**Fundamental and Novel Applications of Electrocaloric Effect**

by

Farrukh Najmi

A dissertation submitted to the Graduate Faculty of
Auburn University
in partial fulfillment of the
requirements for the Degree of
Doctor of Philosophy

Auburn, Alabama
August 8, 2020

Keywords: Electrocaloric effect, pyroelectricity, thermal analysis, thermal cycles, transient heat conduction, solid-state heat pump, ECE-based device, solid-state cooling



Approved by

Zhongyang Cheng, Chair, Alumni Professor of Materials Engineering
Dong-Joo Kim, Alumni Professor of Materials Engineering
Lorenzo Cremaschi, Associate Professor of Mechanical Engineering
Majid Beidaghi, Assistant Professor of Materials Engineering
Pengyu Chen, Assistant Professor of Materials Engineering

## Abstract

The discovery of materials with a giant electrocaloric (EC) coefficient in the last decade triggered the research community to explore the materials with high pyroelectric and electrocaloric coefficient that revived the research on the development of EC-based solid-state cooling devices, as alternatives of conventional vapor compression (VC)-based technology, which was abandoned few decades back due to less pyroelectric and electrocaloric coefficient of then known materials. Electrocaloric materials (ECMs) offer a great potential for solid-state cooling applications and currently the research on the subject is being carried out in two different domains: the development of *new ECMs* and design of *EC-based cooling device.* For the former, the characterization of the EC effect is the key and several ECMs have been studied and reported for last 15 years where primarily two methods are used for their characterization: *direct and indirect methods*. A challenge, which is associated with the characterization of the ECMs, is that huge variations in the coefficients of the electrocaloric effect (ECE) have been observed during characterization by these two methods. For the latter, one of the problems in the development of EC-based solid-state cooling device is the involvement of moving parts – either active components or cooling/ heating fluids are moved physically to transfer heat from the source (cold end) to the sink (hot end). This approach reduces the efficiency of EC-based coolers/ heat pumps and adds complexities limiting their exploitation in small scale applications. In this research, the above mentioned issues with EC cooling technologies have been addressed.

Indirect method *that is based on the thermodynamic relations* and direct method *that is the direct measurement of temperature change in dielectric materials upon application/removal of electric field* should give the same results in characterization coefficients for linear dielectric materials. However, most ECMs are nonlinear in nature that causes the difference in the EC coefficient obtained using direct and indirect methods. Moreover, the mechanical condition has a strong influence on the EC coefficient, but during the measurements, either perfect *constant stress* or *constant strain* condition cannot be achieved. Additionally, adiabatic process is needed, but it is difficult to achieve, especially when dealing with the thin films where substrates act as thermal anchors, and complete adiabatic conditions are not achievable. More importantly, giant EC coefficient has been obtained in relaxor ferroelectrics, but the results from direct and indirect

methods show a huge difference. By fundamental physics, the relaxor ferroelectrics should not have the EC effect. The fundamental factors behind these phenomena are discussed using phenomenological theory by considering nonlinear effects, such as the *electric field and temperature dependence of the permittivity* of the dielectric material. New relationships are introduced. Based on these, a new EC-like phenomenon is studied that is independent of crystal structure and becomes dominant at the higher electric fields that are involved in the EC characterization.

On the device side, to address the issue of moving parts, a multilayer system of EC and non-EC bodies is devised that is capable to achieve the directional heat flow without the involvement of any moving parts in the system. In other words, all the bodies remain in thermal contact throughout the heat conduction process in the system and no moving parts are involved. Two EC layers have been sandwiched between source (SO) and sink (SI) and the heat is pumped from source to sink in a complete silent operation. A thermal cycle (precisely an electric field cycle) is applied on the EC layers alternatively in such a way that it creates a temperature gradient to achieve a directional heat flow in a system of bodies (SI/ECs/SO), that are otherwise in thermal equilibrium. Most of the ECMs being anisotropic may be simplified to one dimensional case. So, the problem of one-dimensional (1D) transient heat conduction within a multilayer system of four connecting bodies (SI/ECs/SO), in which two finite bodies that are EC, and two semi-infinite bodies that are non-EC, has been solved analytically. The temperature of EC-bodies can be instantaneously changed by external electric field to establish the initial temperature profile. Then, the temperature distribution in the bodies as a function of time/space (1D) and the heat flux through the interfaces as a function of time have been determined analytically. Each of these analytical solutions includes five infinite summation series. It is proved that each of these series is convergent, and the sum of each infinite series can be approximated and calculated using the first $N$ terms of the series. The formula for calculating the value of $N$ is provided.

This idea of multilayer system of EC/non-EC bodies has been employed to achieve a directional heat flow from source to sink with complete silent operation, i.e., without involvement of any physical movements of the components, in an EC-based heat pump. For a sustainable operation, a specially designed thermal cycle comprising of three steps is applied on EC bodies, where in first step heat is pumped from source to sink and in the subsequent steps, EC bodies are recovered for the next cycle. In these two steps, the net heat flow between SO and SI through the interfaces

cancels each other so the net heat transfer is the heat that was transferred in the first step. The analytical solution has been implemented numerically for several scenarios depending on the thermal properties of EC and non-EC materials and has been found that a huge thermal mismatch between ECMs and SI/SO (i.e. low value of contacting coefficient), offers ideal conditions for the continuous operation of heat pump. This novel approach can be a viable solution in thermal management of high power density electronics and for portable medical applications.

Moreover, most of the typical ECE-based devices reported in the literature are either prototypes or numerical simulations, so the performance of the device is mostly based on the experimental results. The optimization of the devices requires that there must be some formulation so that the EC devices can be designed for high efficiency and cooling power. During absorption of heat (depolarization of ECM), the typical ECM is coupled with source on one side and there is air/ or other material on the other side. On the other hand, during polarization, the ECM is coupled with sink on one side and with air/other material on the other side to reject the heat. This scenario has been solved analytically, and the transient solution for generalized initial conditions, and for bodies with different thermal properties has been given that is much versatile and flexible to be used in the thermal analysis of most of the ECE-based devices for the determination of relaxation time, temperature profiles and heat fluxes.

**Acknowledgements**

First, I would like to acknowledge my supervisor, Dr. Zhongyang Cheng for his guidance towards my research. He has been a great source of knowledge, technical insight, and encouragement throughout my journey to PhD. His continuous support not only motivated me to work diligently but also created a sense of inquisitiveness that helped me being determined and focused to achieve my goal. Secondly, my words will not complete without thanking my peers, friends, and colleagues specially Dr. Hossein Talebinezhad and Dr. Yang Tong for their support, cooperation and help during my studies at Auburn.

I would also like to thank Dr. Lorenzo Cremaschi for his valuable time for long discussions for in-depth understanding of scientific and engineering aspects of my research that opened new prospects for an impactful contribution in the field. I also really appreciate Dr. Wenxian Shen for her verification and validation of the analytical solution of the problem and for her meticulous observations to present the mathematical model in systematic and scientific way.

My successful journey towards my destination is indebted to the continuous support, self-sacrificing hard work, kindness, and everlasting prayers of my parents. They guided me rightly at each step of my life and helped me to make difficult decisions for a brighter future. Moreover, this long journey would not have been possible without love, patience and support of my lovely wife who is a great blessing in my life and has proved herself a perfect life partner. During this time, she not only fulfilled her maternal duties nicely to look after three kids but also completed her MS with distinction along with challenging professional assignments as a teaching assistant.

I consider it pertinent to thank my friend Mr. Zaheer Iqbal – a civil servant and a Humphrey fellow – for his selfless motivation to bring me out of my comfort zone and guiding me towards my expedition to knowledge and research.

I would also like to acknowledge the cooperation and support of hopper administration of Auburn University to provide access to the supercomputer for carrying out the highly intensive finite element simulations.

In the end, I would definitely like to appreciate the financial support from the U.S. Department of State, Bureau of Educational and Cultural Affairs (ECA) and the United States Agency for International Development (USAID), as well as the administrative support from the

United States Educational Foundation in Pakistan (USEFP) and the Institute of International Education (IIE), throughout my research as a Ph.D. candidate under the Fulbright Foreign Student Program.

Table of Contents

Abstract ..... 2

Acknowledgements ..... 5

Table of Contents ..... 7

List of Figures ..... 13

List of Tables ..... 18

List of Abbreviations and Symbols ..... 19

Chapter 1 Electrocaloric Effect: Theory, Characterization and Applications ..... 21

1.1 Historical Background ..... 21

1.2 Fundamentals of Electrocaloric Effect (ECE) ..... 24

1.3 Theory of Electrocaloric Effect (ECE) ..... 26

1.3.1 General Thermodynamics ..... 26

1.3.1.1 Primary Pyroelectric Effect ..... 27

1.3.1.2 Secondary Pyroelectric Effect ..... 28

1.3.1.3 Relationship between Primary and Secondary Pyroelectricity ..... 29

1.3.1.4 Measurement of Electrocaloric Effect ..... 31

1.3.2 Thermodynamics of Ferroelectrics – Landau, Ginzburg and Devonshire Theory ..... 33

1.3.2.1 Second Order Phase Transition ($\xi > 0$) ..... 34

1.3.2.2 First Order Phase Transition ($\xi < 0$) ..... 36

1.3.3 Electrocaloric Characterization ..... 38

1.3.3.1 Indirect EC Measurements by Maxwell Approach ..... 39

1.3.3.2 Direct Measurements ..... 41

1.3.3.3 Comparison of Indirect and Direct Methods ..... 47

1.3.4 Classification of Electrocaloric Materials (ECMs) ..... 49

1.3.4.1 Normal Ferroelectric (FE) Materials ..... 49

1.3.4.2 Antiferroelectric (AFE) Materials ..... 51

1.3.4.3 Relaxor Ferroelectric (RFE) Materials ..... 52

1.3.4.4 Highly Researched EC Materials and Current Status ..... 54
1.4 Working Principle of ECE-based Cooling and Figure of Merits (FoM) ..... 57
1.4.1 Comparison of VC-based and EC-based Cooling Cycles ..... 57
1.4.2 Comparison of MC-based and EC-based Cooling Technology ..... 59
1.4.3 Thermodynamic Cycles for EC Cooling ..... 59
1.4.3.1 Carnot Cycle ..... 59
1.4.3.2 Brayton Cycle ..... 60
1.4.3.3 Ericsson Cycle ..... 61
1.4.4 Basic Concept of EC-based Device ..... 62
1.4.5 Performance Criteria of the EC-Device ..... 63
1.4.5.1 Coefficient of Performance (COP) ..... 63
1.4.5.2 Refrigeration Capacity (RC) ..... 64
1.4.5.3 Specific Cooling Power ..... 65
1.4.5.4 Efficiency of EC Device ..... 65
1.5 Current Status of the EC-based Cooling Devices ..... 65
1.5.1 Regeneration Designs ..... 69
1.5.1.1 EC-based Devices with Liquid Regenerator ..... 69
1.5.1.1 EC-based Devices with Solid Regenerator ..... 71
1.5.1.2 Design Concept without External Heat Regenerator ..... 72
1.5.2 Cascade Designs ..... 73
1.5.2.1 EC Devices with Mechanical / Motorized Actuating Systems ..... 74
1.5.2.2 EC Devices based on Electrostatic Actuation ..... 75
1.5.2.3 EC-devices with Electromechanical Actuation ..... 76
1.5.2.4 EC Devices with Thermal Diodes/ Heat Switches ..... 77
1.5.3 Solid-state Cooling Line ..... 79
1.6 Research Objectives ..... 83
1.6.1 Objective # 1 ..... 83
1.6.2 Objective # 2 ..... 83
1.6.3 Objective # 3 ..... 83
1.6.4 Objective # 4 ..... 84
Chapter 2 Electrocaloric-like Effect at High Electric Field ..... 85

2.1 Nonlinear Contribution to Temperature Change ..... 85
2.1.1 First Approach ..... 91
2.1.1.1 Temperature Dependence of Permittivity ..... 91
2.1.1.2 Temperature Dependence of Static Permittivity ..... 93
2.1.2 Second Approach ..... 94
2.1.2.1 Temperature Dependence of Permittivity ..... 94
2.1.2.2 Temperature Dependence of Static Permittivity ..... 95
2.1.3 Determination of Constants *a*, α and β ..... 96
2.1.4 Case Study-I (BST) ..... 97
2.1.4.1 Determination of Constant *"a"* using PE Loops ..... 97
2.1.4.2 Determination of Constants α and β ..... 99
2.1.4.3 Determination of ΔT Contribution due to Higher Fields ..... 100
2.1.5 Case Study-II (PMN-0.1 PT) ..... 102
2.1.5.1 Determination of Constant *"a"* using PE Loops ..... 103
2.1.5.2 Determination of Constants α and β ..... 104
2.1.5.3 Determination of ΔT Contribution due to Higher Fields ..... 105
2.1.6 Conclusion and Comments ..... 106
2.2 Primary and Secondary Pyroelectricity with Nonlinear and Higher Order Coupling ..... 106
2.2.1 Case-I Principle and Linear Coupling Coefficients ..... 107
2.2.2 Case-II Principle and Nonlinear Coefficients ..... 108
2.3 Concluding Remarks ..... 111

Chapter 3 Analytical Solution of a Multilayer System ..... 112

3.1 Model and Analytical Solution ..... 113
3.1.1 Physical Model ..... 113
3.1.2 Mathematical Model and Governing Equations ..... 113
3.1.2.1 Assumptions and Considerations ..... 113
3.1.2.2 Initial Conditions (ICs) ..... 114
3.1.2.3 Boundary Conditions (BCs) ..... 114
3.1.2.4 Physical Conditions (PCs) ..... 115
3.1.3 Solution of the Heat Equations ..... 115

3.1.3.1 Laplace Transformation ..... 116
3.1.3.2 Considerations and Conditions ..... 116
3.1.3.3 Determining the Constants of Integration ..... 117
3.1.3.4 Manipulating the Constants of Integration ..... 118
3.1.3.5 Equations in Laplace Domain ..... 121
3.1.3.6 Inverse Laplace Transform of the System of Equations ..... 123
3.1.4 Temperature Profiles of the Bodies ..... 124
3.1.5 Validation of the Analytical Solution ..... 125
3.1.6 Temperature Gradients in the Bodies ..... 127
3.1.7 Heat Flux through the Interfaces ..... 128
3.1.8 Heat Energy Transfer through the Interfaces ..... 130
3.2 Summary of Analytical Solution ..... 132
3.3 Estimating the Summation Terms ..... 133
3.3.1 Determination of Number of Terms Needed ..... 133
3.3.2 A Case Study ..... 138
3.4 Concluding Remarks ..... 140

Chapter 4 Heat Pump without Moving Parts/ Silent Operation ..... 141

4.1 Heat Pump Model for Directional Heat Flow ..... 141
4.2 Physical Model and Working Principle ..... 141
4.3 Mathematical Model and Analytical Solution ..... 145
4.3.1 Initial Conditions for Thermal Cycle ..... 145
4.3.2 Boundary Conditions (BCs) ..... 146
4.3.3 Physical Conditions ..... 147
4.3.4 Analytical Solution ..... 147
4.4 Temperature Profiles of the Bodies ..... 147
4.5 Temperature Gradients in the Bodies ..... 149
4.6 Heat Flux through the Interfaces ..... 151
4.7 Heat Energy Transfer through the SI|EC1 and EC2|SO Interfaces ..... 153
4.7.1 Heat Energy Transfer through the SI|EC1 Interface ..... 154
4.7.2 Heat Energy Transfer through the EC2|SO Interface ..... 154
4.8 Net Heat Energy Transfer through the Interfaces in One Cycle ..... 155

4.8.1 Heat Energy Transfer in Step-I ..... 156
4.8.2 Heat Energy Transfer in Step-II ..... 156
4.8.3 Heat Energy Transfer in Step-III ..... 156
4.9 Temperature Profile and Corresponding Heat Flow through EC2|SO Interface ..... 157
4.9.1 Step-II and Step-III ..... 158
4.9.2 Step-I ..... 164
4.9.3 Summary of an Ideal Three-step Process ..... 168
4.10 Operation to Achieve Net Heat Transfer from SO to SI for One Cycle for $K_\varepsilon << 1$ ..... 170
4.11 Concluding Remarks ..... 172

Chapter 5 Analytical Solution of a Multilayer Problem with Different Source and Sink ..... 174

5.1 Model and Analytical Solution ..... 174
5.1.1 Physical Model ..... 174
5.1.2 Mathematical Model and Governing Equations ..... 175
5.1.2.1 Assumptions and Considerations ..... 175
5.1.2.2 Initial Conditions (ICs) ..... 175
5.1.2.3 Boundary Conditions (BCs) ..... 176
5.1.2.4 Physical Conditions (PCs) ..... 176
5.1.3 Solution of the Heat Equations ..... 177
5.1.3.1 Laplace Transformation ..... 177
5.1.3.2 Determining the Constants of Integration ..... 178
5.1.3.3 Solving Simultaneous Equations ..... 179
5.1.3.4 Manipulation of Constants of Integration ..... 179
5.1.3.5 Equations in Laplace Domain ..... 180
5.1.3.6 Inverse Laplace Transform of the System of Equations ..... 182
5.1.4 Temperature Profiles of the Bodies ..... 183
5.1.5 Heat Flux through the Interfaces ..... 184
5.1.6 Heat Energy Transfer through the Interfaces ..... 186
5.2 Estimating the Infinite Series ..... 186
5.3 Application of Analytical Solution on Real Scenarios ..... 190
5.3.1 Case Study of a Device ..... 191
5.3.1.1 Parameters to be Used in the Simulation ..... 191

5.3.1.2 Temperature Profiles and Heat Flux ..... 192
5.3.2 Implementing the Analytical Solution in Thin Film Characterization ..... 196
5.4 Concluding Remarks ..... 197
Bibliography ..... 199
Appendix - A Generic Solution of the Heat Equation ..... A-1
Appendix - B Constants of Integration (Analytical Solution for Same Sink/Source) ..... B-1
Appendix - C Manipulating the Denominator for Analytical Solution in Chapter 3 ..... C-1
Appendix - D Validation of the Analytical Solution ..... D-1
Appendix - E Thermal Properties of Several EC and non-EC Materials ..... E-1
Appendix - F Definitions of Material Properties of a Dielectric Material ..... F-1
Appendix - G Tensorial Ranks of Material Properties ..... G-1
Appendix - H Matrix and Tensor Notations ..... H-1
Appendix - I Proof of Geometric Series ..... I-1
Appendix - J Constants of Integration (Analytical Solution for Different Sink/Source) ..... J-1
Appendix - K Manipulating the Denominator for Analytical Solution in Chapter 5 ..... K-1

List of Figures

Figure 1.1 A Schematic presentation of dipoles orientation in a dielectric material, (a). No electric field, (b). External electric field applied adiabatically at constant strain, (c). External electric field applied isothermally at constant strain, (d). External electric field applied adiabatically at constant stress, (e). External electric field applied isothermally at constant stress ..... 25
Figure 1.2 Heckman diagram for primary and secondary pyroelectricity ..... 30
Figure 1.3 Typical curves for second order phase transition[32], (a). Free energy vs P, (b). Temperature dependence of spntaneous polarization, (c). Temperature dependence of reciprocal permittivity ..... 36
Figure 1.4 Typical curves for first order phase transition[32], (a). Free energy vs P, (b). Temperature dependence of spontaneous polarization, (c). Temperaure dependence fo reciprocal permittivity ..... 37
Figure 1.5 Temperature and electric field dependence of polarization of normal ferroelectrics, (a). Second order phase transition, (b). First order phase transition[29,54] ..... 38
Figure 1.6 Typical steps for indirect EC measurements, (a). Typical PE curves, (b). Temperature dependence of polarization at constant electric field, (c). $(\partial P/\partial T)_E$ as a function of temperature at different constant electric fields, (d). $(\partial P/\partial T)_E$ functions obtained by appropriate curve fitting[10]40
Figure 1.7 Typical steps for indirect characterization of ECMs where phase transition is involved (first order in this case)[52] ..... 41
Figure 1.8 Schematic of a modified DSC for direct EC measurements[23] ..... 43
Figure 1.9 EC Measurements using typical DSC technique[52,57] ..... 43
Figure 1.10 Schematic of an adiabatic calorimeter[23] ..... 44
Figure 1.11 Typical EC measurements using adiabatic calorimetry (AC)[52] ..... 44
Figure 1.12 Direct ECE measurements using IR thermometry[58] ..... 45
Figure 1.13 Comparison of ECE obtained by HRC and IR thermometry[58] ..... 45
Figure 1.14 EC temperature changes at different points (shown Left) on MLC surface[59,60] ..... 46
Figure 1.15 (a). Thin resistive electrode as temperature sensing element, (b). Temperature sensing element on an MLC ..... 46
Figure 1.16 Direct and indirect measurement in PMN-PT single crystal[63] ..... 47

Figure 1.17 Comparison of directly and indirectly measured ECE in NKN[65] ..... 47
Figure 1.18 Comparison of direct and indirect measurements of PLZT bulk ceramics[66], (a). PLZT RFE, (b). PLZT AFE ..... 48
Figure 1.19 Comparison of directly and indirectly measured EC coefficient in PVDF RFE polymer[56] ..... 48
Figure 1.20 Comparison of direct and indirect ECE measurements in BST bulk ceramics[67] ..... 48
Figure 1.21 (a). EC coefficient for several organic and inorganic ECMs, (b). ΔT/ΔE vs electric field for several organic and inorganic ECMs ..... 51
Figure 1.22 A typical P-E loop for AFEs ..... 52
Figure 1.23 Negative ECE in Ba-doped Lead Zirconate (PBZ) - An AFE material[82] ..... 52
Figure 1.24 Broad peak in permittivity vs temperature in typical RFEs (PMN-0.13PT)[87] ..... 53
Figure 1.25 ΔT as a function of T for increasing electric fields for PMN-0.13PT – A RFE with a permittivity peak temperature of 48ºC[87] ..... 53
Figure 1.26 Sharp peak in a typical normal FE (BT single crystal)[88] ..... 54
Figure 1.27 ΔT vs T for increasing electric fields for BT single crystal – a normal FE with FE-to-PE phase transition temperature of 402K[88] ..... 54
Figure 1.28 Working principle (thermodynamic cycle) of VC and EC cooling[104] ..... 58
Figure 1.29 Thermodynamic cycles for EC cooling on T-S diagram[106], (a). Brayton cycle, (b). Ericsson cycle ..... 61
Figure 1.30 Simplest EC cooling device: EC sandwiched between heat sink and heat source, (a). Equilibrium state, (b). Polarized state, ECM heats up, (c). Depolarization state, ECM cools down ..... 62
Figure 1.31 Basic working principle of an efficient ECE-based cooling device, (a). Adiabatic polarization, (b). Heat rejection under constant E, (c). Adiabatic depolarization, (d). Heat absorption under constant E ..... 63
Figure 1.32 Classification of EC-based cooling devices[113] ..... 67
Figure 1.33 Schematic of translational fluidic AER (Top), translational solid AER (bottom) .... 69
Figure 1.34 Schematic of cascade, (a). Moving elements, (b). Heat switches/ diodes, (c). Static/ no movement ..... 69
Figure 1.35 (a). First EC device based on AER, (b). Temperature span achieved by AER-based device[117] ..... 70

Figure 1.36 EC cooler with electrostatically driven diaphragms to control the motion of the liquid[118] ..... 71
Figure 1.37 Peristaltic pump driven fluid control for AER in EC-based device[120] ..... 71
Figure 1.38 Prototype EC oscillatory refrigerator (ECOR) based on solid-state regenerator[122] .. 72
Figure 1.39 Basic principle of solid regenerator[122] ..... 72
Figure 1.40 (a). Device concept for self EC to EC regeneration, (b). S-T diagram of a Brayton cycle for rotary EC refrigerator[123] ..... 73
Figure 1.41 EC device with motorized actuator[119] ..... 74
Figure 1.42 EC cooler with mechanical heat switch[126] ..... 74
Figure 1.43 Electrostatic actuation – cross-sectional view of μECM device in flexural mode[127] 76
Figure 1.44 PVDF film based EC device using electrostatic actuation to alternatively make contact with heat source/ sink[13] ..... 76
Figure 1.45 (a). Electromechanical actuation of ECM cantilevers for thermal coupling/ decoupling, (b). Temperature span achieved as a function of number of cycles[128] ..... 77
Figure 1.46 Working stages of TE-EC-TE heat pump[104] ..... 79
Figure 1.47 Thin film based heat switch[109] ..... 79
Figure 1.48 Solid-state cooling line and temperature gradients[23,132] ..... 80
Figure 1.49 (a).Variations of the electric field applied on the EC elements adiabatically and isothermally, (b). Derivative of electric field[132] ..... 80
Figure 1.50 (a). Solid-state cooling line, (b). Electric pulses applied on the EC element, (c). Temperature distribution along the cooling line for two different EC elements (PMN-25 PT and PMN-4.5PT)[134] ..... 81
Figure 2.1 Typical PE loop to determine D and $P_S$ ..... 97
Figure 2.2 Determination of α and β by curve fitting ..... 97
Figure 2.3 Comparison of directly and indirectly measured ECE for BST[67] ..... 98
Figure 2.4 PE loops of BST for *(x = 0.25);* approximated values for D and $P_S$[67] ..... 98
Figure 2.5 Temperature dependence of permittivity for four compositions of BST[67] ..... 99
Figure 2.6 Data deduced from experimental results to determine α and β by curve fitting ..... 100
Figure 2.7 Comparison of direct and indirect ECE measured at E = 30 kV/cm[67] ..... 101
Figure 2.8 Comparison of reported ECE and contribution to ECE due to nonlinear effect ..... 102

Figure 2.9 Comparison of experimentally measured ECE in PMN-0.1PT by direct and indirect method: Solid blue and black dots represent indirect EC data, while stars or other shapes represent direct EC data[120] ..... 102
Figure 2.10 PE loops of PMN-0.1PT[140], (a). P and $P_S$ at 0.5 kV/cm, (b). P and $P_S$ at 20 kV/cm103
Figure 3.1 Theoretical model of heat conduction problem ..... 113
Figure 3.2 A problem from a reference book to validate the analytical solution[143] ..... 126
Figure 3.3 Dependence of *N* on $\gamma$ (=$3a^2$) with fixed |*h*| and $\delta$ , (a). $\delta = 10^{-4}$, (b). $\delta = 10^{-6}$ ..... 137
Figure 3.4 Dependence of N on |*h*| and $\gamma$ for typical ranges of |h| = 0.55 – 0.85 and $\gamma$ = 0.01 – 10, (a). $\delta = 10^{-4}$, (b). $\delta = 10^{-6}$ ..... 138
Figure 3.5 Dependence of N on t and R for BT as ECM and Al as *end* bodies for, (a). $\delta = 10^{-4}$, (b). $\delta = 10^{-6}$ ..... 139
Figure 3.6 Dependence of N on tolerance using BT as ECMs and Al as *end* bodies for t = 10s and R = 1 mm. ..... 140
Figure 4.1 Conceptual model of EC heat pump ..... 141
Figure 4.2 Operational process of the three-step cycles for the system shown in Figure 4.1 ..... 142
Figure 4.3 Electric field cycle and corresponding temperature variations at center of EC1 and EC2 (three cycles shown). ..... 143
Figure 4.4 Temperature profiles of system-1 during, (a). Step-II, (b). Step-III ..... 159
Figure 4.5 Temperature profiles at different times for system-2, (a). Step-II, (b). Step-III ..... 160
Figure 4.6 Time dependence of heat energy transferred through SI|EC1 (blue) and EC2|SO (red) interface for system-2: (a). Step-II, (b). Step-III. ..... 161
Figure 4.7 Temperature profiles $K_\varepsilon << 1$ at different times for system-3, (a). Step-II, (b). Step-III ..... 162
Figure 4.8 Time dependence of heat energy transferred through SI|EC1 (blue) and EC2|SO (red) interface for system-3: (a). Step-II, (b). Step-III. ..... 163
Figure 4.9 Step-I of system-1, (a). Temperature profiles at different times, arrowhead shows the curve at the time $t_r$ $(\partial T_s(t_r)/\partial x|_R = 0)$, (b). Time dependence of heat energy transferred through SI|EC1 and EC2|SO interfaces ..... 164
Figure 4.10 Step-I of system-2, (a). Temperature profiles at different times, arrowhead shows the curve at the time $t_r$ $(\partial T_s(t_r)/\partial x|_R = 0)$, (b). Time dependence of heat energy transferred through SI|EC1 and EC2|SO interfaces ..... 166

Figure 4.11 Step-I of system-3 $K_\varepsilon = 0.0172 << 1$ with R = 1 mm, $\Delta T = 1^oC$, (a). Temperature profiles at different times, arrowhead shows the curve at the time $t_r$, $(\partial T_s(t_r)/\partial x|_R = 0)$, (b). Time dependence of heat energy transferred through SI|EC1 and EC2|SO interfaces ..... 167
Figure 5.1 Theoretical model of heat conduction problem for different source and sink bodies 174
Figure 5.2 An electrostatic actuation based EC cooler: ECM is PVDF and sink/source are AL blocks ..... 191
Figure 5.3 Schematic diagram for working principle of EC cooler shown in Figure 5.2, (a). Heat absorption, (b). Heat rejection ..... 192
Figure 5.4 Heat flux through ECM|SO interface for $\Delta T = 1.3\ ^oC$ at 50MV/m[13] taking PVDF (thickness 6mm) as ECM and AL as source at frequency (0.06 Hz); (a). Simulation using analytical solution, (b). Experimental results[13] ..... 192
Figure 5.5 Heat absorption for PVDF as ECM, AL as source for f = 0.06 Hz (using analytical solution) ..... 193
Figure 5.6 Temperature profile of EC cooler for extended times to absorb more heat energy from source ..... 194
Figure 5.7 Heat flux through the interfaces during heat absorption from the source ..... 194
Figure 5.8 Modification of device shown in Figure 5.3 to two-layered model ..... 195
Figure 5.9 Temperature profile showing the quick relaxation of ECMs in two-layered heat pump as compared to profile shown in Figure 5.6..... 196
Figure 5.10 (a) Typical arrangements of direct ECE measurement in thin film by infrared (IR) camera, (b). Physical model of thin film measurements..... 197

List of Tables

Table 1.1 Efficiency* and status of different cooling technologies[6] ..... 24
Table 1.2 Thermodynamic potentials[32,37] ..... 27
Table 1.3 Primary and secondary pyroelectric effects of several pyroelectric materials at RT[40–42] ..... 30
Table 1.4 Recently reported intensively studied ECMs..... 55
Table 1.5 Analogy between Electrocaloric Effect (ECE) and Magnetocaloric Effect (MCE)..... 59
Table 1.6 Typical COP range for solid-state cooling technologies[23]..... 64
Table 1.7 Several reported EC-based devices and working principle of directional heat flow.... 82
Table 2.1 Calculating *"a"* at electric field 10 kV/cm (1x10$^6$ V/m), 1μC/cm$^2$ = 10$^{-2}$ C/m$^2$ ..... 99
Table 2.2 Determination of ΔT using constants a, α and β for E = 3 MV/m (30 kV/cm..... 100
Table 2.3 Comparison of directly and indirectly measured ECE with nonlinear contribution to ΔT (BST025)..... 101
Table 2.4 Approximation of constant *"a"* from PE loops of PMN-0.1PT using assumption k = a/T ..... 103
Table 2.5 Approximation of constant *"a"* from PE loops of PMN-0.1PT using assumption k = a/T$^2$ ..... 104
Table 2.6 Comparison of difference between experimental measured data (approximately extracted from Figure 2.9) and data deduced from the mathematical formulation at E = 57 kV/cm (Assumption k = a / T$^2$)..... 105
Table 2.7 Comparison of difference between experimental measured data (approximately extracted from Figure 2.9) and ΔT contribution due to nonlinear effect (Assumption k = a / T) ..... 106
Table 4.1 Contacting coefficient (**Kε**), interface temperature (T$_s$) at EC2|SO interface at *t = 0*, time $t_r$ and Q($t_r$) for systems using BT and PMN-4.5PT as ECM and different materials as SO and SI (δ = 10$^{-5}$) ..... 169
Table 4.2 Step-I of System-3 when it is operated with different ΔT. (δ = 10$^{-5}$) ..... 171
Table 4.3 System-3 is modified to use different R, PMN-4.5PT as ECM and Cu as SO/SI ..... 172

List of Abbreviations and Symbols

| | |
|---|---|
| $\alpha_{\mu}^{E}$ | Thermal Expansion Coefficient Matrix (2nd Rank Tensor), μ: 1 – 6 |
| $C^{E,X}$ | Heat Capacity at constant Electric Field and Stress |
| $C^{E,x}$ | Heat Capacity at constant Electric Field and Strain |
| COP | Coefficient of Performance |
| $c_{\mu\nu}^{E,T}$ | Stiffness Matrix |
| D | Electric Displacement (Scalar Form) |
| $d_{m\mu}^{T}$ | Piezoelectric Coefficient Matrix (3rd Rank Tensor) |
| E | Electric Field (Scalar Form) |
| $E_m$ | Electric Field Vector (1st Rank Tensor) |
| EC1 | Electrocaloric Layer 1 |
| EC2 | Electrocaloric Layer 2 |
| ECE | Electrocaloric Effect |
| ECM | Electrocaloric Material |
| FWHM | Full Width at Half Maximum |
| MCE | Magnetocaloric Effect |
| MCM | Magnetocaloric Material |
| $p_m$ | Pyroelectric Vector, m: 1 – 3 |
| P | Polarization |
| $P_s$ | Spontaneous Polarization |
| $P_S$ | Saturation Polarization |
| S | Entropy |
| SI | Sink |
| SO | Source |
| $s_{\mu\nu}^{E,T}$ | Compliance Matrix |
| T | Temperature |
| $T_C$ | Curie Temperature |
| $T_c$ | Cold Reservoir Temperature |

| | |
|---|---|
| $T_h$ | Hot Reservoir Temperature |
| TD | Thermodynamics |
| VC | Vapor Compression |
| $x_\mu$ | Strain Matrix |
| $X_\mu$ | Stress Matrix |

# Chapter 1 Electrocaloric Effect: Theory, Characterization and Applications

## 1.1 Historical Background

Human civilization has evolved through a long history of struggle for food, shelter and against natural calamities. Perhaps one of the greatest challenges, the humankind had to strive against, was to save himself from severe environmental conditions and harsh climates, and this great motive of survival, and desire for better living laid down the foundation of modern engineering of HVAC (Heating, Ventilating and Air-conditioning). Vapor compression (VC) technology has served the humanity for more than a century for air-conditioning, refrigeration, and heat pumping purposes. The refrigerants, i.e., Freon gases like Chlorofluorocarbons (CFC) and Hydrochlorofluorocarbons (HCFCs), to drive these systems, however, had a detrimental effect on environment, ozone depletion potential (ODP), by depleting the atmospheric ozone layer. Ozone layer is a natural barrier against ultraviolet (UV) radiation and human exposure to UV radiation can cause skin cancers and other adverse medical issues[1]. In 1987, a convention called *"Montreal Protocol on Substances that Deplete the Ozone Layer*[2]*"* and in 1997 *"Kyoto Protocol to the United Nation Framework Convention on Climate Change*[3]*"* provided a route map to regulate these materials and emphasized the importance to find the alternative new technologies for refrigeration and air-conditioning. Hydrofluorocarbons (HFCs) were developed to successfully reduce the ODP but they came with global warming potential (GWP)[4].

Moreover, the ever-expanding microelectronics industry and the advent of the miniaturization of the electronics as envisioned by Moore put forward a new challenge of cooling down the electronic systems for sustainable and reliable operation and vapor compression-based technologies could not offer a viable solution due to their limitations in scalability. The future of Moore's prediction of *doubling of components in IC in every 18-24 months*[5] depends on the on-chip refrigeration technology as increased thermal power generation in such small areas limits the performance if not properly cooled. In addition, several emerging technologies also rely on the innovative cooling technologies as a critical part of their systems design, i.e., superconductor-based technologies require high-sensitivity cryogenic temperature control, the development of reliable and efficient hybrid and electric vehicles, having performance equivalent to internal combustion engine vehicles, suffers from excessive heat generated by a vehicle's mechanical and electrical systems

and electrolytic-based capacitors degrade their performance above 70 ºC[6], so reliable, efficient and ecofriendly cooling systems are a dire need of industry.

It is an era of compactness and energy efficiency. About 17% of the total power production of the world goes towards HVAC needs[7]. It is inevitable now that highly efficient, compact and environment friendly cooling systems would be developed. Research community is determined in developing new refrigeration techniques to limit, eliminate, and hopefully reverse the disastrous environmental effects and to address the small-scale cooling issues. Liquids and solids are being considered potential candidates for next generation refrigeration technologies not only because of their higher energy density, low cost and eco-friendly nature but also for compact and vibration free systems to fulfill the wide industry demand of efficient, flexible, small-scale and environmental friendly refrigeration and cooling systems. In pursuit of alternatives for VC technology, about twelve not-in-kind (NIK) technologies were considered to be the potential candidates for next generation cooling, refrigeration and/or heat pumping systems[8]. The term NIK refers to any technology for refrigeration and air conditioning that is not based on VC technology. Keeping this in view, tremendous scientific efforts to explore the potential candidates were carried out but most of them have not been proved more than a laboratory curiosity[8]. Thermoelectric (TE)-based coolers offered advantages of small-scale manufacturing, spot thermal management, flexibility, static-operation and durability, the biggest disadvantage associated with them, however, was poor efficiency due to joule heating and high manufacturing costs making them far less likely to be used for refrigeration purposes[9,10].

In the recent years, the *caloric* refrigeration has showed a great potential to address these challenges. Caloric refrigeration exploits the caloric properties of the materials with different type of external stimuli to produce the thermal changes in materials, i.e., magnetocaloric (MC), electrocaloric (EC), elastocaloric (eC) and barocaloric (BC)[11–14]. Among them elastocaloric and barocaloric have not got much attention of the research community and still are in their novice state. Magnetocaloric technology is playing a pivotal role in cryogenics applications and many magnetocaloric-based systems were successfully developed and commercialized. The involvement of high magnetic fields, however, has always been an issue and hindered their scalability to be used in microelectronics and for IC thermal management[9,10,15]. The miniaturization of magnetocaloric devices is a big challenge due to difficulty in producing inexpensively sufficiently large magnetic fields in small devices and this limits their use in small

scale application of microcooling and IC thermal management. For example, magnetic induction higher than 1.8 T is very unlikely to be produced using permanent magnets[7] and to produce magnetic fields above 5 T, large and expensive superconductive magnets are required. Also, higher costs and availability of rare earth metals to produce permanent magnets are major concerns.

Electrocaloric (EC) cooling has recently come forward to address the current challenges of industry and is being considered a promising candidate for future solid-state cooling and refrigeration. Electrocaloric effect (ECE) is not new to the science community, the idea was first proposed theoretically by William Thomson in 1878 as converse effect of pyroelectricity[16]. It was, however, experimentally observed in Rochelle salt about 50 years later in 1930[17] and EC temperature change was investigated experimentally in 1943[18]. The results were not very promising as only a minute temperature change of 0.003K was observed and then research on electrocalorics (ECs) witnessed a long pause for next few decades and no considerable efforts were carried out by the research community. One of the reasons was the industry demands for cryogenic applications in the field of superconductors and MC cooling addressed and achieved these scientific goals successfully. The first idea of the EC refrigerator was proposed in 1979[19]. Due to much less EC coupling coefficients of then known electrocaloric materials (ECMs), however, they were not considered alternative of MC and VC technologies so this field could not get considerable attention of research community and was not much explored and abondended[6]. It was not until the years 2006 and 2008, when the giant ECE in PZT thin films and PVDF polymers were reported, respectively[20,21], they got attention again and triggered the research community to explore the ECE in the next generation cooling devices[22]. After these breakthrough discoveries, an avalanche of research publications was observed in which various organic and inorganic materials (i.e., both normal ferroelectrics (FEs) and relaxor ferroelectrics (RFEs)) in the form of bulk ceramics, single crystals, thick and thin films, and polymer thin films were investigated to achieve a high temperature change ($\Delta T_{EC}$) upon the application of the external electric field[20,23–27].

The ECE is analogous to the magnetocaloric effect (MCE) except that in the case of EC material, the temperature change is achieved by changing the external electric field instead of magnetic field. In contrast to MCE, refrigeration using EC phenomenon offers easiness in producing higher electric fields on much lower costs[23] and has the potential to achieve the efficiency comparable to MCE-based cooling devices[9]. This great advantage opens the possibility for miniaturization and ECE-based devices can be tailored for almost any application in micro-robotics, microelectronics,

and a broad variety of other niche applications. Besides, they also have strong potential to be used in different standard cooling and heating devices, such as commercial refrigerators, heating pumps, and air conditioners. Table 1.1 shows the efficiencies of some developed and developing solid-state cooling technologies in comparison with conventional VC refrigeration technology[6].

**Table 1.1 Efficiency*and status of different cooling technologies[6]**

| Technology | Efficiency (%) | Status and Comments |
|---|---|---|
| Vapor Compression (VC) | 40-50 | Fully Developed, widely utilized, and optimized, Involves ODP and GWP due to CFC and HCFC gases |
| Magnetocaloric Effect (MCE) | 60-70 | Successfully Addressing Cryogenic Applications<br>Utilized in Cryogenic Application, Required Large Magnetic Field and Large Magnets, Scalability is the issue. |
| Thermoelectric (TE) | 10 | 60 years of extensive research has not delivered a practical and efficient device; Easy to be miniaturized, Expensive to manufacture |
| Electrocaloric Effect (ECE) | 60-70[28] | Has potential to be manufactured in small scale<br>Small Effect in bulk materials<br>Large Effect in Thin Films<br>No commercial device is available, and research is going through its evolutional stages |

*Efficiency of a cooling device/ system is defined with respect to Carnot cycle efficiency, (Ref: section 1.4.5)

## 1.2 Fundamentals of Electrocaloric Effect (ECE)

Electrocaloric effect (ECE) is a physical phenomenon observed in dielectric materials in which a dielectric material undergoes a reversible temperature change when it is subjected to the external electric field[9,10,29]. When an external electric field is applied on a dielectric material, an electric polarization is induced due to the dipole orientation (*alignment*) that reflects the change in the order degree of the dipoles, and the reverse effect happen when the electric field is removed (*randomness*). Therefore, if an electric field is applied on a dielectric material adiabatically ($\Delta S = 0$, where $S$ is the entropy), the change in the polarization would result in a change in the temperature of the dielectric as shown in Figure 1.1(b), whereas on the other hand, if the electric field is applied on a dielectric material under an isothermal condition ($\Delta T = 0$, where T is the temperature), the change in the polarization would result in a heat exchange between the dielectric

and surrounding as shown in Figure 1.1(c). The ECE is a reversible process and can be used for cooling applications[30].

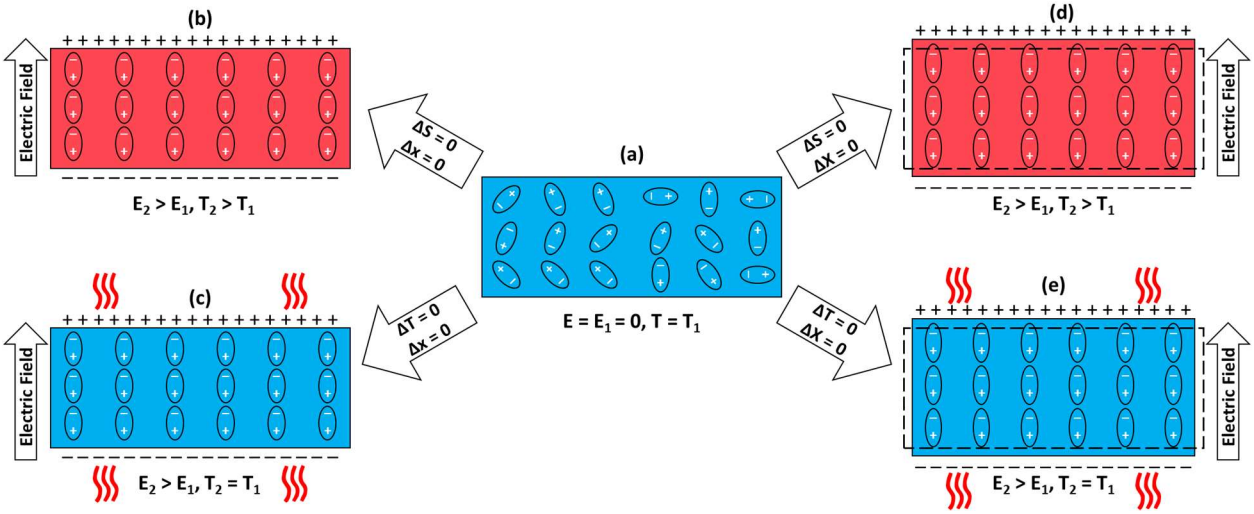


**Figure 1.1 A Schematic presentation of dipoles orientation in a dielectric material, (a). No electric field, (b). External electric field applied adiabatically at constant strain, (c). External electric field applied isothermally at constant strain, (d). External electric field applied adiabatically at constant stress, (e). External electric field applied isothermally at constant stress**

By physics, the ECE may be expressed by Eq. (1.1), where $p_m^x$ is electrocaloric coefficient, that represents a change in entropy ($S$) of the dielectric material with external electric field ($E_m$) at constant strain ($x$) and temperature. The dielectric materials where this phenomenon happens are anisotropic in nature and the ECE is a vector quantity (first rank tensor), where $m = 1,2,3$ represents three crystallographic directions.

$$p_m^x(T) = \left(\frac{\partial S}{\partial E_m}\right)_{x,T} \qquad \text{(m=1,2,3)} \qquad (1.1)$$

The crystals based on their macroscopic symmetry have been divided into 32 point groups. The symmetry of a crystal is related to symmetry of its physical property. It is a fundamental postulate of the crystal physics known as Neumann's principle. *"The symmetry elements of any physical property of a crystal must include the symmetry elements of the point group of the crystal*[31]*"*. Among these 32 point groups, 11 are centrosymmetric and characterize no polar properties (i.e. non-polar). The remaining 21 are non-centric point groups. 20 out of them, except cubic 432 point group, can exhibit polar properties upon the application of external stress so they are *piezoelectric* in nature. Among these 20 point groups, 10 point groups (6, 6mm, 4, 4mm, 3, 3m, mm2, 2, m, 1)

have unique polar axis and possess *spontaneous polarization* (electric moment per unit volume), and this spontaneous polarization changes with the temperature of the crystal, which is called *pyroelectric effect* (PEE). These polar classes are also referred to as pyroelectric classes[31–33]. *Electrocaloric Effect* (ECE) is the thermodynamic equivalent of pyroelectric effect. Moreover, *ferroelectric* is pyroelectric when its spontaneous polarization can be switched using external electric field.

## 1.3 Theory of Electrocaloric Effect (ECE)

A general theory for microscopic explanation of ECE has not yet been fully developed[10,20,23]. Macroscopically this phenomenon can be understood using standard thermodynamic relations. Dielectric, piezoelectric, and pyroelectric properties of homogeneous dielectric materials may be expressed by three independent variables each chosen from three conjugate pairs of variables $(E_m, D_m), (X_\mu, x_\mu)$ & $(T, S)$. These conjugate pairs can be used to express electrical, mechanical and thermal work in the dielectric materials, respectively. Since $E_m$ and $D_m$ are vectors (three components), and $X_\mu$ and $x_\mu$ are tensors (six components), it should be realized that to express the energy state of a crystal, ten variables (nine plus temperature/entropy) are required. There exists a unique function of these ten variables called thermodynamic potential or free energy function[33]. For instant, choosing $D_m, x_\mu, S$ as independent variables, gives us internal energy – a thermodynamic potential that can be an easiest starting point to understand the ECE thermodynamically.

### 1.3.1 General Thermodynamics

Mathematically, ECE may be understood using laws of thermodynamics. That is, according to the first law of thermodynamics: the change in the internal energy $(dU)$ per unit volume of a piece of a dielectric material because of external electrical work $(\delta w_E = E_m dD_m)$ and mechanical work $(\delta w_E = E_m dD_m)$, can be expresses as:

$$dU = TdS - X_\mu dx_\mu + E_m dD_m \tag{1.2}$$

$dS = \frac{\delta q}{T}$ (second law of thermodynamics)

$E_m$: Electric field (V/m) vector (1st rank tensor)

$D_m$: Electric displacement (C/m$^2$) vector (1st rank tensor)

$X_\mu$: Stress (Pa = N/m$^2$) matrix (2nd rank tensor)

$x_\mu$: Strain Matrix (2nd rank tensor)

$T$: Temperature (K)

$S$: Entropy (J/K)

There are eight ways to choose independent variables from three pairs of variables that constitute eight thermodynamic potentials shown in Table 1.2. Reader is referred to classical books on ferroelectricity for details[32,34–36].

**Table 1.2 Thermodynamic potentials**[32,37]

| Thermodynamic Potential | Independent Variables | Definition | Differential Form |
|---|---|---|---|
| Internal Energy | $S, x_\mu, D_m$ | $U$ | $dU = TdS - X_\mu dx_\mu + E_m dD_m$ |
| Helmholtz Free Energy | $T, x_\mu, D_m$ | $A = U - TS$ | $dS = -SdT - X_\mu dx_\mu + E_m dD_m$ |
| Enthalpy | $S, X_\mu, E_m$ | $H = U + X_\mu x_\mu - E_m D_m$ | $dH = TdS + x_\mu dX_\mu - D_m dE_m$ |
| Elastic Enthalpy | $S, X_\mu, D_m$ | $H_1 = U + X_\mu x_\mu$ | $dH_1 = TdS + x_\mu dX_\mu + E_m dD_m$ |
| Electric Enthalpy | $S, x_\mu, E_m$ | $H_2 = U - E_m D_m$ | $dH_2 = TdS - X_\mu dx_\mu - D_m dE_m$ |
| Gibbs Free Energy | $T, X_\mu, E_m$ | $G = U - TS + X_\mu x_\mu - E_m D_m$ | $dG = -SdT + x_\mu dX_\mu - D_m dE_m$ |
| Elastic Gibbs Energy | $T, X_\mu, D_m$ | $G_1 = U - TS + X_\mu x_\mu$ | $dG_1 = -SdT + x_\mu dX_\mu + E_m dD_m$ |
| Electric Gibbs Energy | $T, x_\mu, E_m$ | $G_2 = U - TS - E_m D_m$ | $dG_2 = -SdT - X_\mu dx_\mu - D_m dE_m$ |

#### 1.3.1.1 Primary Pyroelectric Effect

Considering $T, x_\mu, E_m$ as independent variables, the natural thermodynamic potential is electric Gibbs energy that can be given as,

$$dG_2 = -SdT - X_\mu dx_\mu - D_m dE_m \tag{1.3}$$

Differentiating a thermodynamic potential with respect to one independent variable, we get the dependent variable of the corresponding conjugate pair, So from Eq. (1.3),

$$\left(\frac{\partial G_2}{\partial E_m}\right)_{x,T} = -D_m \qquad \left(\frac{\partial G_2}{\partial x_\mu}\right)_{T,E} = -X_\mu \qquad \left(\frac{\partial G_2}{\partial T}\right)_{x,E} = -S$$

Differentiating again,

$$\left(\frac{\partial^2 G_2}{\partial T \partial E_m}\right)_x = -\left(\frac{\partial D_m}{\partial T}\right)_{x,E} \qquad \left(\frac{\partial^2 G_2}{\partial E_m \partial T}\right)_x = -\left(\frac{\partial S}{\partial E_m}\right)_{x,T}$$

Electric Gibbs energy, being an exact differential, gives

$$\left(\frac{\partial D_m}{\partial T}\right)_{x,E} = p_m^x(T) = \left(\frac{\partial S}{\partial E_m}\right)_{x,T} \tag{1.4}$$

This is called *primary pyroelectric effect.* That is, change in electric displacement of dielectric material with temperature at constant strain. It is also called true pyroelectricity[31]. Based on Neumann's principle, only pyroelectric materials exhibit the pyroelectric effect. Right hand side of Eq. (1.4) is called *electrocaloric effect*, that is, change in entropy of dielectric material with temperature, so pyroelectric effect and electrocaloric effect (ECE) are thermodynamically equal.

#### 1.3.1.2 Secondary Pyroelectric Effect

If $T, X_\mu, E_m$ are taken as independent variable, the natural thermodynamic potential is Gibbs free energy that can be given as,

$$G(T, X, E) = U - TS + X_\mu x_\mu - E_m D_m \tag{1.5}$$

Taking differential of Eq. (1.5), we get

$$dG = dU - TdS - SdT + X_\mu dx_\mu + x_\mu dX_\mu - E_m dD_m - D_m dE_m$$

Putting Eq. (1.2) in Eq. (1.5), we get

$$dG = TdS - X_\mu dx_\mu + E_m dD_m - TdS - SdT + X_\mu dx_\mu + x_\mu dX_\mu - E_m dD_m - D_m dE_m$$

$$dG = -SdT + x_\mu dX_\mu - D_m dE_m \tag{1.6}$$

Similarly, differentiating Eq. (1.6) with respect to independent variables,

$$\left(\frac{\partial G}{\partial T}\right)_{X,E} = -S \qquad \left(\frac{\partial G}{\partial X_\mu}\right)_{T,E} = x_\mu \qquad \left(\frac{\partial G}{\partial E_m}\right)_{X,T} = -D_m$$

Differentiating again

$$\left(\frac{\partial^2 G}{\partial E_m \partial T}\right)_X = -\left(\frac{\partial S}{\partial E_m}\right)_{X,T} \qquad \left(\frac{\partial^2 G}{\partial T \partial E_m}\right)_X = -\left(\frac{\partial D_m}{\partial T}\right)_{X,E}$$

Gibbs free energy, being an exact differential, gives

$$\left(\frac{\partial S}{\partial E_m}\right)_{X,T} = p_m^X = \left(\frac{\partial D_m}{\partial T}\right)_{X,E} \tag{1.7}$$

This is *secondary pyroelectric effect,* that is, change in electric displacement of dielectric with temperature at constant stress. Right hand side of Eq. (1.7) is *electrocaloric effect,* that is, change in entropy of dielectric material with external electric field, so both effects are thermodynamically equal. It has been observed that relative differences between primary and secondary pyroelectric effect can be very high (of the order of 100%). For example, the primary and secondary

pyroelectric coefficient can have different signs. In other words, the experimental measuring conditions play an important role in the results for the characterization of the pyroelectric effect as well as of electrocaloric effect.

### 1.3.1.3 Relationship between Primary and Secondary Pyroelectricity

Several classical books have discussed the relative difference of the properties of the materials at different measuring conditions[31,38]. The relation between primary and secondary pyroelectricity using the method adopted by Nye[31] has been determined.

A small change in the electric displacement of a dielectric material may be given as,

$$dD_m(E,T,x) = \left(\frac{\partial D_m}{\partial E_n}\right)_{x,T} dE_n + \left(\frac{\partial D_m}{\partial T}\right)_{x,E} dT + \left(\frac{\partial D_m}{\partial x_\mu}\right)_{T,E} dx_\mu$$

The strain may be expressed as a function of $E_m, T, X_\mu$ as follows,

$$dx_\mu(E,T,X) = \left(\frac{\partial x_\mu}{\partial E_m}\right)_{T,X} dE_m + \left(\frac{\partial x_\mu}{\partial T}\right)_{E,X} dT + \left(\frac{\partial x_\mu}{\partial X_\nu}\right)_{T,E} dX_\nu$$

Pyroelectric measurements are done at constant Electric Field, i.e., $dE = 0$, so

$$dD_m(E,T,x) = \left(\frac{\partial D_m}{\partial T}\right)_{E,x} dT + \left(\frac{\partial D_m}{\partial x_\mu}\right)_{T,E} dx_\mu$$

$$dx_\mu(E,T,X) = \left(\frac{\partial x_\mu}{\partial T}\right)_{E,X} dT + \left(\frac{\partial x_\mu}{\partial X_\nu}\right)_{T,E} dX_\upsilon$$

$$dD_m(E,T,x) = \left(\frac{\partial D_m}{\partial T}\right)_{E,x} dT + \left(\frac{\partial D_m}{\partial x_\mu}\right)_{T,E} \left(\left(\frac{\partial x_\mu}{\partial T}\right)_{E,X} dT + \left(\frac{\partial x_\mu}{\partial X_\nu}\right)_{T,E} dX_\nu\right)$$

Differentiating with respect to T keeping X constant

$$\left(\frac{\partial D_m(E,T,x)}{\partial T}\right)_{E,X} = \left(\frac{\partial D_m}{\partial T}\right)_{E,x} + \left(\frac{\partial D_m}{\partial x_\mu}\right)_{T,E} \left(\frac{\partial x_\mu}{\partial T}\right)_{E,X}$$

$$p_m^X = p_m^x + \left(\frac{\partial D_m}{\partial X_\mu}\right)_{T,E} \left(\frac{\partial X_\mu}{\partial x_\nu}\right)_{T,E} \left(\frac{\partial x_\mu}{\partial T}\right)_{E,X}$$

$$p_m^X = p_m^x + d_{m\mu}^T c_{\mu\nu}^{T,E} \alpha_\mu^E \tag{1.8}$$

Where $d_{m\mu}^T$ is piezoelectric matrix (3rd rank tensor), $c_{\mu\nu}^{T,E}$ is elastic stiffness matrix (4th rank tensor) and $\alpha_\mu^E$ is thermal expansion coefficient matrix (2nd rank tensor). Relation (1.8) may be understood better using the Heckmann diagram[31,36] shown in Figure 1.2. Two terms on the right side of Eq.

(1.8) represent two paths in Heckmann diagram for change in electric displacement with temperature; the direct path shows the displacement change with temperature when volume of the material is fixed, i.e. constant strain, whereas in the second path, the material is free to deform, i.e., constant stress. The temperature will cause a thermal expansion in the material, that in turn will change the electric displacement by piezoelectric effect, so an additional pyroelectricity has produced in the material. This secondary pyroelectricity is sometimes referred to as false pyroelectricity of first kind[31,39]. Moreover, for a dielectric material that has no piezoelectric effect, the difference between primary and secondary pyroelectricity would be zero.

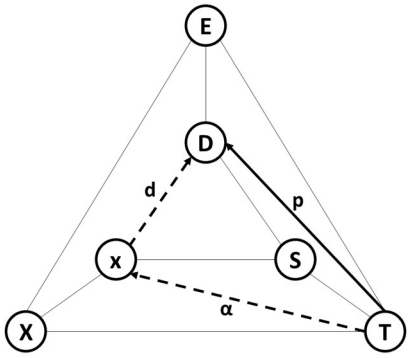


**Figure 1.2 Heckman diagram for primary and secondary pyroelectricity**

Several ferroelectric and non-ferroelectric materials showing primary and secondary pyroelectricity have been summarized in Table 1.3.

**Table 1.3 Primary and secondary pyroelectric effects of several pyroelectric materials at RT**[40–42]

| **Materials** | **Type** | **Symmetry** | **Experimental Value ($p_m^X$) μC m$^{-2}$/K)** | **[a]Calculated Secondary Effect ($p_m^X - p_m^x$) μC m$^{-2}$/K)** | **Primary Effect ($p_m^x$) (μC m$^{-2}$/K)** |
|---|---|---|---|---|---|
| $PbZr_{0.52}Ti_{0.48}O_3$ | Poled Ceramic | ∞ m | -50 | +60 | -110 |
| $PbZr_{0.95}Ti_{0.05}O_3$ | Poled Ceramic | ∞ m | -268 | +37.7 | -305.7 |
| BT | Poled Ceramic | ∞ m | -200 | +60 | -260 |
| $Ba_2NaNb_5O_{15}$ | [b]SC | 2mm | -100 | +41.7 | -141.7 |
| TGS | SC | 2 | -270 | -330 | +60 |
| SBN | SC | 4mm | -550 | -48 | -502 |
| PVDF | Organic | 2mm | -27 | -13 | -14 |

[a] Calculated using $d_{m\mu}^T, c_{\mu\nu}^{T,E}$ and $\alpha_\mu^E$ values
[b] Single Crystal

From Table 1.3, it may be observed that the primary and secondary effects are of the same order in most cases. It means that the measuring conditions play an important role in the characterization[40,42] and the value of the pyroelectric coefficient is strongly dependent on the mechanical condition. The negative value of pyroelectric effect shows that the electric displacement/polarization decreases with increasing temperature. In other words, from electrocaloric point of view, the entropy of the dielectric material decreases with applied electric field that is the diploes arrange themselves when dielectric is subjected to external electric field[40].

#### 1.3.1.4 Measurement of Electrocaloric Effect

As we have already discussed that the experimental conditions are important in characterizing the EC materials. EC characterization may be done at either constant strain or constant stress conditions like pyroelectric measurements

**Constant Strain Conditions:**

At constant strain $(dx = 0)$, the entropy of a dielectric material as a function of electric field and temperature can be expressed as[43],

$$dS(E,T) = \left(\frac{\partial S}{\partial E_m}\right)_{x,T} dE_m + \left(\frac{\partial S}{\partial T}\right)_{x,E} dT \tag{1.9}$$

If the electric field is applied on the dielectric material isothermally $(dT = 0)$, then the change in entropy of the materials is called *isothermal entropy change* and is expressed as,

$$\Delta S_{iso} = \int_{E_1}^{E_2} \left(\frac{\partial S}{\partial E_m}\right)_{x,T} dE_m \tag{1.10}$$

From the definition of primary pyroelectricity from the Eq. (1.4), Eq. (1.10) becomes,

$$\Delta S_{iso} = \int_{E_1}^{E_2} \left(\frac{\partial D_m}{\partial T}\right)_{x,E} dE_m \tag{1.11}$$

From the application point of view, it is the change in temperature that is important rather that change in the entropy with applied electric field. So, applying electric field on a material adiabatically, we get

$$\left(\frac{\partial S}{\partial E_m}\right)_{x,T} dE_m = -\left(\frac{\partial S}{\partial T}\right)_{x,E} dT$$

Differentiating above equation with E at constant strain,

$$\left(\frac{\partial S}{\partial E_m}\right)_{x,T} = -\left(\frac{\partial S}{\partial T}\right)_{x,E} \left(\frac{\partial T}{\partial E_m}\right)_{x,S}$$

Using Maxwell's relations[44] of the definition of the pyroelectricity, we get

$$\left(\frac{\partial D_m}{\partial T}\right)_{x,E} = -\left(\frac{\partial S}{\partial T}\right)_{x,E}\left(\frac{\partial T}{\partial E_m}\right)_{x,S}$$

$$\left(\frac{\partial T}{\partial E_m}\right)_{x,S} = -\left(\frac{\partial D_m}{\partial T}\right)_{x,E}\left(\frac{\partial T}{\partial S}\right)_{x,E}$$

Heat capacity at constant electric field and strain is defined as,

$$\left(\frac{\partial S}{\partial T}\right)_{x,E} = \frac{C^{x,E}}{T}$$

Putting this relation in above equation, we get

$$\left(\frac{\partial T}{\partial E_m}\right)_{x,S} = -\frac{T}{C^{x,E}}\left(\frac{\partial D_m}{\partial T}\right)_{x,E}$$

The adiabatic temperature change of a dielectric materials at constant strain conditions can be given as,

$$\Delta T_{ad} = -\frac{T}{C^{x,E}}\int_{E_1}^{E_2}\left(\frac{\partial D_m}{\partial T}\right)_{x,E} dE_m \tag{1.12}$$

**Constant Stress Conditions:**

Similarly, from the definition of the total entropy as a function of electric field and temperature at constant stress may be gives as,

$$dS(E,T) = \left(\frac{\partial S}{\partial E_m}\right)_{X,T} dE_m + \left(\frac{\partial S}{\partial T}\right)_{X,E} dT$$

From the definition of secondary pyroelectricity from the Eq. (1.4), the following relations may be determined,

$$\Delta S_{iso} = \int_{E_1}^{E_2}\left(\frac{\partial D_m}{\partial T}\right)_{X,E} dE_m \tag{1.13}$$

Heat capacity at constant electric field and stress is defined as,

$$\left(\frac{\partial S}{\partial T}\right)_{x,E} = \frac{C^{X,E}}{T}$$

$$\Delta T_{ad} = -\frac{T}{C^{X,E}}\int_{E_1}^{E_2}\left(\frac{\partial D_m}{\partial T}\right)_{X,E} dE_m \tag{1.14}$$

Eqs. (1.11) – (1.14) are the foundations of the characterization of the ECMs by indirect method (section 1.3.3.1). From these equation, it can be obviously seen that to obtain a large isothermal entropy change ($\Delta S_{ist}$) and a large adiabatic temperature change ($\Delta T_{ad}$) in a dielectric material, a

high pyroelectric coefficient (i.e., EC coefficient) is required, i.e. a strong temperature dependence of the polarization of a dielectric material under a constant electric field[9,10,29]. Eqs. (1.11) & (1.12) give the isothermal entropy change and electrocaloric temperature achage at constant strain conditions, whereas Eqs. (1.13) & (1.14) give these changes at constant stress. Eqs. (1.12) and (1.14) show that a high temperature change (ECE) may also be achieved if the heat capacity of the dielectric material is small. For cooling applications, however, as we will see later, that high values of both isothermal entropy change and adiabatic temperature change are required[45]. The relation between heat capacities at constant strain (mechanically clamped) and stress (mechanically free) conditions[42] is given as,

$$C^{x,E} - C^{X,E} = T\alpha_{\mu}^{E} c_{\mu\nu}^{T,E} \alpha_{\nu}^{E} \tag{1.15}$$

Where $\alpha_{\mu}^{E}$ / $\alpha_{\nu}^{E}$ is thermal expansion coefficient matrix (2nd rank tensor), and $c_{\mu\nu}^{T,E}$ is elastic stiffness matrix (4th rank tensor). The pyroelectric coefficient $p_m$ is a material property of 1st rank tensor. For a ferroelectric material, its Gibbs free energy can be further studied using Landau, Ginzburg and Devonshire (LGD) theory.

### 1.3.2 Thermodynamics of Ferroelectrics – Landau, Ginzburg and Devonshire Theory

Although the general thermodynamics is enough to define and describe the pyroelectric effect and ECE, it does not give further information or details of the pyroelectric effect. To further study the pyroelectric effect, a phenomenological theory known as LGD phenomenological theory[46] may be used. LGD got the name due to significant works by Landau[47] who originally described the second order phase transitions of the order parameter (i.e. polarization) in ferroelectrics, Ginzburg and Landau[48,49] who added the order parameter gradient terms in the free energy relation, and Devonshire[50,51] who successfully described the temperature dependence of dielectric properties in barium titanate (BT) and extended the theory to first order phase transition.

This theory can also be used to explain EC entropy change in ferroelectric and antiferroelectric (NOT relaxor ferroelectrics) materials induced by the order-disorder transition near the phase-transition temperature[10,41,52]. In this section, G vs. D, $P_s$ vs. T curves are discussed that can define the permittivity, polarization and pyroelectric coefficient, below and above the ferroelectric-to-paraelectric phase transition temperature (i.e. $T_C$ ) for both 1st and 2nd order phase transitions and then ECE may be determined from these curves indirectly.

Under constant stress conditions, the elastic Gibbs free energy ($G_1$), which is a function of T and D, can be used (see Table 1.2). For most ferroelectrics, the difference between D and P is very small so that P and D are treated as the same and interchangeable in most texts. Use of both D and P has been reported in several texts. Also, for simplicity, $D_m/P_m$ is considered only in one crystallographic direction (spontaneous polarization occurs in that direction only) and the electric field is restricted only in the same direction, so electric displacement (polarization) tensor may be reduced to a scalar property ($D_m/P_m = D/P$)[44]. Here P has been used as the original theory has used P[34]. LGD theory assumes that free energy may be written in a simple polynomial form using the Taylor series as,

$$G_1 = G_{10} + \frac{1}{2}\alpha P^2 + \frac{1}{4}\xi P^4 + \frac{1}{6}\zeta P^6 \tag{1.16}$$

Where $\alpha = (T - T_0)/\beta$, where the $T_0$ is Curie-Weiss temperature and is related to the phase transition temperature $T_C$ (i.e. Curie Temperature) between the ferroelectric-to-paraelectric phase[32–34]. β (>0), ξ and ζ are phenomenological coefficients and are assumed as temperature invariant, and $G_1|_{P=0} = G_{10}$. The details of the theory may be found in the classical books on ferrolectricity[33,37,44,53]. $\zeta$ is always taken as positive for the divergence issues. $\xi$ can be either negative or positive. If $\xi$ is positive, the phase transition between the ferroelectric and paraelectric phase is second order and $T_C = T_0$. If $\xi$ is negative, the phase transition between the ferroelectric (FE) and paraelectric (PE) phase is first order and $T_C > T_0$.

#### 1.3.2.1 Second Order Phase Transition ($\xi > 0$)

Second order phase transition is defined as a transition where entropy and polarization change continuously across the phase transition point (i.e., $T_C$). Important relations for both below and above the phase transition temperature are summarized below[33,34].

**For Paraelectric Phase *($T > T_C$)***

Above $T_C$, the paraelectric phase is the stable phase and the material loses its spontaneous polarization (i.e., $P_S = 0$), it is obtained:

$$\kappa^{T,X} = \left(\frac{\partial E}{\partial P}\right)_{X,T} = \frac{1}{\varepsilon^{X,T}} = \frac{(T - T_0)}{\beta} = \frac{(T - T_C)}{\beta} \tag{1.17}$$

This is Curie-Weiss law. Some generic curves for an arbitrary ferroelectric material are shown in Figure 1.3.

**For Ferroelectric Phase *($T < T_C$)***

In thermodynamic equilibrium, $\left(\frac{\partial G_1}{\partial D}\right)_T = E$, from Eq. (1.16)

$$E = \alpha P + \xi P^3 + \zeta P^5 \tag{1.18}$$

Eq. (1.18) gives the relationship between polarization and electric field in the ferroelectric phase and is called equation of state.

For $T < T_C$, α is negative and ferroelectric phase is stable. From (1.18), it may be found as ($P_s = P$) in the absence of electric field

$$P_s^2 = \frac{-\xi + \sqrt{\xi^2 - 4\zeta\alpha}}{2\zeta} \tag{1.19}$$

$P_s^2 > 0$ holds only if $\alpha < 0$ as $\zeta > 0$ always.

The reciprocal permittivity (dielectric constant) of the ferroelectric material below the phase transition,

$$\kappa^{T,X} = \left(\frac{\partial E}{\partial P}\right)_{X,T} = \frac{1}{\varepsilon^{X,T}} = 2\frac{(T_0 - T)}{\beta} = 2\frac{(T_C - T)}{\beta} \tag{1.20}$$

Spontaneous polarization in the ferroelectric phase gives the dielectric contribution to the entropy near the phase transition. So from Eq. (1.16) as $\xi$, $\zeta$ are independent of temperature, dielectric contribution to entropy at the zero field[44] may be given by Eq. (1.21), where $P = P_s$

$$S = \left(\frac{\partial G_1}{\partial T}\right)_P = P^2\left(\frac{\partial \alpha}{\partial T}\right)_P = -\frac{1}{2\beta}P_s^2 \tag{1.21}$$

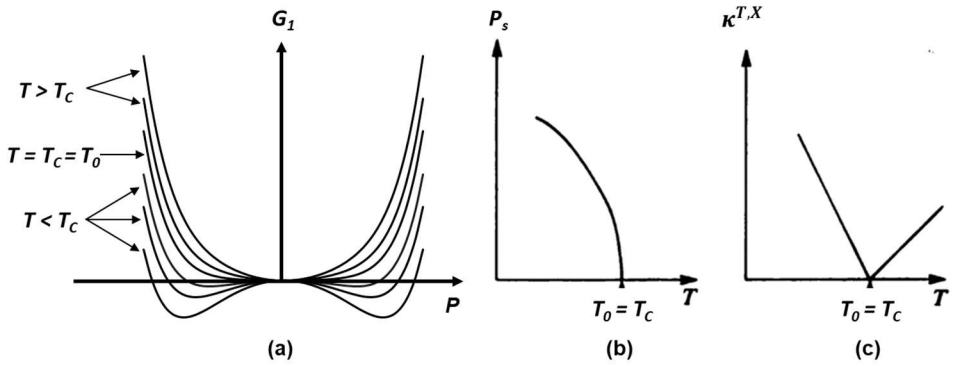


**Figure 1.3 Typical curves for second order phase transition[32], (a). Free energy vs P, (b). Temperature dependence of spntaneous polarization, (c). Temperature dependence of reciprocal permittivity**

### 1.3.2.2 First Order Phase Transition ($\xi < 0$)

In this first order phase transition, the entropy and polarization change discontinuously cross the phase transiton[37]. In the following, some results are being summarized. The details may be found in the classical books on ferroelectricity[33,44,53].

**For Paraelectric Phase ($T > T_C$)**

Above phase transition temperature, the permittivity may be written simply using Devonshire approximation, the reciprocal permittivity above $T_C$ may be determined using Eq. (1.24) as,

$$\kappa^{X,T} = \frac{1}{\varepsilon^{X,T}} = \frac{(T - T_0)}{\beta} \tag{1.22}$$

**For Ferroelectric Phase ($T < T_C$)**

Now Eq. (1.16) becomes as follows.

$$G_1 = G_{10} + \frac{1}{2}\alpha P^2 + \frac{1}{4}\xi P^4 + \frac{1}{6}\zeta P^6 \tag{1.23}$$

Where again by the basic Devonshire assumption that $\alpha = \frac{(T-T_0)}{\beta}$ near the phase transition. The dielectric equation of state may be written as,

$$E = \alpha P + \xi P^3 + \zeta P^5 \tag{1.24}$$

In the FE phase, the polarization without electric field becomes may be determined from Eq. (1.24) and it is called spontaneous polarization.

$$P_s^2 = \frac{-\xi + \sqrt{\xi^2 - 4\zeta\alpha}}{2\zeta} \tag{1.25}$$

In this case, as $\alpha < 0$ and $\zeta > 0$ always, so only the +ve part of the radical holds.

$$T_C = T_0 + \frac{\beta\xi^2}{2\zeta} \tag{1.26}$$

In the above equations, $\beta > 0, \xi^2 > 0, \zeta > 0$, so $T_C > T_0$ as shown in the Figure 1.4. Reciprocal permittivity below $T_C$ is given as,

$$\kappa^{X,T} = \frac{1}{\varepsilon^{X,T}} = 4\frac{(T_x - T)}{\beta} \tag{1.27}$$

The relation (1.27) shows that permittivity in the case of first order transition is discontinuous but finite as shown in Figure 1.4c. The discontinuous change in polarization causes a discontinuous change in entropy. From Eq. (1.23) we can find $S = \left(\frac{\partial G_1}{\partial T}\right)_P = \frac{1}{2}\beta P_0^2$ at $T_0$. Since the dielectric entropy becomes zero (or no contribution in entropy due to dielectric behavior) in the nonpolar phase, so the entropy discontinuity at $T_0$ may be given as (1.28)[44]. In other words, if we go from the FE-to-PE phase, this is the entropy that decreases and that causes temperature change in the material.

$$\Delta S = \frac{1}{2}\beta P_0^2 \tag{1.28}$$

Some typical graphs in the first order transition are shown in Figure 1.4

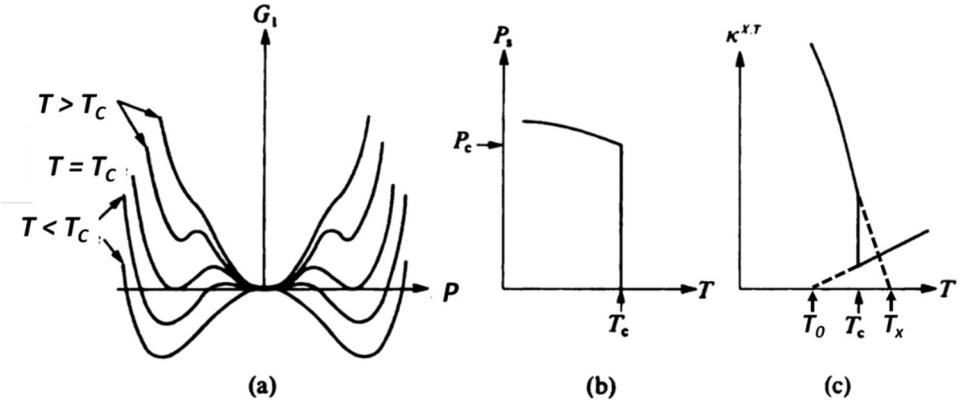


**Figure 1.4 Typical curves for first order phase transition[32], (a). Free energy vs P, (b). Temperature dependence of spontaneous polarization, (c). Temperaure dependence fo reciprocal permittivity**

As discussed above, paraelectric phase does not exhibit the pyroelectric effect. The pyroelectric coefficient of ferroelectric phase for the ferroelectric materials can be calculated using Eq. (1.18) and (1.24) by the definition: $p_m^X = \left(\frac{\partial D_m}{\partial T}\right)_{E=0}$ . This is what usually reported for the pyroelectric coefficient of ferroelectric materials.

$$p_m^X = \left(\frac{\partial D_m}{\partial T}\right)_{E=0} = -\frac{1}{\zeta}\left[\frac{\xi}{\sqrt{\xi^2 - 4\zeta\alpha}} + 1\right] \tag{1.29}$$

The variations of the temperature dependence of polarization and Curie point with electric field for second order and first order phase transition are in Figure 1.5 (a) and (b), respectively. In the second order transition, for electric fields E > 0, there is no well-defined curie temperature and the curve becomes smooth as shown in Figure 1.5 (a). For first order phase transition, the curie temperature increases with the electric field and at some point, the vertical line of the first order transition (FE-PE phase transition) disappears and above that point both phases may be present. This temperature is called critical temperature $T_{CP}$ and the corresponding electric field is called critical electric field $E_{CP}$ as shown in Figure 1.5 (b).

For understanding the physics behind this phenomenon and for mathematical relations of temperature dependence of Curie temperature and polarization, the reader is referred to the books on advanced ferroelectricity.

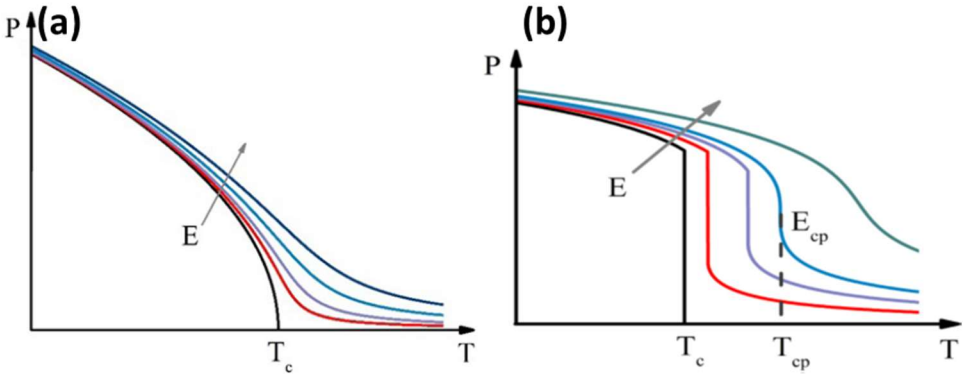


**Figure 1.5 Temperature and electric field dependence of polarization of normal ferroelectrics, (a). Second order phase transition, (b). First order phase transition**[29,54]

### 1.3.3 Electrocaloric Characterization

Reliable EC characterization is required to exploit this physical phenomenon for solid-state cooling applications and for fundamental understanding of ECE in different materials. Over the years, research community has developed two main approaches, i.e., *indirect, and direct method*s, to determine the EC coefficient of a material. Indirect method is based on the thermodynamic equations derived based on Maxwell relations (section 1.3.1.4), whereas in the direct method, the temperature change in the EC material upon the application of electric field is measured directly using thermal devices. That is, the heat generated in the dielectric material upon the application of

external electric field is measured. A brief introduction of these approaches is given here for a quick reference. The reader is referred to the literature for details[52,55].

#### 1.3.3.1 Indirect EC Measurements by Maxwell Approach

Eqs. (1.12) and (1.14), shown again here, derived by Maxwell relations, are used to determine the ECE indirectly depending on the measuring conditions like constant strain and constant stress respectively.

$$\Delta T_{ad} = -\frac{T}{C^{x,E}} \int_{E_1}^{E_2} \left(\frac{\partial D_m}{\partial T}\right)_{x,E} dE_m \tag{1.12}$$

$$\Delta T_{ad} = -\frac{T}{C^{X,E}} \int_{E_1}^{E_2} \left(\frac{\partial D_m}{\partial T}\right)_{X,E} dE_m \tag{1.14}$$

By experimentally determined $\frac{\partial D_m}{\partial T}$, one can use Eq. (1.12) or (1.14) to calculate $\Delta T_{ad}$. This is called as the indirect method to determine the ECE. That is, in indirect approach, ECE of a dielectric material is determined/calculated from the temperature dependence of the polarization under a constant electric field, i.e. $P(T, E)$. For this purpose, electric field dependence of polarization is measured under isothermal conditions (PE loop) and then the temperature dependence of the polarization is measured at constant electric field. The mechanical conditions *clamped or free*, on the sample are also important so that respective heat capacity must be used for reliable calculations. Typical steps used to measure the ECE indirectly are shown in the Figure 1.6 (a) – (d)[6,55].

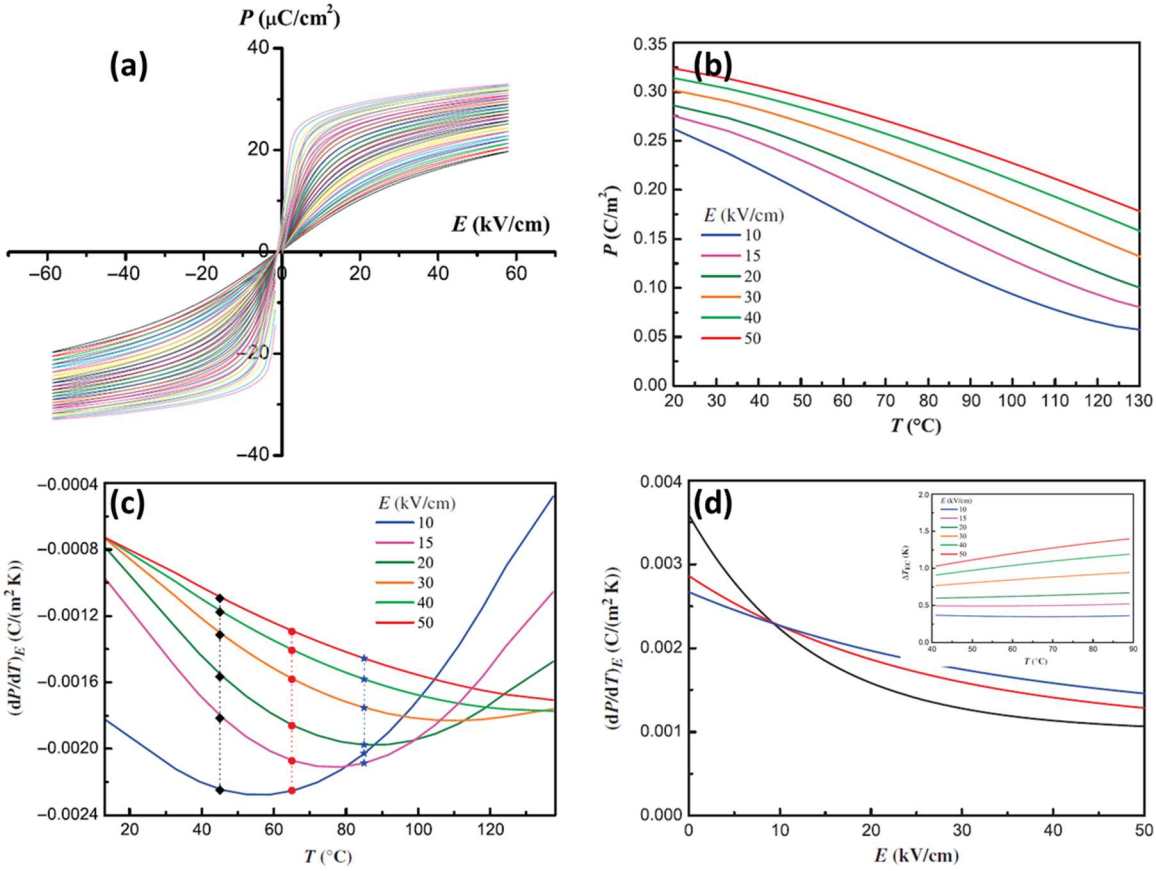


**Figure 1.6 Typical steps for indirect EC measurements, (a). Typical PE curves, (b). Temperature dependence of polarization at constant electric field, (c). $(\partial P/\partial T)_E$ as a function of temperature at different constant electric fields, (d). $(\partial P/\partial T)_E$ functions obtained by appropriate curve fitting**[10]

1 Plotting the hysteresis loops (aka P-E curves) of the dielectric material (polarization vs electric field) at different temperatures as shown in Figure 1.6 (a).

2 Plotting the polarization as a function of temperature at constant electric field as shown in Figure 1.6 (b), and the P (T, E) is determined. There are two polarization values for a single field due to hysteresis effects, the average value of P is normally taken for further calculations.

3 The temperature variations of $(\partial P/\partial T)_E$ are then plotted for different constant fields as shown in Figure 1.6 (c).

4 Smooth $(\partial P/\partial T)_E$ functions at a given temperature are then obtained by appropriate curve fitting as shown in Figure 1.6 (d).

5 These functions are then used in Eqs. (1.12) or (1.14) for each particular temperature in order to evaluate $\Delta T_{EC}$ (T) as shown in Figure 1.6 (d) (inset).

Figure 1.6 shows the steps in the indirect method to determine ECE where no transition in involved. The indirect method involves highly complicated functions when the phase transitions between ferroelectric to paraelectric phase are involved in the temperature range where the characterization is being carried out[52]. Without electric field, the phase transition temperature is a well-defined point in both types of transitions (first and second order) as shown in Figure 1.5 but in the presence of electric field, the well-defined phase transition point vanishes as may be observed in Figure 1.5 (b), so this method should be used with extreme caution especially taking derivatives $(\partial P/\partial T)_E$ in the vicinity of phase transitions and for nonergodic systems[10,56]. Figure 1.7 shows the typical steps in EC characterization where phase transition is involved.

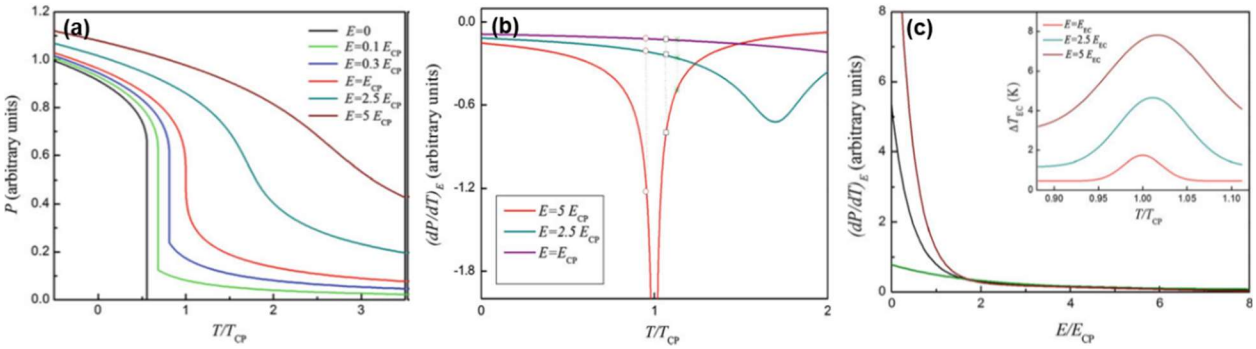


**Figure 1.7 Typical steps for indirect characterization of ECMs where phase transition is involved (first order in this case)**[52]

These complications have been discussed in phenomenological theory by Landau and Devonshire as discussed in section 1.3.2.

### 1.3.3.2 Direct Measurements

Indirect measurement techniques have long been used to find the EC coefficients in materials. The uncertainties, however, in some cases were observed when indirectly measured results were validated by the direct measurements. These uncertainties may occur if the indirect approach is not properly used and due to discontinuity in the case of first order transition at critical point. Secondly the heat capacity is strongly T and E dependent, but in the relations (1.11) – (1.14), it is normally taken out of the integral as constant[55]. This gives a major drawback to the indirect methods as heat capacity is highly dependent on the temperature and even electric field. To address these issues, the establishment of a direct measurement method was realized inevitable so that the results may be reported with extended confidence and reliability.

Direct measurements may be subdivided into two categories namely thermometric and calorimetric based on the condition that electric field is either applied adiabatically or isothermally. Thermometric measurement is the measurements of the EC temperature change ($\Delta T_{EC}$) directly using thermocouples and thermistors upon the application/ removal of electric field adiabatically on the dielectric material[6,55], while calorimetric measurement is the measurement of the heat exchange between the dielectric material and surrounding when external electric field is applied isothermally. A brief introduction to the direct methods is being given here as a quick reference. For in-depth understanding, the reader is referred to the literature[10,23,52,55].

**Differential Scanning Calorimetry (DSC):**

Differential scanning calorimetry (DSC) is by far the most used calorimetric technique for precise EC measurements. Modifications are required to the commercially available calorimeters – that are designed to determine zero-field heat capacity – to apply the electric field to the sample. The working principle of the DSC is that a constant heat flow is applied to a *reference sample* (whose heat capacity is known) and to the *sample under test*. After the thermal equilibrium in achieved, the electric field is applied/ removed on the sample and the heat flow into and out of the sample under test is measured isothermally. Under applied electric field, the sample generates heat and exchanges it with the environment, which is detected as an exothermal peak, whereas upon removal of electric field, the endothermic peaks are measured. The heat flow $Q$ inside/ outside the sample as a function of time is shown in Figure 1.9. The height of the exothermic/ endothermic peaks corresponds to the EC temperature change, and the total heat flow is determined by time integrating these peaks. The entropy change is calculated using the relation $\Delta S = Q/T$ and EC temperature changes is often calculate using $\Delta T = T\Delta S/C(0)$, where $C(0)$ is zero-field heat capacity – an unrealistic assumption[55]. This method has advantages of relatively good sensitivity and optimally designed DSC can perform high sensitivity measurements of 0.2 μW and enthalpy change measurements of about 0.01J/g[52]. DSC works well with the bulk materials where relatively high heat flows are involved, it shows, however, some limitation in dealing with thick and films where extremely small heat flows are involved. Longer times are normally required to bring the sample and apparatus in thermal equilibrium, which makes this technique slower[6,10,23,55]. Heat dissipation through the leads, and the internal joule heating that cause difference in the endothermic/ exothermic peaks are associated issue with this technique[23,52].

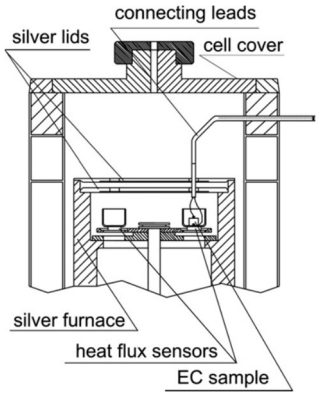


**Figure 1.8 Schematic of a modified DSC for direct EC measurements**[23]

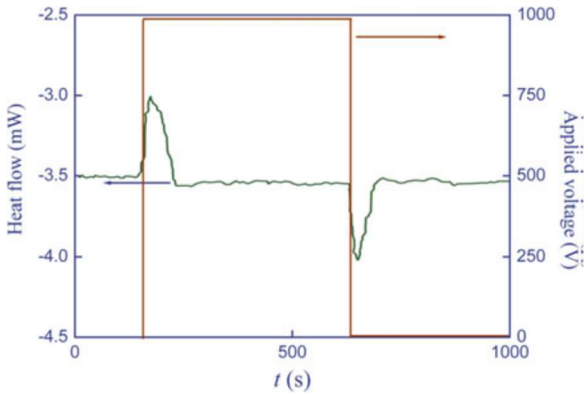


**Figure 1.9 EC Measurements using typical DSC technique**[52,57]

## High Resolution Calorimetry (HRC):

In this technique, high resolution measurement under enhanced thermal shielding are used to measure the temperature of the sample under adiabatic conditions[52]. Extra arrangements are made in the conventional calorimeters to apply high voltage electric signal to the sample, which adds complexities to the system. With proper arrangements, temperature changes as low as $10^{-4}$ K may be measured[23]. As no calorimeter can be a perfect insulator, so an important condition is that heat capacities of the thermocouples, holders, electrodes, and heaters etc. should be negligible as compared to specimen. For this purpose, the thermal mass of the specimen is kept large compared to thermal mass of the environment to minimize the measurement error[23]. The long electrical pulses are usually applied to allow the thermal relaxation of the sample temperature back to the bath temperature. as shown in Figure 1.11[52]. In case of thin films, the internal relaxation happens quickly, and the thin film releases/absorbs its heat to/from the substrate in the order of few milliseconds and this thermally equilibrium system, comes in equilibrium to the external bath in much longer time scale. The final EC temperature change is measured using relation (1.30)[10,52].

$$\Delta T_{EC} = \Delta T \frac{\sum_i C_p^i}{C_p^{EC}} \tag{1.30}$$

Where $C_p^i$ is the heat capacities of the sample without electrodes, wires, thermistors, and the electrodes and $C_p^{EC}$ is the heat capacity of sample with electrodes. The entropy change is determined by Eq. (1.31)

$$\Delta S = \frac{mc_p \Delta T_{EC}}{T} \tag{1.31}$$

A typical error in case of thin/thick films is 10% and in bulk materials is about 1%[10].

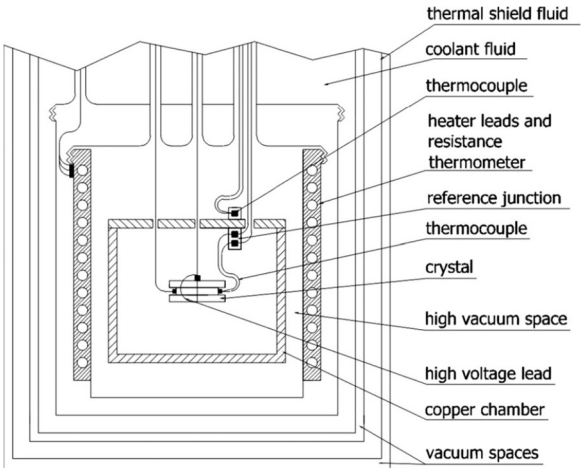


**Figure 1.10 Schematic of an adiabatic calorimeter**[23]

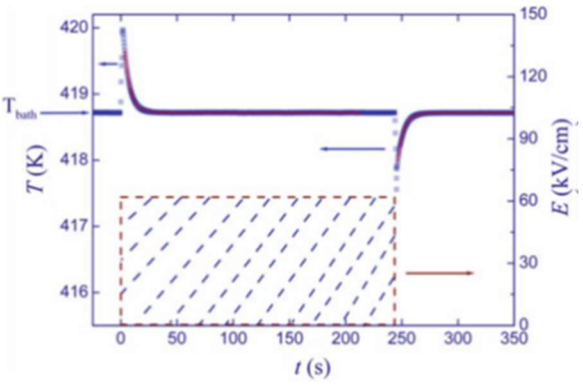


**Figure 1.11 Typical EC measurements using adiabatic calorimetry (AC)**[52]

**Fast Thermometry Approach/Infra-red Photometry:**

Conventional calorimetry techniques provide reliable results in bulk, thick and thin films. This technique is, however, slow and involves longer time periods for external thermal relaxation as discussed above. Calorimetry techniques have limitations in measuring very quick and online adiabatic temperature changes in thin films solely upon the application of electric field. Also, the spatial variations in the thin films has become a big concern as it provides information about the film quality[52]. To tackle this problem, high speed infra-red thermometry technique has been introduced by S Lu. *et. al*[58]. An IR sensor is used to measure the temperature of the thin film as shown in Figure 1.12. This technique was applied on the relaxor terpolymer, P(VDF-TrFE-CFE) and the results were compared to the conventional calorimetric technique as shown in Figure 1.13. These two results which have come from two completely different testing methodologies have a great agreement which shows its validation[6,58]. This technique has shown very impressive results to find the special resolution of thin films. This great feature can be exploited to maintain the quality of this films and to measure ECE across the film[10,52,59] as shown in Figure 1.14.

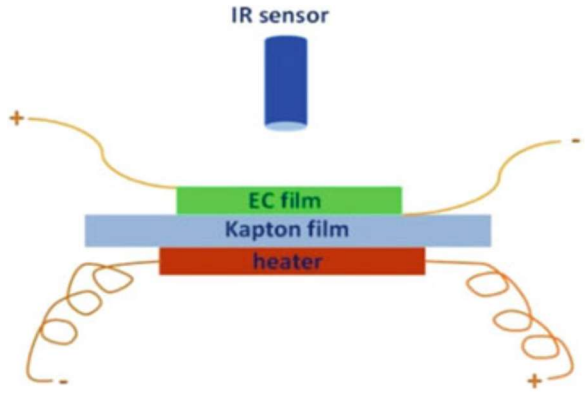


**Figure 1.12 Direct ECE measurements using IR thermometry**[58]

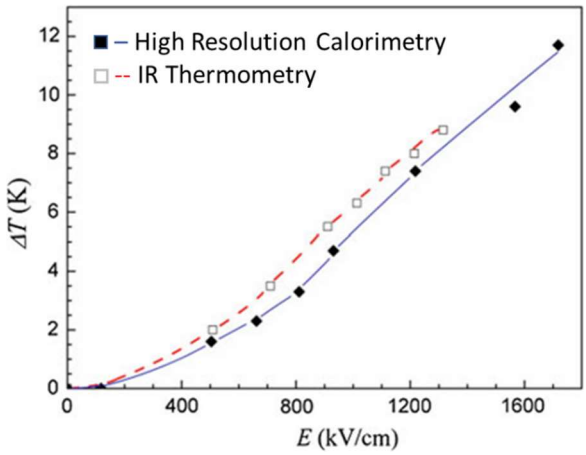


**Figure 1.13 Comparison of ECE obtained by HRC and IR thermometry**[58]

A drawback associated with this technique is that a high accuracy and high speed IR camera is required as the temperature changes vanish too quickly due to high thermal coupling of thin films with substrate[52]. A properly calibrated IR thermometry can deliver results with 10% accuracy[52]. IR thermometry is an excellent and quick technique to measure the surface temperature. It does not, however, give any information about the thermal gradients inside the material. In designing the ECE-based devices, the information about the internal temperature profile is necessary for finding the thermal relaxation times of the materials involved, for the application of thermal cycle and for the heat fluxes inside the devices so that the performance of the device may be calculated. Currently most of the devices are only conceptual or simulation based or prototypes. A relationship between the interface temperature and the body temperature is certainly needed, but not exist. An analytical solution may provide the answer for this.

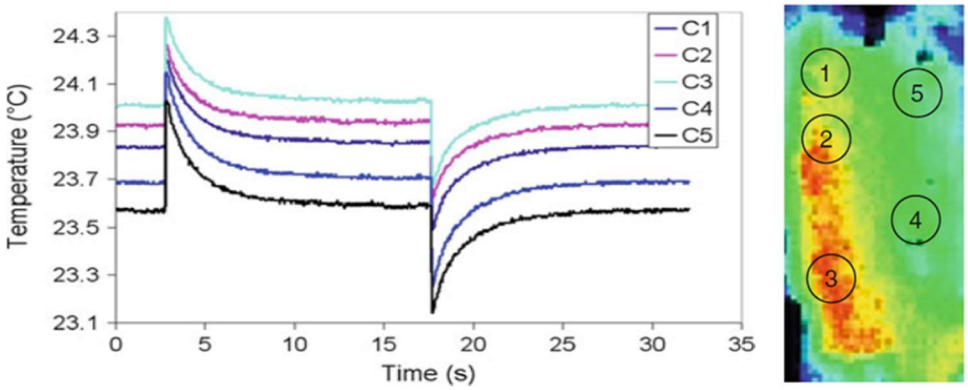


**Figure 1.14 EC temperature changes at different points (shown Left) on MLC surface**[59,60]

## Scanning Thermal Microscopy (SThM):

As it is already mentioned that in thin films, the thermal relaxation occurs so quickly that there is very short time to measure the temperature change. Several efforts have been carried out to enhance the time response of the thermometer to measured high dynamic temperature variation in thin films. In this context, the exploitation of the change in resistivity of very thin electrode attached to the thin film has been reported[59]. A thin-film metal thermometer is attached to the EC thin films whose resistance changes with temperature as shown in Figure 1.15. The EC temperature change can be monitored during the application and removal of electric field on thin films. As the mass of this metallic thin film is very low so sufficiently low response time can provide reliable estimate of the temperature change[52,61].

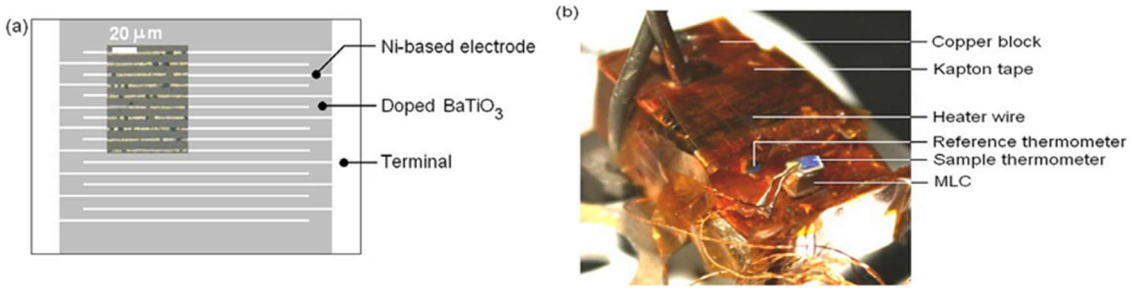


**Figure 1.15 (a). Thin resistive electrode as temperature sensing element, (b). Temperature sensing element on an MLC**

C. Molin *et. al*. compared all the direct methods in characterization of PMN-PT MLCs are found results that were very much similar[62].

In short, measurement of ECE in thin films was a major concern due to bulky nature of thermocouples and other thermometers so these bulky thermocouples were replaced by much

sophisticated and sensitive thermistors which had the capability to sense temperature variation in much higher resolution[52] so the use of the direct measurement techniques is on rise now.

### 1.3.3.3 Comparison of Indirect and Direct Methods

Although indirect method is still the mostly used method for EC characterization, but recently several comparative studies on the EC characterization for the reliability concerns of the results have been reported[62–65]. For some cases, a good agreement is observed in the EC coefficient measured by both direct and indirect methods for ferroelectric materials as shown in Figure 1.16, but clear and unignorable difference can be observed sometimes, as shown in Figure 1.17 specially at higher temperatures. Figure 1.17 shows the comparison of EC results measure by direct and indirect methods where exo and endo represent the exothermal and endothermal peaks upon the applications and removal of external electric field during the direct measurements.

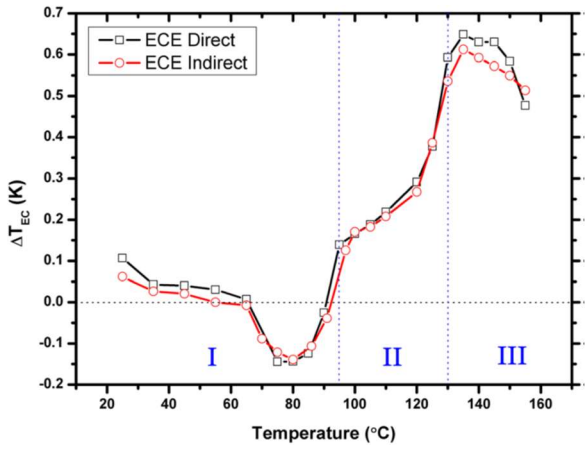


**Figure 1.16 Direct and indirect measurement in PMN-PT single crystal[63]**

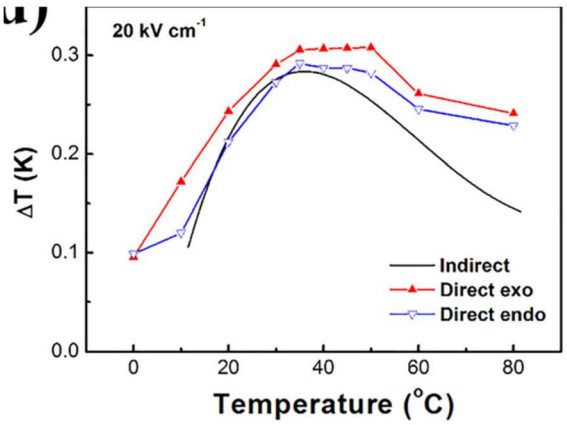


**Figure 1.17 Comparison of directly and indirectly measured ECE in NKN[65]**

In the relaxor ferroelectrics (RFEs) and antiferroelectrics (AFEs), however, significant differences have been observed in the measurements of direct and indirect methods[63] as shown in Figure 1.18 and Figure 1.19[56,66] . Moreover these disagreements in coefficients become pronounced specially when ultrahigh electric fields are involved[65]. For example, Figure 1.19 shows a comparison of direct and indirect measurements of a standalone thick film of 4-6 µm of PVDF relaxor polymer. It may be noticed that at the field of 70 MV/m, in the vicinity of 310K, the ECE of about 3.7K (blue triangles) by the direct measurement and about 0.9K (blue hollow circles) by the indirect measurements has been determined and the ECE is about 4 times greater in case of direct measurements. Figure 1.18 shows the results of EC characterization of PLZT bulk ceramics by

using both direct and indirect methods (Maxwell and LGD techniques). from Figure 1.18 (b), it may be clearly noted that at 300 K, the difference is much bigger! In an AFE PLZT, ECE measured at 3MV by direct method (purple triangle) is about 4 times greater that value deduced by the Maxwell relation (Red continuous line).

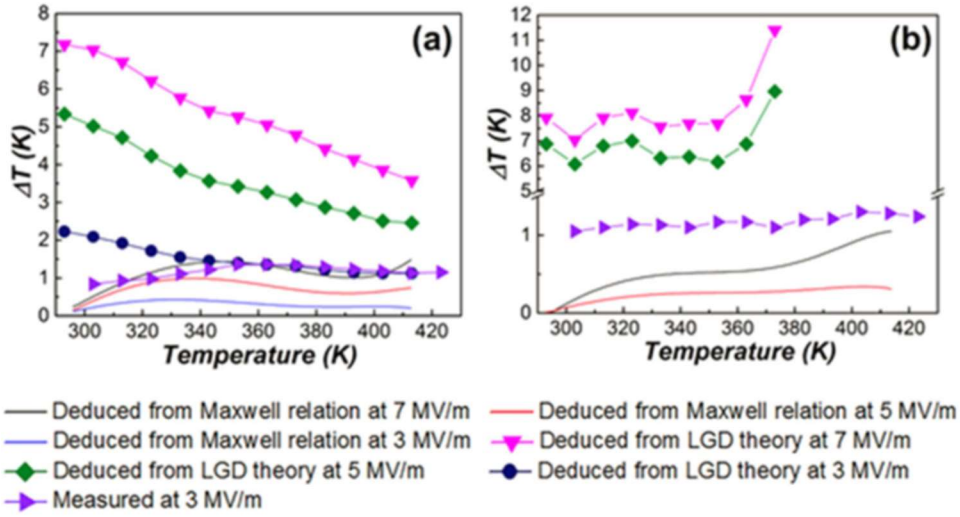


**Figure 1.18 Comparison of direct and indirect measurements of PLZT bulk ceramics[66], (a). PLZT RFE, (b). PLZT AFE**

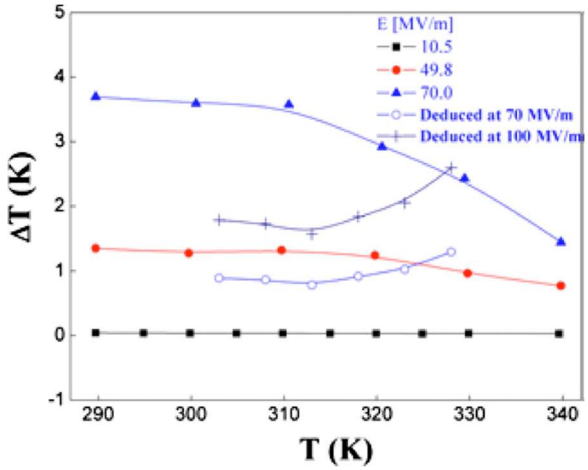


**Figure 1.19 Comparison of directly and indirectly measured EC coefficient in PVDF RFE polymer[56]**

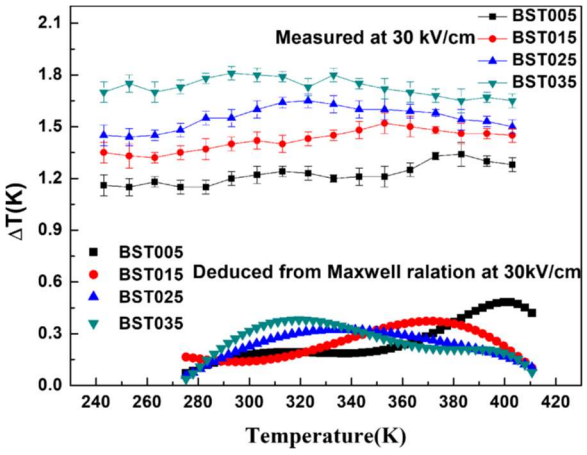


**Figure 1.20 Comparison of direct and indirect ECE measurements in BST bulk ceramics[67]**

Several studies have revealed the reasons behind this disagreement and indicated that thermodynamic theories are based on ideal conditions of single crystals and ergodic states[21,23,56,66] whereas the RFEs are nonergodic materials[68]. Some authors have reports that AFE and RFE materials are not in thermal equilibrium, but the Maxwell's equations are derived for thermal

equilibrium. It was found that relaxor ferroelectrics are not at equilibrium state, so the Maxwell equations cannot be used[62]. One of the other several reasons behind the discrepancy is that Maxwell relations are derived based on the linear relations, and the nonlinear and higher order coupling coefficients have been neglected in the calculations whereas in RFEs the nonlinear effects are also strong *(i.e., electrostriction)*, so these parts must be considered to find the entropy change specially when higher electric fields are involved. Moreover, in the characterization, perfect constant stress and constant strain conditions are not achievable with high accuracy especially in the case of thin films where the substrate act as thermal anchors and perfect adiabatic conditions are difficult to achieve.

Sometimes clear and unignorable difference in direct and indirect measurements are observed in normal FEs as well as shown in Figure 1.20 in case of BST bulk ceramics where a difference of 3 – 4 times has been reported[67]. It may be inferred from the above discussed results that there is some strong mechanism that is being ignored in derivation of equation for indirect method and that mechanism needs to be addressed so that an agreement between these two approaches may be achieved for reliable EC measurements.

### 1.3.4 Classification of Electrocaloric Materials (ECMs)

In last two decades, a great deal of research on ECE has been done, especially on the development of ECMs. Many ECMs with strong ECE have been reported. These ECMs may be categorized based on several parameters like organic and inorganics, polycrystalline and single crystals, and bulk and think/thin films, and on crystal structures. By the structure, all reported ECMs with a strong ECE can be classified into ferroelectric, antiferroelectric and relaxor ferroelectrics.

#### 1.3.4.1 Normal Ferroelectric (FE) Materials

FEs are the organic and inorganic polar materials that show a spontaneous polarization that can be by reversed by inverting external electric filed[69]. As mentioned in Section 1.3, all FEs exhibit a phase transition between their ferroelectric and paraelectric phase at a temperature called Curie temperature[43]. In their ferroelectric phase, an ECE is expected, but no ECE is expected for paraelectric phase. Near this phase transition, a high ECE may be achieved due to very strong temperature dependence of $P_S$ polarization. The phase transition temperature increases with electric field applied on the material as shown in Fig. 1.18.

Both organic and inorganic FEs in the form of thick and thin films, bulk ceramics and single crystals have been researched over the years. In inorganic family, bulk ceramic materials (thickness: t > 100 μm) due to their high thermal mass are considered promising candidate to be exploited in the development of ECE-based cooling devices. These systems include barium titanate (BT), lead zirconate titanate (PZT), barium strontium titanate (BST), Ammonium-based and glycine-based sulfates and selenates, etc. A limitation, however, associated with bulk materials is their failure at higher electric fields before reaching the saturation (i.e. dielectric strength limited)[23], due to the fact that the breakdown field of a dielectric material decreases with increasing thickness. Other associated issues with some bulk ceramics are conductivity and joule heating caused by electronic and/ or ionic leakage currents at higher electric fields. For example, Ammonium-based and glycine-based sulfates and selenates have shown higher ECE but have high ionic current as well[70]. Thin films (t < 1μm), on the other hand, offer a great potential to sustain at the extremely higher electric fields, but a major problem associated with them is low specific heat (low thermal mass) and can pump less heat during the thermal cycle resulting in less cooling power. Development and characterization of the thin films has some associated challenges like smooth film thickness, film orientation, thermal clams and misfit strains, etc.[23].

To overcome the issued associated with bulk and thin film, thick ceramic films (10μm < t < 100μm) in the form of multilayer capacitors (MLCs) structures have been reported[71–73]. MLCs can have large thermal mass as compared to thin films and at the same time can sustain higher electric fields to generate higher ECE [74]. EC change of 1.8 K in BT based MLCs at the electric field of 17.6Mv/m has been reported. Pb $(Sc_{0.5}Ta_{0.5})O_3$-based MLCs were investigated to get much higher ECE of 2.3 K[23,75]. This makes them a strong candidate to be used in the new generation electrocaloric refrigeration and cooling devices.

To further enhance the range, organic ferroelectric like polyvinylidene-fluoride (PVDF) copolymers and terpolymers are the most researched organic materials for EC applications because of their high dielectric strength, high flexibility, high electric resistance, and low joule heating. The application of electric field on P(VDF-TrFE) films at the temperatures around the ferroelectric transition induces a large entropy change. An entropy change of 56 J/kgK[21] has been observed in polymers which is much higher than 10 J/kg K for oxide (PZT) films[20]. The high entropy change in polymers films is indebted to its ability to withstand extremely high electric field of 209 MV/m which is several times higher than the breakdown field for oxide films. The EC Coefficient[76] (i.e.,

ΔT/ΔE) – a parameter to judge the suitability of a material for ECE-based cooling devices – of the polymer films is, however, small as compared to oxides, making them unsuitable for EC cooling applications. Figure 1.21(a) and Figure 1.21(b) show the temperature change in the reported materials and the ΔT/ΔE values of several EC systems, respectively. It is evident from these figures that despite to the fact that thin films show high ECE due to their ability to sustain high electric field without breakdown failure, still thin films are not considered good candidate for development of the EC-based cooling device[23] due their low thermal mass. The best materials for the development of the EC coolers are still bulk ceramics in spite of their inbuilt limitations of dielectric breakdown at relatively lower electric field[23]. Moreover for a piratical high performance EC cooling device, high entropy change is also required along with high ECE[45].

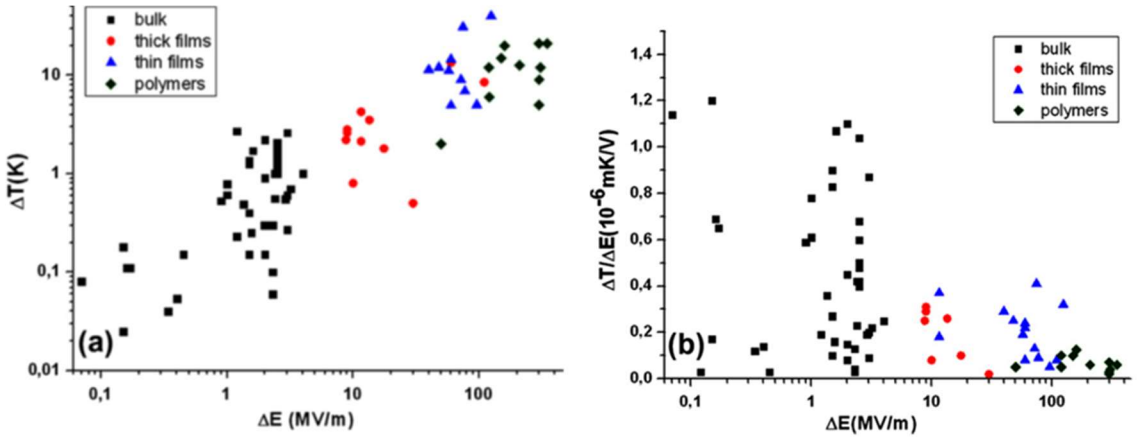


**Figure 1.21 (a). EC coefficient for several organic and inorganic ECMs, (b). ΔT/ΔE vs electric field for several organic and inorganic ECMs**

### 1.3.4.2 Antiferroelectric (AFE) Materials

Antiferroelectric behavior is normally observed in inorganic materials whereas and antiferroelectric organic materials are very rare. The dielectric properties of antiferroelectric materials can be significantly enhanced at a high field due to the electric field induced transition from an AFE-to-FE phase[77]. Antiferroelectric (AFE) materials exhibit low coercive fields and dielectric losses (at low field), as well as a high saturated polarization. The high saturation polarization originates from the field-induced AFE-FE phase transition, that is, realignment of antiparallel dipoles under an external electric field[78]. The characteristic P–E double hysteresis loop, a typical for AFEs, is shown in Figure 1.22. AFEs undergo a phase transition under zero electric field from a high-temperature unpolarized state to an anti-parallel state (AFE phase) where

two adjacent dipoles are in opposite direction that cancel each other resulting no macroscopic polarization (i.e. zero spontaneous polarization). Thus, the material goes from ordered to disordered phase (i.e. Or from ordered state to another ordered state with different order degrees) when electric field is applied adiabatically. That is, the dipolar entropy increases leading to a negative ECE ($\Delta T_{EC} < 0$)[10]. Physically it can be described as that AFE in stabilized with a nominal entropy and when electric field is applied, the local dipoles will rotate in the direction of electric filed until local domains switch from AFE to FE and the system becomes disordered[55]. Unlike normal FEs, the electric field induced macroscopic polarization may decreases with decreasing T resulting in negative ECE[10]. There are conflicting results in the literature where positive and negative ECE of same AFEs materials have been reported[79–82] (see Table 1.4 for details). The reasons behind it may be the unjustified nature of antiferroelectricity and wrong curve fitting of $(\partial P/\partial T)_E$ without considering the temperature and field dependence of heat capacity[55].

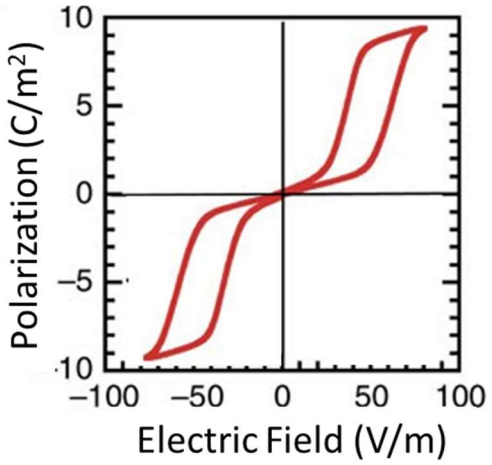


**Figure 1.22 A typical P-E loop for AFEs**

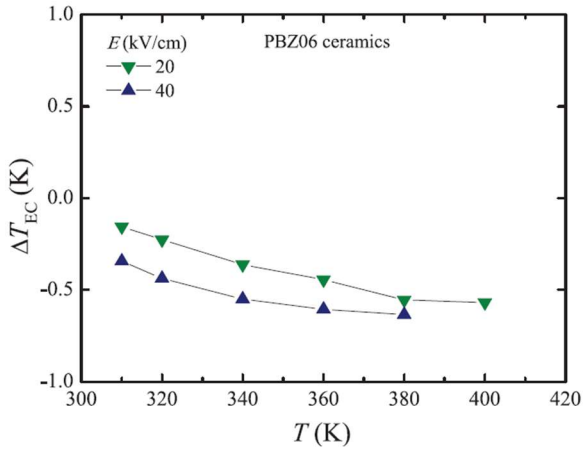


**Figure 1.23 Negative ECE in Ba-doped Lead Zirconate (PBZ) - An AFE material[82]**

### 1.3.4.3 Relaxor Ferroelectric (RFE) Materials

Relaxor ferroelectric (RFE) materials or relaxor ferroelectrics (RFEs) or simply relaxors are a special category of both organic[68] and inorganic ferroelectric materials[58] that have high dielectric constant and exhibit a broad peak in the dielectric constant vs temperature curve[83]. They normally show neither a spontaneous polarization nor a phase transition to ferroelectric phase but undergo a phase transition to ferroelectric phase under an electric field. Therefore, their phase transition is called as diffused phase transition (DPT) without a well-defined Curie temperature[10,43]. Although RFEs don't belong to the 10 non-symmetric polar point groups, yet they can exhibit, piezoelectric

and electrocaloric effect due to their unique mechanism of dielectric relaxation[84,85]. The key to the relaxation behavior is the formation of polar nanoregions (PNRs) above the temperature of permittivity maximum in the relaxors. These PNRs bring extra contribution to entropy change that leads to the enhanced ECE[63,64]. At lower temperature, there is a strong frequency dispersion of dielectric due to freezing of the fluctuation of these PNRs[69]. High ECE is observed in REFs over a broader temperature range whereas, while a high ECE is only observed in normal FEs over a narrow temperature range (i.e., a few degrees) as shown in Figure 1.25 and Figure 1.27 respectively. The temperature dependence of the permittivity for a RFE and normal FE are shown in Figure 1.24 and Figure 1.25 showing clearly a broad peak and sharp peak respectively. This special character of RFEs make them a strong candidate for ECE-based devices, so several RFEs like PMN, PMN-PT, PLZT, PSN, and PST have been extensively studies[6,85,86]. But it has to be mentioned that there is no pyroelectric effect observed in RFEs.

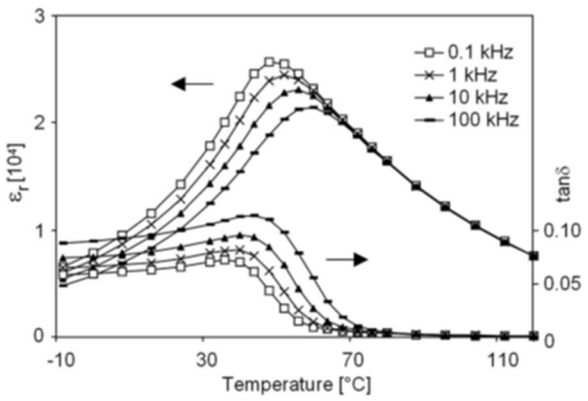


**Figure 1.24 Broad peak in permittivity vs temperature in typical RFEs (PMN-0.13PT)**[87]

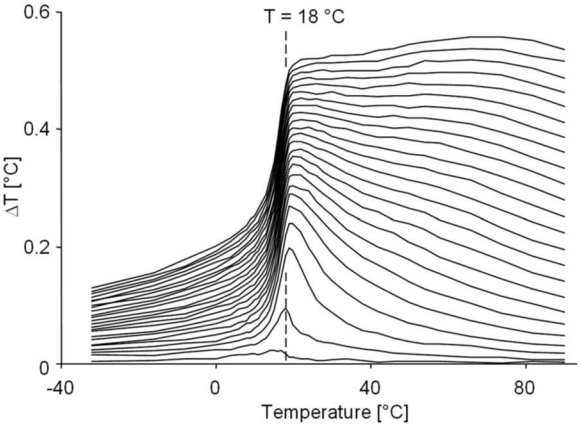


**Figure 1.25 ΔT as a function of T for increasing electric fields for PMN-0.13PT – A RFE with a permittivity peak temperature of 48°C**[87]

Although high EC performance has been observed in the REFs, the physics behind the phenomena is still an open question since the structure of REFs does not belong to any of ten polar point groups required for pyroelectric crystals.

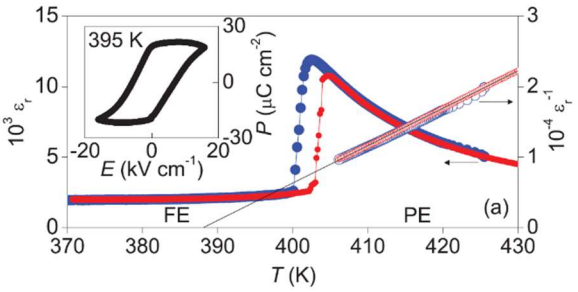


**Figure 1.26 Sharp peak in a typical normal FE (BT single crystal)**[88]

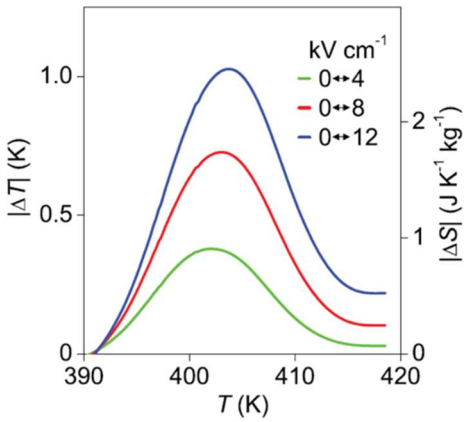


**Figure 1.27 ΔT vs T for increasing electric fields for BT single crystal – a normal FE with FE-to-PE phase transition temperature of 402K**[88]

### 1.3.4.4 Highly Researched EC Materials and Current Status

Since the breakthrough discovery of giant ECE in organic and inorganic thin films, considerable research activities have been carried out to develop materials with giant ECE that resulted in an avalanche of research publications in which several monolithic and single crystal ceramics, thick and thin film ceramics, polymer thin films and relaxor ferroelectrics were investigated to achieve high electrocaloric effect ($\Delta T_{EC}$) [12,23,24,26,27,58,61,68,89–91]. The detailed information about newly developed high-performance ECMs has been summarized in some recent review articles[23,55,76,92]. Some of the highly researched ECMs are summarized in Table 1.4 for a ready reference.

**Table 1.4 Recently reported intensively studied ECMs**

| ECM | Type | T[a] (°C) | ΔT (°C) | ΔE[b] (MV/m) | \|ΔT/ΔE\| ($10^{-6}$ °C/Vm$^{-1}$) | Characterization Method | Ref. |
|---|---|---|---|---|---|---|---|
| **Normal Ferroelectrics (FEs)** | | | | | | | |
| BT | Bulk | 124 | 1.6 | 3.0 | 0.53 | Direct | [93] |
| BST | Bulk | 25 | 1.0 | 2.4 | 0.42 | [c]DSC | [94] |
| BZT | Bulk | 39 | 4.5 | 14.5 | 0.31 | Direct | [24] |
| PMN-8PT | Bulk | 23 | 1.35 | 1.5 | 0.9 | Direct | [95] |
| PMN-10PT | Bulk | 127 | 3.5 | 16.0 | 0.22 | Direct | [61] |
| PLT | Bulk | 147 | 1.67 | 5 | 0.334 | Indirect | [89] |
| BT | Thick | 60 | 7.1 | 80 | 0.089 | Indirect | [27] |
| Co, Sb-doped Pb $(Sc_{0.5}Ta_{0.5})O_3$ | MLC | 18 | 3.5 | 13.5 | 0.26 | AC | [75] |
| 8/65/35 PLZT | Thick Film | 45 | 40 | 120 | 0.33 | Direct | [96] |
| **Antiferroelectrics (AFEs)** | | | | | | | |
| PLZT | [d]Thin Film | -6.8 | 19 | 50 | 0.136 | Indirect | [97] |
| PLZT $Pb_{0.93}La_{0.07}$ $(Zr_{0.82}Ti_{0.18})_{0.9825}O_3$ | Think Film | 141/130 | 1.04/1.3 | 3.5/3 | 0.30/0.433 | Indirect/Direct | [66] |
| PLZT $Pb_{0.97}La_{0.02}(Zr_{0.75}Sn_{0.18}Ti_{0.07})O_3$ | Thick Film | 5 | 53.8 | 90 | 0.06 | Indirect | [98] |
| PLZT $(Pb_{0.97}La_{0.02})(Zr_{0.95}Ti_{0.05})O_3$ | [d]Thin Film | -5 | 30 | 30.8 | 0.016 | Indirect | [79] |
| $Pb_{0.94}Ba_{0.06}ZrO_3$ | Thin Film | 37 | -0.7 | 4.0 | 0.175 | Direct | [99] |
| **Relaxor Ferroelectrics (RFEs) - Inorganic** | | | | | | | |
| $Pb_{0.8}Ba_{0.2}ZrO_3$ | Thin Film | 17 | 45.3 | 59.8 | 0.076 | Indirect | [81] |
| PMN-10PT | Thin Film | 92 | 4.2 | 18.8 | 0.26 | [e]SThM | [61] |
| PMN-10PT | Thick | 92 | 1.3/0.23 | 10 | 0.13/0.0.023 | SThM/Indirect | [61] |

| ECM | Type | T[a] (°C) | ΔT (°C) | ΔE[b] (MV/m) | \|ΔT/ΔE\| ($10^{-6}$ °C/Vm$^{-1}$) | Characterization Method | Ref. |
|---|---|---|---|---|---|---|---|
| PMN-10PT | Thick Film | 75 | | | | Indirect | [100] |
| PZT | Thin Film | 222 | 12 | 48 | 0.25 | Indirect | [20] |
| PLZT | Thin Film | 45 | 40 | 125 | 0.32 | DTR | [58] |
| $(Pb_{0.88}La_{0.08})$ $(Zr_{0.65}Ti_{0.35})O_3$ | Thin Film | 45 | 40 | 125 | 0.32 | DTR | [68] |
| P(VDF-TrFE-CFE) | Thick Film | 25 | 0.87 | | | Indirect | [21] |
| PLZT $Pb_{0.89}La_{0.11}$ $(Zr_{0.7}Ti_{0.3})_{0.9725}O_3$ | RFE | 423/353 | 2.21/1.36 | 7/3 | 0.32/0.453 | Indirect/Direct | [66] |
| PMN-30PT | Bulk | 157 | 2.7 | 9.0 | 0.3 | Direct | [101] |
| 8/65/35 PLZT | Bulk | 110 | 1.8 | 6.8 | 0.26 | Direct | [101] |
| **Relaxor Ferroelectrics (RFEs) – Organic** | | | | | | | |
| P(VDF-TrFE-CFE) 59.2/33.6/7.2 | Thin | 37 | 0.87/3.6 | 70 | 0.012/0.051 | Direct/Indirect | [56] |
| P(VDF-TrFE) 55/45 | Thin | 80 | 12.6 | 209 | 0.06 | Indirect | [21] |
| **Composites[f]** | | | | | | | |
| P(VDF-TrFE-CFE)/BST67 | Bulk | 38 | 9.2 | 75 | 0.12 | - | [102] |
| $0.35(Sr_{0.7}Bi_{0.2})$ $TiO_3/0.65(Na_{0.5}Bi_{0.5})TiO_3$ | Bulk | 45 | 2.4 | 12 | 0.18 | - | [103] |

[a] Temperature at which EC measurements are made
[b] Applied Electric Field
[c] Differential Scanning Calorimetry
[d] Thin film on substrate
[e] Scanning Thermal Microscopy
[f] A composite of organic and inorganic materials

## 1.4 Working Principle of ECE-based Cooling and Figure of Merits (FoM)

Although several FEs and RFEs have offered promising results regarding high EC temperature and entropy changes over the years, yet the ECE-based devices are still going through their evolutional stages as several challenges are associated with their development. One of the challenges is to find a directional heat flow between cold end and hot end in a complete solid-state arrangement without involvement of any moving part. In this section, the short introduction of working principle of the ECE-based device, figure-of-merits, status of the device technology and limitations associated with reported prototypes will be discussed.

### 1.4.1 Comparison of VC-based and EC-based Cooling Cycles

The principle of the vapor compression (VC) cooling is that the *expansion of gases creates cooling*. As vapor compression VC-based cooling technology is fully understood and developed so EC-based cooling technology is illustrated in comparison with it. Both types of cooling cycles resemble with each other. VC-based cooling technology works on two adiabatic and two isothermal stages to complete one thermal cycle whereas EC-based cooling cycle comprises two adiabatic and two isofield steps as shown in Figure 1.28[10].

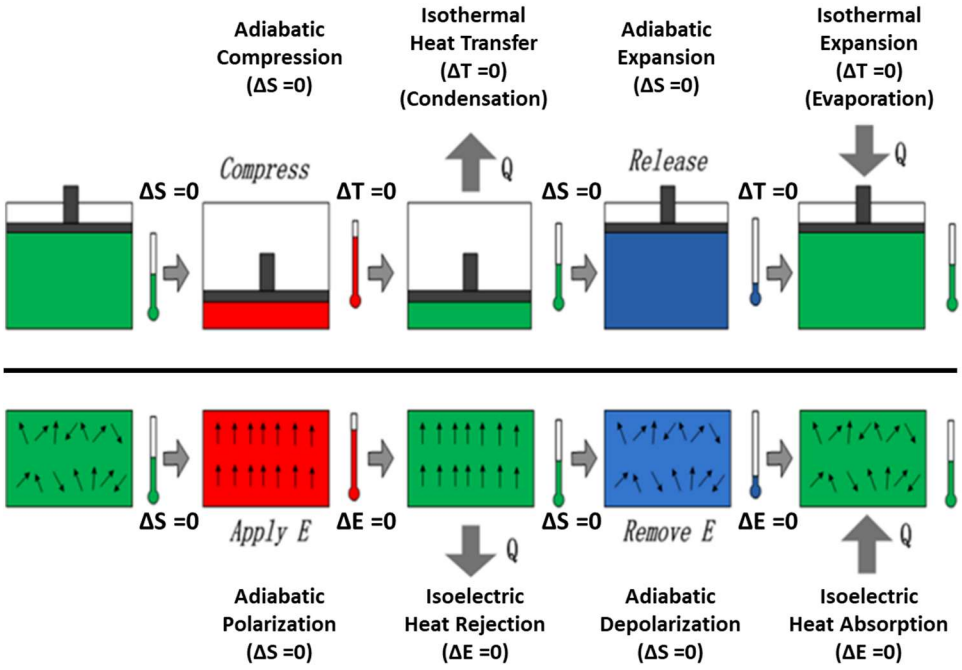


**Figure 1.28 Working principle (thermodynamic cycle) of VC and EC cooling**[104]

The stages for thermodynamic working cycle have been elaborated below.

A. *Adiabatic polarization*: Electric filed is applied on the EC body adiabatically which increases its temperature by ΔT. Temperature increase takes place as a result of decrease in entropy due to alignment of dipoles under electric field. This step resembles with the adiabatic compression in vapor compression refrigeration.

B. *Isoelectric Heat Transfer:* The EC body exchanges its heat with high temperate reservoir under constant electric field. In vapor compression refrigeration, this stage resembles with isothermal compression of the refrigerant.

C. *Adiabatic depolarization:* The electric file is removed adiabatically, and the EC body lowers its temperature by ΔT. This step is called adiabatic expansion in vapor compression refrigerator.

D. *Isoelectric Thermal Absorption:* EC body absorbs heat from the low temperature reservoir under constant electric field. This step is called isothermal expansion in vapor compression refrigeration[23,105].

### 1.4.2 Comparison of MC-based and EC-based Cooling Technology

From application point of view, the magnetocaloric (MC)-based refrigeration has exhibited high cooling efficiencies up to 60% of Carnot efficiency and has successfully been implemented in cryogenic applications[9]. As magnetocaloric cooling is ahead in advancement and is well-established field so mostly the same thermodynamic cycles are being exploited in the EC refrigeration except that the magnetic field is replaced with electric field. Magnetic / electric work is done on the MCM/ECM during magnetization /demagnetization & polarization / depolarization upon the application and removal of the magnetic / electric field[7,30]. An analogy has been given in Table 1.5.

**Table 1.5 Analogy between Electrocaloric Effect (ECE) and Magnetocaloric Effect (MCE)**

| Description | ECE | MCE |
|---|---|---|
| First Law of Thermodynamics | $dU = \delta q - \delta w$ | $dU = \delta q - \delta w$ |
| Thermal Work | $dq = TdS$ | $dq = TdS$ |
| Work due to External Field | $dw = -DdE$ | $dw = -\mu_o HdM$ |
| First Law of Thermodynamics | $dU = TdP + PdE$ | $du = TdS + \mu_o HdM$ |
| Entropy Change | $dS(T,E) = \left(\frac{\partial S}{\partial T}\right)_E dT + \left(\frac{\partial S}{\partial E}\right)_T dE$ | $dS(T,H) = \left(\frac{\partial S}{\partial T}\right)_H dT + \left(\frac{\partial S}{\partial H}\right)_T dH$ |
| Heat Capacity at constant fields | $C^E = \left(\frac{\partial q}{\partial T}\right)_E = T\left(\frac{\partial S}{\partial T}\right)_E$ | $C^H = \left(\frac{\partial q}{\partial T}\right)_H = T\left(\frac{\partial S}{\partial T}\right)_H$ |
| Adiabatic Temperature Change | $\Delta T_{ad} = -\int_{E_1}^{E_2} \frac{T}{C^E}\left(\frac{\partial P}{\partial T}\right)_E dE$ | $\Delta T_{ad} = -\int_{H_1}^{H_2} \frac{\mu_o}{C^H} T\left(\frac{\partial M}{\partial T}\right)_H dH$ |
| Isothermal Entropy Change | $\Delta S_{ist} = \int_{E_1}^{E_2} \left(\frac{\partial P}{\partial T}\right)_E dE$ | $\Delta S_{ist} = \int_{H_1}^{H_2} \mu_o \left(\frac{\partial M}{\partial T}\right)_H dH$ |

### 1.4.3 Thermodynamic Cycles for EC Cooling

Some thermodynamic cycles that are implemented in the development of ECE-based cooling devices are discussed below.

#### 1.4.3.1 Carnot Cycle

It is an ideal cycle which works between two adiabatic (ΔS=0) and two isothermal stages (ΔT=0). Although the efficiency of EC-based devices operating in Carnot cycle is higher than any other thermal cycle, yet this cycle is difficult to apply on real systems, so Brayton and Ericson cycles

are more viable in application due to their easier isofield stages[106]. Carnot cycle is mainly used for the comparison purposes[55]. The efficiency of an ideal cycle can be given as,

$$\eta_{CR} = \frac{T_L}{T_H - T_L} \tag{1.32}$$

Where $T_L$ and $T_H$ are low temperature and high temperature reservoirs, i.e. source and sink, respectively.

#### 1.4.3.2 Brayton Cycle

The Brayton like cycle works between two adiabatic and two isofield stages and is the mostly used cycle in the EC-based devices. Actually it is mostly used in both designs either cascade or regenerative). This cycle on T-S diagram has been shown in Figure 1.29 (a). During the polarization, electric/magnetic field is applied adiabatically ($\Delta S = 0$). This step is represented by line 2 that goes from point B → C. Polarization is normally very fast that there is no time to flow heat either from sink or source side. The during the isofield stage (i.e., thermal relaxation) shown by line 3 from C → D, the heat flows towards sink side unless the EC body is at equilibrium. In the next stage, the electric field is removed (line 4 from D → A) to produce depolarization, as a result the temperature of the body reduces. Now the body is in contact with the source, the heat will flow toward the EC body unless bodies are in thermal equilibrium. Electric field is kept constant during this stage as well (line 1 from A → B). In this way after the one cycle, the EC material is at initial state and is ready for the next thermal cycle. The black lines represent the ideal cycle showing perfect two adiabatic and isothermal stages in on complete cycle. The electrical work done on ECM and efficiency during one Brayton cycle are shown in Eqs. (1.33) & (1.34), respectably[106].

$$W_{Brayton} = (S_L - S_H) \int_{T_L}^{T_H} E dT \tag{1.33}$$

$$\eta_{Bryton} = \frac{Q_L^{in}}{W_{Brayton}} \tag{1.34}$$

Where $Q_L^{in}$ heat absorbed from the low temperaure reservior (cold end) and $W_{Brayton}$is the work done in the one Brayton cycle.

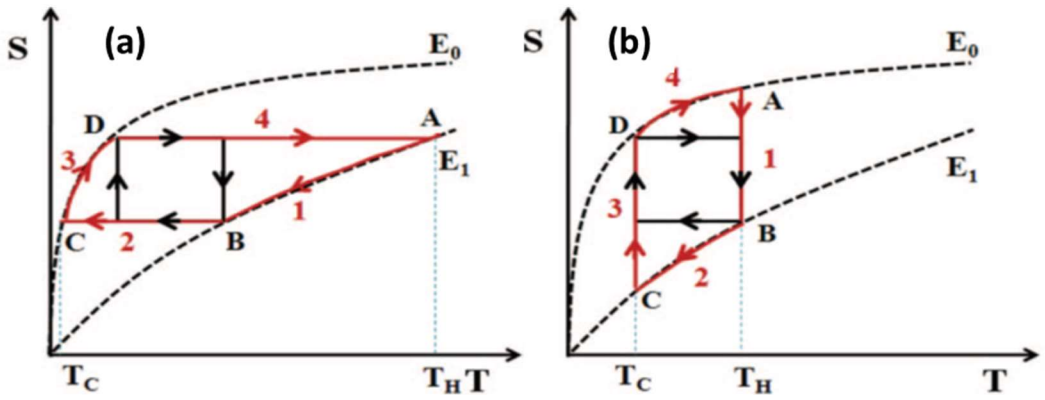


**Figure 1.29 Thermodynamic cycles for EC cooling on T-S diagram[106], (a). Brayton cycle, (b). Ericsson cycle**

### 1.4.3.3 Ericsson Cycle

Unlike Brayton cycle, the Ericsson cycle comprises of two isothermal and two isofield stages as in this thermal cycle the electric field is applied isothermally instead of adiabatically[55] as shown in Figure 1.29 (b). In this thermal cycle, the polarization/ depolarization of ECM is done by applying/ removing the electric field isothermally ($\Delta T = 0$) shown by line 1 from A → B. During the application of electric field, the materials tends to increase its temperature, but the body is kept in contact with the heat reservoir, so ECM rejects its heat to keep the temperature constant or to follow the isothermal conditions. Next, the ECM is brought in contact with the low temperature reservoir and electric field is removed isothermally again (line 3 from C → D), and this time the material will tend to lower its temperature and to compensate it the heat will flow from the lower temperature reservoir to the ECM. Electric work done on the ECM and the efficiency of Ericsson cycle is gives in Eqs. (1.35) & (1.36)[106].

$$W_{Erisson} = -(T_H - T_L)\int_{E_1}^{E_2} PdE \tag{1.35}$$

$$\eta_{Erisson} = \frac{Q_L^{in}}{W_{Erisson}} \tag{1.36}$$

Where $Q_C^{in}$is the heat absorbed from the low temperaure reservios and $W_{Erisson}$ is the work done during one complete cycle. Generally, the Ericsson cycle has more efficiency but it is difficulty to implement[106]. Hence, most of the reported ECE-based devices use Bryton cycle for heat umping and cooling applications. The reader is referred to literature[7,107,108] for detailed understanding of the thermal cycles for EC cooling.

### 1.4.4 Basic Concept of EC-based Device

The working mechanism of the ECE-based device may be understood from the simplest model of an ECE-based device shown in Figure 1.30. The model should be designed is such a way that during polarization ($\Delta E > 0$), the heat generated in ECM should be effectively transferred to the heat sink. On the other hand, during depolarization ($\Delta E < 0$), the heat be absorbed from the heat source. During polarization and depolarization, however, heat transfers to/from both heat sink/ heat source and no heat or small amount of heat is transferred from source to sink, so this type of device cannot work efficiently.

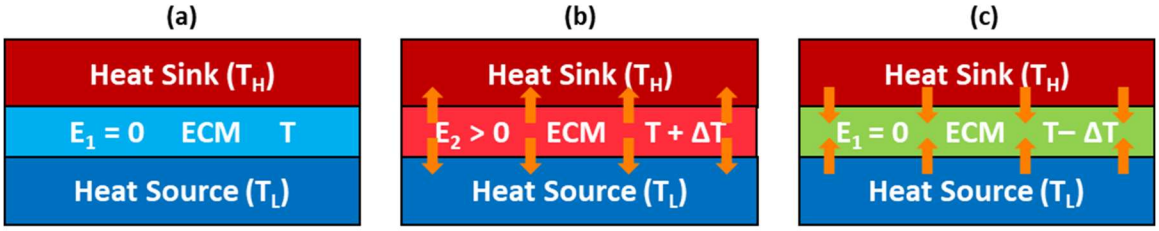


**Figure 1.30 Simplest EC cooling device: EC sandwiched between heat sink and heat source, (a). Equilibrium state, (b). Polarized state, ECM heats up, (c). Depolarization state, ECM cools down**

To achieve high efficiency and high heat transfer during one polarization/ depolarization cycle, there should be some arrangement/mechanism that heat should only transfer to heat sink during polarization and to heat source only during depolarization so that a net directional heat transfer may be achieved for a sustainable pumping operation. That is, *an effective separation of heat flows on polarization and depolarization is the key for an efficient device*. For this purpose, the simplest arrangement is that ECM may be attached / detached to heat sink and source alternatively during the thermodynamic cycle as shown in Figure 1.31. The basic working principle of a practical ECE-based cooling device shown in Figure 1.31 (a) – (d) may be illustrated as follow,

i. Increasing temperature of ECM upon application of electric field adiabatically.
ii. Thermal contact of ECM with heat source and heat rejection under constant electric field.
iii. Detaching it from heat sink and decreasing temperature of ECM upon removal of electric field adiabatically.
iv. Heat absorption from heat source under constant electric field by thermally attaching it to the heat source.

This completes one cycle and the directional heat flow from source to sink has achieved for sustainable pumping operation. It can be noticed from Figure 1.31 (d) that the ECM has come to its initial state ($E_1 = 0$, and equilibrium T), that is, ECM has recovered and is ready for next cycle. ECM recovery is one of the greatest challenges in development of ECE-based device as to implement the TD cycle the ECM must be alternatively attached and detached to heat source and sink that adds the complexities in the system.

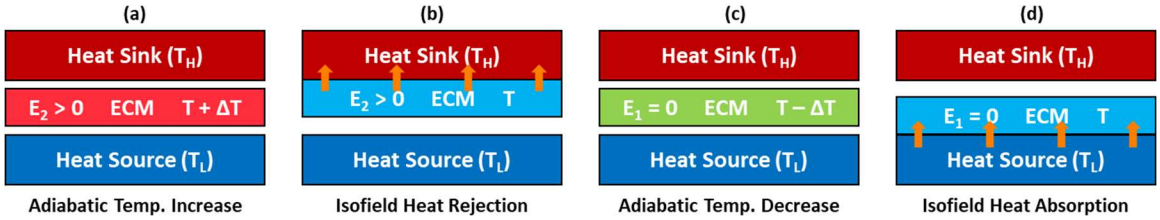


**Figure 1.31 Basic working principle of an efficient ECE-based cooling device, (a). Adiabatic polarization, (b). Heat rejection under constant E, (c). Adiabatic depolarization, (d). Heat absorption under constant E**

### 1.4.5 Performance Criteria of the EC-Device

As this technology is going through its developmental stages so there are no established procedures and parameters to report the performance of the EC device. Here, some of the parameters are being discussed that have been reported in literature by different research groups[6,13,106].

#### 1.4.5.1 Coefficient of Performance (COP)

The coefficient of performance (COP) is defined as ratio of the heat absorbed $Q_L$ at low temperature reservoir (cold end) to the total electrical work done on the electrocaloric materialal[13];

$$COP = \frac{Q_L^{in}}{W_{EC}^{in}} \tag{1.37}$$

Where $Q_L$ is the heat absorbed from the low temperature reservoir and $W_{EC}^{in}$ is the work done (energy supplied) on the ECM during one cycle and can be given as ideally.[9]

$$W_{EC}^{in} = Q_H^{out} - Q_L^{in} \tag{1.38}$$

$$W_{EC}^{in} = Q_H - Q_L = T_H \Delta S_H - T_L \Delta S_L \tag{1.39}$$

$\Delta S_H$ and $\Delta S_L$ are the entropy changes in the high and low temperature reservoirs, respectively. The above relation holds for ideal reversible cycle.

During the application, however, there are various irreversible processes that can generate entropy like temperature gradients in heat switches, electrical resistance, joule heating and hysteresis in the ECM[9,76,109], so the $W_{EC}^{in}$ needs to be determined accordingly. For real systems, more entropy may be generated due to irreversible processes and hysteresis.

$$S_{gen} + \Delta S_L = \Delta S_H \tag{1.40}$$

$S_{gen}$ is the extra entropy generated heat per cycle due to irreversible process. So, the net electrical work in EC material can be written as,

$$W_{EC}^{in} = (T_H - T_L)\Delta S_L + T_H S_{gen} \tag{1.41}$$

In real case (Non-ideal), the COP can be written as,

$$COP = \frac{T_c \Delta S_c}{(T_H - T_L)\Delta S_L + T_H S_{gen}} \tag{1.42}$$

Or the above relation may be given after manipulation as[76,109]

$$COP = \frac{\eta_{CR}}{\left(1 + \frac{\eta_{CR} T_H S_{gen}}{Q_C^{in}}\right)} \tag{1.43}$$

Where $\eta_{CR} = T_L/(T_H - T_L)$

The electrical work done on the EC material can also be calculated from the stored energy in the EC elements as follows[13].

$$W_{EC}^{in} = \frac{1}{2}\varepsilon_o \varepsilon_r E^2 \tag{1.44}$$

**Table 1.6 Typical COP range for solid-state cooling technologies**[23]

| Device Technology | COP |
|---|---|
| Thermoelectric | 0.3 |
| Magnetocaloric | 7-10 |
| Electrocaloric | 7-10 |

### 1.4.5.2 Refrigeration Capacity (RC)

This parameter has been used frequently for magnetocaloric refrigeration but has not been reported much by electrocaloric research community. For a reversible process, refrigeration capacity (RC) can be given as[10,45],

$$RC = \Delta S_L \times (T_H - T_L) \tag{1.45}$$

RC is basically heat transferred in one thermodynamics cycle between temperatures $T_L$ and $T_H$. Some other authors have defined RC is different way by calculating full width at half maximum (FWHM) of ΔS-T graph by taking $T_L$ and $T_H$ as operating temperatures[110,111],

$$RC = \int_{T_c}^{T_h} \Delta S dT \approx -\Delta S_m \times FWHM \tag{1.46}$$

Where $\Delta S_m$ is maximum entropy change.

#### 1.4.5.3 Specific Cooling Power

Cooling power depends on the frequency of the device. In other words, it is the time that how quickly a device comes at thermal equilibrium and is ready for next cycle. The higher the frequency, the higher will be the cooling power[112]. The cooling power depends strongly on the thermal properties of the ECM, i.e., heat capacity, thermal conductivity, and thermal diffusivity. An EC material with high thermal diffusivity will come in thermal equilibrium more quickly. It is a measure of average heat flux during the heat transfer cycle and it a function of the size of ECM involved. It is normally reported in W/g or W/cm$^3$.

#### 1.4.5.4 Efficiency of EC Device

The efficiency of the EC device is normally defined relative to the ideal cycle (Carnot Cycle) as follows[9],

$$\eta_{CR} = \frac{COP}{COP_C} \tag{1.47}$$

Where $COP_C$ is the coefficient of the performance of ideal thermal cycle (i.e. Carnot cycle). In the system design, there may be other mechanisms involved like heat switches, actuators and regenerators to find the directional heat flow so proper mathematical formulations and experimental data is required to calculate the energy taken by the EC layers in one cycle and for the efficiency of the device.

## 1.5 Current Status of the EC-based Cooling Devices

Over the last decade, considerable efforts have been carried out to realize the working of EC-based cooling devices. Several designs have been conceptualized, prototypes and reported to exploit the

ECE in real systems, but most of the proposed devices were never built nor tested. Consequently, no commercial EC-based cooling device is yet available[10]. One of the greatest challenges in designing the EC-based cooling device is to establish a sustainable cyclic directional heat flow from cold end to hot end. All these concepts can be simply illustrated using the principle shown in Figure 1.31, where heat is being absorbed from the heat source at low temperature and is rejected at the sink at high temperature by thermal coupling / decoupling of EC body with source and sink alternatively by physical movement of EC body.

As EC-based cooling technology is going through its evolutional stages so several *functional procedures*[113] have been reported including liquid/solid regeneration, electrostatic actuation, mechanical actuation, heat switches and thermal diodes etc., to achieve directional heat flow between heat source and heat sink and to attain thermal recovery of EC materials for next cycle. These functional principles work efficiently for a specific design and are normally independent of the thermodynamic cycle. No standardization of these underlying principles and categorization of EC-based devices has been carried out by the research community. A systematic classification of function principles and device types which can lead for the development of EC refrigerating systems has been reported[113] and has been shown in Figure 1.32.

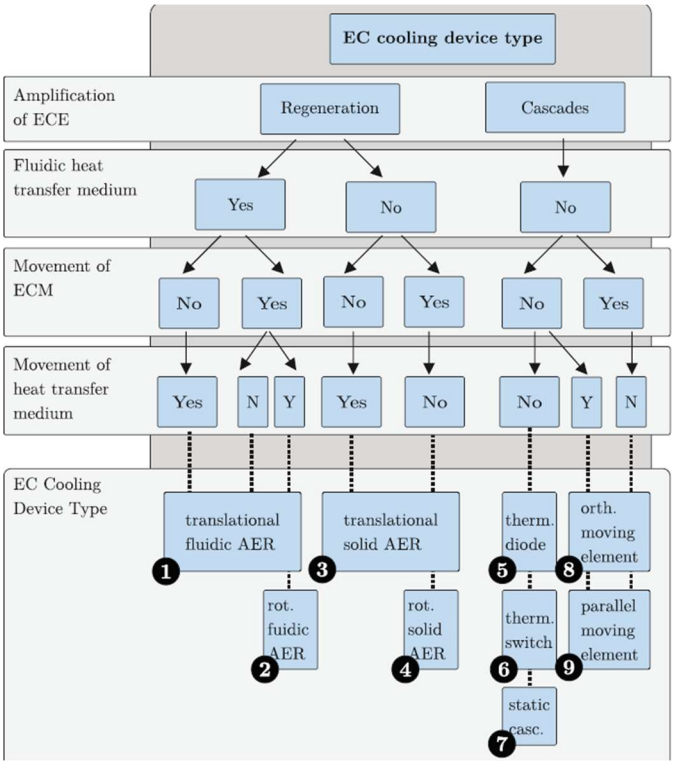


**Figure 1.32 Classification of EC-based cooling devices**[113]

As discussed in 1.4 section that the key for a sustainable operation of an ECE-bases cooling device is the continuous heat flow from the source to sink. This can be achieved either using the concept of *regeneration* or *cascades*[12,113].

What is regenerator? A heat regenerator is a type of indirect heat exchanger where the heat is temporarily stored and then periodically transferred from cold heat exchanger to hot heat exchanger by a working (heat-transfer) fluid. The working fluid is pumped through the porous structure of the regenerative material usually in an oscillatory manner. During the 'hot period', a warmer fluid flows through the regenerative material. and the working fluid exchanges its heat with regenerative material. As a result, the working fluid cools down whereas the regenerative materials heat up, i.e. heat is stored in the regenerative material. During the 'cold period', a cooler fluid flows through previously heated regenerative material. The heat is exchanged again between working fluid and regenerative material, but this time the working fluid heats up, while the regenerative material cools down. Again, this heated working fluid enters in the hot heat exchanger and one cycle completes. After repetition of several such cycles, a temperature gradient is established along the length of the regenerator and a steady state is reached[114]. Here the regenerator

only stores heat temporarily and does not create any heating/cooling itself, so this type of regenerator is called *passive regenerator*. An *active regenerator*, on the other hand, contains an active material as regenerator. In that case the regenerator's function is twofold. It can itself increase/decrease the temperature using an external stimulus enabling an increase in the temperature span and works as heat exchanger for working fluid between the phases of the thermodynamic cycle.

In cascade concept, on the other hand, the directional heat flow between source (cold end) and sink (hot end) is achieved by making a heat-switch-type arrangement between source, ECM and sink by the use of thermal diodes, thermal switches/valves and other mechanical arrangements like physical thermal coupling and decoupling of the bodies involved in ECE-based device. Regeneration can be achieved using fluids and solids whereas the concept of fluids in cascade design is not conceivable. For regeneration, one moving part is essential. Working fluids are normally used for this purpose, but ECM can also be moved but it adds the complexity for the fields to be applied. Cascade devices without involvement of any moving parts have been reported where thermal diodes have been exploited to control the heat flow direction but there are some inbuilt problems with these diodes like internal joule heating, low thermal contrast, and manufacturing costs.

A general concept of regeneration (both liquid/ solid) and cascade has been shown in Figure 1.33 and Figure 1.34 respectively. Finding directional heat flow defines the working principle of the EC device. In the following, some reported EC-devices along with their working principles are discussed to illustrate the challenges and problems associated with them.

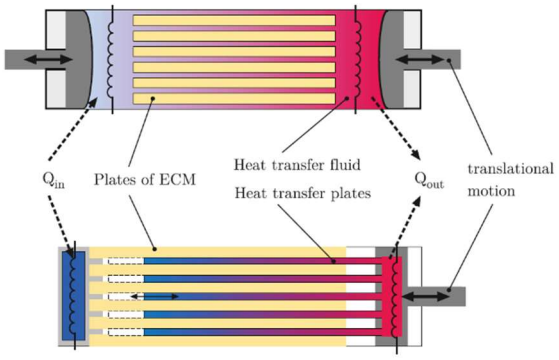


**Figure 1.33 Schematic of translational fluidic AER (Top), translational solid AER (bottom)**

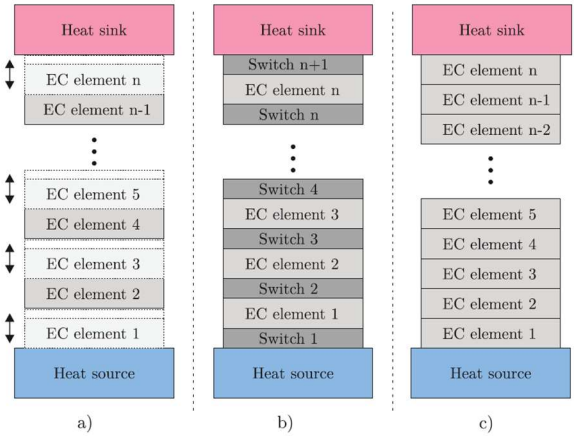


**Figure 1.34 Schematic of cascade, (a). Moving elements, (b). Heat switches/ diodes, (c). Static/ no movement**

### 1.5.1 Regeneration Designs

As most of the practical ECMs (i.e. bulk ceramics) do not offer a wide temperature range and high ECE so different principles are used to increase the temperature span of device greater than $\Delta T_{EC}$ of ECMs. The concept of regeneration has successfully been used in MC refrigeration. In case of magnetic refrigeration, a magnetic material is used as regenerator so the term Active Magnetic Regenerator (AMR). This concept was explained and patented by Baclay, et. al. to exploit MCE as room temperature[115]. Since then, the concept of Active Magnetocaloric Regeneration (AMR) has been the basis of most prototype designs reported for magnetocaloric cooling[114]. The same idea has been exploited in the EC cooling by replacing MCMs with ECMs so the term *active electrocaloric regeneration* (AER). The strong feature of the regeneration is that a temperature span along the device may be achieved greater than the $\Delta T_{EC}$ of ECM at the same electric field[12,116]. The ratio between temperature span across the device and $\Delta T_{EC}$ is called regeneration factor.

#### 1.5.1.1 EC-based Devices with Liquid Regenerator

The first ever EC device based on AER was demonstrated by Siyansky and Broyansky and coworkers[117]. Their prototype concept, as shown in Figure 1.35 (a), includes PST plates as EC bodies (Block 1 & 2) which act as active regenerators and underdo a temperature change of 1.3 - 1.5 K upon the application of external electric field of 2.5 MV/m[117]. External electrical fields are applied on blocks out of phase and are synchronized with the pump so that the working liquids

(silicon oil) takes the heat from the cold end to the hot end. On the other hand, taking off the external field from the EC bodies decrease their temperature and the heat-transfer fluid is pumped in the opposite direction. The warm fluid now gives heat to the EC bodies and cools down and enters the cold end. Several cycles are repeated, it can be seen from Figure 1.35 (b) that a smaller EC temperature change ($\Delta T_{EC} \approx 2\ K$) in active body has made higher temperature changes ($\Delta T = 5K$) in the block 3 and 4 . The most promising feature of regeneration is that the temperature changes of much higher that $\Delta T_{EC}$ can be achieved with it. Heat losses due to long paths of fluid flow, down-scaling, less heat exchange efficiency between PST plates and working fluid, reliability and long-term stability (sealing of liquid) are some associated disadvantages with these designs[113].

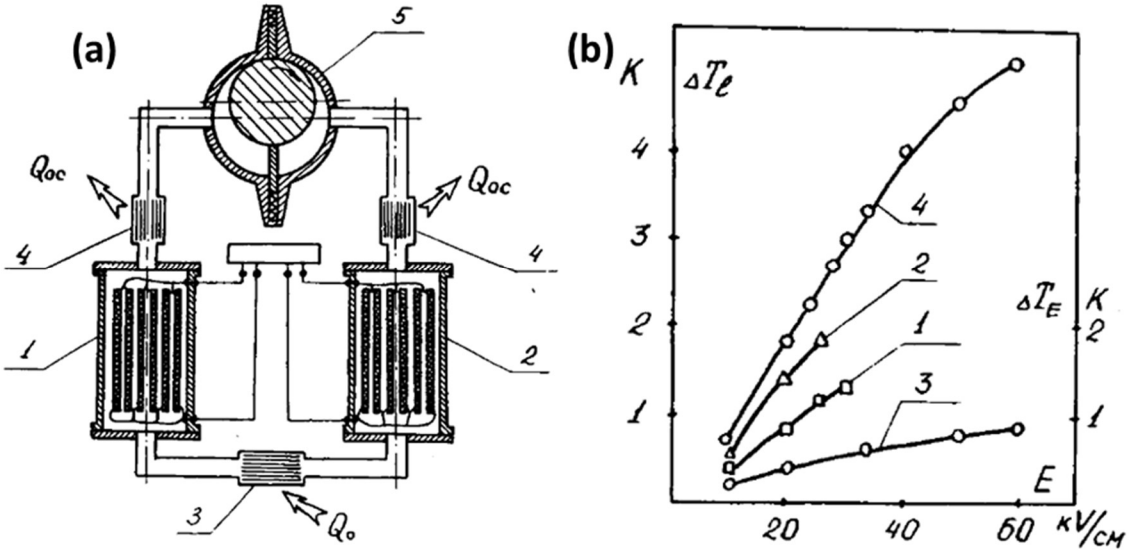


**Figure 1.35 (a). First EC device based on AER, (b). Temperature span achieved by AER-based device**[117]

A similar concept of AER with liquid working fluid has been used by Guo *et al.*[118]. In this design, a concept of electrostatically controlled diaphragms was used to control the flow of the working fluid to achieve the directional heat flow. A cooling power of 3W/cm$^3$, a temperature span of 15K with an efficiency of 31% has been achieved. The low operating frequency (i.e., low cooling power), poor efficiency, and reliability of fluid pumps, however, have hampered their further development[119] and their exploitation in miniature/chip-scale applications. A liquid AER based EC device was also reported by U. Plaznik, et. al[120] where peristaltic pump was used to control the flow of fluid. A temperature span of 14K and regeneration factor of 9.6 has been reported. In another AER based design, P. Blumenthal used PMN-PT and PMN-PT MLC plates as active

regenerator and silicon oil as circulating fluid by piston-driven arrangement as shown in Figure 1.37 to achieve a temperature span of $\Delta T_{device}$ of 0.17 K with $\Delta T_{EC}$ of 0.009 K representing a regeneration factor of 2[121].

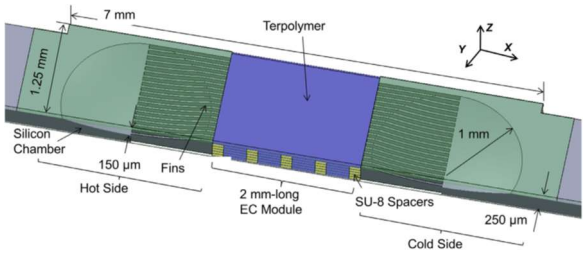


**Figure 1.36 EC cooler with electrostatically driven diaphragms to control the motion of the liquid**[118]

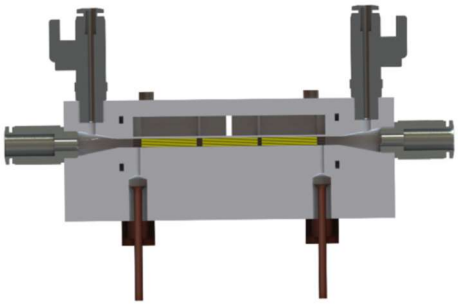

**Figure 1.37 Peristaltic pump driven fluid control for AER in EC-based device**[120]

### 1.5.1.1 EC-based Devices with Solid Regenerator

Haiming Gu *et al*. introduced the new idea of solid-state regenerator to overcome the issues associated with liquid based AER designs[122]. Figure 1.38 shows the prototype *electrocaloric oscillatory refrigerator* (ECOR) where stainless steel plates of 0.5 mm thickness were used as regenerators. Solid state regenerator offers several advantages over liquid based regenerator like ease in accurately driven miniature actuators, reduction in size to chip scale level, no fluid mixing/ leakage problems, fabrication in anisotropic thermal conductivity to reduce the conduction loss from the hot side to the cold side along the regenerator[122]. The working principle of solid regenerator has been illustrated in Figure 1.39(a) – (d). EC module moves to the right side of regenerator and electric field is applied on EC material that increases the temperature of EC module. EC module is fixed on the right side to reject heat from EC module to the regenerator. EC module is then moved to the left side of regenerator and electric field in removed that decreases its temperature. Now EC module stays there, and heat is absorbed from the regenerator at the cold end. As the refrigeration cycle repeats, a temperature gradient of 5K is created between the left side and right side of the regenerator as shown in Figure 1.39. Involvement of actuation mechanism and heating due to metal to metal friction and irreversible conduction losses are the associated issues with this regeneration designs.

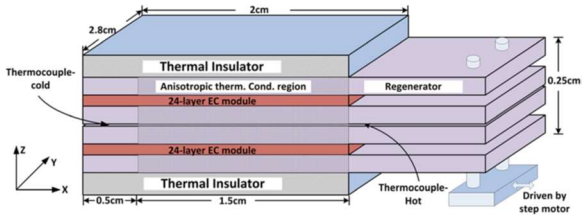


**Figure 1.38 Prototype EC oscillatory refrigerator (ECOR) based on solid-state regenerator**[122]

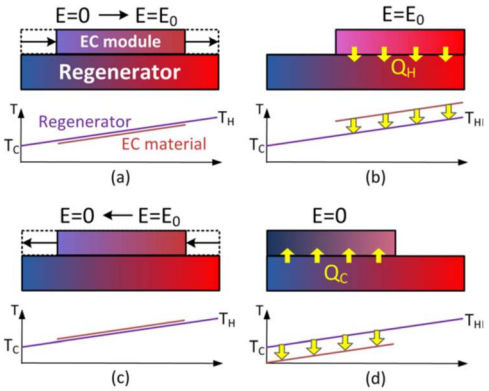


**Figure 1.39 Basic principle of solid regenerator**[122]

### 1.5.1.2 Design Concept without External Heat Regenerator

This idea of EC-based devices without any external regenerators was first studied by Gu *et al*. and simulation results were reported[123]. The original idea of regeneration without external regenerators was first demonstrated in magnetocaloric (MC) device by Hakuraku[124] but faced the problems of restrictions in applying the magnetic fields on the MCM and low cooling due to involvement of long thermal paths. In EC refrigeration, the application of electric field can easily be realized in this configuration so this model was developed by Tian Zhang *et al*[125] as shown in Figure 1.40 (a). and the experimental results were reported. The operation of the device can be understood from the Figure 1.40 (b). The temperature of the elements increases as they move from T2/B2 to T1/B1 under the influence of external electric field. If the increased temperature is higher than the hot end temperature $T_h$, the heat will be rejected from the EC element to heat exchanger (then to external heat sink). As the EC elements T1/B1 rotate to T16/B16,…, to T10/B10, the electric field will be kept on the elements and meanwhile the heat will flow from the elements on top/bottom ring to the elements on bottom/top ring due to a temperature difference between them.

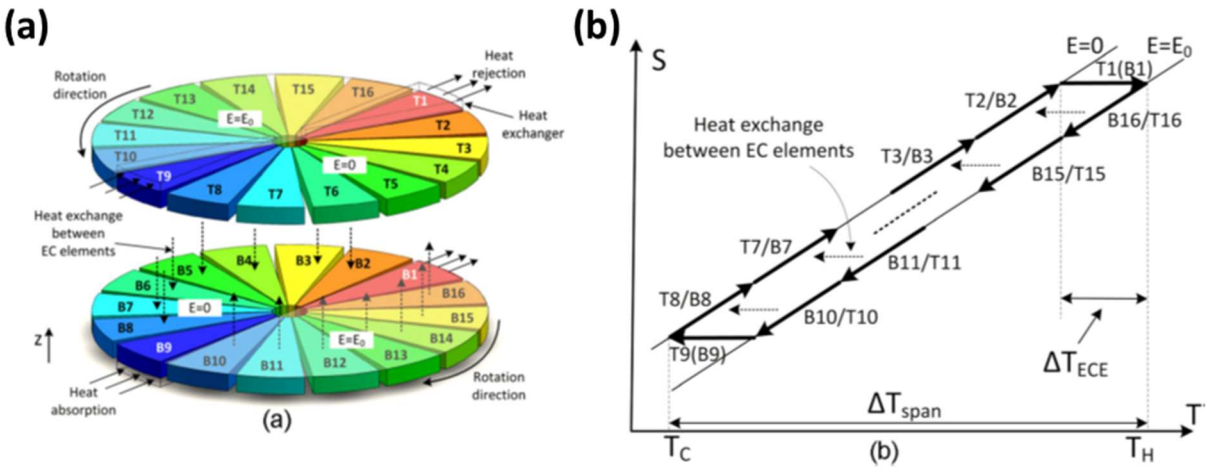


**Figure 1.40 (a). Device concept for self EC to EC regeneration, (b). S-T diagram of a Brayton cycle for rotary EC refrigerator**[123]

When the elements move from T10/B10 to T9/B9, the temperature of the elements decreases due to the removal of external electric field. If the decreased temperature is lower than the temperature of cold end $T_c$, heat will be absorbed from cold heat exchanger $T_c$ to ECMs. During the time period of the rotation from T9/B9 to T8/B8,…, to T2/B2, the electric field on the element will be kept at zero and heat will be exchanged between the elements on bottom/top ring and the elements on top/bottom ring due to a temperature difference. This cycle will repeat. An entropy-temperature (S-T) plot of a Brayton cycle of the refrigerator with adiabatic boundary condition (without heat exchange with the external heat load/sink) is shown in Figure 1.40 (b). This device achieved the regeneration factor higher than the other reported devices based on regeneration

Although the EC devices based on regeneration demonstrated successfully high EC performance by lifting the temperature spans greater than the $\Delta T_{EC}$ of the refrigerants involved, yet there are extra mechanisms involved that are responsible for the movements of the solid/ liquid fluids for regeneration that add the complexities in the device.

### 1.5.2 Cascade Designs

To address the issues like convective heat transfers, involvement of pumps, leakage/sealing issues and longer heat paths associated with regeneration designs, cascade designs were introduced by several research groups.

### 1.5.2.1 EC Devices with Mechanical / Motorized Actuating Systems

The use of a mechanical actuator to alternatively attach/ detach the ECM with high and low temperature bodies has been reported[119]. The key of this study is a use of a *liquid based thermal interface* of high switching ration ($R_{off}/R_{on} > 100\ m^2K/W$) which provides high-off thermal resistance of $R_{off} > 10^{-2}\ m^2K/W$. To achieve a high thermal contact, a layer of Teflon was coated on sink/source and then small hydrophilic islands of diameter (1mm) were patterned lithographically. A liquid, glycerol in this study, is dispensed on the islands of both sides which forms discrete droplets when there is no thermal contact (thermal contact OFF) and makes a thin layer when there is thermal contact (thermal contact ON) interface. It offers some advantages over solid-solid direct contact which has reliability challenges due to stiction and poor thermal contact. The basic principle is same with four stages (polarization, heat rejection to sink, depolarization, heat absorption from source). A schematic has been shown in Figure 1.41 . In this study, Au based heater is used as a constant heat source whose temperature was kept constant at 27 °C (corresponds to a power density of 2.5 kW/m$^2$), whereas the temperature of the sink was maintained at 25 °C. The COP and cooling power have not been reported in the work.

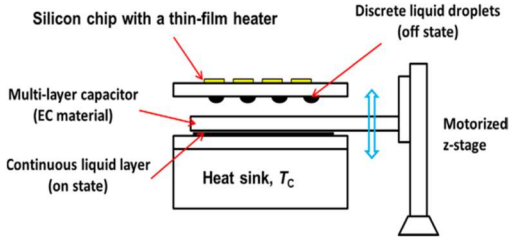


**Figure 1.41 EC device with motorized actuator**[119]

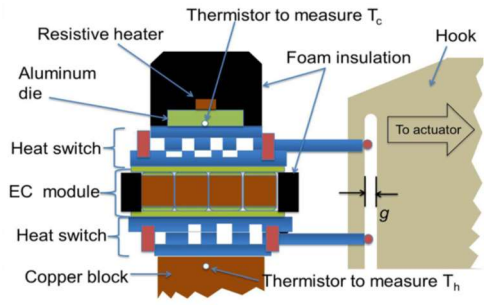


**Figure 1.42 EC cooler with mechanical heat switch**[126]

Y. D. Wang *et. al.* has used a silicon based mechanical heat switch of contrast ratio of 27[126]. In this design, a mechanical heat switch is used to control the heat flow direction by switching it in ON/OFF mode. Its ON mode thermal conductance is more than its OFF mode thermal conductance. This ratio is called contrast ratio. More is the ratio, the better the heat switch will work. The working principle has been illustrated in Figure 1.42. A temperature lift of 0.3 C (60% of the electrocaloric change of BT based-MLC used) and heat flux of 36 mW has been reported.

The major problems associated with this heat switch is that the ON and OFF states are achieved by using a mechanical actuator motors which adds the complexity in the system. Moreover, there are other issues of thermal contact with the active EC body. These limitations make them unsuitable for a compact and efficient design.

#### 1.5.2.2 EC Devices based on Electrostatic Actuation

It has already been discussed that ECE in bulk materials in dielectric strength limited, whereas the thin films have less volumetric heat capacity (less thermal mass) so cannot pump much heat. To overcome these issues, the use of multilayer capacitor (MLC) is on rise, but the problem with them is that slower thermal conduction and longer heat paths have negative effects on cooling power. To address this issue, a novel idea to used MLC laterally as opposed to vertically as shown in Figure 1.43. The working principle is comprised of Bryton cycle with four thermodynamic stages (two adiabatic and two isofield). A detailed parametric study to know the effects of electrode thickness, relaxation time constants, temperature spans has been carried out in this study. COP of 15 has been achieved and an efficiency of 50% has been reported[127]. The reliability of the thermal contact is the major concern in these types of design.

Rujun Ma, et. al. reported a EC-based cooling device using a flexible EC polymer film of P(VDF-TrFE-CFE) and electrostatic mechanism for actuation[13]. The size of the device is 7cm x 3cm x 0.6 cm. A good thermal contact of polymer film with heat sink and source has been achieved using efficient electrostatic mechanism with energy consumption of 0.02 W which also reduces parasitic heating. The actuation is noiseless, compact, and free from the frictional forces which can cause damage. The quality of thermal contact has been confirmed by measuring heat flux through the contact by using a heat flux meter. The working principle is based on Bryton Cycle and EC cycles and electrostatic cycles work together to achieve the directional heat flow as shown in Figure 1.44. Electric Field is applied to EC polymer stack adiabatically which increases its temperature. Heat transfers from the EC polymer stack to the heat sink. After equilibrium, EC polymer stack is moved in contact with bottom aluminum plate (heat source) using electrostatic actuation. Electric field is removed from EC polymer stack adiabatically which decreases its temperature. Now the heat will transfer from the heat source to the EC polymer stack and the operation continues.

A COP of 13 and specific cooling power of 2.8 W/g has been achieved which is higher than mostly reported magnetocaloric and thermoelectric devices. This device also offers flexibility to be conformed in any application and is noiseless. The frequency of the device is 0.8 Hz, electrostatic

actuator can work even at higher frequency but there is some time which is required to transfer heat from the EC polymer stack to the sink/source through other laminated sheet. The electric field on the EC polymer stack can also be increased to maximize the heat flux. A heat flux of 29.7 $mW/cm^2$ has been achieved by an electric field of 6.7 MV/m. The $COP/COP_C$ is only 6% which is not that impressive as compared to other reported devices, but the specific cooling is much better than other cooling devices[13].

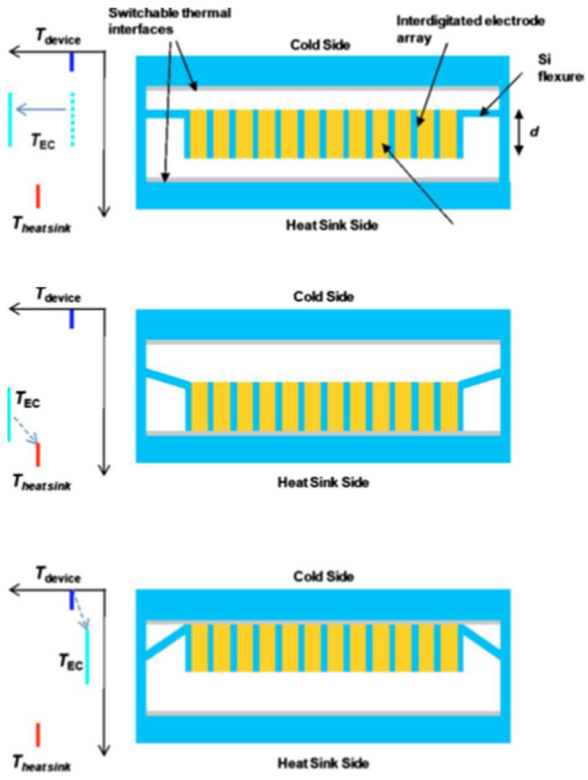


**Figure 1.43 Electrostatic actuation – cross-sectional view of µECM device in flexural mode[127]**

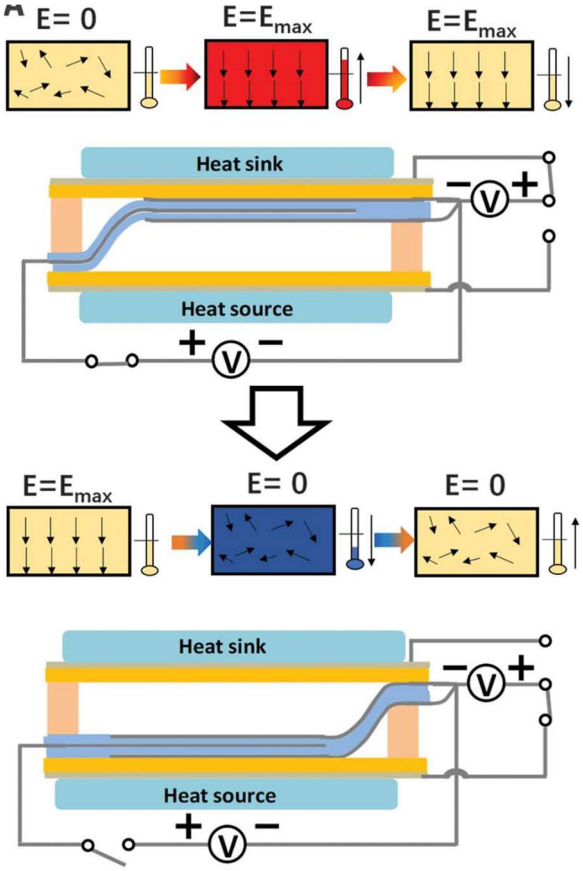


**Figure 1.44 PVDF film based EC device using electrostatic actuation to alternatively make contact with heat source/ sink[13]**

### 1.5.2.3 EC-devices with Electromechanical Actuation

To avoid any external actuation mechanism, the electromechanical coupling effect was used to actuate the ECM for thermal coupling/decoupling between heat sink and heat source[128] as shown in Figure 1.45 (a). This device consists of PMN-0.1PT elements in the form of cantilevers clamped

at one side. This material is also piezoelectric. So, when an electric field is applied, it heats up due EC effect and at the same time it bends due to its piezoelectric properties and makes contacts with the other cantilevers to transfer its heat. By properly establishing a thermodynamic cycle and movement of cantilevers, a net directional heat can be achieved. This device achieves a temperature span of 12.6 K with elements having EC coefficient of 1.5 K giving a generation factor of 10.2 as shown in Figure 1.45 (b). Although this concept does not use any external mechanism for actuation, yet the moving parts are involved in the device and reliable thermal coupling and decoupling is still as issue.

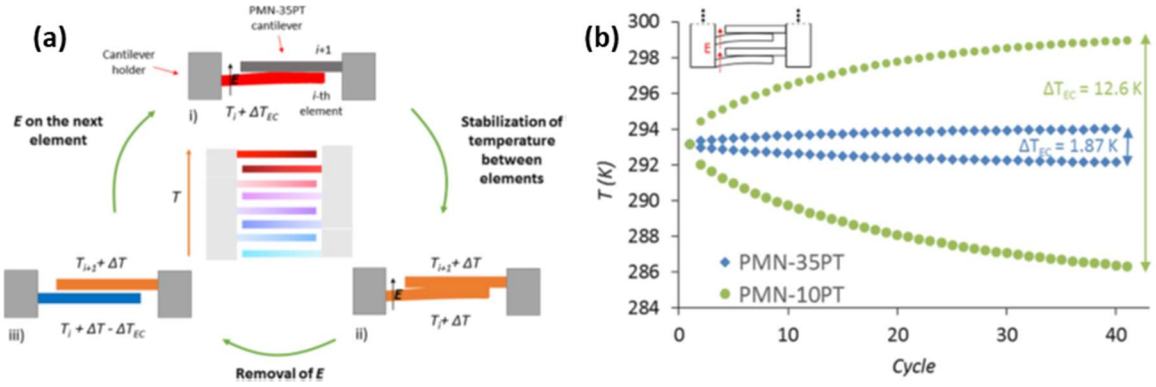


**Figure 1.45 (a). Electromechanical actuation of ECM cantilevers for thermal coupling/ decoupling, (b). Temperature span achieved as a function of number of cycles**[128]

### 1.5.2.4 EC Devices with Thermal Diodes/ Heat Switches

Thermoelectric materials have been reported to be used as thermal switches[104,129]. The physical phenomena behind is that thermal resistance or conductance can be controlled by electrically switching them ON and OFF. These ON/oFF cycles are fully synchronized with the EC cycles which allow more heat flow in one direction as compared to other direction [113,126,130]. A concept of heat pump using thermoelectric (TE) and electrocaloric (EC) materials has been given by D. Feng *et al*[130]. In this device an EC layer has been sandwiched between two TE layers. TE layers control the direct of heat flow as shown in Figure 1.46 and work just like thermal switches but here the main difference is that unlike thermal switches, thermal diodes are semiconductor devices based on Peltier Effect so they can be used for development of complete noiseless EC devices. This idea was first patented in 1988 by Basiulis *et al*[131]. The working principle of this TE-EC-TE element has been illustrated in Figure 1.46. Like other designs, this also works in four stages.

A. The temperature of the EC element is decreased by removing the electric field as shown in Figure 1.46a.

B. TE1 is switched ON and a constant electric current is passed through the TE1element to pump the heat in the direction of the current and the heat will transfer from $T_c$ to EC. When the TE1 and EC bodies are in thermal equilibrium, the TE1 is switched OFF. TE2 is already switched OFF, and will not allow heat to flow from hot side to EC.

C. The electric field is applied on the EC body, it increases the temperature of EC body.

D. Now the TE2 is switched ON and current is passed through it, which allows the heat flow from the EC to hot side ($T_h$). One cycle completes, and some heat has transferred from the cold side ($T_c$) to hot side ($T_h$).

Exploitation of TE materials in EC based heat pumping has given very promising results and achieved a COP of 1.54 and cooling capacity of .80 $W/m^2$. A limitation associated with these types of arrangement, however, that it generates the joule heating which reduces the cooling power of the device[130].

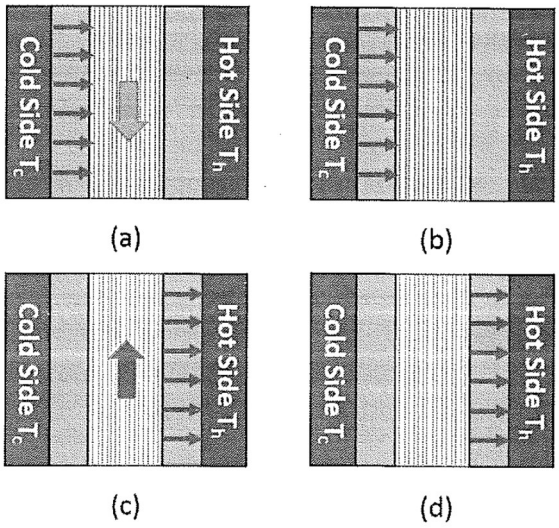


**Figure 1.46 Working stages of TE-EC-TE heat pump**[104]

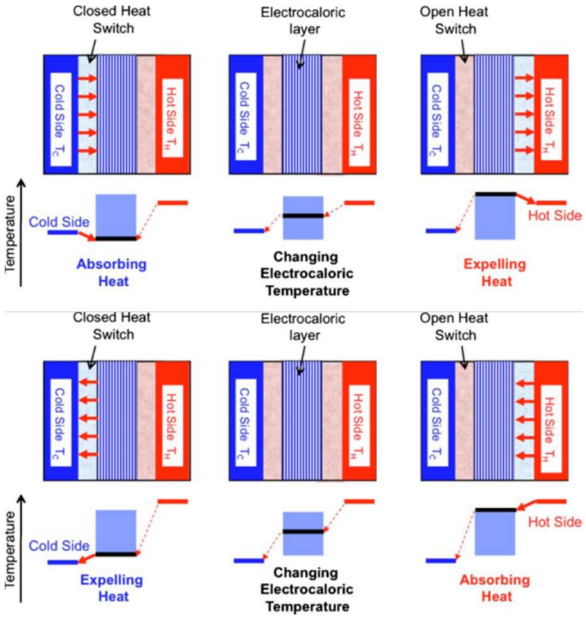


**Figure 1.47 Thin film based heat switch**[109]

Electrocaloric devices based on thin films[109] heat switch has been reported where the anisotropic properties of the liquids are exploited to achieve the directional heat flow as shown in Figure 1.47.

### 1.5.3 Solid-state Cooling Line

S. Karmanenko, et. al. introduced an idea of a solid-state cooling line composed of EC elements and highly thermoconductive metallic elements and investigated the approach suing analytical and computational experiment[132,133]. The model of the solid-state cooling line has been shown in Figure 1.48. In this technique, the electric field is applied adiabatically and is removed isothermally, this creates a thermal flux and temperature gradient along the cooling line. For a completely isolated and symmetric cooling line the average temperature remains same as of initial temperature. Changing the boundary conditions on both extremes, however, disturbs the symmetry and a net heat transfer from the cold end to the hot end is observed[132]. There is critical issue with this all-solid-state cooling line that was not explained/ demonstrated whether they can achieve a continuous cooling/heat pumping operation[23] or it is just a temperature redistribution in the cooling line[132]. Theoretical studies show that with an electrocaloric change of 2K, a temperature gradient of 20K may be achieved with an efficiency of 60%[28].

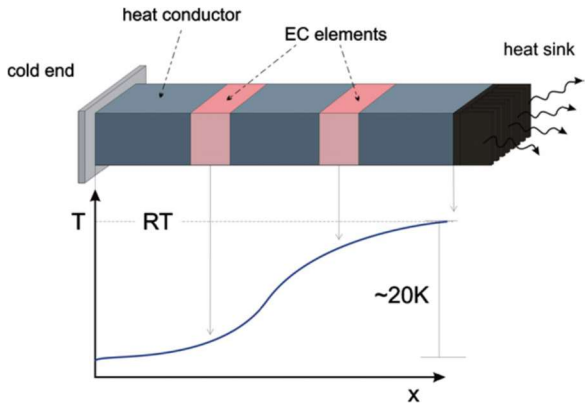


**Figure 1.48 Solid-state cooling line and temperature gradients**[23,132]

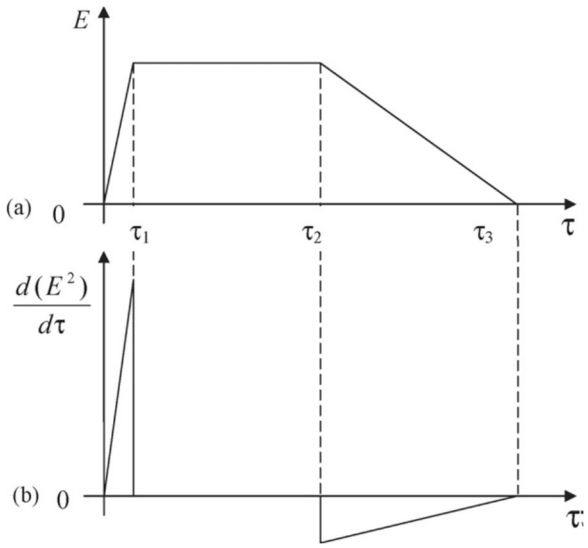


**Figure 1.49 (a).Variations of the electric field applied on the EC elements adiabatically and isothermally, (b). Derivative of electric field**[132]

Some other works based on the same idea have also been reported where one EC element layer between two conduction layers have been reported. Mathematical model of the concept were given but solved numerically and simulation results were given[133,134]. A solid state cooling line comprising three elements (Al-EC-Cu) model has shown in Figure 1.50 (a). Figure 1.50 (b) shows the electric field cycles that were applied on the EC element. The temperature profile of the cooling line for two different EC elements has been shown in Figure 1.50 (c). Still there is an open question that either these devices are able to transfer any heat or it is just a temperature redistribution as the one end is thermally insulated in these types of cooling lines[133,134]. In another all soli-state device, cooling has been achieved by exploiting the kinetic process using different rising and falling rates of the electric fields in an MLC of barium titanate[135]. The reader is referred to the literature for details.

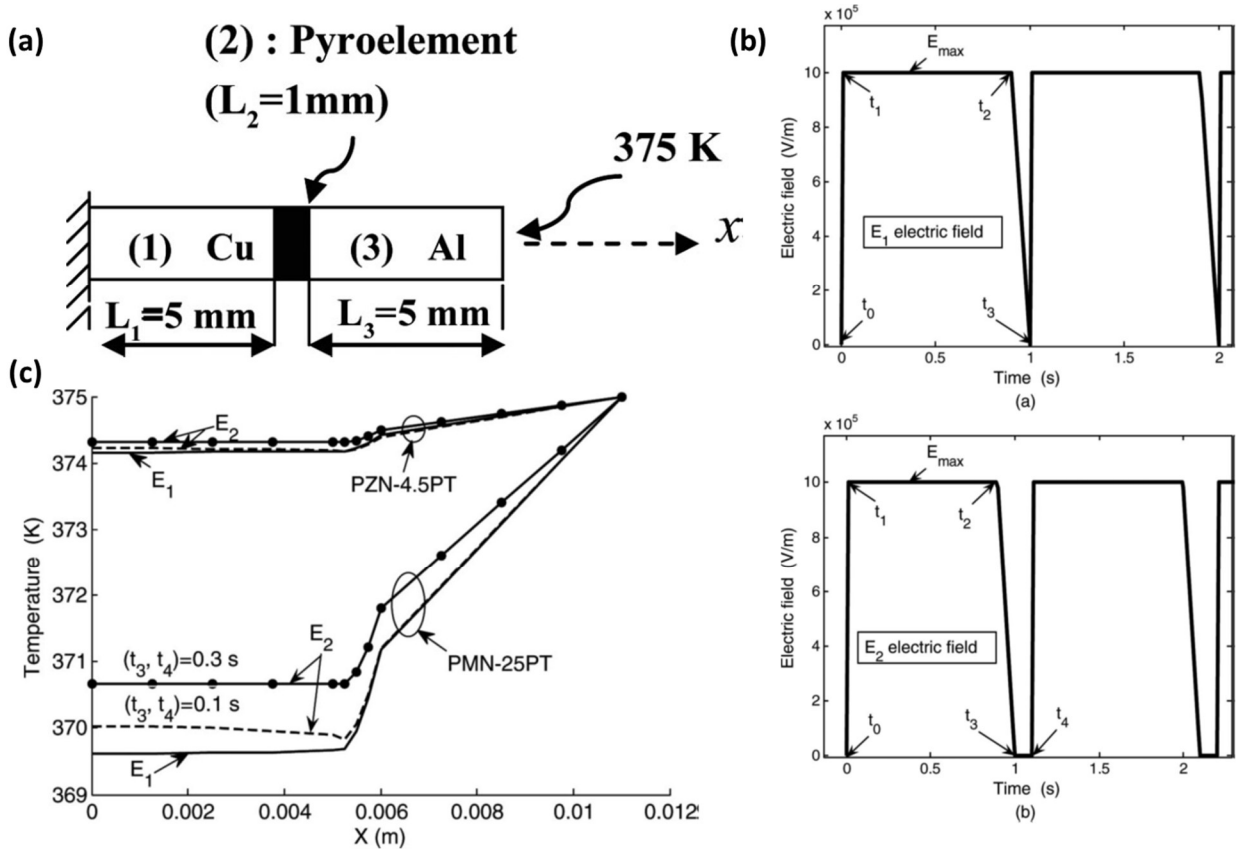


**Figure 1.50 (a). Solid-state cooling line, (b). Electric pulses applied on the EC element, (c). Temperature distribution along the cooling line for two different EC elements (PMN-25 PT and PMN-4.5PT)**[134]

Some recently reported EC-based devices and their cooling performance along with their working principle have been summarized in Table 1.7.

**Table 1.7 Several reported EC-based devices and working principle of directional heat flow**

| Working Principle | Energy Recovery Mechanism | Regeneration Factor $\Delta T/\Delta T_{EC}$ | COP | Cooling Power / Avg. Heat Flux ($mW/cm^2$) | Cooling Capacity (W/g, $W/cm^3$) | Efficiency (%) | Ref. |
|---|---|---|---|---|---|---|---|
| Liquid Crystal Thin Film Heat Switch | Cascade | - | - | - | - | 66 | Epstein, R. I. *et al* (2009)[109] |
| μECM with electrostatic Actuation | Cascade | - | 10 | 10,000 | - | - | Ju, Y. S. *et al* (2010)[127] |
| Solid-Solid Regeneration (without external regenerator) | Regeneration | 3.3 | 8 | - | 37 | 57 | Gu, H., *et al* (2013)[123,125] |
| Liquid based microscale electrostatic Refrigerator | Regeneration | - | - | 3000 | - | 31 | Guo, D. *et al.* (2014)[118] |
| Liquid Based Regenerator (Peristaltic Pump) | Regeneration | 3.7 | - | - | - | - | Plaznik, Uros. *et. al* (2015)[120] |
| Heat Switch Based Device | Cascade | - | - | 36 | - | 60 | Wang, Y. D. *et al* (2015) |
| TE based EC Cooler | Cascade | - | 1.54 | 8000 | - | - | Feng, D. *et al* (2016)[104] |
| Electromechanical Actuation | Multistage Cascade | 12.6/1.5 =10.5 | - | - | 2.34 W/g | - | Bradesko, A. *et. al.* (2016)[128] |
| Cooling with Electrostatic Actuation | Cascade | - | 13 | 29.7 | 2.8 | 6.1 | Ma, R. *et al.* (2017)[13] |
| Solid-state cooling line | - | 20/2=10 | - | - | - | 60 | S. F. Karmanenko, *et. al.* (2009)[28,132,133] |

## 1.6 Research Objectives

### 1.6.1 Objective # 1

For the characterization of ECM, both direct and indirect approaches have been used. Based the linear TD theory, they should result in the same EC coefficient for an ECM. However, as discussed above, they often result in very different EC coefficients. By the definition of ECE and phenomenological theory, the ECE can only be observed in the polar crystals (i.e., 10 point groups). However, strong ECE has been observed in ferroelectrics and even in the paraelectric phase. More interestedly, very promising ECE has been observed in RFEs.

For the thermodynamic theory currently used in the discussion of ECE, only linear coupling effects are considered. It would be important to include the nonlinear coupling effects in the discussion in order to explain the experimental results obtained in the studies of ECM. In chapter 2, nonlinear coupling effects will be included in the thermodynamic theory to exploit the reasons behind the high ECE in RFEs. So ECE has been determined for some typical normal FEs and RFEs by considering effect of *"nonlinear temperature dependence of the dielectric constant"* on the entropy change specially at higher fields.

### 1.6.2 Objective # 2

For the development of ECE-based devices, many different designs have been reported. One can find that the heat conduction in a multilayer structure along the thickness direction is the key to determine the performance of these devices. Unfortunately, all the reports are either conceptual or experimentally try and error. Analytical solution of the heat conduction in a multilayer structure would help to determine and optimize the performance of a design. In this study, the analytical solution for the heat conduction in a four-body structure is established. The solution includes the series with infinite terms, which would limit the application of the solution. A method to get the approximation of the solution is developed so that the numerical calculations can be conducted.

### 1.6.3 Objective # 3

Cooling devices with complete silent operation, without involving any moving body either ECM, or circulation of any fluids for regeneration, is an ultimate objective of EC refrigeration technology. Involvement of moving mechanisms adds the complexities in the system and in turn reduces the cooling power of the device.

Although a great progress has been made in the development of high-performance ECMs and several innovative designs of ECE-based devices have been conceptualized, analyzed and prototyped, there is not a design/ system of ECE-based cooling line that does not use other mechanisms (regenerating fluids, actuators for moving part, thermal diodes and technologies for heat switches). The usage of other mechanisms increases the complexity of the device and reduces their miniaturization capability along with other issue of thermal coupling and decoupling.

In this research, a fundamental issue of involvement of moving parts is addressed and a multilayer design of all-solid ECE-based cooling line is introduced. In this novel idea, double layers of ECM are sandwiched between sink and source, and no moving part or heat switch was used to find directional heat flow. The operation principle of the design is based on independent electric field applied on each ECM layer and a special pattern of the electric field on these two ECM layers. First the unsteady heat conduction problem of multilayer system of EC and sink/ source bodies has been solved analytically. Numeric calculation based on the analytical solution is carried out to determine the heat flow in the multilayer structure. It is demonstrated that the design can achieve a continuous heat flow along one direction without the involvement of any heat switches, thermal diodes, and fluidic regenerators. In this complete solid-state design, all parts are permanently intact with each other and are coupled thermally and no part moves during operation and heat pump works in complete silent mode. This design can help in miniaturization and increases reliability.

### 1.6.4 Objective # 4

Most of the typical ECE-based devices reported in the literature are either prototypes or are FEA-based thermal analysis, so the performance is mostly based on the experimental results or numerical simulations. The optimization of the devices requires that there must be some formulation so that devices can be designed for high efficiency and cooling power. An analytical solution is being devised that can be used to calculate the heat fluxes, temperature profiles and the time of thermal equilibrium for different thermal properties of EC, sink and source materials. During absorption of heat, the typical depolarized ECM is coupled with source on one side and there is air/ other material on the other side. On the other hand, during polarization, the ECM has now coupled with sink on one side and air/ other material on the other side to reject the heat. This scenario has been solved analytically for generalized initial conditions and for bodies with different thermal properties. The analytical solution is much versatile/ flexible to be used in most of the ECE-based device for the determination of relaxation time, temperature profiles and heat fluxes.

# Chapter 2 Electrocaloric-like Effect at High Electric Field

As discussed in SECTION 1.3.3.3, the extensive study of ECE and ECMs discovered that: 1) there is a great discrepancy in EC coefficient determined by direct and indirect approaches; 2) a great difference between the well-known pyroelectric coefficient and EC coefficient, although by physics these two should be the same, 3) strong ECE has been found in RFEs over a wide temperature range, although by physics and their structure, RFE should not have ECE.

For most of pyroelectric devices, the electric field involved is very weak. Therefore, the pyroelectric coefficient is usually characterized under low electric field even zero electric field, such as $dP_s/dT$. However, for the applications of ECE, a high electric field is required in order to achieve a high entropy change in ECM as described by Eqs. (1.12) and (1.14). That is, what is important for the application of ECE is the entropy change rather than the EC coefficient. Therefore, a high electric field is usually applied to achieve high ECE in the ferroelectric-based materials. Unfortunately, the dielectric response of ferroelectric-based materials is nonlinear: the related properties are dependent on the strength of electric field and even the history of the electric field. Therefore, it is interesting to study the contribution of the property's nonlinearity including nonlinear coupling effect on the experimental results, which is currently ignored in the study of ECE and ECM.

This chapter will establish the fundamentals for the influence of nonlinear properties on the ECE and use it to understand the discrepancies in the experimental results reported in the literatures.

## 2.1 Nonlinear Contribution to Temperature Change

Regarding nonlinear contribution to ECE, one was studied in classical book on ferroeletrics[136]. It is the nonlinear contribution to entropy due to the temperature dependence of permittivity, which can be determined by thermodynamics where only temperature dependence of the permittivity was considered. Permittivity is however is strongly dependent on both temperature and electric field. Here we will study the contribution of nonlinear and nonlinear coupling coefficients in the entropy change due to applied external electric field. Gibbs free energy offers a suitable selection of independent variables to define the nonlinear effects, and nonlinear coupling effect and even higher effect of external forces on a dielectric material.

$$
\begin{aligned}
G(E,T,X) = G_0 &+ \overbrace{\frac{1}{2}\varepsilon_{mn}^{T,X}E_mE_n + \frac{1}{2}\frac{C^{E,X}}{T}\Delta T^2 + \frac{1}{2}s_{\mu\upsilon}^{E,T}X_\mu X_\upsilon}^{linear\ principle\ effects} \\
&+ \overbrace{p_m^X E_m\Delta T + \alpha_\mu^E \Delta T X_\mu + d_{m\mu}^T E_m X_\mu}^{linear\ coupling\ effects} \\
&+ Z_{m\mu}D_m\Delta T X_\mu \\
&+ \overbrace{\frac{1}{3}\eta_{mnp}^{T,X}E_mE_nE_p + \frac{1}{3}\delta^{E,X}\Delta T^3 + \frac{1}{3}\varphi_{\mu\upsilon\xi}^{E,T}X_\mu X_\upsilon X_\xi}^{nonlinear\ effects} \\
&+ \overbrace{L_{mn}^X E_mE_n\Delta T + M_m^X E_m(\Delta T)^2 + N_\mu^E(\Delta T)^2X_\mu + O_{\mu\upsilon}^E\Delta T X_\mu X_\upsilon + R_{mn\mu}^T E_mE_nX_\mu + V_{m\mu\upsilon}^T E_mX_\mu X_\upsilon}^{nonlinear\ couling\ effects} \\
&+ \overbrace{\frac{1}{4}\lambda_{mnpq}^{T,X}E_mE_nE_pE_q + \frac{1}{4}\chi^{E,X}\Delta T^4 + \frac{1}{4}\psi_{\mu\upsilon\xi\lambda}^{E,T}X_\mu X_\upsilon X_\xi X_\lambda}^{highe\ \ order\ nonlinea\ \ effects}
\end{aligned}
\tag{2.1}
$$

Where $\eta_{mnp}^{T,X}$, $L_{mn}^X$, $\lambda_{mnpq}^{T,X}$, $\lambda_{mnpq}^{T,X}$, $M_m^X$, $\delta^{E,X}$, $\chi^{E,X}$, $\lambda_{mnpq}^{T,X}$, and $\psi_{\mu\upsilon\xi\lambda}^{E,T}$ all are material properties (see Appendix - F). From the Eq. (2.1), the constitutive equations of electric field, strain and entropy are derived as,

$$
\begin{aligned}
D_m = \left(\frac{\partial G(E,T,X)}{\partial E_m}\right)_{T,X} &= \varepsilon_{mn}^{T,X}E_n + p_m^X\Delta T + d_{m\mu}^T X_\mu + Z_{m\mu}\Delta T X_\mu + \eta_{mnp}^{T,X}E_nE_p + 2L_{mn}^X E_n\Delta T + M_m^X(\Delta T)^2 \\
&+ 2R_{mn\mu}^T E_nX_\mu + V_{m\mu\upsilon}^T X_\mu X_\upsilon + \lambda_{mnpq}^{T,X}E_nE_pE_q
\end{aligned}
\tag{2.2}
$$

$$
\begin{aligned}
x_\mu = \left(\frac{\partial G(E,T,X)}{\partial X_\mu}\right)_{E,T} &= s_{\mu\upsilon}^{E,T}X_\upsilon + \alpha_\mu^E\Delta T X_\mu + d_{m\mu}^T E_m + Z_{m\mu}E_m\Delta T + \varphi_{\mu\upsilon\xi}^{E,T}X_\upsilon X_\xi + N_\mu^E(\Delta T)^2 \\
&+ 2O_{\mu\upsilon}^E\Delta T X_\upsilon + R_{mn\mu}^T E_mE_n + 2V_{m\mu\upsilon}^T E_mX_\upsilon + \psi_{\mu\upsilon\xi\lambda}^{E,T}X_\upsilon X_\xi X_\lambda
\end{aligned}
\tag{2.3}
$$

$$
\begin{aligned}
S = \left(\frac{\partial G(E,T,X)}{\partial T}\right)_{E,X} &= \frac{C^{E,X}}{T}\Delta T + p_m^X E_m + \alpha_\mu^E X_\mu + Z_{m\mu}E_mX_\mu + \delta^{E,X}\Delta T^2 + L_{mn}^X E_mE_n + 2M_m^X D_m(\Delta T) \\
&+ 2N_\mu^E(\Delta T)X_\mu + O_{\mu\upsilon}^E\Delta T X_\mu X_\upsilon + \chi^{E,X}\Delta T^3
\end{aligned}
\tag{2.4}
$$

Most of the nonlinear, nonlinear coupling and higher order effects are either not available or observed extremely weak, so most of the effects will not be considered making a major contribution to the entropy upon the application of external electric filed. Two nonlinear effects,

however, are strong enough that need to be considered while the characterization of ECE in dielectric materials. These effects are

$$L_{mn}^{X} = \left(\frac{\partial^3 G}{\partial E_m \partial E_n \partial T}\right)_X = \frac{\partial}{\partial T}\left(\frac{\partial^2 G}{\partial E_m \partial E_n}\right)_X = \frac{\partial}{\partial T}\left(\frac{\partial D_m}{\partial E_n}\right)_X = \left(\frac{\partial \varepsilon_{mn}^{T,X}}{\partial T}\right)_X$$

$$\eta_{mnp}^{X,T} = \left(\frac{\partial^3 G}{\partial E_m \partial E_n \partial E_p}\right)_{X,T} = \frac{\partial}{\partial E_p}\left(\frac{\partial^2 G}{\partial E_m \partial E_n}\right)_{X,T} = \frac{\partial}{\partial E_p}\left(\frac{\partial^2 D_m}{\partial E_n}\right)_{X,T} = \left(\frac{\partial \varepsilon_{mn}^{T,X}}{\partial E_p}\right)_{X,T}$$

Where $L_{mn}^{X}$ and $\eta_{mnp}^{X,T}$ are temperature and electric field dependence of permittivity, respectively. As we have discussed in detail in Chapter 1 that the EC characterization may be performed using *clamped and free* conditions. From engineering point of view, constant stress conditions are easier to achieve and most of EC characterization of ECMs has been reported for constant stress conditions. These conditions offer an ease in mathematical complication and scientific understanding of the phenomenon. So, it is inevitable to determine the nonlinear electric field dependence of entropy on constant stress conditions so that this nonlinear part may be studied in comparison with the reported results.

At constant stress condition $\left(dX_\mu = 0\right)$, elastic Gibbs energy may be the suitable choice to start with. Recalling elastic Gibbs energy (Table 1.2)

$$dG_1(T, D_m) = -SdT + E_m dD_m \tag{2.5}$$

where $D_m = \varepsilon_{mn}^{T,X} E_n$

The relation of the electric displacement and electric field are given as,

$$D_m(E_n, T) = \varepsilon_{mn}^{T,X}(E_n, T) E_n$$

Above relation in differential form may be written as,

$$dD_m(E_n, T) = \varepsilon_{mn}^{T,X} dE_n + E_n d\varepsilon_{mn}^{T,X} \tag{2.6}$$

For nonlinear dielectrics, permittivity is a strong function of temperature and electric field, so

$$d\varepsilon_{mn}^{T,X}(E_n, T) = \left(\frac{\partial \varepsilon_{mn}^{T,X}}{\partial E_n}\right)_T dE_n + \left(\frac{\partial \varepsilon_{mn}^{T,X}}{\partial T}\right)_E dT \tag{2.7}$$

Putting Eq. (2.7) in (2.6) gives,

$$dD_m = \varepsilon_{mn}^{T,X} dE_n + E_n \left(\frac{\partial \varepsilon_{mn}^{T,X}}{\partial E_n}\right)_T dE_n + E_n \left(\frac{\partial \varepsilon_{mn}^{T,X}}{\partial T}\right)_E dT$$

Using the above relation in Eq. (2.5), we have

$$dG_1(T,E_m) = -SdT + E_m\varepsilon_{mn}^{T,X}dE_n + E_mE_n\left(\frac{\partial\varepsilon_{mn}^{T,X}}{\partial T}\right)_E dT + E_mE_n\left(\frac{\partial\varepsilon_{mn}^{T,X}}{\partial E_n}\right)_T dE_n \tag{2.8}$$

Elastic free energy is an exact differential (i.e., the order of differentiation does not matter), so

$$\left(\frac{\partial}{\partial T}\left(\frac{\partial G_1}{\partial E_n}\right)_T\right)_E = \left(\frac{\partial}{\partial E_n}\left(\frac{dG_1}{\partial T}\right)_E\right)_T \tag{2.9}$$

Differentiating Eq. (2.8) with respect to $E_n$ at constant *T,* and then with respect to *T* at constant electric field, we get

$$\left(\frac{\partial G_1}{\partial E_n}\right)_T = \varepsilon_{mn}^{T,X}E_m + E_mE_n\left(\frac{\partial\varepsilon_{mn}^{T,X}}{\partial E_n}\right)_T$$

$$\left(\frac{\partial}{\partial T}\left(\frac{\partial G_1}{\partial E_n}\right)_T\right)_E = E_m\left(\frac{\partial\varepsilon_{mn}^{T,X}}{\partial T}\right)_E + E_mE_n\frac{\partial}{\partial T}\left(\frac{\partial\varepsilon_{mn}^{T,X}}{\partial E_n}\right)_T \tag{2.10}$$

Differentiating Eq. (2.8) again by changing the order of differentiation, we get

$$\left(\frac{\partial G_1}{\partial T}\right)_E = -S + E_mE_n\left(\frac{\partial\varepsilon_{mn}^{T,X}}{\partial T}\right)_E$$

$$\left(\frac{\partial}{\partial E_n}\left(\frac{\partial G_1}{\partial T}\right)_E\right)_T = -\left(\frac{\partial S}{\partial E_n}\right)_T + 2E_m\left(\frac{\partial\varepsilon_{mn}^{T,X}}{\partial T}\right)_E + E_mE_n\frac{\partial}{\partial E_n}\left(\frac{\partial\varepsilon_{mn}^{T,X}}{\partial T}\right)_E \tag{2.11}$$

Putting Eqs. (2.10) and (2.11) in Eq.(2.9), we get

$$E_m\left(\frac{\partial\varepsilon_{mn}^{T,X}}{\partial T}\right)_E + E_mE_n\frac{\partial}{\partial T}\left(\frac{\partial\varepsilon_{mn}^{T,X}}{\partial E_n}\right)_T = -\left(\frac{\partial S}{\partial E_n}\right)_T + 2E_m\left(\frac{\partial\varepsilon_{mn}^{T,X}}{\partial T}\right)_E + E_mE_n\frac{\partial}{\partial E_n}\left(\frac{\partial\varepsilon_{mn}^{T,X}}{\partial T}\right)_E$$

$$\left(\frac{\partial S}{\partial E_n}\right)_T = E_m\left(\frac{\partial\varepsilon_{mn}^{T,X}}{\partial T}\right)_E \tag{2.12}$$

Where $\varepsilon_{mn}^{T,X} = \varepsilon_0\varepsilon_{r}{}_{mn}^{T,X}$ is permittivity matrix of the dielectric material and its dependence on temperature is also a material property as discussed above. Similarly, for constant strain condition, which is more suitable for theoretical studies, the nonlinear electric field dependence of entropy may be given as,

$$\left(\frac{\partial S}{\partial E_n}\right)_T = E_m\left(\frac{\partial\varepsilon_{mn}^{T,x}}{\partial T}\right)_E \tag{2.13}$$

For a piezoelectric material, the relationship between two values of permittivity can be determined and has been reported in the literature[31,42] as $\varepsilon_{mn}^{x,T} - \varepsilon_{mn}^{X,T} = -d_{m\mu}^{T} d_{m\nu}^{T} c_{\mu\nu}^{E,T}$. For nonlinear dielectrics, Eq. (2.12) and (2.13) hold and the term on the right hand side cannot be considered as constant for integration. That term changes with electric field and becomes evident at higher electric fields. This phenomenon can be observed in any materials irrespective of crystal structure. As in EC characterization, the higher electric fields are involved, so the entropy change may happen even in the non-polar (paraelectric) phase. We may name this entropy change as "apparent/new entropy change" unlike the real entropy change due to EC effect. In RFEs, this can be a strong contribution, so in this research, this entropy change has been addressed and nonlinear electric field dependence of entropy change for few RFEs has been determined as case study and to address the issue of disagreement in direct and indirect methods.

For nonlinear dielectrics Eq. (2.12) may be integrated as,

$$\Delta S_{iso} = \int_0^E \left(\frac{\partial \varepsilon_{mn}^{T,X}}{\partial T}\right)_{X,E} dE_m \tag{2.14}$$

And for nonlinear dependence of the ECE may be determined as,

$$\Delta T = -\int_0^E \frac{T}{C^{E,X}} \left(\frac{\partial \varepsilon_{mn}^{T,X}}{\partial T}\right)_{X,E} E_m dE_n \tag{2.15}$$

Use the similar process, the results for constant strain condition are obtained as,

$$\Delta S = \int_0^E \left(\frac{\partial \varepsilon_{mn}^{T,x}}{\partial T}\right)_{x,E} E_m dE_n \tag{2.16}$$

And for nonlinear dependence of the ECE may be determined as,

$$\Delta T = -\int_0^E \frac{T}{C^{E,x}} \left(\frac{\partial \varepsilon_{mn}^{T,x}}{\partial T}\right)_{x,E} E_m dE_n \tag{2.17}$$

It has to be mentioned that for linear dielectrics, we may integrate Eq. (2.13) to get,

$$S(E,T) = S_0(T) + \frac{1}{2}\left(\frac{\partial \varepsilon_{mn}^{T,x}}{\partial T}\right)_{E} E_m E_n \tag{2.18}$$

This is the exactly what was reported in literature[137]. That is, in the literature only nonlinear term for Gibbs energy was considered is the temperature dependence of permittivity for linear dielectrics. Where $S_0(T)$ is the entropy of the materials under zero electric field that is only dependent on the temperature. According to above relation, if the permittivity of a dielectric

material increases with temperature, the application of external electric field results in the increase of the entropy of the material and heating will occur, whereas on the other hand if the permittivity decreases with increasing temperature, then the cooling will happen in the dielectric material upon the application external electric field. Eq. (2.18) shows the nonlinear electric field dependence of the entropy of a dielectric material, i.e., depends on the square of the electric field applied.

As mentioned in SECTION 1.2 that the ECMs are ferroelectrics and mostly are nonlinear ferroelectric (i.e. RFEs). For ferroelectrics which are nonlinear in nature, it is highly complicated and cumbersome to include the higher terms and to find the symmetries of all the tensors involved, so it can be achieved by using the physical approximations[44]. For nonlinear ferroelectrics, the relation between electric displacement, saturation polarization and electric field has been determined as,

$$D(E,T) = P_S(T)\tanh(k|E|) \tag{2.19}$$

where $P_S(T)$ is the saturation polarization, and $k$ is a constant, and is dependent on the temperature. In general, k should decrease with increasing $T$. Based on the results from orientation effect described by Langevin function[138], here we assume that $k = a/T$, $a$ is independent of $T$. Depending on the nature of the material, here we may adopt two approaches based on the definition of the permittivity as given in (2.20) and (2.21). Also in this section, we will just skip the tensorial representation for convenience.

The permittivity for linear dielectric where DC bias does not affect the permittivity is defined as,

$$\begin{aligned} \varepsilon^{T,X}(E,T) &= \frac{dD(E,T)}{dE} = \frac{\Delta D(E,T)}{\Delta E} = \frac{D}{E} \\ &\cong \frac{dP(E,T)}{dE} = \frac{\Delta P(E,T)}{\Delta E} = \frac{P}{E} \end{aligned} \tag{2.20}$$

The permittivity for nonlinear dielectrics where DC bias does affect the permittivity is defined either way as given in Eq. (2.21) or (2.22). Both are different,

$$\begin{aligned} \varepsilon^{T,X}(E,T) &= \frac{D(E,T)}{E} \neq \frac{dD(E,T)}{dE} \\ &\cong \frac{P(E,T)}{E} \neq \frac{dP(E,T)}{dE} \end{aligned} \tag{2.21}$$

$$\varepsilon^{T,X}(E,T) = \frac{dD(E,T)}{dE} \neq \frac{D(E,T)}{E}$$
$$\cong \frac{dP(E,T)}{dE} \neq \frac{P(E,T)}{E} \tag{2.22}$$

### 2.1.1 First Approach

Using Eq. (2.19) and (2.21), we have

$$\varepsilon^{T,X}(E,T) = P_S(T)\frac{\tanh\left(\frac{a}{T}|E|\right)}{E} \tag{2.23}$$

For electric field approaching zero, the only temperature dependence of the permittivity may be determined as follows,

$$\varepsilon^{T,X}(T) = \lim_{E\to 0} P_S(T)\frac{\tanh\left(\frac{a}{T}|E|\right)}{E}$$
$$\varepsilon^{T,X}(T) = P_S(T)\frac{a}{T}$$
$$\frac{T\cdot\varepsilon^{T,X}(T)}{a} = P_S(T) \tag{2.24}$$

Using (2.24) in (2.19), we have

$$D(E,T) = \frac{T\cdot\varepsilon^{T,X}(T)}{a} tanh\left(\frac{a}{T}|E|\right) \tag{2.25}$$

Mathematical relation for temperature dependence of permittivity has been given by several researchers based on different models.

#### 2.1.1.1 Temperature Dependence of Permittivity

The relation for temperature dependence of permittivity given by Cheng *et. al.*[86] is being used here.

$$\varepsilon^{X,T}(T) = \varepsilon_0 \exp(\alpha - \beta T) \tag{2.26}$$

Where α and β are constants, that can be determined by curve fitting of temperature dependence of permittivity.

Using (2.26) in (2.24), we get the relation

$$P_S(T) = \frac{\varepsilon_0 T}{a} \exp(\alpha - \beta T) \tag{2.27}$$

Putting value of $P_s(T)$ in Eq. (2.23), we have

$$D(E,T) = \varepsilon_0 \frac{T}{a} \tanh\left(\frac{a}{T}|E|\right) \exp(\alpha - \beta T) \tag{2.28}$$

Using (2.28) in Eq. (2.23) becomes, , we get,

$$\varepsilon^{T,X}(E,T) = \frac{D(E,T)}{E} = \frac{\varepsilon_0}{aE} T \tanh\left(\frac{a}{T}|E|\right) \exp(\alpha - \beta T) \tag{2.29}$$

Eq. (2.29) represents the electric field and temperature dependence of permittivity for nonlinear dielectrics and may be used to determine the entropy and temperature change in the dielectric materials on higher electric fields.

Now differentiating Eq. (2.29) with respect to T at constant electric field, we get

$$\left(\frac{\partial \varepsilon^{T,X}(E,T)}{\partial T}\right)_E = \varepsilon_0 \exp(\alpha - \beta T)\left[\frac{1-\beta T}{a\mathrm{E}} \tanh\left(\frac{a}{T}|E|\right) - \frac{1}{T}\mathrm{sech}^2\left(\frac{a}{T}|E|\right)\right] \tag{2.30}$$

Recalling Eq. (2.12), and considering only scalar form

$$\left(\frac{\partial S}{\partial E}\right)_T = E\left(\frac{\partial \varepsilon^{T,X}}{\partial T}\right)_E \tag{2.31}$$

$$\Delta S = \int_0^E \varepsilon_0 \exp(\alpha - \beta T)\left[\frac{1-\beta T}{a\mathrm{E}} \tanh\left(\frac{a}{T}|E|\right) - \frac{1}{T}\mathrm{sech}^2\left(\frac{a}{T}|E|\right)\right] E dE \tag{2.32}$$

Using (2.32) in Eq. (2.15), we have

$$\Delta T = -\frac{\varepsilon_0 T}{C^{E,X}} \exp(\alpha - \beta T) \int_0^E \left[\frac{1-\beta T}{a} \tanh\left(\frac{a}{T}|E|\right) - \frac{E}{T}\mathrm{sech}^2\left(\frac{a}{T}|E|\right)\right] dE \tag{2.33}$$

Integrating (2.33), we have,

$$\begin{aligned}\Delta T = \frac{\varepsilon_0 T}{C^{E,X}} \exp(\alpha - \beta T)\Bigg[&\frac{1-\beta T}{a}\left(\frac{T}{a}\ln\left[\cosh\left(\frac{a}{T}|E|\right)\right]\right) \\ &- \frac{1}{T}\left(\frac{T}{a}E\tanh\left(\frac{a}{T}|E|\right) - \frac{T^2}{a^2}\ln\left[\cosh\left(\frac{a}{T}|E|\right)\right]\right)\Bigg]\end{aligned} \tag{2.34}$$

Manipulating (2.34), the relation for nonlinear contribution to temperature change due to applied electric field is derived as,

$$\Delta T = \frac{\varepsilon_0 T}{C^{E,X}} \exp(\alpha - \beta T) \frac{1}{a^2} \left[ 2T \ln\left[\cosh\left(\frac{a}{T}E\right)\right] - \beta T^2 \ln\left[\cosh\left(\frac{a}{T}E\right)\right] - aE \tanh\left(\frac{a}{T}E\right)\right] \tag{2.35}$$

### 2.1.1.2 Temperature Dependence of Static Permittivity

In literature, sometimes the static permittivity is reported. The temperature dependence of the static permittivity[85,86,139] has been reported in literature as,

$$\varepsilon_S^{X,T}(T) = \frac{1}{T} \exp[\alpha' - \beta'(T - 273.15)] \tag{2.36}$$

Where $\alpha'$ and $\beta'$ are constant and their value can be found in the literature or determined using the curve fitting. Now the relation for temperature and electric field dependence of dielectric displacement and permittivity will change as shown in Eqs. (2.37) and (2.38) respectively.

$$D(E,T) = \varepsilon_0 \frac{1}{a} \tanh\left(\frac{a}{T}|E|\right) \exp[\alpha' - \beta'(T - 273.15)] \tag{2.37}$$

$$\varepsilon^{T,X}(E,T) = \frac{D(E,T)}{E} = \frac{\varepsilon_0}{aE} \tanh\left(\frac{a}{T}|E|\right) \exp[\alpha' - \beta'(T - 273.15)] \tag{2.38}$$

The above calculation may be repeated as follows,

Differentiating Eq. (2.38) with respect to T at constant electric field,

$$\left(\frac{\partial \varepsilon^{T,X}(E,T)}{\partial T}\right)_E = \varepsilon_0 \exp[\alpha' - \beta'(T - 273.15)] \left[ -\frac{\beta'}{a\mathrm{E}} \tanh\left(\frac{a}{T}|E|\right) - \frac{1}{T^2} \operatorname{sech}^2\left(\frac{a}{T}|E|\right)\right]$$

Using above relation in Eq. (2.31)

$$\Delta S = \int_0^E \varepsilon_0 \exp[\alpha' - \beta'(T - 273.15)] \left[ -\frac{\beta'}{a} \tanh\left(\frac{a}{T}|E|\right) - \frac{E}{T^2} \operatorname{sech}^2\left(\frac{a}{T}|E|\right)\right] dE \tag{2.39}$$

Integrating Eq. (2.39) in (2.15), we come to the relation for the temperature change as,

$$\Delta T = -\frac{\varepsilon_0 T}{C^{E,X}} \exp[\alpha' - \beta'(T - 273.15)] \left[ \frac{\ln\left[\cosh\left(\frac{a}{T}E\right)\right]}{a^2} - \frac{\beta' T}{a^2} \ln\left[\cosh\left(\frac{a}{T}E\right)\right] - \frac{E}{Ta} \tanh\left(\frac{a}{T}E\right) \right] \tag{2.40}$$

### 2.1.2 Second Approach

For nonlinear dielectrics, where DC bias does affect the permittivity is given by Eq. (2.22) as,

$$\varepsilon^{T,X} = \left(\frac{\partial D}{\partial E}\right)_{T,X}$$

#### 2.1.2.1 Temperature Dependence of Permittivity

Recalling Eq. (2.28),

$$D(E,T) = \varepsilon_0 \frac{T}{a} \tanh\left(\frac{a}{T}|E|\right) \exp[\alpha - \beta T]$$

Now the permittivity by the definition of Eq. (2.22) may be determined by differentiating above relation as follows,

$$\varepsilon^{T,X}(E,T) = \left(\frac{\partial D(E,T)}{\partial E}\right)_{T,X} = \varepsilon_0 \operatorname{sech}^2\left(\frac{a}{T}|E|\right) \exp[\alpha - \beta T] \tag{2.41}$$

Now differentiating Eq. (2.41) with respect to T

$$\left(\frac{\partial \varepsilon^{T,X}}{\partial T}\right)_E = \varepsilon_0 \left[ -\beta \exp[\alpha - \beta T] \operatorname{sech}^2\left(\frac{a}{T}|E|\right) + \frac{2aE}{T^2} \exp[\alpha - \beta T] \operatorname{sech}^2\left(\frac{a}{T}|E|\right) \tanh\left(\frac{a}{T}|E|\right) \right]$$

$$\left(\frac{\partial \varepsilon^{T,X}}{\partial T}\right)_E = \varepsilon_0 \exp[\alpha - \beta T] \left[ \frac{2aE}{T^2} \operatorname{sech}^2\left(\frac{a}{T}|E|\right) \tanh\left(\frac{a}{T}|E|\right) - \beta \operatorname{sech}^2\left(\frac{a}{T}|E|\right) \right] \tag{2.42}$$

Using the above relations in Eq. (2.31**)** and using the Eq. (2.15),

$$\Delta T = -\frac{\varepsilon_0 T}{C^{E,X}} \exp[\alpha - \beta T] \int_0^E \left[ \frac{2aE^2}{T^2} \operatorname{sech}^2\left(\frac{a}{T}|E|\right) \tanh\left(\frac{a}{T}|E|\right) - \beta E \operatorname{sech}^2\left(\frac{a}{T}|E|\right) \right] dE \tag{2.43}$$

Solving the above relation, we have

$$\Delta T = \frac{\varepsilon_0 T}{C^{E,X}} \exp[\alpha - \beta T] \left[ -\frac{2T \ln\left[\cosh\left(\frac{a}{T}|E|\right)\right]}{a^2} + \frac{\beta T^2 \ln\left[\cosh\left(\frac{a}{T}|E|\right)\right]}{a^2} - \frac{E^2 \operatorname{sech}^2\left(\frac{a}{T}|E|\right)}{T} + \frac{2E \tanh\left(\frac{a}{T}|E|\right)}{a} - \frac{\beta T E \tanh\left(\frac{a}{T}|E|\right)}{a} \right]$$

$$\Delta T = \frac{\varepsilon_0}{C^{E,X}} \exp[\alpha - \beta T] \frac{1}{a^2} \left[ -2T^2 \ln\left[\cosh\left(\frac{a}{T}|E|\right)\right] + \beta T^3 \ln\left[\cosh\left(\frac{a}{T}|E|\right)\right] - a^2 E^2 \operatorname{sech}^2\left(\frac{a}{T}|E|\right) + 2aTE \tanh\left(\frac{a}{T}|E|\right) - a\beta T^2 E \tanh\left(\frac{a}{T}|E|\right) \right] \tag{2.44}$$

#### 2.1.2.2 Temperature Dependence of Static Permittivity

Recalling Eq. (2.37)

$$D(E,T) = \varepsilon_0 \frac{1}{a} \tanh\left(\frac{a}{T}|E|\right) \exp[\alpha' - \beta'(T - 273.15)]$$

Differentiating with $E$ we have,

$$\varepsilon^{T,X}(E,T) = \left(\frac{\partial D(E,T)}{\partial E}\right)_{T,X} = \varepsilon_0 \frac{1}{T} \operatorname{sech}^2\left(\frac{a}{T}|E|\right) \exp[\alpha' - \beta'(T - 273.15)] \tag{2.45}$$

Differentiating with T, the above relation becomes

$$\left(\frac{\partial \varepsilon^{T,X}(E,T)}{\partial T}\right)_E = \varepsilon_0 \exp[\alpha' - \beta'(T - 273.15)] \left[ -\frac{\operatorname{sech}^2\left(\frac{a}{T}|E|\right)}{T^2} - \frac{\beta' \operatorname{sech}^2\left(\frac{a}{T}|E|\right)}{T} + \frac{2aE \operatorname{sech}^2\left(\frac{a}{T}|E|\right) \tanh\left(\frac{a}{T}|E|\right)}{T^3} \right] \tag{2.46}$$

Using the above relations in Eq. (2.31**)**, and using the relation (2.15),we get

$$\Delta T = -\frac{\varepsilon_0 T}{C^{E,X}} \exp[\alpha' - \beta'(T - 273.15)] \int_0^E \left[ -\frac{E\ \operatorname{sech}^2\left(\frac{a}{T}|E|\right)}{T^2} - \frac{\beta' E \operatorname{sech}^2\left(\frac{a}{T}|E|\right)}{T} + \frac{2aE^2 \operatorname{sech}^2\left(\frac{a}{T}|E|\right) \tanh\left(\frac{a}{T}|E|\right)}{T^3} \right] dE$$

$$\Delta T = -\frac{\varepsilon_0}{T^2 C^{E,X}} \exp[\alpha' - \beta'(T - 273.15)] \int_0^E \left[ -T\ E \operatorname{sech}^2\left(\frac{a}{T}|E|\right) - T^2 \beta' E \operatorname{sech}^2\left(\frac{a}{T}|E|\right) + 2aE^2 \operatorname{sech}^2\left(\frac{a}{T}|E|\right) \tanh\left(\frac{a}{T}|E|\right) \right] E dE$$

After integrating, we get

$$\begin{aligned} \Delta T = -\frac{\varepsilon_0}{T^2 C^{E,X}} & \exp[\alpha' - \beta'(T - 273.15)] \\ & \times \left[ -\frac{T^3 \ln\left[\cosh\left(\frac{a}{T}|E|\right)\right]}{a^2} + \frac{\beta' T^4 \ln\left[\cosh\left(\frac{a}{T}|E|\right)\right]}{a^2} \right. \\ & - TE^2 \operatorname{sech}^2\left(\frac{a}{T}|E|\right) + \frac{T^2 E \tanh\left(\frac{a}{T}|E|\right)]}{a} \\ & \left. - \frac{\beta' T^3 \mathrm{E} \tanh\left(\frac{a}{T}|E|\right)}{a} \right] \end{aligned} \tag{2.47}$$

Eqs. (2.35), (2.40), (2.44) and (2.47) may be used to determine the nonlinear contribution to the ECE depending on the nature of the dielectric material and the permittivity being measured. In these equations, the constants may be determined from the experimental data like PE loops and from temperature dependence of permittivity graph.

### 2.1.3 Determination of Constants *a*, α and β

The constants *a*, α and β in Eqs. (2.35), (2.40), (2.44) and (2.47) are determined using the experimental data. Unfortunately, the constant *"a"* may not be determined analytically using (2.25), this value, however, can be approximated using PE loops as shown in Figure 2.10.

The constants *a* can be determined using the D and $P_S$ values from PE loops of the dielectric materials at different temperatures. Whereas the constant α and β are determined from the temperature dependence of permittivity graph by curve fitting as shown in Figure 2.2.

Recalling Eq. (2.23)

$$\varepsilon^{X,T}(T) = \varepsilon_0 \exp(\alpha - \beta T)$$

Taking natural log of the above equation

$$\ln\left(\varepsilon^{X,T}(T)\right) = \ln \varepsilon_0 + \alpha - \beta T \tag{2.48}$$

Eq. (2.48) is an equation of straight line, so from the $\ln\left(\varepsilon^{X,T}(T)\right)$ vs T graph, the values of α and β can be determined using curve fitting as β represents the slope of the line and the term $\ln \varepsilon_0 + \alpha$ is y-intercept.

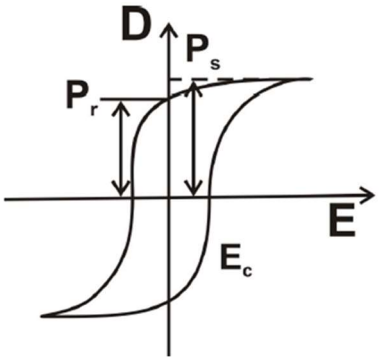


**Figure 2.1 Typical PE loop to determine D and $P_S$**

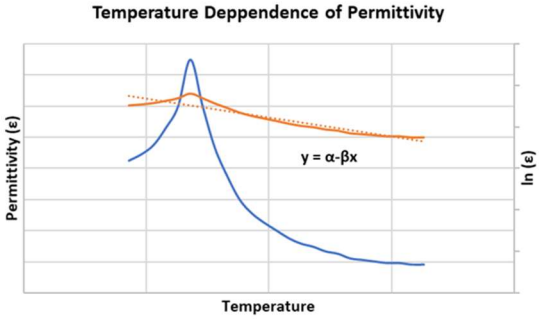


**Figure 2.2 Determination of α and β by curve fitting**

### 2.1.4 Case Study-I (BST)

To determine the nonlinear contribution towards ECE, a case study is being carried out to understand the discrepancies of direct and indirect methods. In BST material a huge difference in the directly measured and deduced ECE from Maxwell relations has been reported[67] as shown in Figure 2.3. The formulation derived above will used to determine the nonlinear contribution to ECE which is neglected in the derivation of the indirect relations as discussed in Chapter 1. The constants are determined from the experimental data reported in the article and the ΔT due to nonlinear effects will be calculated. The article has reported four different compositions of $Ba_{1-x}Sr_xTiO_3$ (BST), but in this work we have just taken composition bases on x = 0.25 to validate our theory and formulation.

#### 2.1.4.1 Determination of Constant *"a"* using PE Loops

Using the relation,

$$D(E,T) = P_S(T) \tanh\left(\frac{a}{T}|E|\right)$$

$$a = \frac{T}{E}\tanh^{-1}\left(\frac{D}{P_S}\right) \tag{2.49}$$

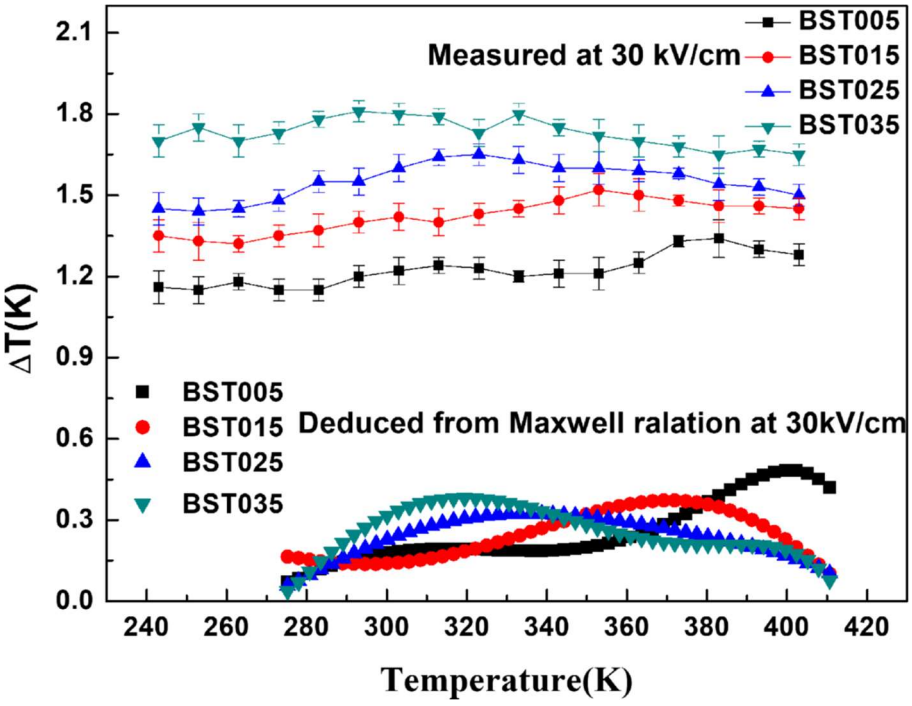


**Figure 2.3 Comparison of directly and indirectly measured ECE for BST**[67]

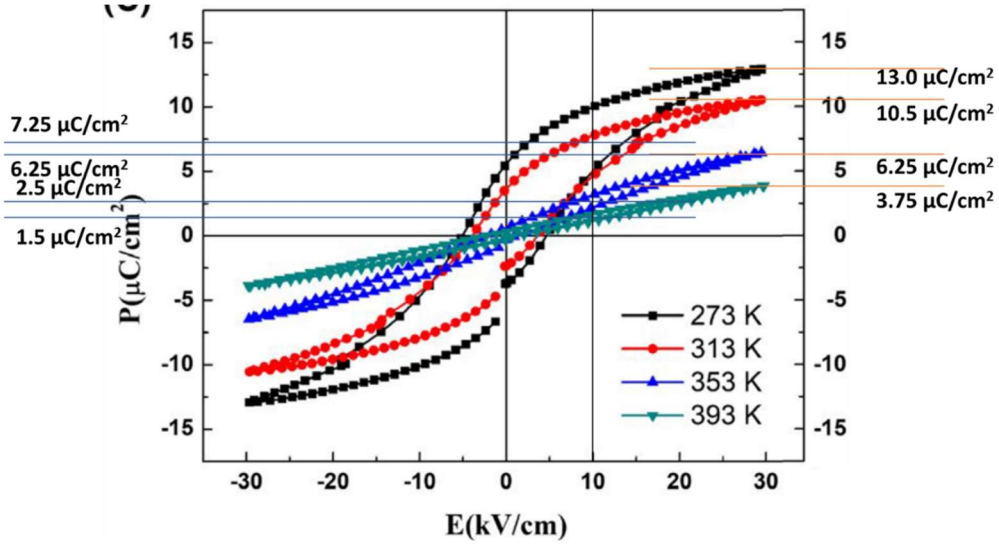


**Figure 2.4 PE loops of BST for *(x = 0.25);* approximated values for D and Ps**[67]

The values of "*a*" is calculated using the PE loops shown in Figure 2.4 and the relation given in Eq. (2.49).

**Table 2.1 Calculating *"a"* at electric field 10 kV/cm (1x10$^6$ V/m), 1μC/cm$^2$ = 10$^{-2}$ C/m$^2$**

| T(K) | D (E, T) / P (E, T) (C/m$^2$) | $P_s$(T) (C/m$^2$) | $a$ |
|---|---|---|---|
| 273 | 0.0725 | 0.13 | 0.000172 |
| 313 | 0.0625 | 0.105 | 0.000215 |
| 353 | 0.025 | 0.0625 | 0.000150 |
| 393 | 0.015 | 0.0375 | 0.000166 |

### 2.1.4.2 Determination of Constants α and β

The constants α and β can be determined from the temperature dependence of permittivity graphs shown in Figure 2.5 by curve fitting. The data has been extracted from the Figure 2.5 for Extracting BST025 (i.e. x = 0.25) and the curve fitting is shown in Figure 2.6.

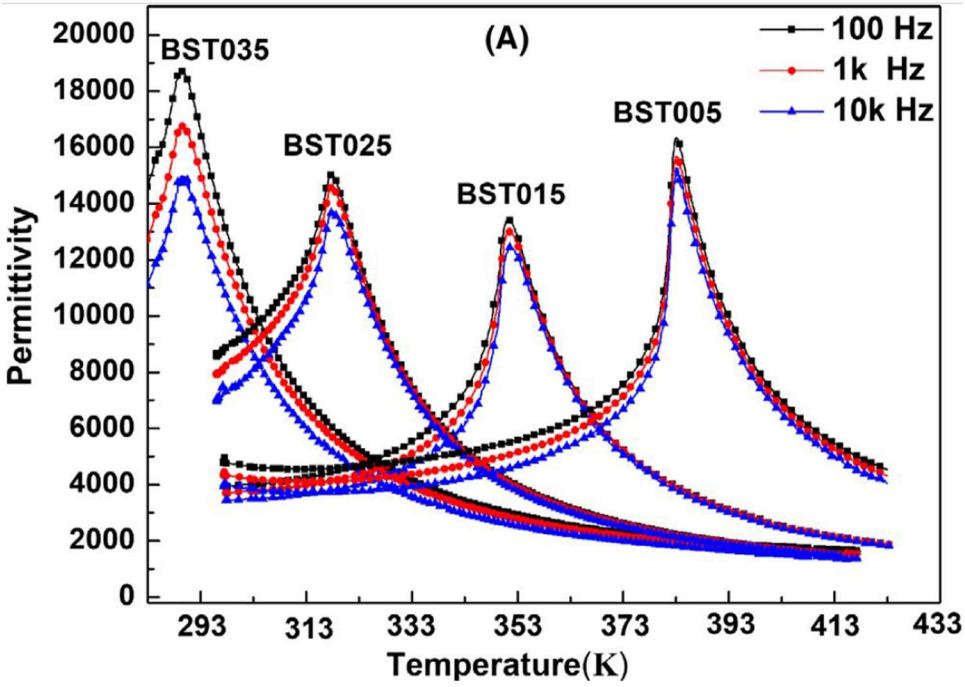


**Figure 2.5 Temperature dependence of permittivity for four compositions of BST**[67]

Using the relation for temperature dependent permittivity as

$$\varepsilon^{X,T}(T) = \exp(\alpha - \beta T)$$

$$\ln\left(\varepsilon^{X,T}(T)\right) = \alpha - \beta T$$

From the curve fitting shown in Figure 2.6, we have

$$\alpha = 14.921 \;\&\; \beta = 0.0185K^{-1}$$

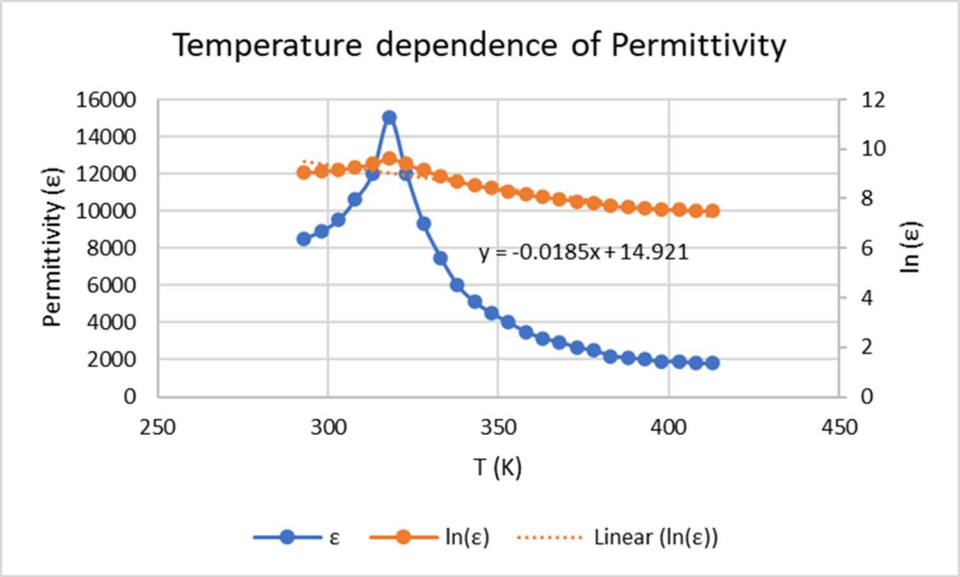


**Figure 2.6 Data deduced from experimental results to determine α and β by curve fitting**

### 2.1.4.3 Determination of ΔT Contribution due to Higher Fields

Using the definition of permittivity given in Eq. (2.21)

$$\varepsilon^{T,X}(E,T) = \frac{D(E,T)}{E}$$

$$\varepsilon^{T,X}(E,T) = \frac{\varepsilon_0}{aE} T \tanh\left(\frac{a}{T}|E|\right) \exp(\alpha - \beta T)$$

We have the relation

$$\Delta T = \frac{\varepsilon_0 T}{C^{E,X}} \exp(\alpha - \beta T) \frac{1}{a^2} \left[2T \ln\left[\cosh\left(\frac{a}{T}E\right)\right] - \beta T^2 \ln\left[\cosh\left(\frac{a}{T}E\right)\right] - aE \tanh\left(\frac{a}{T}E\right)\right]$$

**Table 2.2 Determination of ΔT using constants a, α and β for E = 3 MV/m (30 kV/cm**

| T (K) | $C^{E,X}$ (J/Kkg) | $a$ | $\frac{a}{T}E$ | ΔT (K) |
|---|---|---|---|---|
| 273 | 450 | 0.000172 | 1.888 | 0.93 |
| 313 | 450 | 0.000215 | 2.057 | 0.49 |
| 353 | 450 | 0.000150 | 1.271 | 0.34 |
| 393 | 450 | 0.000166 | 1.271 | 0.18 |

ΔT in Table 2.2 is the nonlinear contribution to the ECE. Now this value is compared to the directly and indirectly reported ECE to see the nonlinear effect that is ignored in the indirect formulation.

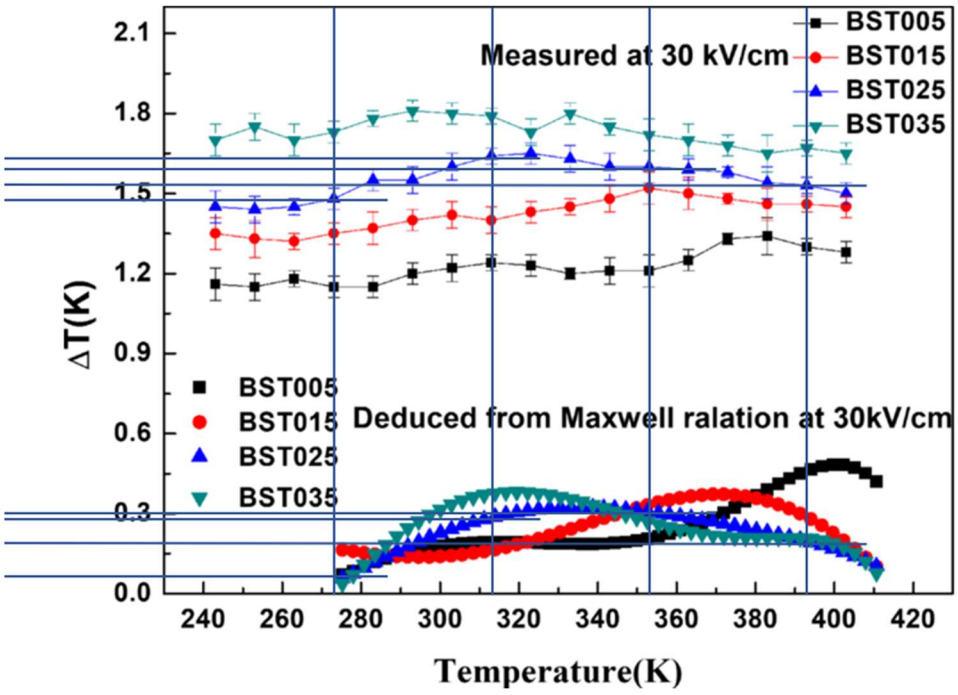


**Figure 2.7 Comparison of direct and indirect ECE measured at E = 30 kV/cm**[67]

The directly and indirectly measured ECE values extracted from the Figure 2.7 have been tabulated in Table 2.3 and are compared with the contribution to ΔT due to nonlinear effect.

**Table 2.3 Comparison of directly and indirectly measured ECE with nonlinear contribution to ΔT (BST025)**

| T (K) | $\Delta T_{direct}$ (K) | $\Delta T_{indirect}$ (K) | $\Delta T_{direct} - \Delta T_{indirect}$ (K) | ΔT (K) Nonlinear contribution (calculated) |
|---|---|---|---|---|
| 273 | 1.485 | 0.060 | 1.425 | 0.93 |
| 313 | 1.635 | 0.285 | 1.350 | 0.49 |
| 353 | 1.590 | 0.300 | 1.290 | 0.34 |
| 393 | 1.538 | 0.195 | 1.343 | 0.18 |

Figure 2.8 compares the directly and indirectly measured results with nonlinear contribution to ΔT due to temperature dependence of permittivity. It may be concluded from the comparison that the if we add calculated ΔT to the indirectly measured ECE, the results are closer to the directly measured values. It can be inferred from this analysis that the nonlinear effects have significant contribution and must be taken into account in the future EC measurements for a better agreement between direct and indirect results.

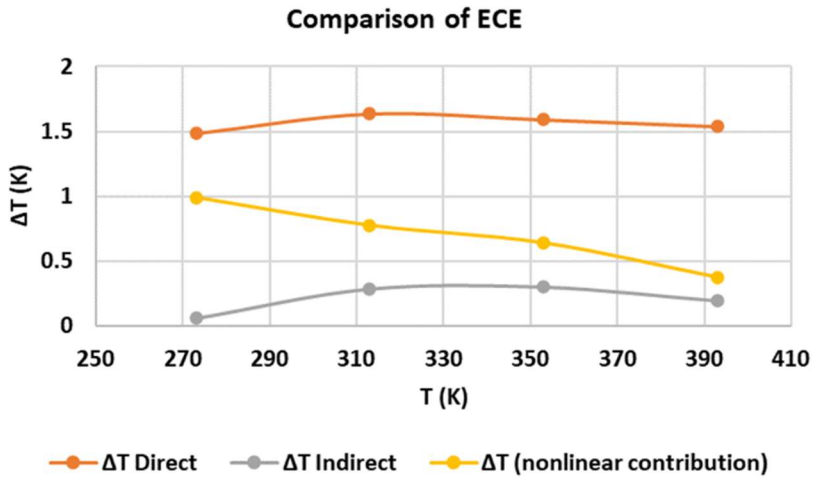


**Figure 2.8 Comparison of reported ECE and contribution to ECE due to nonlinear effect**

### 2.1.5 Case Study-II (PMN-0.1 PT)

Another case study was carried out to demonstrate the nonlinear contribution to temperature change (ΔT) and to find the origin of the difference between directly and indirectly determined ECE of PMN-0.1PT, and to compare the results with the formulation derived in our study. PMN-0.1PT is an RFE material and has been extensively studied for the application of EC cooling devices. Figure 2.9 compares the directly and indirectly measured ECE for PMN-0.1PT for the temperature range of 300 K to 400 K.

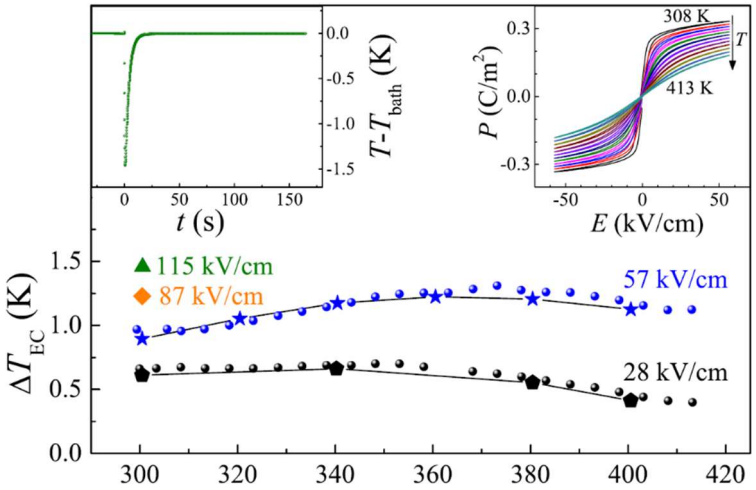


**Figure 2.9 Comparison of experimentally measured ECE in PMN-0.1PT by direct and indirect method: Solid blue and black dots represent indirect EC data, while stars or other shapes represent direct EC data**[120]

### 2.1.5.1 Determination of Constant *"a"* using PE Loops

This value of constant "*a"* may be approximated using PE loops as shown in Figure 2.10.

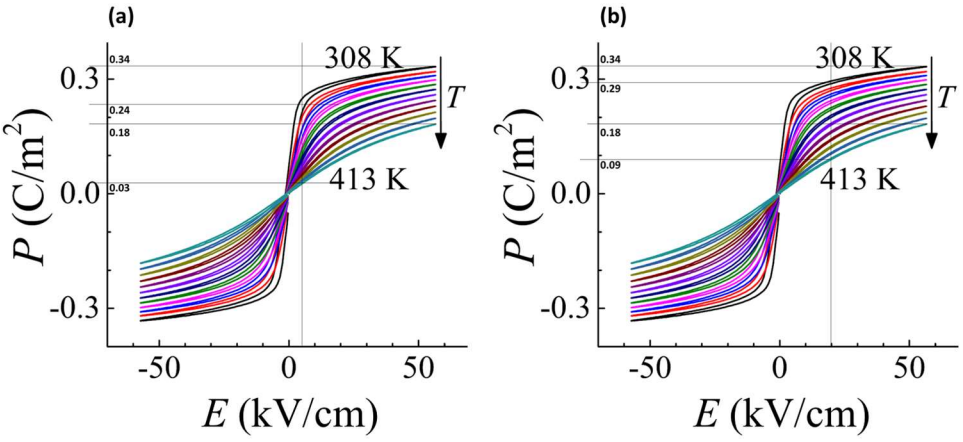


**Figure 2.10 PE loops of PMN-0.1PT[140], (a). P and $P_S$ at 0.5 kV/cm, (b). P and $P_S$ at 20 kV/cm**

From Figure 2.10[140] the values of P (or D) and $P_S$ are found for T =308 K and T=413 K for two different field E=5 kV/cm and 20 kV/cm as shown in Table 2.4. The value of $a$ has been calculated from the following relation where k has been approximated by k = a/T.

$$D(E,T) = P_S(T)\tanh\left(\frac{a}{T}|E|\right)$$

**Table 2.4 Approximation of constant *"a"* from PE loops of PMN-0.1PT using assumption k = a/T**

| Temperature | E (MV/m) | D (C/m²) | $P_S$(T)(C/m²) | $a$ |
|---|---|---|---|---|
| T = 308 K | 2 | 0.29 | 0.34 | 0.000195 |
| T= 413 K | 2 | 0.09 | 0.18 | 0.000113 |
| T = 308 K | 0.5 | 0.24 | 0.34 | 0.000541 |
| T= 413 K | 0.5 | 0.03 | 0.18 | 0.000139 |

In the Table 2.4, it may be noticed that there is a big difference in the values of $a$ determined at different temperatures and fields. It may be inferred that our assumption $k = a/T$ may not be accurate enough to represent variations of polarization with temperature and electric field accurately. We may make another assumption $k = a/T^2$. Based on this assumption, the value of $a$ is calculated again as shown in Table 2.5. It may be observed that the value of $a$ is better approximated and variations of $a$ values are small so $k = a/T^2$ is the much accurate assumption in this case.

**Table 2.5 Approximation of constant *"a"* from PE loops of PMN-0.1PT using assumption k = a/T²**

| Temperature | E (MV/m) | D (C/m²) | $P_S$(T)(C/m²) | $a$ |
|---|---|---|---|---|
| T = 308 K | 2 | 0.29 | 0.34 | 0.06 |
| T= 413 K | 2 | 0.09 | 0.18 | 0.05 |
| T = 308 K | 0.5 | 0.24 | 0.34 | 0.167 |
| T= 413 K | 0.5 | 0.03 | 0.18 | 0.057 |

The nonlinear contribution to ΔT for this assumption has been determined and in given in (2.51) and (2.52) for both definitions of permittivity ($\varepsilon^{T,X} = D(E,T)/E$ and $\varepsilon^{T,X} = \partial D(E,T)/\partial E$), respectively.

Using this assumption, now the relation (2.25) becomes.

$$D(E,T) = \frac{T^2 \cdot \varepsilon^{T,X}(T)}{a} \tanh\left(\frac{a}{T^2}|E|\right) \tag{2.50}$$

**From $\boldsymbol{\varepsilon^{T,X} = D(E,T)/E}$**

$$\Delta T = \frac{\varepsilon_0 T}{C^{E,X}} \exp(\alpha - \beta T) \frac{1}{a^2}\left[3T^2 \ln\left[\cosh\left(\frac{a}{T^2}E\right)\right] - \beta T^3 \ln\left[\cosh\left(\frac{a}{T^2}E\right)\right] - 2aE \tanh\left(\frac{a}{T^2}E\right)\right] \tag{2.51}$$

**From $\boldsymbol{\varepsilon^{T,X} = \partial D(E,T)/\partial E}$**

$$\Delta T = \frac{\varepsilon_0 T}{C^{E,X}} \exp[\alpha - \beta T]\left[-\frac{4T^3 \ln\left[\cosh\left(\frac{a}{T^2}|E|\right)\right]}{a^2} + \frac{\beta T^4 \ln\left[\cosh\left(\frac{a}{T^2}|E|\right)\right]}{a^2} - \frac{2E^2 \operatorname{sech}^2\left(\frac{a}{T^2}|E|\right)}{T} + \frac{4ET \tanh\left(\frac{a}{T^2}|E|\right)}{a} - \frac{\beta T^2 E \tanh\left(\frac{a}{T^2}|E|\right)}{a}\right] \tag{2.52}$$

### 2.1.5.2 Determination of Constants α and β

Unfortunately, the experimental results of the temperature dependence of permittivity are not given in the article[140]. The values of constants $\alpha$ & $\beta$ for PMN-0.1PT have been found from literature[85,86] as α = 15.67 and β = 0.0182 K$^{-1}$.

### 2.1.5.3 Determination of ΔT Contribution due to Higher Fields

The ΔT values extracted from Figure 2.9 have been tabulated in Table 2.6. Data shows that there is not a significant difference between directly and indirectly measured ECE in this temperature range. The nonlinear contribution to temperature change (ΔT) due to temperature dependence of permittivity has been calculated using relation (2.51) and is compared with the directly and indirectly measured values which shows that nonlinear contribution is not strong enough (column 5 of Table 2.6) and that was the reason that there were small variations in the direct and indirect measured values. Moreover, the directly measured ECE is slightly less than the indirectly measured effect (contrary to results discussed in section 1.3.3.3 where direct values were higher than the indirectly measured values).

**Table 2.6 Comparison of difference between experimental measured data (approximately extracted from Figure 2.9) and data deduced from the mathematical formulation at E = 57 kV/cm (Assumption k = a / $T^2$)**

| T (K) | Cp (J/kg/K) | $\Delta T_{direct}$ (K) (Measured) | $\Delta T_{indirect}$ (K) (Measured) | $\Delta T_{direct} - \Delta T_{indirect}$ (K) | ΔT (K) Nonlinear contribution (Calculated) $\varepsilon^{T,X} = \frac{D}{E}$ |
|---|---|---|---|---|---|
| 300 | 325 | 0.925 | 0.975 | -0.005 | 0.012 |
| 320 | 335 | 1.03 | 1.06 | -0.03 | 0.009 |
| 340 | 340 | 1.15 | 1.18 | -0.03 | 0.007 |
| 360 | 345 | 1.23 | 1.25 | -0.02 | 0.005 |
| 380 | 347 | 1.25 | 1.20 | 0.05 | 0.004 |
| 400 | 347 | 1.18 | 1.12 | 0.06 | 0.003 |

Table 2.7 shows the comparison of the experimental measured values and the values determined from the relations (2.35) and (2.44) that were based on the assumption $k = a/T$. As we explained that that assumption was not accurate enough so it may be noticed that ΔT is marginally greater than the difference between the directly and indirectly measured values.

**Table 2.7 Comparison of difference between experimental measured data (approximately extracted from Figure 2.9) and ΔT contribution due to nonlinear effect (Assumption k = a / T)**

| T (K) | Cp (J/kg/K)[99] | $\Delta T_{direct}$ (K) (Measured) | $\Delta T_{indirect}$ (K) (Measured) | ΔT (K) (Calculated) at E =57 kV/cm $\varepsilon^{T,X} = \frac{D}{E}$ | ΔT (K) (Calculated) at E =57 kV/cm $\varepsilon^{T,X} = \left(\frac{\partial D}{\partial E}\right)_{T,X}$ |
|---|---|---|---|---|---|
| 300 | 325 | 0.925 | 0.975 | 1.90 | 0.17 |
| 320 | 335 | 1.03 | 1.06 | 1.47 | 0.15 |
| 340 | 340 | 1.15 | 1.18 | 1.14 | 0.12 |
| 360 | 345 | 1.23 | 1.25 | 0.88 | 0.10 |
| 380 | 347 | 1.25 | 1.20 | 0.67 | 0.09 |
| 400 | 347 | 1.18 | 1.12 | 0.52 | 0.07 |

### 2.1.6 Conclusion and Comments

We conclude that by using the advanced thermodynamics, the nonlinear contribution to the ECE of the dielectric material has been determined by considering the temperature dependence of the permittivity (i.e. $L_{mn}^{X} = (\partial \varepsilon_{mn}^{T,X}/\partial T)_{X}$). $L_{mn}^{X}$ is a second rank tensor and contributes to ΔT irrespective of the crystal symmetry (i.e. both in FE and PE regions) and the effect becomes stronger at higher electric field so it must be considered during the characterization of the ECMs. The formulation derived above can help to address the issues that result in the discrepancies in the indirect and direct measurements of the ECE. Both accurate data analysis and the reasonable assumptions are the key to find the discrepancies in the direct and indirect methods. A generalized methodology has been proposed to incorporate the nonlinear and nonlinear coupling effect in the determination of the ECE. This technique may be extended for all models that can be used to approximate the temperature dependence of permittivity and also for different definitions/approaches of the permittivity because the presence of the hysteresis in the ferroelectric materials makes it a complicated problem, and also the reported results are not consistent.

## 2.2 Primary and Secondary Pyroelectricity with Nonlinear and Higher Order Coupling

In most of the classical books[31,38,42] on ferroelectricity, the relation between primary and secondary pyroelectricity has been determined using different methods considering primarily only principle effects as it was explained in SECTION 1.3.1.3. As it has been discussed that the nonlinear and

nonlinear coupling effects are strong in the nonlinear ferroelectrics so the relation for pyroelectricity at different conditions needs to be modified accordingly so that the higher order effect may be incorporated. Here the relation between primary and secondary pyroelectricity is determined using nonlinear and higher order coupling coefficients using the same methodology mentioned in the classical books on ferroelectricity.

### 2.2.1 Case-I Principle and Linear Coupling Coefficients

As the pyroelectric measurement are done at constant electric field ($dE = 0$), so the electric displacement *D (T, x)* in differential form may be expanded considering only principle and linear coupling coefficients. The following relation may be found by expanding electric Gibbs energy by Taylor series.

$$dD_m(T,x) = \left(\frac{\partial D_m}{\partial T}\right)_{E,x} dT + \left(\frac{\partial D_m}{\partial x_\mu}\right)_{T,E} dx_\mu + \left(\frac{\partial^2 D_m}{\partial x_\mu \partial T}\right)_E dx_\mu dT \tag{2.53}$$

Where the strain is a function of temperature and stress, $x = f(T, X)$ and may be expressed as,

$$dx_\mu(E,T,X) = \left(\frac{\partial x_\mu}{\partial T}\right)_{E,X} dT + \left(\frac{\partial x_\mu}{\partial X_\nu}\right)_{T,E} dX_\upsilon + \left(\frac{\partial^2 x_\mu}{\partial X_\nu \partial T}\right)_E dX_\nu dT \tag{2.54}$$

Using (2.54) in (2.53) and manipulating, we get

$$D_m(E,T,x) = \left(\frac{\partial D_m}{\partial T}\right)_{E,x} dT + \left(\frac{\partial D_m}{\partial x_\mu}\right)_{T,E} \left[\left(\frac{\partial x_\mu}{\partial T}\right)_{E,X} dT + \left(\frac{\partial x_\mu}{\partial X_\nu}\right)_{T,E} dX_\upsilon + \left(\frac{\partial^2 x_\mu}{\partial X_\nu \partial T}\right)_E dX_\nu dT\right] + \left(\frac{\partial^2 D_m}{\partial x_\mu \partial T}\right)_E \left[\left(\frac{\partial x_\mu}{\partial T}\right)_{E,X} dT + \left(\frac{\partial x_\mu}{\partial X_\nu}\right)_{T,E} dX_\upsilon + \left(\frac{\partial^2 x_\mu}{\partial X_\nu \partial T}\right)_{E,X} dX_\nu dT\right] dT$$

Differentiating with T keeping X constant (Definition of secondary pyroelectric effect)

$$\left(\frac{D_m(E,T,x)}{\partial T}\right)_X = \left(\frac{\partial D_m}{\partial T}\right)_{E,x} + \left(\frac{\partial D_m}{\partial x_\mu}\right)_{T,E} \left(\frac{\partial x_\mu}{\partial T}\right)_{E,X} + 2\left(\frac{\partial^2 D_m}{\partial x_\mu \partial T}\right)_E \left(\frac{\partial x_\mu}{\partial T}\right)_{E,X} dT$$

Where, by definition, from Eqs. (1.4) and (1.7),

$$p_m^X = p_m^x + \left(\frac{\partial D_m}{\partial x_\mu}\right)_{T,E}\left(\frac{\partial x_\mu}{\partial T}\right)_{E,X} + 2\left(\frac{\partial x_\mu}{\partial T}\right)_{E,X}\left(\frac{\partial^2 D_m}{\partial x_\mu \partial T}\right)_E dT$$

Using chain rule, we may write the above equation as,

$$p_m^X = p_m^x + \left(\frac{\partial D_m}{\partial X_\mu}\right)_{T,E}\left(\frac{\partial X_\mu}{\partial x_\nu}\right)_{T,E}\left(\frac{\partial x_\mu}{\partial T}\right)_{E,X} + 2\left(\frac{\partial x_\mu}{\partial T}\right)_{E,X}\frac{\partial}{\partial T}\left(\left(\frac{\partial D_m}{\partial X_\mu}\right)_{T,E}\left(\frac{\partial X_\mu}{\partial x_\nu}\right)_{T,E}\right)_E dT$$

$$p_m^X = p_m^x + d_{m\mu}^T c_{\mu\nu}^{T,E}\alpha_\mu^E + 2\alpha_\mu^E\frac{\partial}{\partial T}\left(d_{m\mu}^T c_{\mu\nu}^{T,E}\right)_E dT \tag{2.55}$$

In Eq. (2.55) $d_{m\mu}^T$, $c_{\mu\nu}^{T,E}$, and $\alpha_\mu^E$ all are material properties. Eq. (2.55) may be compared with Eq. (1.8). This equation has extra term that is showing the temperature dependence of piezoelectric and stiffness of the dielectric material. In normal FEs, these terms may be weak and can be neglected, but in nonlinear ferroelectrics (i.e. RFEs), these may be strong enough and must be considered to find the reliable values of the primary and secondary pyroelectric effect.

### 2.2.2 Case-II Principle and Nonlinear Coefficients

In this case, only principal and nonlinear coefficients are being considered. Expanding D again, at constant, $dE = 0$, as a function of temperature and strain $D = f(T, x)$ and strain as a function of temperature and stress $x = g(T, X)$ as follows,

$$\begin{aligned} dD_m(E,T,x) = &\left(\frac{\partial D_m}{\partial T}\right)_{E,x} dT + \left(\frac{\partial D_m}{\partial x_\mu}\right)_{T,E} dx_\mu \\ &+ \left(\frac{\partial^2 D_m}{\partial T \partial T}\right)_{E,x} dT dT + \left(\frac{\partial^2 D_m}{\partial x_\mu \partial x_\nu}\right)_{T,E} dx_\mu dx_\nu \end{aligned} \tag{2.56}$$

$$\begin{aligned} dx_\mu(E,T,X) = &\left(\frac{\partial x_\mu}{\partial T}\right)_{E,X} dT + \left(\frac{\partial x_\mu}{\partial X_\nu}\right)_{T,E} dX_\nu \\ &+ \left(\frac{\partial^2 x_\mu}{\partial T \partial T}\right)_{E,X} dT dT + \left(\frac{\partial^2 x_\mu}{\partial X_\nu \partial X_\xi}\right)_{E,X} dX_\nu dX_\xi \end{aligned} \tag{2.57}$$

Putting Eq.(2.57) in (2.56) in Eq. and manipulating

$$dD_m(E,T,x) = \left(\frac{\partial D_m}{\partial T}\right)_{E,x} dT + \left(\frac{\partial D_m}{\partial x_\mu}\right)_{T,E}\left[\left(\frac{\partial x_\mu}{\partial T}\right)_{E,X} dT + \left(\frac{\partial x_\mu}{\partial X_\nu}\right)_{T,E} dX_\nu + \left(\frac{\partial^2 x_\mu}{\partial T \partial T}\right)_{E,X} dTdT + \left(\frac{\partial^2 x_\mu}{\partial X_\nu \partial X_\xi}\right)_{E,X} dX_\nu dX_\xi\right] + \left(\frac{\partial^2 D_m}{\partial T \partial T}\right)_{E,x} dTdT + \left(\frac{\partial^2 D_m}{\partial x_\mu \partial x_\nu}\right)_{T,E}\left[\left(\frac{\partial x_\mu}{\partial T}\right)_{E,X} dT + \left(\frac{\partial x_\mu}{\partial X_\nu}\right)_{T,E} dX_\nu + \left(\frac{\partial^2 x_\mu}{\partial T \partial T}\right)_{E,X} dTdT + \left(\frac{\partial^2 x_\mu}{\partial X_\nu \partial X_\xi}\right)_{E,X} dX_\nu dX_\xi\right]\left[\left(\frac{\partial x_\mu}{\partial T}\right)_{E,X} dT + \left(\frac{\partial x_\mu}{\partial X_\nu}\right)_{T,E} dX_\nu + \left(\frac{\partial^2 x_\mu}{\partial T \partial T}\right)_{E,X} dTdT + \left(\frac{\partial^2 x_\mu}{\partial X_\nu \partial X_\xi}\right)_{E,X} dX_\nu dX_\xi\right]$$

Differentiating $dD_m$ with respect to $T$ keeping $X_\mu$ constant (Definition of secondary pyroelectricity)

$$\left(\frac{\partial D_m(E,T,x)}{\partial T}\right)_{E,X} = \left(\frac{\partial D_m}{\partial T}\right)_{E,x} + \left(\frac{\partial D_m}{\partial x_\mu}\right)_{T,E}\left[\left(\frac{\partial x_\mu}{\partial T}\right)_{E,X} + 2\left(\frac{\partial^2 x_\mu}{\partial T \partial T}\right)_{E,X} dT\right] + 2\left(\frac{\partial^2 D_m}{\partial T \partial T}\right)_{E,x} dT + \left(\frac{\partial^2 D_m}{\partial x_\mu \partial x_\nu}\right)_{T,E}\left[2\left(\frac{\partial x_\mu}{\partial T}\right)_{E,X} dT + 6\left(\frac{\partial^2 x_\mu}{\partial T \partial T}\right)_{E,X} dTdT + 4\left(\frac{\partial^2 x_\mu}{\partial T \partial T}\right)_{E,X} dTdTdT\right]$$

$$p_m^X = p_m^x + \left(\frac{\partial D_m}{\partial x_\mu}\right)_{T,E}\left(\frac{\partial x_\mu}{\partial T}\right)_{E,X} + 2\left(\frac{\partial D_m}{\partial x_\mu}\right)_{T,E}\left(\frac{\partial^2 x_\mu}{\partial T \partial T}\right)_{E,X} dT + 2\left(\frac{\partial^2 D_m}{\partial T \partial T}\right)_{E,x} dT + \left(\frac{\partial^2 D_m}{\partial x_\mu \partial x_\nu}\right)_{T,E}\left[2\left(\frac{\partial x_\mu}{\partial T}\right)_{E,X} dT + 6\left(\frac{\partial^2 x_\mu}{\partial T \partial T}\right)_{E,X} dTdT + 4\left(\frac{\partial^2 x_\mu}{\partial T \partial T}\right)_{E,X} dTdTdT\right]$$

$$p_m^X = p_m^x + \left(\frac{\partial D_m}{\partial X_\mu}\right)_{T,E}\left(\frac{\partial X_\mu}{\partial x_\nu}\right)_{T,E}\left(\frac{\partial x_\mu}{\partial T}\right)_{E,X} + 2\left(\frac{\partial D_m}{\partial X_\mu}\right)_{T,E}\left(\frac{\partial X_\mu}{\partial x_\nu}\right)_{T,E}\frac{\partial}{\partial T}\left(\frac{\partial x_\mu}{\partial T}\right)_{E,X} dT$$
$$+ 2\frac{\partial}{\partial T}\left(\frac{\partial D_m}{\partial T}\right)_{E,x} dT$$
$$+ \overbrace{\left(\frac{\partial^2 D_m}{\partial x_\mu \partial x_\nu}\right)_{T,E}}^{Term}\left[2\left(\frac{\partial x_\mu}{\partial T}\right)_{E,X} dT + 6\left(\frac{\partial^2 x_\mu}{\partial T \partial T}\right)_{E,X} dTdT + 4\left(\frac{\partial^2 x_\mu}{\partial T \partial T}\right)_{E,X} dTdTdT\right]$$

The $Term$ may be manipulated as follows,

$$\overbrace{\left(\frac{\partial^2 D_m}{\partial x_\mu \partial x_\nu}\right)_{T,E}}^{Term} = \frac{\partial}{\partial x_\mu}\left(\frac{\partial D_m}{\partial x_\nu}\right)_{T,E}$$
$$= \frac{\partial}{\partial x_\mu}\left[\left(\frac{\partial D_m}{\partial X_\mu}\right)_{T,E}\left(\frac{\partial X_\mu}{\partial x_\nu}\right)_{T,E}\right]$$
$$= \frac{\partial}{\partial X_\mu}\frac{\partial X_\mu}{\partial x_\nu}\left[\left(\frac{\partial D_m}{\partial X_\mu}\right)_{T,E}\left(\frac{\partial X_\mu}{\partial x_\nu}\right)_{T,E}\right]$$
$$= \frac{\partial}{\partial X_\mu}\frac{\partial X_\mu}{\partial x_\nu}\left[\left(\frac{\partial D_m}{\partial X_\mu}\right)_{T,E}\left(\frac{\partial X_\mu}{\partial x_\nu}\right)_{T,E}\right]$$

Using this relation in the above equation, we have,

$$p_m^X = p_m^x + \left(\frac{\partial D_m}{\partial X_\mu}\right)_{T,E}\left(\frac{\partial X_\mu}{\partial x_\nu}\right)_{T,E}\left(\frac{\partial x_\mu}{\partial T}\right)_{E,X} + 2\left(\frac{\partial D_m}{\partial X_\mu}\right)_{T,E}\left(\frac{\partial X_\mu}{\partial x_\nu}\right)_{T,E}\frac{\partial}{\partial T}\left(\frac{\partial x_\mu}{\partial T}\right)_{E,X} dT$$
$$+ 2\frac{\partial}{\partial T}\left(\frac{\partial D_m}{\partial T}\right)_{E,x} dT$$
$$+ \frac{\partial}{\partial X_\mu}\frac{\partial X_\mu}{\partial x_\nu}\left[\left(\frac{\partial D_m}{\partial X_\mu}\right)_{T,E}\left(\frac{\partial X_\mu}{\partial x_\nu}\right)_{T,E}\right]\left[2\left(\frac{\partial x_\mu}{\partial T}\right)_{E,X} dT + 6\left(\frac{\partial^2 x_\mu}{\partial T \partial T}\right)_{E,X} dTdT\right.$$
$$\left. + 4\left(\frac{\partial^2 x_\mu}{\partial T \partial T}\right)_{E,X} dTdTdT\right]$$

$$p_m^X = p_m^x + d_{m\mu}^T c_{\mu\nu}^{T,E}\alpha_\mu^E + 2d_{m\mu}^T c_{\mu\nu}^{T,E}\frac{\partial \alpha_\mu^E}{\partial T} dT + 2\frac{\partial p_m^x}{\partial T} dT$$
$$+ c_{\mu\nu}^{T,E}\frac{\partial}{\partial X_\mu}\left[d_{m\mu}^T c_{\mu\nu}^{T,E}\right]\left[2\alpha_\mu^E dT + 6\delta^{E,X} dTdT\right. \quad (2.58)$$
$$\left. + 4\chi^{E,X} dTdTdT\right]$$

Eq. (2.58) gives the relationship of primary and secondary pyroelectricity when the nonlinear coefficients are considered. Not all the coefficients make a significant contribution and can be neglected. In RFEs, not only the piezoelectric effect but also electrostriction effect may contribute significantly, so these nonlinear effects may not be neglected during the characterization to get reliable results. Similarly the relations between primary and secondary pyroelectricity including higher order coupling coefficient may be derived but these are normally considered very weak and do not make significant contribution and are difficult to determine experimentally.

## 2.3 Concluding Remarks

This chapter is concluded by emphasizing that with the ever increasing exploitation of RFEs and other nonlinear FEs in ECE-based applications, where higher electric fields are involved, the nonlinear and nonlinear coupling effects make a significant contribution to the temperature change ($\Delta T$) that may be the main source for the observed discrepancies in the ECE measured by two methods. Therefore, these nonlinear and nonlinear coupling effects must be considered in the future studies of ECMs. Based on the advanced thermodynamics, the generalized relations to measure nonlinear contribution towards entropy and temperature change due to higher electric fields have been derived based on the few models for temperature dependence of the permittivity reported in the literature. This method can, however, be applied to any model that expresses/approximates the temperature dependence of permittivity.

Regarding the discrepancy found in direct and indirect methods, it is concluded that both mechanical and thermal conditions, both of which can be different in direct and indirect measurement setups, play an important role. Therefore, a detail analysis of the mechanical and thermal condition should be carried out for each experimental condition. By doing so, the real ECE can be determined so that the same results will be obtained using both direct and indirect approaches. Moreover, as the higher order effects are stronger in RFEs and in other nonlinear FEs, the modified relations to find the difference for the pyroelectric coefficients (i.e. EC coefficients) measured on different conditions *(clamped or free)* have been derived for reliable measurements of these pyroelectric and electrocaloric effects. If these higher order effects are negligibly weak, the relations may be reduced to the linear relations reported in literature.

## Chapter 3 Analytical Solution of a Multilayer System

The discovery of ferroelectrics with a giant electrocaloric effect (ECE)[20,21], which means the temperature of a dielectric material can be changed by external electric field, revives the research in both exploring electrocaloric materials (ECM)[23–27] and designing ECE-based cooling devices[13,121,125,126]. In terms of the device design, several innovative designs based on either active regeneration[122,123,125] or cascade techniques[13,109,129,130] as working principle[113] have been reported (discussed in details in section 1.5) where heat is transferred from cold side to hot side through complex heat paths mostly by heat conduction. There are two approaches widely used in the development of ECE device: experimental demonstration of prototype devices[13,125,126,129]; and numerical simulations using finite element analysis[118,123,127,128,130,141]. The former is limited by its time-consuming process, problems in prototype fabrication and availability of ECM for a researcher. The latter is fast and can be done by any researcher without ECM, it, however, requires too much information about the exact design and the materials used including ECM and surrounding materials. That is, a small change in the design and choice of ECM would require a new simulation. Therefore, it is interesting to have analytical solutions that govern the heat transformation in the ECE device. The analytical solution would help to advance the fundamental understanding of the physics and working principles of an ECE device and would provide a powerful tool to guide and optimize the design of ECE based devices.

In an EC device, the temperature profiles of ECM can be changed instantaneously using the localized external electric field which means a certain temperature profile can be established in the ECM during the heat conduction process. That is, temperature profiles are much more controllable in the ECE-based devices as compared to classical scenarios solved by diffusion heat theory [142–146]. The temperature profile established by the ECE will change with time due to heat fluxes determined by the thermal conductivities of ECM and surrounding materials. The transient heat conduction problem of cooling down of an infinite plate in a medium[145], and the solution of the two semi-infinite bodies in contact having different initial temperatures and thermal properties have been solved classically[143]. Here a multilayer system of four bodies comprising both ECMs and non-ECMs is solved analytically that has the potential to be used as ECE-based pump in complete silent operation (without moving parts).

## 3.1 Model and Analytical Solution

### 3.1.1 Physical Model

All the ECE-based devices use thin layer(s) of ECM, in which the electric field is applied along the thickness direction, so the heat conduction in the ECE-based devices can be simplified as one-dimensional (1D) heat conduction problem. In this chapter, a 1D transient heat conduction of a system of four bodies is solved analytically to simulate the ECE devices, in which both ECM and non-ECM are used. As shown in Figure 3.1, the model consists of four bodies: the two at the *end*s are semi-infinite bodies (B1 and B4) and the two in the *center* are finite ECM bodies (B2 and B3) that have been sandwiched between end bodies. The unsteady heat conduction problem has been solved analytically to find temperature profiles as a function of time and space, and heat fluxes through the interfaces as a function of time. This analytical solution will be used to numerically calculate the temperature profiles and heat fluxes in our novel idea of heat pump that will achieve the direction heat flow with complete silent operation. The thermal properties of the *center* and the *end* bodies can be either different or the same, the problem has been solved for a generalized case. The initial temperature profile is established in two ECMs using ECE. It is assumed that an electric field is applied on ECM (B2 and B3) at time zero ($t = 0$) and prior to this all bodies have the same temperature (say T). B1|B2, B2|B3, and B3|B4 are the interfaces through which the heat will transfer by heat conduction.

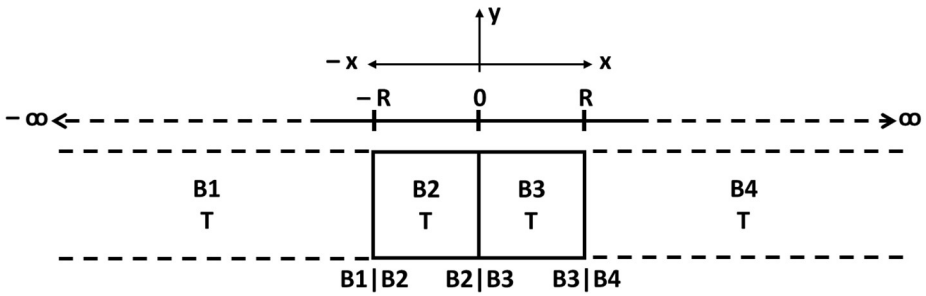


**Figure 3.1 Theoretical model of heat conduction problem**

### 3.1.2 Mathematical Model and Governing Equations

#### 3.1.2.1 Assumptions and Considerations

To analytically solve the heat conduction in the system shown in Figure 3.1, the following assumptions are used: 1) there is no heat loss to the environment through convection and/or radiation, 2) the interfaces are considered the perfect thermal contacts (i.e. zero thermal resistance), 3) the gradients in the y and z direction are neglected, only the gradients along the x-direction are

considered, 4) the materials properties are temperature invariant, 5) bodies B1 and B4 are considered infinite heat sink/source bodies. In this unsteady heat diffusion problem, the 1D heat equations for each of the bodies are given in Eqs. (3.1) – (3.4).

$$\frac{\partial T_1(x,t)}{\partial t} = \alpha_1 \frac{\partial^2 T_1(x,t)}{\partial x^2} \qquad -\infty < \boldsymbol{x} < -\boldsymbol{R} \tag{3.1}$$

$$\frac{\partial T_2(x,t)}{\partial t} = \alpha_2 \frac{\partial^2 T_2(x,t)}{\partial x^2} \qquad -\boldsymbol{R} < \boldsymbol{x} < \boldsymbol{0} \tag{3.2}$$

$$\frac{\partial T_3(x,t)}{\partial t} = \alpha_3 \frac{\partial^2 T_3(x,t)}{\partial x^2} \qquad \boldsymbol{0} < \boldsymbol{x} < \boldsymbol{R} \tag{3.3}$$

$$\frac{\partial T_4(x,t)}{\partial t} = \alpha_4 \frac{\partial^2 T_4(x,t)}{\partial x^2} \qquad \boldsymbol{R} < \boldsymbol{x} < \infty \tag{3.4}$$

Where $T_j\ (x,t)\ (j = 1,2,3,4)$ are the temperatures at time $t$ and location $x$ in the bodies from B1 ($j=1$) to B4 ($j=4$). $\alpha_j = k_j/\rho_j c_{p_j}$ ($m^2/s$) are the thermal diffusivities of body $j$, in which $k_j$ $(Wm^{-1}K^{-1})$, $\rho_j(kg/m^3)$, and $c_{p_j}(J/Kkg)$ are the thermal conductivity, mass density and specific heat capacity of body $j$, respectively.

### 3.1.2.2 Initial Conditions (ICs)

Based on the physical model shown in Figure 3.1, the ECE is used to change the temperature of bodies B2 and B3 by application/ removal of external electric field at any time. The followings are the generalized initial conditions,

$$\begin{aligned} T_1(x,0) &= T_{1i} \\ T_2(x,0) &= T_{2i} \\ T_3(x,0) &= T_{3i} \\ T_4(x,0) &= T_{4i} \end{aligned} \tag{3.5}$$

### 3.1.2.3 Boundary Conditions (BCs)

When two finite bodies at different temperatures are brought in thermal contact, the temperature ($T_s$) at their mutual interface is equal and the value depends on the thermal properties of the materials across the interface[143,147,148]. Based on the first law of thermodynamics, the amount of overall heat released by one body is equal to the amount of heat flowed in the surrounding body

through the interface[143]. So based on *Fourier's law of heat conduction*[149] across the interface, the following boundary conditions for $t > 0$ (also known as the boundary conditions of fourth kind[150]) are set for the model shown Figure 3.1.

**Interface B1|B2 at $x = -R$**

$$T_1(-R,t) = T_2(-R,t)$$

$$-k_1 \left.\frac{\partial T_1(x,t)}{\partial x}\right|_{x=-R} = -k_2 \left.\frac{\partial T_2(x,t)}{\partial x}\right|_{x=-R} \tag{3.6}$$

**Interface B2|B3 at $x = 0$**

$$T_2(0,t) = T_3(0,t)$$

$$-k_2 \left.\frac{\partial T_2(x,t)}{\partial x}\right|_{x=0} = -k_3 \left.\frac{\partial T_3(x,t)}{\partial x}\right|_{x=0} \tag{3.7}$$

**Interface B3|B4 at $x = R$**

$$T_3(R,t) = T_4(R,t)$$

$$-k_3 \left.\frac{\partial T_3(x,t)}{\partial x}\right|_{x=R} = -k_4 \left.\frac{\partial T_4(x,t)}{\partial x}\right|_{x=R} \tag{3.8}$$

#### 3.1.2.4 Physical Conditions (PCs)

The two semi-infinite end bodies (B1 and B4) being very large are considered a continuous source and sink of energy (i.e. infinite source/sink of heat energy). The lateral surfaces are perfectly insulated and there is no heat transfer to the surroundings at $x = \pm\infty$.

$$\left.\frac{\partial T_1(x,t)}{\partial x}\right|_{x=-\infty} = \left.\frac{\partial T_4(x,t)}{\partial x}\right|_{x=\infty} = 0 \tag{3.9}$$

### 3.1.3 Solution of the Heat Equations

Laplace transform method[151] is used to solve the system of the heat equations (3.1) – (3.4).

### 3.1.3.1 Laplace Transformation

The Laplace transform of the system of Eqs. (3.1) – (3.4) may be written as follows, (see Appendix - A),

$$W_1(x,s) - \frac{T_{1i}}{s} = A_1\, e^{\sqrt{\frac{s}{\alpha_1}}x} + B_1\, e^{-\sqrt{\frac{s}{\alpha_1}}x} \tag{3.10}$$

$$W_2(x,s) - \frac{T_{2i}}{s} = A_2\, e^{\sqrt{\frac{s}{\alpha_2}}x} + B_2\, e^{-\sqrt{\frac{s}{\alpha_2}}x} \tag{3.11}$$

$$W_3(x,s) - \frac{T_{3i}}{s} = A_3\, e^{\sqrt{\frac{s}{\alpha_3}}x} + B_3\, e^{-\sqrt{\frac{s}{\alpha_3}}x} \tag{3.12}$$

$$W_4(x,s) - \frac{T_{4i}}{s} = A_4\, e^{\sqrt{\frac{s}{\alpha_4}}x} + B_4\, e^{-\sqrt{\frac{s}{\alpha_4}}x} \tag{3.13}$$

We have 8 constants of integration. Boundary conditions may be used to calculate them. For the temperature of the bodies to be finite at $x = \pm\infty$, the constants $B_1\ and\ A_4$ vanish instantly. (i.e. $B_1 = 0\ and\ A_4 = 0$), and the Eqs. (3.10) – (3.13) become as follow,

$$W_1(x,s) - \frac{T_{1i}}{s} = A_1\, e^{\sqrt{\frac{s}{\alpha_1}}x} \tag{3.14}$$

$$W_2(x,s) - \frac{T_{2i}}{s} = A_2\, e^{\sqrt{\frac{s}{\alpha_2}}x} + B_2\, e^{-\sqrt{\frac{s}{\alpha_2}}x} \tag{3.15}$$

$$W_3(x,s) - \frac{T_{3i}}{s} = A_3\, e^{\sqrt{\frac{s}{\alpha_3}}x} + B_3\, e^{-\sqrt{\frac{s}{\alpha_3}}x} \tag{3.16}$$

$$W_4(x,s) - \frac{T_{4i}}{s} = B_4\, e^{-\sqrt{\frac{s}{\alpha_4}}x} \tag{3.17}$$

Boundary conditions on each interface may be used to get six equations that can be determined by solving them simultaneously.

### 3.1.3.2 Considerations and Conditions

Before we proceed further, some simplifications are being made. For simplification, the EC bodies B2 & B3 have been considered here as the same, whereas B1 & B4 bodies are the same but different from B2 & B3. That is,

$$\alpha_2 = \alpha_3 = \alpha^c \ \&\ \alpha_1 = \alpha_4 = \alpha^o$$

$$k_2 = k_3 = k^c \ \& \ k_1 = k_4 = k^o$$

$$c_{p_2} = c_{p_3} = c_p^c \ \& \ c_{p_1} = c_{p_4} = c_p^o$$

$$\rho_2 = \rho_3 = \rho^c \ \& \ \rho_1 = \rho_4 = \rho^o$$

where superscripts represent ***c***enter and ***o***uter bodies. Using this substitution, Eqs. (3.14) – (3.17) become,

$$W_1(x,s) - \frac{T_{1i}}{s} = A_1 \, e^{\sqrt{\frac{s}{\alpha^o}}x} \tag{3.18}$$

$$W_2(x,s) - \frac{T_{2i}}{s} = A_2 \, e^{\sqrt{\frac{s}{\alpha^c}}x} + B_2 \, e^{-\sqrt{\frac{s}{\alpha^c}}x} \tag{3.19}$$

$$W_3(x,s) - \frac{T_{3i}}{s} = A_3 \, e^{\sqrt{\frac{s}{\alpha^c}}x} + B_3 \, e^{-\sqrt{\frac{s}{\alpha^c}}x} \tag{3.20}$$

$$W_4(x,s) - \frac{T_{4i}}{s} = B_4 \, e^{-\sqrt{\frac{s}{\alpha^o}}x} \tag{3.21}$$

### 3.1.3.3 Determining the Constants of Integration

Boundary conditions (3.6) – (3.8) and are used to determine the integration constants;

Two equations from the boundary conditions at $x = -R$

$$W_1(-R,s) = W_2(-R,s)$$

$$\frac{T_{1i}}{s} + A_1 \, e^{-\sqrt{\frac{s}{\alpha^o}}R} = \frac{T_{2i}}{s} + A_2 \, e^{-\sqrt{\frac{s}{\alpha^c}}R} + B_2 \, e^{\sqrt{\frac{s}{\alpha^c}}R} \tag{3.22}$$

$$-k^o \frac{\partial W_1(x,s)}{\partial x}\bigg|_{x=-R} = -k^c \frac{\partial W_2(x,s)}{\partial x}\bigg|_{x=-R}$$

$$\sqrt{\frac{s}{\alpha^o}}\left(A_1 \, e^{-\sqrt{\frac{s}{\alpha^o}}R}\right) = \frac{k^c}{k^o}\sqrt{\frac{s}{\alpha^c}}\left(A_2 \, e^{-\sqrt{\frac{s}{\alpha^c}}R} - B_2 \, e^{\sqrt{\frac{s}{\alpha^c}}R}\right)$$

$$\left(A_1 \, e^{-\sqrt{\frac{s}{\alpha^o}}R}\right) = \frac{k^c}{k^o}\sqrt{\frac{\alpha^o}{\alpha^c}}\left(A_2 \, e^{-\sqrt{\frac{s}{\alpha^c}}R} - B_2 \, e^{\sqrt{\frac{s}{\alpha^c}}R}\right)$$

$$A_1 \, e^{-\sqrt{\frac{s}{\alpha^o}}R} = K_\varepsilon\left(A_2 \, e^{-\sqrt{\frac{s}{\alpha^c}}R} - B_2 \, e^{\sqrt{\frac{s}{\alpha^c}}R}\right) \tag{3.23}$$

Two equations from the boundary conditions at interface $x = 0$

$$W_2(0,s) = W_3(0,s)$$

$$\frac{T_{2i}}{s} + A_2 \, e^{\sqrt{\frac{s}{\alpha_2}}(0)} + B_2 \, e^{-\sqrt{\frac{s}{\alpha_2}}(0)} = \frac{T_{3i}}{s} + A_3 \, e^{\sqrt{\frac{s}{\alpha_3}}(0)} + B_3 \, e^{-\sqrt{\frac{s}{\alpha_3}}(0)}$$

$$\frac{T_{2i}}{s} + A_2 + B_2 = \frac{T_{3i}}{s} + A_3 + B_3 \tag{3.24}$$

$$-k^c \frac{\partial W_2(x,s)}{\partial x}\Big|_{x=0} = -k^c \frac{\partial W_3(x,s)}{\partial x}\Big|_{x=0}$$

$$\sqrt{\frac{s}{\alpha^c}}\left(A_2\, e^{\sqrt{\frac{s}{\alpha}}(0)} - B_2\, e^{-\sqrt{\frac{s}{\alpha}}(0)}\right) = \sqrt{\frac{s}{\alpha^c}}\left(A_3\, e^{\sqrt{\frac{s}{\alpha}}(0)} - B_3\, e^{-\sqrt{\frac{s}{\alpha}}(0)}\right)$$

$$A_2 - B_2 = A_3 - B_3 \tag{3.25}$$

Two equations from the boundary conditions at $x = R$

$$W_3(R,s) = W_4(R,s)$$

$$\frac{T_{3i}}{s} + A_3\, e^{\sqrt{\frac{s}{\alpha^c}}R} + B_4\, e^{-\sqrt{\frac{s}{\alpha^c}}R} = \frac{T_{4i}}{s} + B_4\, e^{-\sqrt{\frac{s}{\alpha^o}}R} \tag{3.26}$$

$$-k^c \frac{\partial W_3(x,s)}{\partial x}\Big|_{x=R} = -k^o \frac{\partial W_4(x,s)}{\partial x}\Big|_{x=R}$$

$$\frac{k^c}{k^o}\sqrt{\frac{s}{\alpha^c}}\left(A_3\, e^{\sqrt{\frac{s}{\alpha^c}}R} - B_3\, e^{-\sqrt{\frac{s}{\alpha^c}}R}\right) = -\sqrt{\frac{s}{\alpha^o}}\left(B_4\, e^{-\sqrt{\frac{s}{\alpha^o}}R}\right)$$

$$\frac{k^c}{k^o}\sqrt{\frac{\alpha^o}{\alpha^c}}\left(A_3\, e^{\sqrt{\frac{s}{\alpha^c}}R} - B_3\, e^{-\sqrt{\frac{s}{\alpha^c}}R}\right) = -\left(B_4\, e^{-\sqrt{\frac{s}{\alpha^o}}R}\right)$$

$$K_\varepsilon\left(A_3\, e^{\sqrt{\frac{s}{\alpha^c}}R} - B_3\, e^{-\sqrt{\frac{s}{\alpha^c}}R}\right) = -\left(B_4\, e^{-\sqrt{\frac{s}{\alpha^o}}R}\right) \tag{3.27}$$

where $K_\varepsilon = \frac{k^c}{k^o}\sqrt{\frac{\alpha^o}{\alpha^c}}$ is referred to as contacting coefficient and characterizes the thermal activity of one body relative to other body[144].

### 3.1.3.4 Manipulating the Constants of Integration

Eqs. (3.22) – (3.27) are solved simultaneously using Mathematica to find the constants of integration $(A_1, A_2, B_2, A_3, B_3, B_4)$ and have been tabulated in Appendix - B, where $h$ is defined as

$$h = \frac{1 - K_\varepsilon}{1 + K_\varepsilon} \quad |h| < 1$$

Luckily, the denominator of the all constants is in same form (see Appendix - B), that can be manipulated in the following way (see Appendix - C)

$$\frac{1}{2e^{4R\sqrt{\frac{s}{\alpha^c}}}(1+K_\varepsilon)^2 s - 2(1-K_\varepsilon)^2 s} = \frac{1}{s}\frac{1}{2(1+K_\varepsilon)^2}\sum_{n=1}^{\infty} h^{2(n-1)}\exp\left(-4nR\sqrt{\frac{s}{\alpha^c}}\right) \tag{3.28}$$

Using the above relation, $A_2, B_2, A_3, B_3$ may be further manipulated as follows,

$A_2$

$$= \frac{2e^{R\sqrt{\frac{s}{\alpha^c}}}(1-K_\varepsilon)(T_{2i}-T_{1i}) - e^{2R\sqrt{\frac{s}{\alpha^c}}}(1-K_\varepsilon{}^2)(T_{2i}-T_{3i}) - 2e^{3R\sqrt{\frac{s}{\alpha^c}}}(1+K_\varepsilon)(T_{3i}-T_{4i}) - e^{4R\sqrt{\frac{s}{\alpha^c}}}(1+K_\varepsilon)^2(T_{2i}-T_{3i})}{2e^{4R\sqrt{\frac{s}{\alpha^c}}}(1+K_\varepsilon)^2 s - 2(1-K_\varepsilon)^2 s}$$

$$A_2 = \frac{(T_{2i}-T_{1i})\cdot h}{1+K_\varepsilon}\frac{1}{s}\sum_{n=1}^{\infty} h^{2(n-1)}\exp\left(-(4n-1)R\sqrt{\frac{s}{\alpha^c}}\right)$$
$$- \frac{(T_{2i}-T_{3i})\cdot h}{2}\frac{1}{s}\sum_{n=1}^{\infty} h^{2(n-1)}\exp\left(-(4n-2)R\sqrt{\frac{s}{\alpha^c}}\right)$$
$$- \frac{(T_{3i}-T_{4i})}{1+K_\varepsilon}\frac{1}{s}\sum_{n=1}^{\infty} h^{2(n-1)}\exp\left(-(4n-3)R\sqrt{\frac{s}{\alpha^c}}\right)$$
$$- \frac{(T_{2i}-T_{3i})}{2}\frac{1}{s}\sum_{n=1}^{\infty} h^{2(n-1)}\exp\left(-(4n-4)R\sqrt{\frac{s}{\alpha^c}}\right)$$

$B_2$

$$= \frac{(1-K_\varepsilon)^2(T_{2i}-T_{3i}) + 2e^{R\sqrt{\frac{s}{\alpha^c}}}(1-K_\varepsilon)(T_{3i}-T_{4i}) + e^{2R\sqrt{\frac{s}{\alpha^c}}}(1-K_\varepsilon{}^2)(T_{2i}-T_{3i}) - 2e^{3R\sqrt{\frac{s}{\alpha^c}}}(1+K_\varepsilon)(T_{2i}-T_{1i})}{2e^{4R\sqrt{\frac{s}{\alpha^c}}}(1+K_\varepsilon)^2 s - 2(1-K_\varepsilon)^2 s}$$

$$B_2 = \frac{(T_{2i}-T_{3i})\cdot h^2}{2}\frac{1}{s}\sum_{n=1}^{\infty} h^{2(n-1)}\exp\left(-(4n-0)R\sqrt{\frac{s}{\alpha^c}}\right)$$
$$+ \frac{(T_{3i}-T_{4i})\cdot h}{1+K_\varepsilon}\frac{1}{s}\sum_{n=1}^{\infty} h^{2(n-1)}\exp\left(-(4n-1)R\sqrt{\frac{s}{\alpha^c}}\right)$$
$$+ \frac{(T_{2i}-T_{3i})\cdot h}{2}\frac{1}{s}\sum_{n=1}^{\infty} h^{2(n-1)}\exp\left(-(4n-2)R\sqrt{\frac{s}{\alpha^c}}\right)$$
$$- \frac{(T_{2i}-T_{1i})}{1+K_\varepsilon}\frac{1}{s}\sum_{n=1}^{\infty} h^{2(n-1)}\exp\left(-(4n-3)R\sqrt{\frac{s}{\alpha^c}}\right)$$

$A_3$

$$= \frac{-(1-K_\varepsilon)^2(T_{2i}-T_{3i}) + 2e^{R\sqrt{\frac{s}{\alpha^c}}}(1-K_\varepsilon)(T_{2i}-T_{1i}) - e^{2R\sqrt{\frac{s}{\alpha^c}}}\left(1-K_\varepsilon{}^2\right)(T_{2i}-T_{3i}) - 2e^{3R\sqrt{\frac{s}{\alpha^c}}}(1+K_\varepsilon)(T_{3i}-T_{4i})}{2e^{4R\sqrt{\frac{s}{\alpha^c}}}(1+K_\varepsilon)^2 s - 2(1-K_\varepsilon)^2 s}$$

$$A_3 = -\frac{(T_{2i}-T_{3i})\cdot h^2}{2}\frac{1}{s}\sum_{n=1}^{\infty} h^{2(n-1)} \exp\left(-(4n-0)R\sqrt{\frac{s}{\alpha^c}}\right)$$

$$+ \frac{(T_{2i}-T_{1i})\cdot h}{1+K_\varepsilon}\frac{1}{s}\sum_{n=1}^{\infty} h^{2(n-1)} \exp\left(-(4n-1)R\sqrt{\frac{s}{\alpha^c}}\right)$$

$$- \frac{(T_{2i}-T_{3i})\cdot h}{2}\frac{1}{s}\sum_{n=1}^{\infty} h^{2(n-1)} \exp\left(-(4n-2)R\sqrt{\frac{s}{\alpha^c}}\right)$$

$$- \frac{(T_{3i}-T_{4i})}{1+K_\varepsilon}\frac{1}{s}\sum_{n=1}^{\infty} h^{2(n-1)} \exp\left(-(4n-3)R\sqrt{\frac{s}{\alpha^c}}\right)$$

$B_3$

$$= \frac{2e^{R\sqrt{\frac{s}{\alpha^c}}}(1-K_\varepsilon)(T_{3i}-T_{4i}) + e^{2R\sqrt{\frac{s}{\alpha^c}}}(1-K_\varepsilon{}^2)(T_{2i}-T_{3i}) - 2e^{3R\sqrt{\frac{s}{\alpha^c}}}(1+K_\varepsilon)(T_{2i}-T_{1i}) + e^{4R\sqrt{\frac{s}{\alpha^c}}}(1+K_\varepsilon)^2(T_{2i}-T_{3i})}{2e^{4R\sqrt{\frac{s}{\alpha^c}}}(1+K_\varepsilon)^2)s - 2(1-K_\varepsilon)^2 s}$$

$$B_3 = \frac{(T_{3i}-T_{4i})\cdot h}{(1+K_\varepsilon)}\frac{1}{s}\sum_{n=1}^{\infty} h^{2(n-1)} \exp\left(-(4n-1)R\sqrt{\frac{s}{\alpha^c}}\right)$$

$$+ \frac{(T_{2i}-T_{3i})\cdot h}{2}\frac{1}{s}\sum_{n=1}^{\infty} h^{2(n-1)} \exp\left(-(4n-2)R\sqrt{\frac{s}{\alpha^c}}\right)$$

$$- \frac{(T_{2i}-T_{1i})}{1+K_\varepsilon}\frac{1}{s}\sum_{n=1}^{\infty} h^{2(n-1)} \exp\left(-(4n-3)R\sqrt{\frac{s}{\alpha^c}}\right)$$

$$+ \frac{(T_{2i}-T_{3i})}{2}\frac{1}{s}\sum_{n=1}^{\infty} h^{2(n-1)} \exp\left(-(4n-4)R\sqrt{\frac{s}{\alpha^c}}\right)$$

The constants, $A_1$ *and* $B_4$ may be treated in a different way as the term $\sqrt{\frac{s}{\alpha^o}}$ is involved in them.

$$A_1 = \frac{e^{R\sqrt{\frac{s}{\alpha^o}}}K_\varepsilon\left\{(1-K_\varepsilon)(T_{2i}-T_{1i}) - e^{R\sqrt{\frac{s}{\alpha^c}}}(1-K_\varepsilon)(T_{2i}-T_{3i}) - 2e^{2R\sqrt{\frac{s}{\alpha^c}}}(T_{3i}-T_{4i}) - e^{3R\sqrt{\frac{s}{\alpha^c}}}(1+K_\varepsilon)(T_{2i}-T_{3i}) + e^{4R\sqrt{\frac{s}{\alpha^c}}}(1+K_\varepsilon)(T_{2i}-T_{1i})\right\}}{e^{4R\sqrt{\frac{s}{\alpha^c}}}(1+K_\varepsilon)^2 s - (1-K_\varepsilon)^2 s}$$

$$A_1 = \frac{K_\varepsilon}{1+K_\varepsilon}\Bigg\{(T_{2i}-T_{1i})\cdot h\frac{1}{s}\sum_{n=1}^{\infty}h^{2(n-1)}\exp\left[-\left((4nR-0)\sqrt{\frac{s}{\alpha^c}}\sqrt{\frac{\alpha^o}{s}}+R\right)\sqrt{\frac{s}{\alpha^o}}\right]$$
$$-(T_{2i}-T_{3i})\cdot h\frac{1}{s}\sum_{n=1}^{\infty}h^{2(n-1)}\exp\left[-\left((4nR-1)\sqrt{\frac{s}{\alpha}}\sqrt{\frac{\alpha^o}{s}}+R\right)\sqrt{\frac{s}{\alpha^o}}\right]$$
$$-2(T_{3i}-T_{4i})\frac{1}{s}\sum_{n=1}^{\infty}h^{2(n-1)}\exp\left[-\left((4nR-2)\sqrt{\frac{s}{\alpha}}\sqrt{\frac{\alpha^o}{s}}+R\right)\sqrt{\frac{s}{\alpha^o}}\right]$$
$$-(T_{2i}-T_{3i})\frac{1}{s}\sum_{n=1}^{\infty}h^{2(n-1)}\exp\left[-\left((4nR-3)\sqrt{\frac{s}{\alpha}}\sqrt{\frac{\alpha^o}{s}}+R\right)\sqrt{\frac{s}{\alpha^o}}\right]$$
$$+(T_{2i}-T_{1i})\frac{1}{s}\sum_{n=1}^{\infty}h^{2(n-1)}\exp\left[-\left((4nR-4)\sqrt{\frac{s}{\alpha}}\sqrt{\frac{\alpha^o}{s}}+R\right)\sqrt{\frac{s}{\alpha^o}}\right]\Bigg\}$$

$$B_4 = \frac{e^{R\sqrt{\frac{s}{\alpha^o}}}K_\varepsilon\left\{(1-K_\varepsilon)(T_{3i}-T_{4i})+e^{R\sqrt{\frac{s}{\alpha^c}}}(1-K_\varepsilon)(T_{2i}-T_{3i})-2e^{2R\sqrt{\frac{s}{\alpha^c}}}(T_{2i}-T_{1i})+e^{3R\sqrt{\frac{s}{\alpha^c}}}(1+K_\varepsilon)(T_{2i}-T_{3i})+e^{4R\sqrt{\frac{s}{\alpha^c}}}(1+K_\varepsilon)(T_{3i}-T_{4i})\right\}}{e^{4R\sqrt{\frac{s}{\alpha^c}}}(1+K_\varepsilon)^2)s-(1-K_\varepsilon)^2 s}$$

$$B_4 = \frac{K_\varepsilon}{1+K_\varepsilon}\Bigg\{(T_{3i}-T_{4i})\cdot h\frac{1}{s}\sum_{n=1}^{\infty}h^{2(n-1)}\exp\left[-\left((4nR-0)\sqrt{\frac{s}{\alpha^c}}\sqrt{\frac{\alpha^o}{s}}+R\right)\sqrt{\frac{s}{\alpha^o}}\right]$$
$$+(T_{2i}-T_{3i})\cdot h\frac{1}{s}\sum_{n=1}^{\infty}h^{2(n-1)}\exp\left[-\left((4nR-1)\sqrt{\frac{s}{\alpha^c}}\sqrt{\frac{\alpha^o}{s}}+R\right)\sqrt{\frac{s}{\alpha^o}}\right]$$
$$-2(T_{2i}-T_{1i})\frac{1}{s}\sum_{n=1}^{\infty}h^{2(n-1)}\exp\left[-\left((4nR-2)\sqrt{\frac{s}{\alpha^c}}\sqrt{\frac{\alpha^o}{s}}+R\right)\sqrt{\frac{s}{\alpha^o}}\right]$$
$$+(T_{2i}-T_{3i})\frac{1}{s}\sum_{n=1}^{\infty}h^{2(n-1)}\exp\left[-\left((4nR-3)\sqrt{\frac{s}{\alpha^c}}\sqrt{\frac{\alpha^o}{s}}+R\right)\sqrt{\frac{s}{\alpha^o}}\right]$$
$$+(T_{3i}-T_{4i})\frac{1}{s}\sum_{n=1}^{\infty}h^{2(n-1)}\exp\left[-\left((4nR-4)\sqrt{\frac{s}{\alpha^c}}\sqrt{\frac{\alpha^o}{s}}+R\right)\sqrt{\frac{s}{\alpha^o}}\right]\Bigg\}$$

### 3.1.3.5 Equations in Laplace Domain

By putting the values of constants in Eqs. (3.18) – (3.21), we get

$$W_1(x,s) - \frac{T_{1i}}{s} = A_1\, e^{\sqrt{\frac{s}{\alpha^o}}x}$$

$$\begin{aligned}
&W_1(x,s) - \frac{T_{1i}}{s} \\
&= \frac{K_\varepsilon}{1+K_\varepsilon}\Bigg\{ \frac{(T_{2i}-T_{1i})\cdot h}{s}\sum_{n=1}^{\infty} h^{2(n-1)} \exp\left[-\left(-x-R+(4n-0)RK_\alpha^{-1/2}\right)\sqrt{\frac{s}{\alpha^o}}\right] \\
&\quad - \frac{(T_{2i}-T_{3i})\cdot h}{s}\sum_{n=1}^{\infty} h^{2(n-1)} \exp\left[-\left(-x-R+(4n-1)RK_\alpha^{-1/2}\right)\sqrt{\frac{s}{\alpha^o}}\right] \\
&\quad - \frac{2\,(T_{3i}-T_{4i})}{(1+K_\varepsilon)\,s}\sum_{n=1}^{\infty} h^{2(n-1)} \exp\left[-\left(-x-R+(4n-2)RK_\alpha^{-1/2}\right)\sqrt{\frac{s}{\alpha^o}}\right] \\
&\quad - \frac{T_{2i}-T_{3i}}{s}\sum_{n=1}^{\infty} h^{2(n-1)} \exp\left[-\left(-x-R+(4n-3)RK_\alpha^{-1/2}\right)\sqrt{\frac{s}{\alpha^o}}\right] \\
&\quad + \frac{(T_{2i}-T_{1i})}{s}\sum_{n=1}^{\infty} h^{2(n-1)} \exp\left[-\left(-x-R+(4n-4)RK_\alpha^{-1/2}\right)\sqrt{\frac{s}{\alpha^o}}\right]\Bigg\}
\end{aligned} \tag{3.29}$$

$$W_2(x,s) - \frac{T_{2i}}{s} = A_2\, e^{\sqrt{\frac{s}{\alpha^c}}x} + B_2\, e^{-\sqrt{\frac{s}{\alpha^c}}x}$$

$$\begin{aligned}
&W_2(x,s) - \frac{T_{2i}}{s} \\
&= \frac{(T_{2i}-T_{3i})\cdot\, h^2}{2}\frac{1}{s}\sum_{n=1}^{\infty} h^{2(n-1)} \exp\left(-\sqrt{\frac{s}{\alpha^c}}\left((4n-0)R+x\right)\right) \\
&+ \frac{h}{1+K_\varepsilon}\frac{1}{s}\sum_{n=1}^{\infty} h^{2(n-1)}\left[(T_{2i}-T_{1i})\exp\left(-\sqrt{\frac{s}{\alpha^c}}\left((4n-1)R-x\right)\right) + (T_{3i}-T_{4i})\exp\left(-\sqrt{\frac{s}{\alpha^c}}\left((4n-1)R+x\right)\right)\right] \\
&- \frac{h}{2}\frac{1}{s}\sum_{n=1}^{\infty} h^{2(n-1)}\left[(T_{2i}-T_{3i})\exp\left(-\sqrt{\frac{s}{\alpha^c}}\left((4n-2)R-x\right)\right) - (T_{2i}-T_{3i})\exp\left(-\sqrt{\frac{s}{\alpha^c}}\left((4n-2)R+x\right)\right)\right] \\
&- \frac{1}{1+K_\varepsilon}\frac{1}{s}\sum_{n=1}^{\infty} h^{2(n-1)}\left[(T_{3i}-T_{4i})\exp\left(-\sqrt{\frac{s}{\alpha^c}}\left((4n-3)R-x\right)\right) + (T_{2i}-T_{1i})\exp\left(-\sqrt{\frac{s}{\alpha^c}}\left((4n-3)R+x\right)\right)\right] \\
&- \frac{(T_{2i}-T_{3i})}{2}\frac{1}{s}\sum_{n=1}^{\infty} h^{2(n-1)}\exp\left(-\sqrt{\frac{s}{\alpha^c}}\left((4n-4)R-x\right)\right)
\end{aligned} \tag{3.30}$$

$$W_3(x,s) - \frac{T_{3i}}{s} = A_3\, e^{\sqrt{\frac{s}{\alpha^c}}x} + B_3\, e^{-\sqrt{\frac{s}{\alpha^c}}x}$$

$$
\begin{aligned}
W_3(x,s)-\frac{T_{3i}}{s} &= -\frac{(T_{2i}-T_{3i})\cdot\ h^2}{2}\frac{1}{s}\sum_{n=1}^{\infty}h^{2(n-1)}\exp\left(-\sqrt{\frac{s}{\alpha^c}}\left((4n-0)R-x\right)\right)\\
&+\frac{h}{1+K_\varepsilon}\frac{1}{s}\sum_{n=1}^{\infty}h^{2(n-1)}\left[(T_{2i}-T_{1i})\exp\left(-\sqrt{\frac{s}{\alpha^c}}\left((4n-1)R-x\right)\right)+(T_{3i}-T_{4i})\exp\left(-\sqrt{\frac{s}{\alpha^c}}\left((4n-1)R+x\right)\right)\right]\\
&-\frac{h}{2}\frac{1}{s}\sum_{n=1}^{\infty}h^{2(n-1)}\left[(T_{2i}-T_{3i})\exp\left(-\sqrt{\frac{s}{\alpha^c}}\left((4n-2)R-x\right)\right)-(T_{2i}-T_{3i})\exp\left(-\sqrt{\frac{s}{\alpha^c}}\left((4n-2)R+x\right)\right)\right]\\
&-\frac{1}{1+K_\varepsilon}\frac{1}{s}\sum_{n=1}^{\infty}h^{2(n-1)}\left[(T_{3i}-T_{4i})\exp\left(-\sqrt{\frac{s}{\alpha^c}}\left((4n-3)R-x\right)\right)+(T_{2i}-T_{1i})\exp\left(-\sqrt{\frac{s}{\alpha^c}}\left((4n-3)R+x\right)\right)\right]\\
&+\frac{(T_{2i}-T_{3i})}{2}\frac{1}{s}\sum_{n=1}^{\infty}h^{2(n-1)}\exp\left(-\sqrt{\frac{s}{\alpha^c}}\left((4n-4)R+x\right)\right)
\end{aligned}
\tag{3.31}
$$

$$W_4(x,s)-\frac{T_{4i}}{s}=B_4\ e^{-\sqrt{\frac{s}{\alpha^o}}x}$$

$$
\begin{aligned}
&W_4(x,s)-\frac{T_{4i}}{s}\\
&=\frac{K_\varepsilon}{1+K_\varepsilon}\left\{\frac{(T_{3i}-T_{4i})\cdot h}{s}\sum_{n=1}^{\infty}h^{2(n-1)}\exp\left(-\left[x-R+(4n-0)RK_\alpha^{-1/2}\right]\sqrt{\frac{s}{\alpha^o}}\right)\right.\\
&\quad+\frac{(T_{2i}-T_{3i})\cdot h}{s}\sum_{n=1}^{\infty}h^{2(n-1)}\exp\left(-\left[x-R+(4n-1)RK_\alpha^{-1/2}\right]\sqrt{\frac{s}{\alpha^o}}\right)\\
&\quad-\frac{2\,(T_{2i}-T_{1i})}{(1+K_\varepsilon)\,s}\sum_{n=1}^{\infty}h^{2(n-1)}\exp\left(-\left[x-R+(4n-2)RK_\alpha^{-1/2}\right]\sqrt{\frac{s}{\alpha^o}}\right)\\
&\quad+\frac{T_{2i}-T_{3i}}{s}\sum_{n=1}^{\infty}h^{2(n-1)}\exp\left(-\left[x-R+(4n-3)RK_\alpha^{-1/2}\right]\sqrt{\frac{s}{\alpha^o}}\right)\\
&\quad\left.+\frac{(T_{3i}-T_{4i})}{s}\sum_{n=1}^{\infty}h^{2(n-1)}\exp\left(-\left[x-R+(4n-4)RK_\alpha^{-1/2}\right]\sqrt{\frac{s}{\alpha^o}}\right)\right\}
\end{aligned}
\tag{3.32}
$$

$K_\alpha=\alpha^c/\alpha^o$ is relative thermal inertia[144,145].

### 3.1.3.6 Inverse Laplace Transform of the System of Equations

The analytical solution of temperature profiles in each body is determined by taking the inverse Laplace transform of the relations (3.29) – (3.32) by using Eq. (3.33).

$$L^{-1}\left\{\frac{1}{s}\exp\left[-k\sqrt{s}\right]\right\}=\operatorname{erfc}\left[\frac{k}{2\sqrt{t}}\right] \tag{3.33}$$

### 3.1.4 Temperature Profiles of the Bodies

**Temperature Profile of Body-1 (B1)**

$$
\begin{aligned}
&T_1(x,t) - T_{1i} \\
&= \frac{K_\varepsilon}{1+K_\varepsilon}\Bigg\{(T_{2i}-T_{1i})\,h\sum_{n=1}^{\infty}h^{2(n-1)}\,\mathrm{erfc}\frac{-x-R+(4n-0)K_\alpha^{-1/2}R}{2\sqrt{\alpha^o t}} \\
&\qquad -(T_{2i}-T_{3i})\,h\sum_{n=1}^{\infty}h^{2(n-1)}\,\mathrm{erfc}\frac{-x-R+(4n-1)K_\alpha^{-1/2}R}{2\sqrt{\alpha^o t}} \\
&\qquad -\frac{2(T_{3i}-T_{4i})}{1+K_\varepsilon}\sum_{n=1}^{\infty}h^{2(n-1)}\,\mathrm{erfc}\frac{-x-R+(4n-2)K_\alpha^{-1/2}R}{2\sqrt{\alpha^o t}} \\
&\qquad -(T_{2i}-T_{3i})\sum_{n=1}^{\infty}h^{2(n-1)}\,\mathrm{erfc}\frac{-x-R+(4n-3)K_\alpha^{-1/2}R}{2\sqrt{\alpha^o t}} \\
&\qquad +(T_{2i}-T_{1i})\sum_{n=1}^{\infty}h^{2(n-1)}\,\mathrm{erfc}\frac{-x-R+(4n-4)K_\alpha^{-1/2}R}{2\sqrt{\alpha^o t}}\Bigg\}
\end{aligned}
\tag{3.34}
$$

**Temperature Profile of Body-2 (B2)**

$$
\begin{aligned}
&T_2(x,t) - T_{2i} \\
&= \frac{(T_{2i}-T_{3i})\,h^2}{2}\sum_{n=1}^{\infty}h^{2(n-1)}\,\mathrm{erfc}\frac{(4n-0)R+x}{2\sqrt{\alpha^c t}} \\
&\qquad +\frac{h}{1+K_\varepsilon}\sum_{n=1}^{\infty}h^{2(n-1)}\left[(T_{2i}-T_{1i})\,\mathrm{erfc}\frac{(4n-1)R-x}{2\sqrt{\alpha^c t}}+(T_{3i}-T_{4i})\,\mathrm{erfc}\frac{(4n-1)R+x}{2\sqrt{\alpha^c t}}\right] \\
&\qquad -\frac{h}{2}\sum_{n=1}^{\infty}h^{2(n-1)}\left[(T_{2i}-T_{3i})\,\mathrm{erfc}\frac{(4n-2)R-x}{2\sqrt{\alpha^c t}}-(T_{2i}-T_{3i})\,\mathrm{erfc}\frac{(4n-2)R+x}{2\sqrt{\alpha^c t}}\right] \\
&\qquad -\frac{1}{1+K_\varepsilon}\sum_{n=1}^{\infty}h^{2(n-1)}\left[(T_{3i}-T_{4i})\,\mathrm{erfc}\frac{(4n-3)R-x}{2\sqrt{\alpha^c t}}+(T_{2i}-T_{1i})\,\mathrm{erfc}\frac{(4n-3)R+x}{2\sqrt{\alpha^c t}}\right] \\
&\qquad -\frac{(T_{2i}-T_{3i})}{2}\sum_{n=1}^{\infty}h^{2(n-1)}\,\mathrm{erfc}\frac{(4n-4)R-x}{2\sqrt{\alpha^c t}}
\end{aligned}
\tag{3.35}
$$

**Temperature Profile of Body-3 (B3)**

$$
\begin{aligned}
&T_3(x,t) - T_{3i} \\
&= -\frac{(T_{2i} - T_{3i})\, h^2}{2} \sum_{n=1}^{\infty} h^{2(n-1)} \operatorname{erfc} \frac{(4n-0)R - x}{2\sqrt{\alpha^c t}} \\
&\quad + \frac{h}{1+K_\varepsilon} \sum_{n=1}^{\infty} h^{2(n-1)} \left[ (T_{2i} - T_{1i}) \operatorname{erfc} \frac{(4n-1)R - x}{2\sqrt{\alpha^c t}} + (T_{3i} - T_{4i}) \operatorname{erfc} \frac{(4n-1)R + x}{2\sqrt{\alpha^c t}} \right] \\
&\quad - \frac{h}{2} \sum_{n=1}^{\infty} h^{2(n-1)} \left[ (T_{2i} - T_{3i}) \operatorname{erfc} \frac{(4n-2)R - x}{2\sqrt{\alpha^c t}} - (T_{2i} - T_{3i}) \operatorname{erfc} \frac{(4n-2)R + x}{2\sqrt{\alpha^c t}} \right] \\
&\quad - \frac{1}{1+K_\varepsilon} \sum_{n=1}^{\infty} h^{2(n-1)} \left[ (T_{3i} - T_{4i}) \operatorname{erfc} \frac{(4n-3)R - x}{2\sqrt{\alpha^c t}} + (T_{2i} - T_{1i}) \operatorname{erfc} \frac{(4n-3)R + x}{2\sqrt{\alpha^c t}} \right] \\
&\quad + \frac{(T_{2i} - T_{3i})}{2} \sum_{n=1}^{\infty} h^{2(n-1)} \operatorname{erfc} \frac{(4n-4)R + x}{2\sqrt{\alpha^c t}}
\end{aligned} \tag{3.36}
$$

**Temperature Profile of Body-4 (B4)**

$$
\begin{aligned}
&T_4(x,t) - T_{4i} \\
&= \frac{K_\varepsilon}{1+K_\varepsilon} \Bigg\{ (T_{3i} - T_{4i})\, h \sum_{n=1}^{\infty} h^{2(n-1)} \operatorname{erfc} \frac{x - R + (4n-0) K_\alpha^{-1/2} R}{2\sqrt{\alpha^o t}} \\
&\qquad + (T_{2i} - T_{3i})\, h \sum_{n=1}^{\infty} h^{2(n-1)} \operatorname{erfc} \frac{x - R + (4n-1) K_\alpha^{-1/2} R}{2\sqrt{\alpha^o t}} \\
&\qquad - \frac{2(T_{2i} - T_{1i})}{1+K_\varepsilon} \sum_{n=1}^{\infty} h^{2(n-1)} \operatorname{erfc} \frac{x - R + (4n-2) K_\alpha^{-1/2} R}{2\sqrt{\alpha^o t}} \\
&\qquad + (T_{2i} - T_{3i}) \sum_{n=1}^{\infty} h^{2(n-1)} \operatorname{erfc} \frac{x - R + (4n-3) K_\alpha^{-1/2} R}{2\sqrt{\alpha^o t}} \\
&\qquad + (T_{3i} - T_{4i}) \sum_{n=1}^{\infty} h^{2(n-1)} \operatorname{erfc} \frac{x - R + (4n-4) K_\alpha^{-1/2} R}{2\sqrt{\alpha^o t}} \Bigg\}
\end{aligned} \tag{3.37}
$$

### 3.1.5 Validation of the Analytical Solution

Before proceeding further, it is considered pertinent to validate this analytical solution. For this purpose, the initial conditions of this solution may be modified to the solution already available in literature. If the identical initial temperatures of ECM bodies (B2 and B3) are considered ($T_{2i} = T_{3i}$), then the temperature gradient at the interface (B2|B3) vanishes ($\partial T_2(x,t)/\partial x = \partial T_3(x,t)/\partial x = 0$) and also considering equal initial temperatures of End Bodies ($T_{1i} = T_{4i}$), the problem becomes the classic case mentioned in introduction part[144] and is shown in Figure 3.2, in which an infinite plate with a finite uniform thickness is cooled/heated by heat conduction in two semi-infinite media on both sides (considering 1D case). By replacing, $T_{2i} = T_{3i}$, $T_{1i} = T_{4i}$ and

$T_{2i} = T_{3i} > T_{1i} = T_{4i}$ (cooling in this case) in Eqs. (3.34) – (3.37) our solution with some manipulation yields to the solution[143] mentioned in Eq. (3.38) and (3.39) validating the analytical solution determined here (Appendix - D for details).

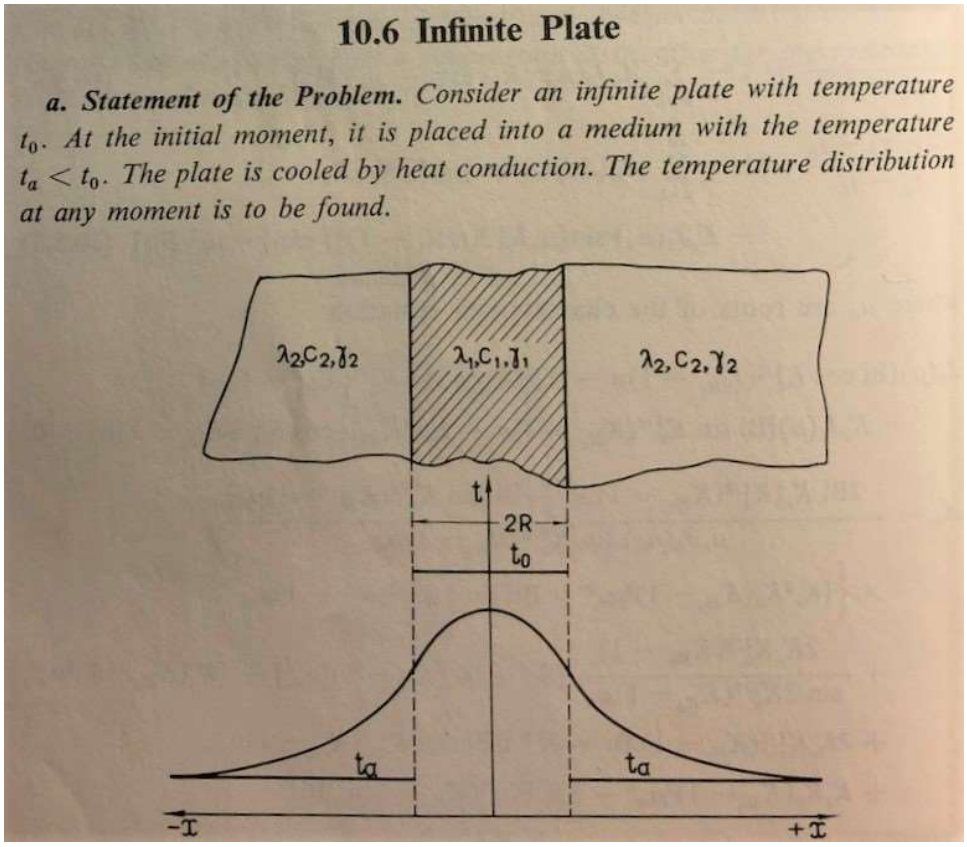


**Figure 3.2 A problem from a reference book to validate the analytical solution**[143]

$$\frac{T_2(x,t) - T_{2i}}{(T_{2i} - T_{4i})} = -\frac{1}{1+K_\varepsilon} \times \sum_{n=1}^{\infty} (-h)^{n-1} \left[ \operatorname{erfc} \frac{(2n-1)R - x}{2\sqrt{\alpha^c t}} + \operatorname{erfc} \frac{(2n-1)R + x}{2\sqrt{\alpha^c t}} \right] \tag{3.38}$$

$$\frac{T_4(x,t) - T_{4i}}{(T_{2i} - T_{4i})} = \frac{K_\varepsilon}{1+K_\varepsilon} \operatorname{erfc} \frac{x - R}{2\sqrt{\alpha^o t}} - \frac{K_\varepsilon(1+h)}{1+K_\varepsilon} \times \sum_{n=1}^{\infty} (-h)^{n-1} \operatorname{erfc} \frac{x - R + 2nRK_\alpha^{-1/2}}{2\sqrt{\alpha^o t}} \tag{3.39}$$

### 3.1.6 Temperature Gradients in the Bodies

Using the following relation, the gradients of the Eqs. (3.34) – (3.37) may be written as,

$$\frac{\partial}{\partial x}\left[\operatorname{erfc}\left(\frac{x}{2\sqrt{\alpha t}}\right)\right] = -\frac{1}{\sqrt{\pi\alpha t}}\exp\left(-\frac{x^2}{4\alpha t}\right)$$

$$\frac{\partial}{\partial x}\left[\operatorname{erfc}\left(\frac{-x}{2\sqrt{\alpha t}}\right)\right] = \frac{1}{\sqrt{\pi\alpha t}}\exp\left(-\frac{x^2}{4\alpha t}\right)$$

**Temperature Gradient in Body-1 (B1)**

$$\begin{aligned}\frac{\partial T_1(x,t)}{\partial x} &= \frac{K_\varepsilon}{1+K_\varepsilon}\frac{1}{\sqrt{\pi\alpha^o t}} \\ &\times\Bigg\{(T_{2i}-T_{1i})\,h\sum_{n=1}^{\infty}h^{2(n-1)}\exp\left(-\left[\frac{-x-R+(4n-0)RK_\alpha^{-1/2}}{2\sqrt{\alpha^o t}}\right]^2\right) \\ &-(T_{2i}-T_{3i})\,h\sum_{n=1}^{\infty}h^{2(n-1)}\exp\left(-\left[\frac{-x-R+(4n-1)RK_\alpha^{-1/2}}{2\sqrt{\alpha^o t}}\right]^2\right) \\ &-\frac{2(T_{3i}-T_{4i})}{(1+K_\varepsilon)}\sum_{n=1}^{\infty}h^{2(n-1)}\exp\left(-\left[\frac{-x-R+(4n-2)RK_\alpha^{-1/2}}{2\sqrt{\alpha^o t}}\right]^2\right) \\ &-(T_{2i}-T_{3i})\sum_{n=1}^{\infty}h^{2(n-1)}\exp\left(-\left[\frac{-x-R+(4n-3)RK_\alpha^{-1/2}}{2\sqrt{\alpha^o t}}\right]^2\right) \\ &+(T_{2i}-T_{1i})\sum_{n=1}^{\infty}h^{2(n-1)}\exp\left(-\left[\frac{-x-R+(4n-4)RK_\alpha^{-1/2}}{2\sqrt{\alpha^o t}}\right]^2\right)\Bigg\}\end{aligned} \tag{3.40}$$

**Temperature Gradient in Body-2 (B2)**

$$\begin{aligned}&\frac{\partial T_2(x,t)}{\partial x} \\ &=\frac{1}{\sqrt{\pi\alpha^c t}}\Bigg\{-\frac{(T_{2i}-T_{3i})\,h^2}{2}\sum_{n=1}^{\infty}h^{2(n-1)}\exp\left(-\left[\frac{(4n-0)R+x}{2\sqrt{\alpha^c t}}\right]^2\right) \\ &+\frac{h}{1+K_\varepsilon}\sum_{n=1}^{\infty}h^{2(n-1)}\left[(T_{2i}-T_{1i})\exp\left(-\left[\frac{(4n-1)R-x}{2\sqrt{\alpha^c t}}\right]^2\right)-(T_{3i}-T_{4i})\exp\left(-\left[\frac{(4n-1)R+x}{2\sqrt{\alpha^c t}}\right]^2\right)\right] \\ &-\frac{h}{2}\sum_{n=1}^{\infty}h^{2(n-1)}\left[(T_{2i}-T_{3i})\exp\left(-\left[\frac{(4n-2)R-x}{2\sqrt{\alpha^c t}}\right]^2\right)+(T_{2i}-T_{3i})\exp\left(-\left[\frac{(4n-2)R+x}{2\sqrt{\alpha^c t}}\right]^2\right)\right] \\ &-\frac{1}{1+K_\varepsilon}\sum_{n=1}^{\infty}h^{2(n-1)}\left[(T_{3i}-T_{4i})\exp\left(-\left[\frac{(4n-3)R-x}{2\sqrt{\alpha^c t}}\right]^2\right)-(T_{2i}-T_{1i})\exp\left(-\left[\frac{(4n-3)R+x}{2\sqrt{\alpha^c t}}\right]^2\right)\right] \\ &-\frac{(T_{2i}-T_{3i})}{2}\sum_{n=1}^{\infty}h^{2(n-1)}\exp\left(-\left[\frac{(4n-4)R-x}{2\sqrt{\alpha^c t}}\right]^2\right)\Bigg\}\end{aligned} \tag{3.41}$$

**Temperature Gradient in Body-3 (B3)**

$$\frac{\partial T_3(x,t)}{\partial x}$$
$$= \frac{1}{\sqrt{\pi\alpha^c t}}\Bigg\{-\frac{(T_{2i}-T_{3i})\,h^2}{2}\sum_{n=1}^{\infty} h^{2(n-1)}\exp\left(-\left[\frac{(4n-0)R-x}{2\sqrt{\alpha^c t}}\right]^2\right)$$
$$+\frac{h}{1+K_\varepsilon}\sum_{n=1}^{\infty} h^{2(n-1)}\left[(T_{2i}-T_{1i})\exp\left(-\left[\frac{(4n-1)R-x}{2\sqrt{\alpha^c t}}\right]^2\right)-(T_{3i}-T_{4i})\exp\left(-\left[\frac{(4n-1)R+x}{2\sqrt{\alpha^c t}}\right]^2\right)\right]$$
$$-\frac{h}{2}\sum_{n=1}^{\infty} h^{2(n-1)}\left[(T_{2i}-T_{3i})\exp\left(-\left[\frac{(4n-2)R-x}{2\sqrt{\alpha^c t}}\right]^2\right)+(T_{2i}-T_{3i})\exp\left(-\left[\frac{(4n-2)R+x}{2\sqrt{\alpha^c t}}\right]^2\right)\right] \quad (3.42)$$
$$-\frac{1}{1+K_\varepsilon}\sum_{n=1}^{\infty} h^{2(n-1)}\left[(T_{3i}-T_{4i})\exp\left(-\left[\frac{(4n-3)R-x}{2\sqrt{\alpha^c t}}\right]^2\right)-(T_{2i}-T_{1i})\exp\left(-\left[\frac{(4n-3)R+x}{2\sqrt{\alpha^c t}}\right]^2\right)\right]$$
$$-\frac{(T_{2i}-T_{3i})}{2}\sum_{n=1}^{\infty} h^{2(n-1)}\exp\left(-\left[\frac{(4n-4)R+x}{2\sqrt{\alpha^c t}}\right]^2\right)\Bigg\}$$

**Temperature Gradient in Body-4 (B4)**

$$\frac{\partial T_4(x,t)}{\partial x} = -\frac{K_\varepsilon}{1+K_\varepsilon}\frac{1}{\sqrt{\pi\alpha^o t}}$$
$$\times\Bigg\{(T_{3i}-T_{4i})\,h\sum_{n=1}^{\infty} h^{2(n-1)}\exp\left(-\left[\frac{x-R+(4n-0)RK_\alpha^{-1/2}}{2\sqrt{\alpha^o t}}\right]^2\right)$$
$$+(T_{2i}-T_{3i})\,h\sum_{n=1}^{\infty} h^{2(n-1)}\exp\left(-\left[\frac{x-R+(4n-1)RK_\alpha^{-1/2}}{2\sqrt{\alpha^o t}}\right]^2\right)$$
$$-\frac{2(T_{2i}-T_{1i})}{(1+K_\varepsilon)}\sum_{n=1}^{\infty} h^{2(n-1)}\exp\left(-\left[\frac{x-R+(4n-2)RK_\alpha^{-1/2}}{2\sqrt{\alpha^o t}}\right]^2\right) \quad (3.43)$$
$$+(T_{2i}-T_{3i})\sum_{n=1}^{\infty} h^{2(n-1)}\exp\left(-\left[\frac{x-R+(4n-3)RK_\alpha^{-1/2}}{2\sqrt{\alpha^o t}}\right]^2\right)$$
$$+(T_{3i}-T_{4i})\sum_{n=1}^{\infty} h^{2(n-1)}\exp\left(-\left[\frac{x-R+(4n-4)RK_\alpha^{-1/2}}{2\sqrt{\alpha^o t}}\right]^2\right)\Bigg\}$$

### 3.1.7 Heat Flux through the Interfaces

The conductive heat flux can be written by Fourier law[146] in 1-D as follows,

$$q = -k\frac{\partial T}{\partial x}$$

**Heat Flux through the Interface B1|B2 at x = – R**

$$q_{B1|B2} = -k^o\left.\frac{\partial T_1(x,t)}{\partial x}\right|_{x=-R} = -k^c\left.\frac{\partial T_2(x,t)}{\partial x}\right|_{x=-R}$$

Putting Eq. (3.40) in above Eq. and replacing $x = -R$ we get

$$q_{B1|B2}(t) = -k^o \left.\frac{\partial T_1(x,t)}{\partial x}\right|_{x=-R}$$

$$= -\frac{k^o}{\sqrt{\pi\alpha^o t}} \frac{K_\varepsilon}{1+K_\varepsilon}$$

$$\times \left\{ (T_{2i} - T_{1i}) h \sum_{n=1}^{\infty} h^{2(n-1)} \exp\left( -\left[\frac{(4n-0)R}{2\sqrt{\alpha^c t}}\right]^2 \right) \right.$$

$$- (T_{2i} - T_{3i}) h \sum_{n=1}^{\infty} h^{2(n-1)} \exp\left( -\left[\frac{(4n-1)R}{2\sqrt{\alpha^c t}}\right]^2 \right)$$

$$- \frac{2(T_{3i} - T_{4i})}{(1+K_\varepsilon)} \sum_{n=1}^{\infty} h^{2(n-1)} \exp\left( -\left[\frac{(4n-2)R}{2\sqrt{\alpha^c t}}\right]^2 \right)$$

$$- (T_{2i} - T_{3i}) \sum_{n=1}^{\infty} h^{2(n-1)} \exp\left( -\left[\frac{(4n-3)R}{2\sqrt{\alpha^c t}}\right]^2 \right)$$

$$\left. + (T_{2i} - T_{1i}) \sum_{n=1}^{\infty} h^{2(n-1)} \exp\left( -\left[\frac{(4n-4)R}{2\sqrt{\alpha^c t}}\right]^2 \right) \right\} \quad (3.44)$$

**Heat Flux through the Interface B2|B3 at x = 0**

$$q_{B2|B3} = -k^c \left.\frac{\partial T_2(x,t)}{\partial x}\right|_{x=0} = -k^c \left.\frac{\partial T_3(x,t)}{\partial x}\right|_{x=0}$$

Putting Eq. (3.41), we get

$$q_{B2|B3}(t) = -k^c \left.\frac{\partial T_2(x,t)}{\partial x}\right|_{x=0}$$

$$= -\frac{k^c}{\sqrt{\pi\alpha^c t}} \left\{ -\frac{(T_{2i} - T_{3i})}{2} h^2 \sum_{n=1}^{\infty} h^{2(n-1)} \exp\left( -\left[\frac{(4n-0)R}{2\sqrt{\alpha^c t}}\right]^2 \right) \right.$$

$$+ \frac{h}{1+K_\varepsilon} (T_{2i} - T_{1i} - T_{3i} + T_{4i}) \sum_{n=1}^{\infty} h^{2(n-1)} \exp\left( -\left[\frac{(4n-1)R}{2\sqrt{\alpha^c t}}\right]^2 \right)$$

$$- (T_{2i} - T_{3i})\, h \sum_{n=1}^{\infty} h^{2(n-1)} \exp\left( -\left[\frac{(4n-2)R}{2\sqrt{\alpha^c t}}\right]^2 \right)$$

$$- \frac{1}{1+K_\varepsilon} (T_{3i} - T_{4i} - T_{2i} + T_{1i}) \sum_{n=1}^{\infty} h^{2(n-1)} \exp\left( -\left[\frac{(4n-3)R}{2\sqrt{\alpha^c t}}\right]^2 \right)$$

$$\left. - \frac{(T_{2i} - T_{3i})}{2} \sum_{n=1}^{\infty} h^{2(n-1)} \exp\left( -\left[\frac{(4n-4)R}{2\sqrt{\alpha^c t}}\right]^2 \right) \right\} \quad (3.45)$$

**Heat Flux through the Interface B3|B4 at x = R**

$$q_{B3|B4} = -k^c \left.\frac{\partial T_3(x,t)}{\partial x}\right|_{x=R} = -k^o \left.\frac{\partial T_4(x,t)}{\partial x}\right|_{x=R}$$

Putting Eq. (3.43) in the above equation, we get

$$\begin{aligned} q_{B3|B4}(t) &= -k^o \left.\frac{\partial T_4(x,t)}{\partial x}\right|_{x=R} \\ &= \frac{k^o}{\sqrt{\pi \alpha^o t}} \frac{K_\varepsilon}{1+K_\varepsilon} \\ &\times \left\{ (T_{3i} - T_{4i})\, h \sum_{n=1}^{\infty} h^{2(n-1)} \exp\left( -\left[\frac{(4n-0)R}{2\sqrt{\alpha^c t}}\right]^2 \right) \right. \\ &+ (T_{2i} - T_{3i})\, h \sum_{n=1}^{\infty} h^{2(n-1)} \exp\left( -\left[\frac{(4n-1)R}{2\sqrt{\alpha^c t}}\right]^2 \right) \\ &- \frac{2(T_{2i} - T_{1i})}{(1+K_\varepsilon)} \sum_{n=1}^{\infty} h^{2(n-1)} \exp\left( -\left[\frac{(4n-2)R}{2\sqrt{\alpha^c t}}\right]^2 \right) \\ &+ (T_{2i} - T_{3i}) \sum_{n=1}^{\infty} h^{2(n-1)} \exp\left( -\left[\frac{(4n-3)R}{2\sqrt{\alpha^c t}}\right]^2 \right) \\ &\left. + (T_{3i} - T_{4i}) \sum_{n=1}^{\infty} h^{2(n-1)} \exp\left( -\left[\frac{(4n-4)R}{2\sqrt{\alpha^c t}}\right]^2 \right) \right\} \end{aligned} \tag{3.46}$$

### 3.1.8 Heat Energy Transfer through the Interfaces

The total amount of heat transfer per unit area through the interface may be determined by integrating heat flux over time as follows,

$$Q = \int_0^t q\,dt$$

From Eqs. (3.44) – (3.46), it may be seen that the form of heat flux is as follows,

$$q = \frac{1}{\sqrt{t}} \exp\left(-\frac{A}{t}\right)$$

Where $A = \left[\frac{(4n-4)R}{2\sqrt{\alpha^c}}\right]^2$

The solution of such integral may be found in any book of calculus[152] or may be solved using Mathematica as,

$$\int_0^t \frac{1}{\sqrt{t}} \exp\left(-\frac{A}{t}\right) dt = 2\sqrt{t}\exp\left(-\frac{A}{t}\right) - 2\sqrt{A}\sqrt{\pi}\,\mathrm{erfc}\left(\frac{A}{\sqrt{t}}\right) \tag{3.47}$$

Where $1 - \mathrm{erf}(x) = \mathrm{erfc}(x)$

**Heat Energy through the Interface B1|B2**

Total heat transfer through any interface B1|B2 throughout the heat conduction process may be determined using the following relation,

$$Q_{B1|B2} = \int_0^t q_{B1|B2} dt$$

Using Eq. (3.47), we may integrate Eq. (3.45) from $t = 0 \rightarrow t$ as follows to determine total heat energy transfer through interface B1|B2,

$$\begin{aligned}
&Q_{B1|B2} \\
&= -\frac{2k^o}{\sqrt{\pi\alpha^o}} \frac{K_\varepsilon}{1+K_\varepsilon} \\
&\times \Bigg\{ (T_{2i} - T_{1i})\, h \sum_{n=1}^{\infty} h^{2(n-1)} \left[ \sqrt{t}\exp\left(-\left[\frac{(4n-0)R}{2\sqrt{\alpha^c t}}\right]^2\right) - \frac{(4n-0)R}{2\sqrt{\alpha^c}}\sqrt{\pi}\,\mathrm{erfc}\frac{(4n-0)R}{2\sqrt{\alpha^c t}} \right] \\
&- (T_{2i} - T_{3i})\, h \sum_{n=1}^{\infty} h^{2(n-1)} \left[ \sqrt{t}\exp\left(-\left[\frac{(4n-1)R}{2\sqrt{\alpha^c t}}\right]^2\right) - \frac{(4n-1)R}{2\sqrt{\alpha^c}}\sqrt{\pi}\,\mathrm{erfc}\frac{(4n-1)R}{2\sqrt{\alpha^c t}} \right] \\
&- \frac{2(T_{3i} - T_{4i})}{(1+K_\varepsilon)} \sum_{n=1}^{\infty} h^{2(n-1)} \left[ \sqrt{t}\exp\left(-\left[\frac{(4n-2)R}{2\sqrt{\alpha^c t}}\right]^2\right) - \frac{(4n-2)R}{2\sqrt{\alpha^c}}\sqrt{\pi}\,\mathrm{erfc}\frac{(4n-2)R}{2\sqrt{\alpha^c t}} \right] \\
&- (T_{2i} - T_{3i}) \sum_{n=1}^{\infty} h^{2(n-1)} \left[ \sqrt{t}\exp\left(-\left[\frac{(4n-3)R}{2\sqrt{\alpha^c t}}\right]^2\right) - \frac{(4n-3)R}{2\sqrt{\alpha^c}}\sqrt{\pi}\,\mathrm{erfc}\frac{(4n-3)R}{2\sqrt{\alpha^c t}} \right] \\
&+ (T_{2i} - T_{1i}) \sum_{n=1}^{\infty} h^{2(n-1)} \left[ \sqrt{t}\exp\left(-\left[\frac{(4n-4)R}{2\sqrt{\alpha^c t}}\right]^2\right) - \frac{(4n-4)R}{2\sqrt{\alpha^c}}\sqrt{\pi}\,\mathrm{erfc}\frac{(4n-4)R}{2\sqrt{\alpha^c t}} \right] \Bigg\}
\end{aligned} \tag{3.48}$$

**Heat Energy through the Interface B3|B4**

Using Eq. (3.47), we may integrate Eq. (3.46) from $t = 0 \rightarrow t$ as follows to determine total heat energy transfer through interface B3|B4,

$$
\begin{aligned}
Q_{B3|B4} &= \frac{2k^o}{\sqrt{\pi\alpha^o t}}\frac{K_\varepsilon}{1+K_\varepsilon} \\
&\times\Bigg\{(T_{3i}-T_{4i})\,h\sum_{n=1}^{\infty}h^{2(n-1)}\left[\sqrt{t}\exp\left(-\left[\frac{(4n-0)R}{2\sqrt{\alpha^c t}}\right]^2\right)-\left(\frac{4R}{2\sqrt{\alpha^c}}\right)\sqrt{\pi}\,\mathrm{erfc}\left(\frac{4R}{2\sqrt{\alpha^c t}}\right)\right] \\
&+(T_{2i}-T_{3i})\,h\sum_{n=1}^{\infty}h^{2(n-1)}\left[\sqrt{t}\exp\left(-\left[\frac{(4n-1)R}{2\sqrt{\alpha^c t}}\right]^2\right)-\left(\frac{4R}{2\sqrt{\alpha^c}}\right)\sqrt{\pi}\,\mathrm{erfc}\left(\frac{(4n-1)R}{2\sqrt{\alpha^c t}}\right)\right] \\
&-\frac{2\,(T_{2i}-T_{1i})}{(1+K_\varepsilon)}\sum_{n=1}^{\infty}h^{2(n-1)}\left[\sqrt{t}\exp\left(-\left[\frac{(4n-2)R}{2\sqrt{\alpha^c t}}\right]^2\right)-\left(\frac{4R}{2\sqrt{\alpha^c}}\right)\sqrt{\pi}\,\mathrm{erfc}\left(\frac{(4n-2)R}{2\sqrt{\alpha^c t}}\right)\right] \\
&+(T_{2i}-T_{3i})\sum_{n=1}^{\infty}h^{2(n-1)}\left[\sqrt{t}\exp\left(-\left[\frac{(4n-3)R}{2\sqrt{\alpha^c t}}\right]^2\right)-\left(\frac{4R}{2\sqrt{\alpha^c}}\right)\sqrt{\pi}\,\mathrm{erfc}\left(\frac{(4n-3)R}{2\sqrt{\alpha^c t}}\right)\right] \\
&+(T_{3i}-T_{4i})\sum_{n=1}^{\infty}h^{2(n-1)}\left[\sqrt{t}\exp\left(-\left[\frac{(4n-4)R}{2\sqrt{\alpha^c t}}\right]^2\right)-\left(\frac{4R}{2\sqrt{\alpha^c}}\right)\sqrt{\pi}\,\mathrm{erfc}\left(\frac{(4n-4)R}{2\sqrt{\alpha^c t}}\right)\right]\Bigg\}
\end{aligned}
\tag{3.49}
$$

Using the relations in Eqs. (3.48) and (3.49), the total heat flow may be determined through the interfaces B1|B2 and B3|B4 respectively during the specified time.

## 3.2 Summary of Analytical Solution

A complete analytical solution of the unsteady heat conduction problem in a multilayer system of four bodies has been determined. Temperature profiles of all the bodies involved as a function of space and time may be determined using Eqs. (3.34) – (3.37). Eqs. (3.44) – (3.46) may be used to determine heat flux through the interfaces (B1|B2, B2|B3, and B3|B4) as a function of time. The total heat through the interfaces in a specified time may be determined using relations (3.48) and (3.49). It may be observed that the solutions, temperature profiles and heat fluxes, energy transfers obtained above have infinite summation series. That is, each solution is the sum of five series and each series has infinite terms. Directly using above solutions requests the determination of the sum of these series, which is not convenient for further study and makes it difficult to get any conclusion from it. Based on the nature of the problem and the physics, the sum of the series should be a finite number. In the following, a procedure is being devised where we will present a solution to replace infinite series to a finite series to a reasonable approximation to use the analytical solution for the numerical calculations.

## 3.3 Estimating the Summation Terms

### 3.3.1 Determination of Number of Terms Needed

The solutions, temperature profiles and heat fluxes, obtained in the analytical solution have infinite number of terms. That is, each solution is the sum of five series and each series has infinite terms. All these series can be represented by the series $S_n(x,t)$ $(n = 1,2,3 \dots)$ or $S_{n'}(x,t)$ $(n' = 0,1,2, \dots)$, i.e., $n' = n - 1$ or $n = n' + 1$ as,

$$S_n(x,t) = h^{2(n-1)} \exp\left(-\left[\frac{(4n-m)R}{2\sqrt{\alpha^c t}}\right]^2\right) \tag{3.50}$$

$$S_{n'}(x,t) = h^{2n'} \exp\left(-\left[\frac{(4n'+4-m)R}{2\sqrt{\alpha^c t}}\right]^2\right) \tag{3.51}$$

where m = 0, 1, 2, 3, 4, respectively. Directly using above solutions requests the determination of the sum of these series, which is not convenient for further study and makes it difficult to get any conclusion from it.

Based on the nature of the problem and the physics, the sum of the series shown in Eqs. (3.50) and (3.51) should be a finite number. It is also found that

$$\frac{S_{n+2}}{S_{n+1}} = \frac{h^{2(n+1)} \exp\left(-\left[\frac{(4(n+2)-m)R}{2\sqrt{\alpha^c t}}\right]^2\right)}{h^{2n} \exp\left(-\left[\frac{(4(n+1)-m)R}{2\sqrt{\alpha^c t}}\right]^2\right)}$$

$$\frac{S_{n+2}}{S_{n+1}} = h^2 B \exp(-A \cdot n) \qquad (< 1) \tag{3.52}$$

where $A = \frac{8R^2}{\alpha^c t} > 0$ and $B = \exp\left(-\frac{(12-2m)R^2}{\alpha^c t}\right) < 1$. As mentioned above $h^2 < 1$, one can get that $\frac{S_{n+2}}{S_{n+1}}$ is less than one (see Appendix - I) and, more importantly, decreases with increasing *n*, which means that these series are convergent. That is, there should be a sufficiently large integer *N* such that the subsequent terms have no significant effect on the overall summation value as,

$$\sum_{n=1}^{\infty} S_n(x,t) = \sum_{n=1}^{N} S_n(x,t) + \sum_{n=N+1}^{\infty} S_n(x,t)$$
$$= \sum_{n=1}^{N} S_n(x,t) + \Delta \tag{3.53}$$
$$\cong \sum_{n=1}^{N} S_n(x,t)$$

$$\sum_{n=1}^{\infty} S_n(x,t) = \sum_{n'=0}^{\infty} S_{n'}(x,t)$$
$$= \sum_{n'=0}^{N-1} S_{n'}(x,t) + \Delta \tag{3.54}$$
$$\cong \sum_{n'=0}^{N-1} S_{n'}(x,t)$$

Therefore, it is interesting to determine the *N* so that the calculation of these series can be carried out and the sum of the first *N* terms can be used as the value of the series as follows. In Eq. (3.53),

$$\Delta = \sum_{n'=N}^{\infty} S_{n'}(x,t)$$
$$= \sum_{n'=N}^{\infty} h^{2n'} \exp\left(-\left[\frac{4R}{2\sqrt{\alpha^c t}} n' + \frac{4R - mR}{2\sqrt{\alpha^c t}}\right]^2\right)$$
$$= \sum_{n'=N}^{\infty} h^{2n'} \exp(-[an' + b]^2)$$
$$= \sum_{n'=N}^{\infty} h^{2n'} \exp\left(-a^2 n'^2\right) \exp(-2abn') \exp(-b^2)$$

where $a = 4R/2\sqrt{\alpha^c t}$ & $b = (4-m)R/2\sqrt{\alpha^c t} \geq 0$. Replacing $n'^2$ with $3n'$ and assuming $n' > 3$ (or the *N* is at least 4), the following relation will hold:

$$\Delta = \sum_{n'=N}^{\infty} h^{2n'} \exp\left(-a^2 n'^2\right) \exp(-2abn') \exp(-b^2)$$

$$< \sum_{n'=N}^{\infty} h^{2n'} \exp(-3a^2 n') \exp(-2abn') \exp(-b^2) \tag{3.55}$$

$$= \sum_{n'=N}^{\infty} C(h^2 \exp(-\gamma))^{n'}$$

where $\gamma = 3a^2 + 2ab > 0$ and $C = \exp(-b^2)$. Therefore, $h^2 \exp(-\gamma) < 1$ as $|h| < 1$ and $\exp(-\gamma) < 1$. The summation of right-hand side of inequality (3.55) being a geometric series is given as:

$$\sum_{n'=N}^{\infty} C(h^2 \exp(-\gamma))^{n'} = C \frac{h^{2N} \exp(-\gamma N)}{1 - h^2 \exp(-\gamma)} > \Delta$$

To determine the value of *N*, any value of first *N* terms can be used to compare with the Δ. For example, if $S_1(x,t)$ is used and a very small positive real number $\delta$ is selected ($0 < \delta \ll 1$), as long as,

$$C \frac{h^{2N} \exp(-\gamma N)}{1 - h^2 \exp(-\gamma)} = S_1(x,t) \cdot \delta$$

the approximation in Eq. (3.53)/(3.54) can be used. That is,

$$\Delta < C \frac{h^{2N} \exp(-\gamma N)}{1 - h^2 \exp(-\gamma)} = \delta\, h^{2(n-1)} \exp\left( - \left[ \frac{(4n-m)R}{2\sqrt{\alpha^c t}} \right]^2 \right) \Bigg|_{n=1}$$

$$\Delta < \exp(-b^2) \frac{h^{2N} \exp(-\gamma N)}{1 - h^2 \exp(-\gamma)} = \delta h^{2(1-1)} \exp(-[a_1]^2)$$

where $a_1 = (4-m)R/2\sqrt{\alpha^c t} = b$ so that

$$h^{2N} \exp(-\gamma N) = \delta[1 - h^2 \exp(-\gamma)] \tag{3.56}$$

Since $0 < h^2 < 1$ and $\exp(-\gamma) < 1$, $[1 - h^2 \exp(-\gamma)] > 0$. Therefore, the N can be written as:

$$\mathrm{N} = \frac{-\ln\delta - \ln(1 - h^2\exp(-\gamma))}{\gamma - \ln h^2} \qquad \geq 4) \qquad (3.57)$$

From Eq. (3.57), one can find that the higher the value of $m$, the bigger is the *N*. Therefore, to simplify the calculation so that one value of *N* can be used for all series with different values of $m$, the constants in Eq. (3.57) is further modified by using m = 4. That is, b = 0 and

$$\gamma = 3a^2 = 12R^2/(\alpha^c t) \qquad (3.58)$$

That is, Eqs. (3.57) and (3.58) and are used to determine the *N*.

From Eq. (3.57) one can find that if $|h| \to 1$ and $\gamma \to \infty$ (i.e., either R is very big or t is very small), $N \to 0$. In this case, the sum of first four terms of the series (i.e., $N = 4$) shown in Eq.(3.53)/(3.54) can be used as the sum of the series. On the other side, if $|h| \to 0$, the $N \to 0$ for all values of $\gamma$. In this case, again the sum of only first four terms of the series (i.e., $N = 4$) shown in Eq. (3.53)/(3.54) can be used as the sum of the series. For a constant $h$, the *N* decreases as the $\gamma$ increases. Typical value of $|h|$ for ceramics as ECM and metals for end materials is 0.5 – 0.9. As long as the $\gamma$ is more than 3 (i.e., $4R^2 > \alpha^c t$), the *N* is less than 4 for the δ being $10^{-5}$ or bigger. Again, in this case, the $N = 4$ can be used for the calculation of the series.

Dependence of *N* on the $\gamma$ for a typical range of $\gamma$ (0.01 – 10) for different values of $|h|$ are shown in Figure 3.3. Clearly, the *N* is always smaller than 70. For a constant value of $h$, *N* decreases as $\gamma$ increases. The rate is, however, not constant as $|h|$ increases, *N* decreases with a higher rate as the γ increases. For a constant γ, the N decreases with decreasing |h|.

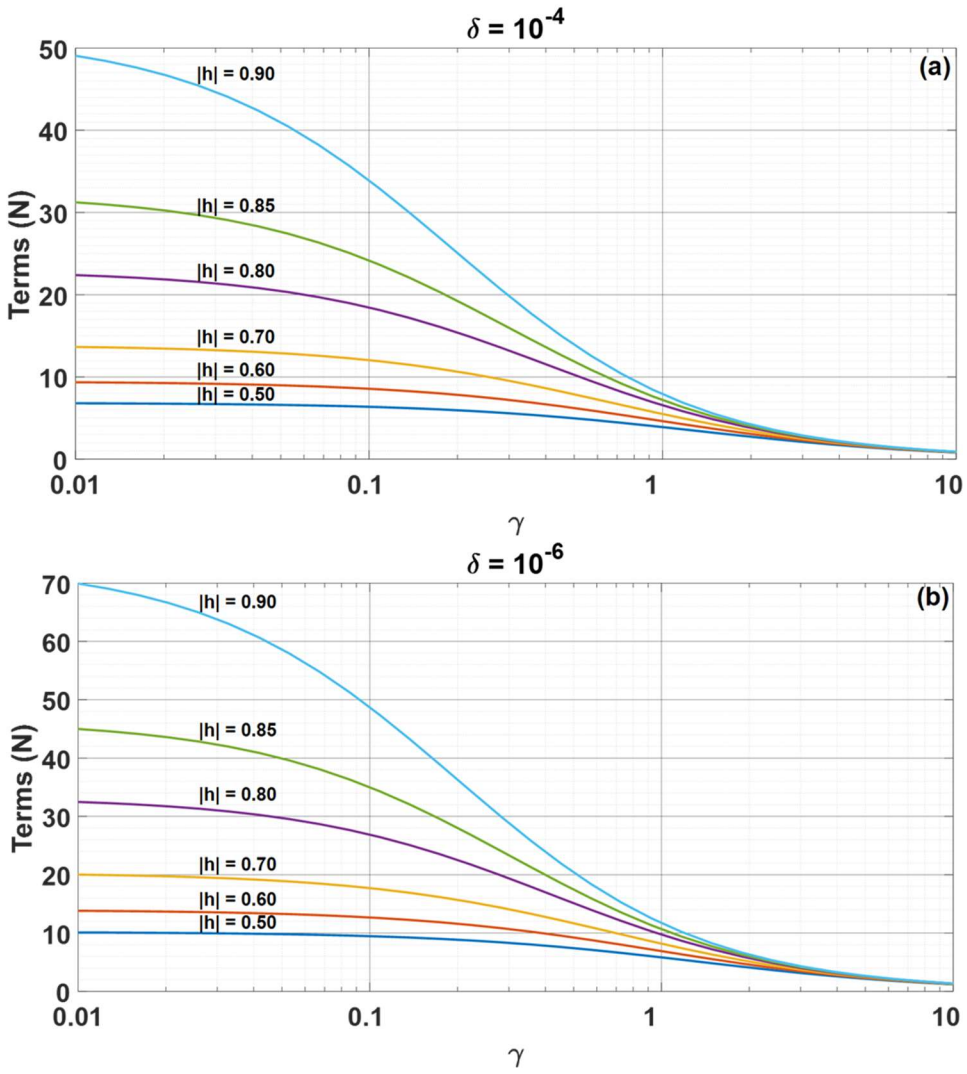


**Figure 3.3 Dependence of $N$ on $\gamma$ (=3a$^2$) with fixed $|h|$ and δ , (a). δ = 10$^{-4}$, (b). δ =10$^{-6}$**

The γ shown in Eq. (3.58) is dependent on the ECM's diffusivity ($\alpha^c$~10$^{-7}$), size of ECM and time of the conduction process. Dependence of $N$ on $|h|$ and $\gamma$ for some typical values is shown in Figure 3.4. Again, it shows that the $N$ is not a big number.

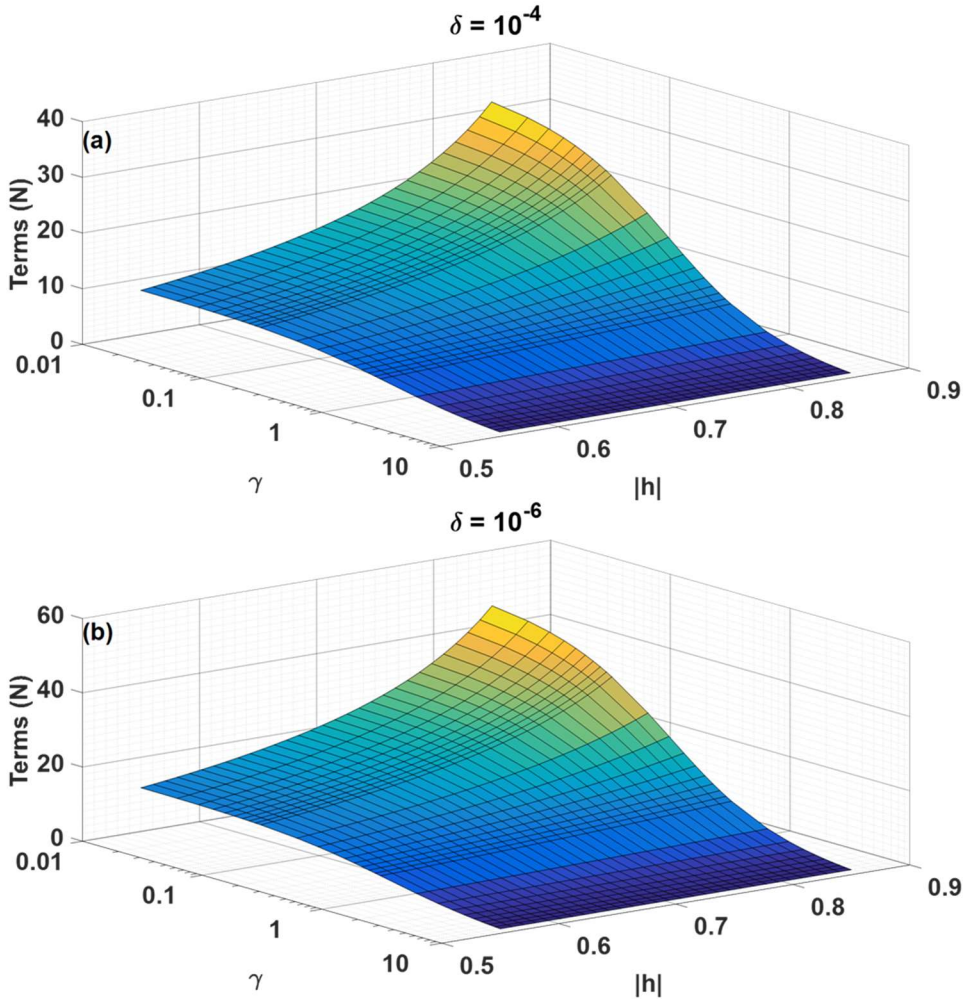


**Figure 3.4 Dependence of N on $|h|$ and $\gamma$ for typical ranges of |h| = 0.55 – 0.85 and $\gamma$ = 0.01 – 10, (a). $\delta = 10^{-4}$, (b). $\delta = 10^{-6}$**

It has to be mentioned that the upper limit $N$ obtained from Eqs. (3.57) and (3.58) is obtained based on the heat flux solution. That is, one can use the $N$ determined to the calculations of Eqs. (3.44) – (3.46).

### 3.3.2 A Case Study

As shown by Eq. (3.57) and (3.58), the value of $N$ is dependent on the values of $\delta$, $h$, and $\gamma$, while the $\gamma$ is determined by $R$, $\alpha^c$ and $t$ (i.e., size of ECM body, thermal diffusivity of the materials, and time). As an example, let us select barium titanate (BT) having thermal properties ($\rho^c$: 6060 $kgm^{-3}$, $k^c$: 6 $Wm^{-1}K^{-1}$, $c_p^c$: 527 $Jkg^{-1}K^{-1}$) as the ECM and aluminum with thermal

properties ($\rho^o$: 2689 $kgm^{-3}$, $k^o$: 237.5 $Wm^{-1}K^{-1}$, $c_p^o$: 951 $Jkg^{-1}K^{-1}$) as the end bodies. Figure 3.5 (a) – (b) shows the dependence of $N$ on both $t$ and $R$ for two different values of for $\delta$.

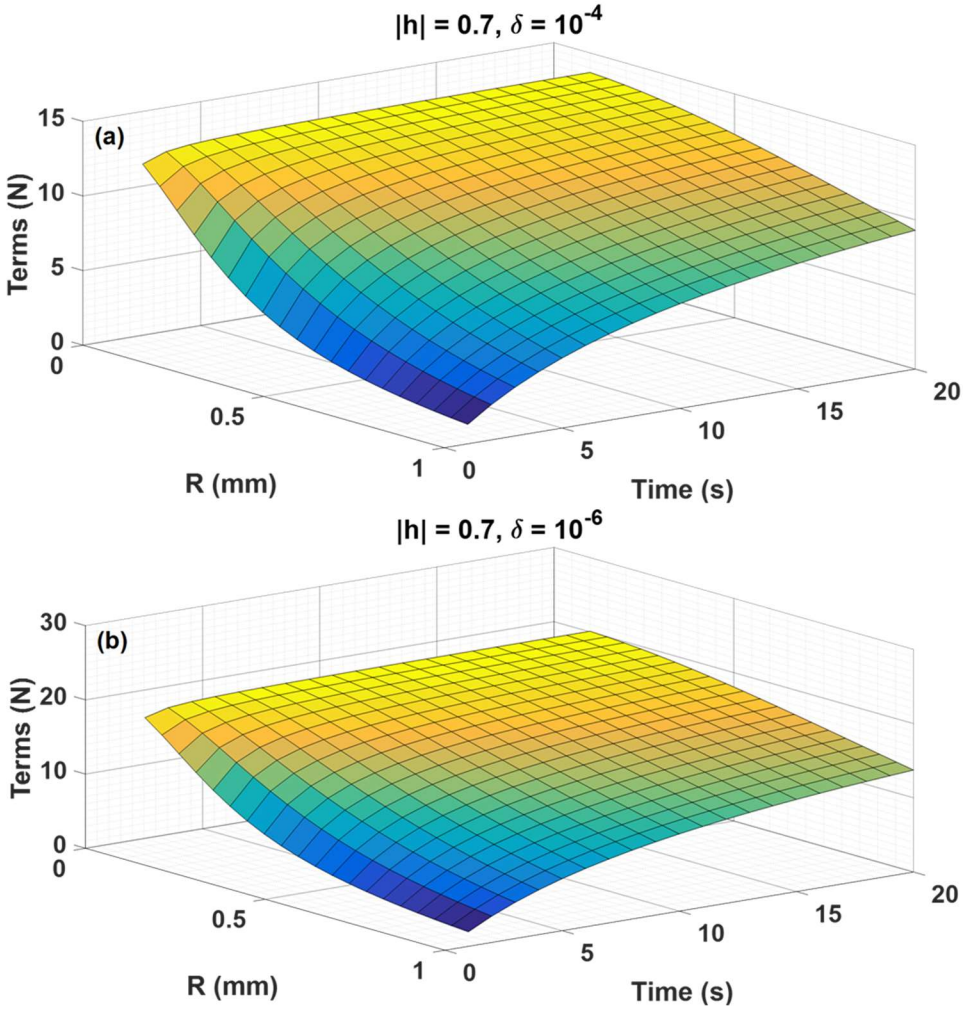


**Figure 3.5 Dependence of N on t and R for BT as ECM and Al as *end* bodies for, (a). δ =10$^{-4}$, (b). δ =10$^{-6}$**

Clearly, longer the time, the higher the value of $N$ is. But, as time gets longer, the increase in the $N$ is very slow. Also, more terms are needed if the sizes of ECMs are reduced. However, the results shown in Figure 3.5 demonstrate that the increase in the $N$ is slow at a longer time and/or smaller size. It seems that for this case, for the numerical calculations, the $N$ is no more than 15. As it is evident from solution (3.57) that $N$ also depends on the tolerance $\delta$. The dependence of $N$ on $\delta$ is shown in Figure 3.6 on a semi logarithmic scale. As expected, the smaller the tolerance, the bigger the value of $N$ is.

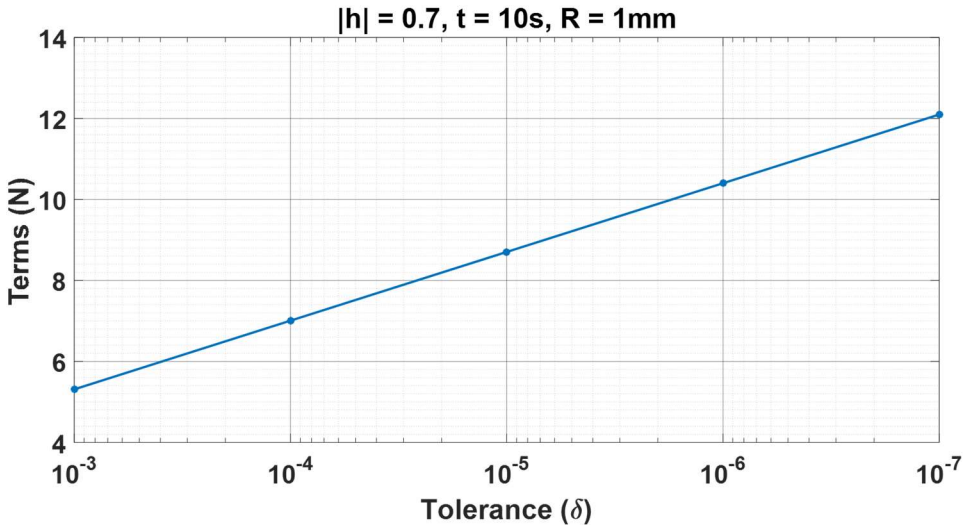


**Figure 3.6 Dependence of N on tolerance using BT as ECMs and Al as *end* bodies for t = 10s and R = 1 mm.**

## 3.4 Concluding Remarks

A one dimensional (1D) analytical solution of dynamic heat conduction problem for a system of four bodies has been determined, which gives the time dependence of both the temperature profiles in all four bodies and heat flux through all three interfaces. The solution includes series with infinite terms. It is proved that these series are convergent so that the sum of first $N$ terms of a series can be used as the sum of the series. An analysis for the estimation of the $N$ was carried out and a formula to calculate the $N$ is introduced. For most of cases, the $N$ is less than 70. When barium titanate (BT) is used as the ECM and aluminum is used as surrounding material, the case study shows that the $N$ is mostly less than 20. The approximation is simple, and yet accurate enough, to be adopted in future engineering models. For example, by using multiplayer model and the results reported here, a new design of ECE-based heat pump with complete silent operation (without any moving parts, regenerators, and/or thermal switches) is introduced in the next chapter.

# Chapter 4 Heat Pump without Moving Parts/ Silent Operation

## 4.1 Heat Pump Model for Directional Heat Flow

This chapter presents a heat pumping concept where the heat energy can be transferred from heat source (SO) to heat sink (SI) without the involvement of any moving parts, i.e. *working materials, circulating fluids, mechanical actuation and/or heat switches/ diodes, etc.* A four-body system has been conceived in which two ECM layers have been sandwiched between two semi-infinite bodies as shown in Figure 4.1. In this multilayer structure, two semi-infinite layers on left and right represent the heat source (SO) and heat sink (SI), respectively, while two layers (EC1 and EC2) of ECM are sandwiched into the SO and SI whose temperature profile may be changed instantaneously using external electric filed. All four bodies/layers are permanently bonded together, and nothing moves. That is, in this all-solid design, neither moving part nor actuator, nor heat switch is used. Therefore, a high reliability is expected.

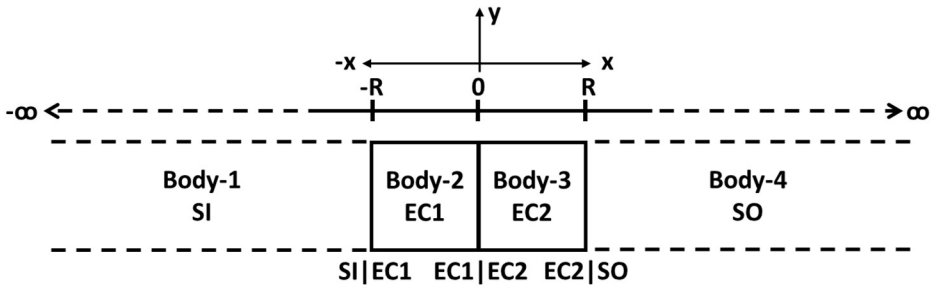


**Figure 4.1 Conceptual model of EC heat pump**

## 4.2 Physical Model and Working Principle

Considering the case that all bodies reach a thermal equilibrium state (i.e., at the same temperature T), and then a three-step electric field cycle as shown in Figure 4.3 is applied on the two ECM layers. Assume that the change in the electric field is so fast that the temperature change in the ECM layer due to the ECE can be treated as an adiabatic process, which is exactly what has been observed in typical ECE-based devices[132,134].

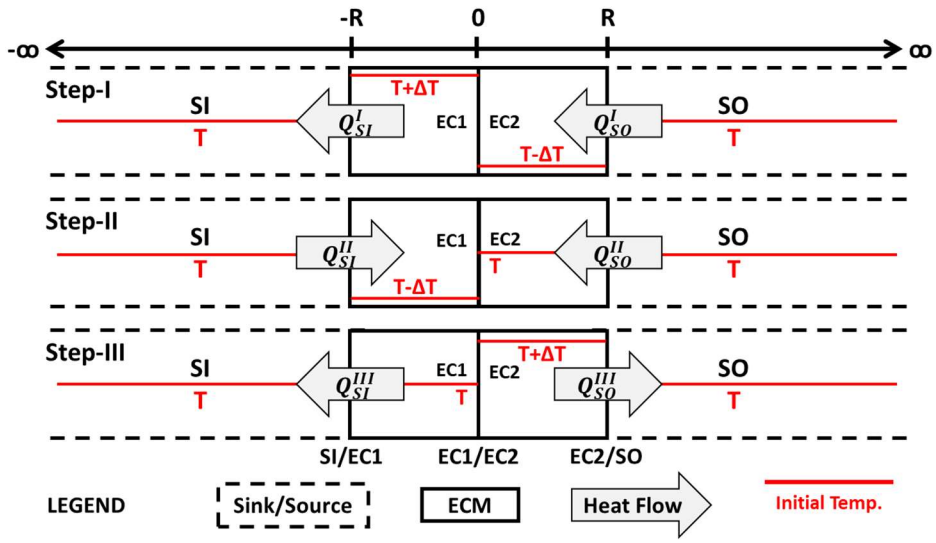


**Figure 4.2 Operational process of the three-step cycles for the system shown in Figure 4.1**

The details about the three-step process/cycle are:

**Step-I**: the electric field on both EC1 and EC2 is changed so that the temperature of EC1 increases by $\Delta T$ $(> 0)$ and the temperature of EC2 decreases by $\Delta T$; and then the electric field on both EC1 and EC2 is kept for a certain time to allow the temperature in all four bodies reaches their new thermal equilibrium state (i.e., the same temperature T) due to the heat conduction.

During Step-I, it is expected that a certain amount of heat ($Q^I_{SO}$) will be transferred from right (SO) to EC2 and a certain amount of heat ($Q^I_{SI}$) will be transferred from EC1 to left (SI) as shown in Figure 4.2.

**Step-II**: the electric field on EC2 is still kept as it is in Step-I, but the electric field on EC1 is changed so that the temperature of the EC1 is decreased by $\Delta T$, and then the electric field on EC1 and EC2 is kept to allow the system reach their thermal equilibrium state (i.e., the same temperature T) again due to the thermal conduction.

During Step-II, it is expected that a certain amount of heat ($Q^{II}_{SO}$) will be transferred from right (SO) to EC2 and a certain amount of heat ($Q^{II}_{SI}$) will be transferred from left (SI) to EC1 as shown in Figure 4.2.

**Step-III**: the electric field on EC1 is kept as it is in Step-II, but the electric field on EC2 is changed so that the temperature of EC2 is increased by $\Delta T$, and then it is kept to allow four bodies to reach their thermal equilibrium state (i.e., the same temperature T) again.

During Step-III, it is expected that a certain amount of heat ($Q_{SO}^{III}$) will be transferred from EC2 to right (SO) and a certain amount of heat ($Q_{SI}^{III}$) will be transferred from EC1 to left (SI) as shown in Figure 4.2.

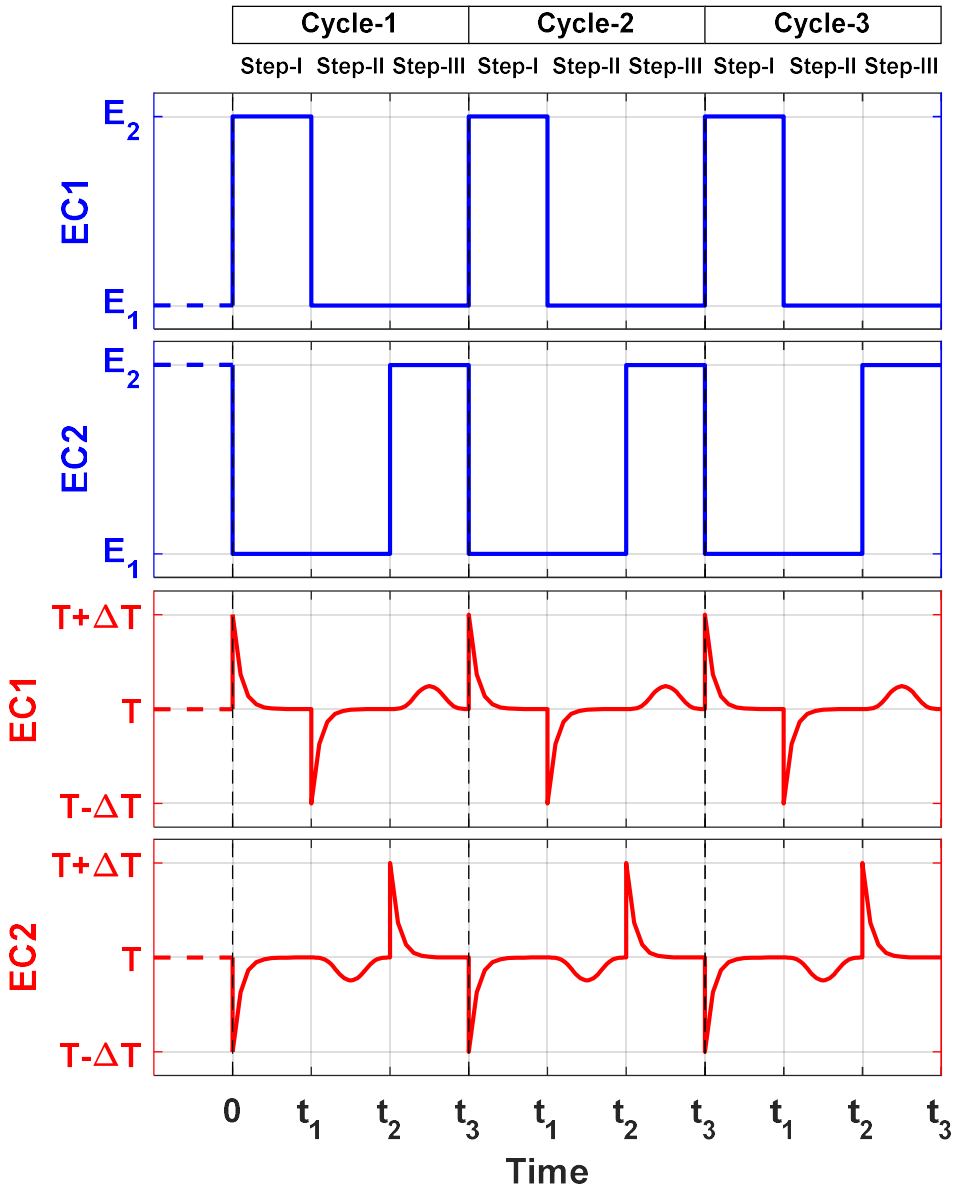


**Figure 4.3 Electric field cycle and corresponding temperature variations at center of EC1 and EC2 (three cycles shown).**

The change in the electric field on both EC1 and EC2 is schematically shown in Figure 4.3, in order to achieve the thermal process shown in Figure 4.2. Clearly, after one cycle, the electric field on both EC1 and EC2 restores its original condition. In other words, the three-step process shown

in Figure 4.2 is repeatable. That is, the three-step process can be continuously repeated. Therefore, if a certain amount of heat can be transferred from right (SO) to left (SI) during one cycle of the three-step process, a continuous heat flow from SO to SI can be achieved. That is, a continuous heat flow from one body to the other can be achieved even two bodies are at the same temperature. Regarding the heat flow during one cycle of the three-step process, as shown in Figure 4.2, there will be an amount of heat (Q) transferred from SO to EC2 as: $Q = -Q_{SO}^{I} - Q_{SO}^{II} + Q_{SO}^{III}$. Similarly, there will be the same amount of heat transferred from EC1 to SI as: $Q = -Q_{SI}^{I} + Q_{SI}^{II} - Q_{SI}^{III}$. That is, during one cycle of the three-step process, an amount of heat (Q) is transferred from right (SO) to left (SI), even though both SO and SI have the same temperature. Since the three-step process shown in Figure 4.2 can be repeated as shown in Figure 4.3, a continuous heat flow from SO (right) to SI (left) can be achieved by continuously repeating the process shown in Figure 4.3. That is, a constant heat flow from SO to SI is expected, although both SO and SI have the same temperature. First of all, let us assume all four bodies are exactly the same material, the heat conduction during Step-II and Step-III becomes a classic heat conduction problem[143]: an infinite plate with a finite uniform thickness is sandwiched into two semi-infinite media on both two sides of the plate. For this case, it is well known: $Q_{SO}^{II} = Q_{SI}^{II}$ and $Q_{SO}^{III} = Q_{SI}^{III}$. Based on the model shown in Figure 4.2, one can get that $Q_{SO}^{II} = Q_{SO}^{III}$. Therefore, $Q_{SO}^{II} = Q_{SI}^{II} = Q_{SO}^{III} = Q_{SI}^{III}$. That is, $Q = Q_{SI}^{I} = Q_{SO}^{I}$. In other words, through one cycle of the three-step process illustrated in Figure 4.3, the amount of heat (Q) transferred from right to left is only determined by the Step-I.

It must be mentioned that during this three-step process, no movement of any part of the system is required and there are no other mechanisms involved. Only the thermal conduction among four bodies is involved. Since all four bodies are permanently bonded together, an excellent thermal contact can be achieved on three interfaces (SI|EC1, EC1|EC2, EC2|SO) and the thermal contact of these interfaces would not change with time. This is the principal advantage of the design introduced here over all reported ECE-based devices.

For the design introduced here, the key is that whether any heat transferred during the process or the Q is zero. If the Q is not zero, what is the condition (materials used for ECs, sink and source layers) to achieve a high Q and what is the time duration of each of these three steps? To answer these questions, numerical calculation is carried out below.

## 4.3 Mathematical Model and Analytical Solution

The unsteady heat equations for the four bodies in this heat pump may be written as the same way we did in Chapter 3, the only difference is that Boby-1 here will be heat sink and Body-2 will be heat source. B2 and B3 bodies are ECM and have been names here as EC1 and EC2, so our system of heat equations become as follows,

$$\frac{\partial T_{SI}(x,t)}{\partial t} = \alpha_1 \frac{\partial^2 T_{SI}(x,t)}{\partial x^2} \qquad -\infty < \boldsymbol{x} < -\boldsymbol{R} \qquad (4.1)$$

$$\frac{\partial T_{EC1}(x,t)}{\partial t} = \alpha_2 \frac{\partial^2 T_{EC1}(x,t)}{\partial x^2} \qquad -\boldsymbol{R} < \boldsymbol{x} < \boldsymbol{0} \qquad (4.2)$$

$$\frac{\partial T_{EC2}(x,t)}{\partial t} = \alpha_3 \frac{\partial^2 T_{EC2}(x,t)}{\partial x^2} \qquad \boldsymbol{0} < \boldsymbol{x} < \boldsymbol{R} \qquad (4.3)$$

$$\frac{\partial T_{SO}(x,t)}{\partial t} = \alpha_4 \frac{\partial^2 T_{SO}(x,t)}{\partial x^2} \qquad \boldsymbol{R} < \boldsymbol{x} < \infty \qquad (4.4)$$

Where $\alpha_j = k_j/\rho_j c_{p_j}$ $(j = 1,2,3,4)$ is thermal diffusivity. In our heat pump model, Body-1 Body-2 are EC bodies (EC1 & EC2) and have been considered here as the same, whereas Body-1 and Body-4 are SI and SO bodies and are the same but different from EC bodies. So the following replacements may be made for simplification.

$$\alpha_2 = \alpha_3 = \alpha^c \;\&\; \alpha_1 = \alpha_4 = \alpha^o$$
$$k_2 = k_3 = k^c \;\&\; k_1 = k_4 = k^o$$
$$c_{p_2} = c_{p_3} = c_p^c \;\&\; c_{p_1} = c_{p_4} = c_p^o$$
$$\rho_2 = \rho_3 = \rho^c \;\&\; \rho_1 = \rho_4 = \rho^o$$

where superscripts represent **c**enter (EC1 and EC2) and **o**uter bodies (SI and SO). The assumptions, initial and boundary conditions, and the complete analytical solution for temperature profiles and the heat flux through the interfaces has been determined in Chapter 3.

### 4.3.1 Initial Conditions for Thermal Cycle

The initial conditions (ICs) for above mentioned steps (Step-I to Step-III) are given in Eqs.(4.5) – (4.7).

**ICs for Step-I**

$$T_{SI}(x,0) = T_{SI,i} = T$$
$$T_{EC}\ (x,0) = T_{EC}\ _{,i} = T + \Delta T$$
$$T_{EC2}(x,0) = T_{EC2,i} = T - \Delta T \quad (4.5)$$
$$T_{SO}(x,0) = T_{SO,i} = T$$

**ICs for Step-II**

$$T_{SI}(x,0) = T_{SI,i} = T$$
$$T_{EC}\ (x,0) = T_{EC1,i} = T - \Delta T \quad (4.6)$$
$$T_{EC2}(x,0) = T_{EC2,i} = T$$
$$T_{SO}(x,0) = T_{SO,i} = T$$

**ICs for Step-III**

$$T_{SI}(x,0) = T_{SI,i} = T$$
$$T_{EC1}(x,0) = T_{EC1,i} = T \quad (4.7)$$
$$T_{EC}\ (x,0) = T_{EC2,i} = T + \Delta T$$
$$T_{SO}(x,0) = T_{SO,i} = T$$

### 4.3.2 Boundary Conditions (BCs)

If two bodies at different temperature are brought in contact, their temperature at the interface (surface temperature, $T_s$) is equal and its value depends of the thermal properties of the materials across the interface[143,147,148]. Based on the first law of thermodynamics, the amount of overall heat released by one body is equal to the amount of heat flowed in the surrounding body through the interface[143] ( The interfaces have been considered as perfect interfaces, i.e., no thermal resistance). So based on *Fourier's law of heat conduction*[149] across the interface, the following boundary conditions for $t > 0$ (also known as the boundary conditions of fourth kind[150]) are set for the model shown in Figure 4.1.

**Interface SI|EC1 at $x = -R$**

$$T_{SI}(-R,t) = T_{EC1}(-R,t)$$

$$-k^o \frac{\partial T_{SI}(x,t)}{\partial x}\bigg|_{x=-R} = -k^c \frac{\partial T_{EC1}(x,t)}{\partial x}\bigg|_{x=-R} \tag{4.8}$$

**Interface EC1|EC2 at $x = 0$**

$$T_{EC1}(0,t) = T_{EC2}(0,t)$$

$$-k^c \frac{\partial T_{EC1}(x,t)}{\partial x}\bigg|_{x=0} = -k^c \frac{\partial T_{EC2}(x,t)}{\partial x}\bigg|_{x=0} \tag{4.9}$$

**Interface EC2|SO at $x = R$**

$$T_{EC2}(R,t) = T_{SO}(R,t)$$

$$-k^c \frac{\partial T_{EC2}(x,t)}{\partial x}\bigg|_{x=R} = -k^o \frac{\partial T_{SO}(x,t)}{\partial x}\bigg|_{x=R} \tag{4.10}$$

### 4.3.3 Physical Conditions

The source and sink have been considered bodies of infinite size and lateral surfaces are insulated so there will be no heat transfer to the surrounding at $x = \pm\infty$.

$$\frac{\partial T_{SI}(x,t)}{\partial x}\bigg|_{x=-\infty} = \frac{\partial T_{SO}(x,t)}{\partial x}\bigg|_{x=\infty} = 0 \tag{4.11}$$

### 4.3.4 Analytical Solution

The assumptions, initial and boundary and conditions and the complete analytical solution for temperature profiles and the heat flux through the interfaces has been determined in Chapter 3. Here the analytical relations for temperature profiles in the bodies involved in heat pump (SI, EC1, EC2 and SO) and heat fluxes through the interface SI|EC1, EC1|EC2 and EC2|SO is given without going into details of the solution (see Chapter 3 for detailed solution).

## 4.4 Temperature Profiles of the Bodies

The temperature profiles in each region of the heat pump model is given as,

**Temperature Profile of SI as Function of Space (1D) and Time**

$$
\begin{aligned}
&T_{SI}(x,t) - T_{SI,i} \\
&= \frac{K_\varepsilon}{1+K_\varepsilon}\Bigg\{\left(T_{EC1,i} - T_{SI,i}\right) h \sum_{n=1}^{\infty} h^{2(n-1)} \operatorname{erfc}\frac{-x-R+(4n-0)K_\alpha^{-1/2}R}{2\sqrt{\alpha^o t}} \\
&\qquad - \left(T_{EC1,i} - T_{EC2,i}\right) h \sum_{n=1}^{\infty} h^{2(n-1)} \operatorname{erfc}\frac{-x-R+(4n-1)K_\alpha^{-1/2}R}{2\sqrt{\alpha^o t}} \\
&\qquad - \frac{2\left(T_{EC2,i} - T_{SO,i}\right)}{1+K_\varepsilon} \sum_{n=1}^{\infty} h^{2(n-1)} \operatorname{erfc}\frac{-x-R+(4n-2)K_a^{-1/2}R}{2\sqrt{\alpha^o t}} \\
&\qquad - \left(T_{EC1,i} - T_{EC\ ,i}\right) \sum_{n=1}^{\infty} h^{2(n-1)} \operatorname{erfc}\frac{-x-R+(4n-3)K_\alpha^{-1/2}R}{2\sqrt{\alpha^o t}} \\
&\qquad + \left(T_{EC1,i} - T_{SI,i}\right) \sum_{n=1}^{\infty} h^{2(n-1)} \operatorname{erfc}\frac{-x-R+(4n-4)K_\alpha^{-1/2}R}{2\sqrt{\alpha^o t}}\Bigg\}
\end{aligned}
\tag{4.12}
$$

**Temperature Profile of EC1 as Function of Space (1D) and Time**

$$
\begin{aligned}
&T_{EC1}(x,t) - T_{EC1,i} \\
&= \frac{\left(T_{EC1,i} - T_{EC\ ,i}\right) h^2}{2} \sum_{n=1}^{\infty} h^{2(n-1)} \operatorname{erfc}\frac{(4n-0)R+x}{2\sqrt{\alpha^c t}} \\
&+ \frac{h}{1+K_\varepsilon} \sum_{n=1}^{\infty} h^{2(n-1)} \left[\left(T_{EC1,i} - T_{SI,i}\right) \operatorname{erfc}\frac{(4n-1)R-x}{2\sqrt{\alpha^c t}} + \left(T_{EC2,i} - T_{SO,i}\right) \operatorname{erfc}\frac{(4n-1)R+x}{2\sqrt{\alpha^c t}}\right] \\
&- \frac{h}{2} \sum_{n=1}^{\infty} h^{2(n-1)} \left[\left(T_{EC1,i} - T_{EC2,i}\right) \operatorname{erfc}\frac{(4n-2)R-x}{2\sqrt{\alpha^c t}} - \left(T_{EC1,i} - T_{EC2,i}\right) \operatorname{erfc}\frac{(4n-2)R+x}{2\sqrt{\alpha^c t}}\right] \\
&- \frac{1}{1+K_\varepsilon} \sum_{n=1}^{\infty} h^{2(n-1)} \left[\left(T_{EC2,i} - T_{SO,i}\right) \operatorname{erfc}\frac{(4n-3)R-x}{2\sqrt{\alpha^c t}} + \left(T_{EC1,i} - T_{SI,i}\right) \operatorname{erfc}\frac{(4n-3)R+x}{2\sqrt{\alpha^c t}}\right] \\
&- \frac{\left(T_{EC1,i} - T_{EC\ ,i}\right)}{2} \sum_{n=1}^{\infty} h^{2(n-1)} \operatorname{erfc}\frac{(4n-4)R-x}{2\sqrt{\alpha^c t}}
\end{aligned}
\tag{4.13}
$$

**Temperature Profile of EC2 as Function of Space (1D) and Time**

$$
\begin{aligned}
&T_{EC2}(x,t) - T_{EC2,i} \\
&= -\frac{\left(T_{EC1,i} - T_{EC2i}\right) h^2}{2} \sum_{n=1}^{\infty} h^{2(n-1)} \operatorname{erfc} \frac{(4n-0)R - x}{2\sqrt{\alpha^c t}} \\
&+ \frac{h}{1+K_\varepsilon} \sum_{n=1}^{\infty} h^{2(n-1)} \left[ \left(T_{EC\ ,i} - T_{SI,i}\right) \operatorname{erfc} \frac{(4n-1)R - x}{2\sqrt{\alpha^c t}} + \left(T_{EC\ ,i} - T_{SO,i}\right) \operatorname{erfc} \frac{(4n-1)R + x}{2\sqrt{\alpha^c t}} \right] \\
&- \frac{h}{2} \sum_{n=1}^{\infty} h^{2(n-1)} \left[ \left(T_{EC\ ,i} - T_{EC\ ,i}\right) \operatorname{erfc} \frac{(4n-2)R - x}{2\sqrt{\alpha^c t}} - \left(T_{EC1,i} - T_{EC\ ,i}\right) \operatorname{erfc} \frac{(4n-2)R + x}{2\sqrt{\alpha^c t}} \right] \\
&- \frac{1}{1+K_\varepsilon} \sum_{n=1}^{\infty} h^{2(n-1)} \left[ \left(T_{EC\ ,i} - T_{SO,i}\right) \operatorname{erfc} \frac{(4n-3)R - x}{2\sqrt{\alpha^c t}} + \left(T_{EC\ ,i} - T_{SI,i}\right) \operatorname{erfc} \frac{(4n-3)R + x}{2\sqrt{\alpha^c t}} \right] \\
&+ \frac{\left(T_{EC\ ,i} - T_{EC\ ,i}\right)}{2} \sum_{n=1}^{\infty} h^{2(n-1)} \operatorname{erfc} \frac{(4n-4)R + x}{2\sqrt{\alpha^c t}}
\end{aligned}
\tag{4.14}
$$

**Temperature Profile of SO as Function of Space (1D) and Time**

$$
\begin{aligned}
&T_{SO}(x,t) - T_{SO,i} \\
&= \frac{K_\varepsilon}{1+K_\varepsilon} \Bigg\{ \left(T_{EC\ ,i} - T_{SO,i}\right) h \sum_{n=1}^{\infty} h^{2(n-1)} \operatorname{erfc} \frac{x - R + (4n-0) K_\alpha^{-1/2} R}{2\sqrt{\alpha^o t}} \\
&\qquad + \left(T_{EC1,i} - T_{EC2,i}\right) h \sum_{n=1}^{\infty} h^{2(n-1)} \operatorname{erfc} \frac{x - R + (4n-1) K_\alpha^{-1/2} R}{2\sqrt{\alpha^o t}} \\
&\qquad - \frac{2\left(T_{EC1,i} - T_{SI,i}\right)}{1+K_\varepsilon} \sum_{n=1}^{\infty} h^{2(n-1)} \operatorname{erfc} \frac{x - R + (4n-2) K_\alpha^{-1/2} R}{2\sqrt{\alpha^o t}} \\
&\qquad + \left(T_{EC1,i} - T_{EC\ ,i}\right) \sum_{n=1}^{\infty} h^{2(n-1)} \operatorname{erfc} \frac{x - R + (4n-3) K_\alpha^{-1/2} R}{2\sqrt{\alpha^o t}} \\
&\qquad + \left(T_{EC\ ,i} - T_{SO,i}\right) \sum_{n=1}^{\infty} h^{2(n-1)} \operatorname{erfc} \frac{x - R + (4n-4) K_\alpha^{-1/2} R}{2\sqrt{\alpha^o t}} \Bigg\}
\end{aligned}
\tag{4.15}
$$

## 4.5 Temperature Gradients in the Bodies

Using the following relations, the gradients of the temperature profiles may be given in Eqs. (4.16) – (4.19).

$$
\frac{\partial}{\partial x}\left[\operatorname{erfc}\left(\frac{x}{2\sqrt{\alpha t}}\right)\right] = -\frac{1}{\sqrt{\pi \alpha t}} \exp\left(-\frac{x^2}{4\alpha t}\right)
$$

$$
\frac{\partial}{\partial x}\left[\operatorname{erfc}\left(\frac{-x}{2\sqrt{\alpha t}}\right)\right] = \frac{1}{\sqrt{\pi \alpha t}} \exp\left(-\frac{x^2}{4\alpha t}\right)
$$

**Temperature Gradient in Sink (SI)**

$$\frac{\partial T_{SI}(x,t)}{\partial x} = \frac{K_\varepsilon}{1+K_\varepsilon}\frac{1}{\sqrt{\pi\alpha^o t}}$$
$$\times\left\{\left(T_{EC1,i}-T_{SI,i}\right)h\sum_{n=1}^{\infty}h^{2(n-1)}\exp\left(-\left[\frac{-x-R+(4n-0)RK_\alpha^{-1/2}}{2\sqrt{\alpha^o t}}\right]^2\right)\right.$$
$$-\left(T_{EC1,i}-T_{EC2,i}\right)h\sum_{n=1}^{\infty}h^{2(n-1)}\exp\left(-\left[\frac{-x-R+(4n-1)RK_\alpha^{-1/2}}{2\sqrt{\alpha^o t}}\right]^2\right)$$
$$-\frac{2\left(T_{EC\ ,i}-T_{SO,i}\right)}{(1+K_\varepsilon)}\sum_{n=1}^{\infty}h^{2(n-1)}\exp\left(-\left[\frac{-x-R+(4n-2)RK_\alpha^{-1/2}}{2\sqrt{\alpha^o t}}\right]^2\right)$$
$$-\left(T_{EC1,i}-T_{EC\ ,i}\right)\sum_{n=1}^{\infty}h^{2(n-1)}\exp\left(-\left[\frac{-x-R+(4n-3)RK_\alpha^{-1/2}}{2\sqrt{\alpha^o t}}\right]^2\right)$$
$$\left.+\left(T_{EC1,i}-T_{SI,i}\right)\sum_{n=1}^{\infty}h^{2(n-1)}\exp\left(-\left[\frac{-x-R+(4n-4)RK_\alpha^{-1/2}}{2\sqrt{\alpha^o t}}\right]^2\right)\right\} \quad (4.16)$$

## Temperature Gradient in EC1

$$\frac{\partial T_{EC1}(x,t)}{\partial x} = \frac{1}{\sqrt{\pi\alpha^c t}}$$
$$\times\left\{-\frac{\left(T_{EC1,i}-T_{EC2,i}\right)h^2}{2}\sum_{n=1}^{\infty}h^{2(n-1)}\exp\left(-\left[\frac{(4n-0)R+x}{2\sqrt{\alpha^c t}}\right]^2\right)\right.$$
$$+\frac{h}{1+K_\varepsilon}\sum_{n=1}^{\infty}h^{2(n-1)}\left[\left(T_{EC1,i}-T_{SI,i}\right)\exp\left(-\left[\frac{(4n-1)R-x}{2\sqrt{\alpha^c t}}\right]^2\right)-\left(T_{EC2,i}-T_{SO,i}\right)\exp\left(-\left[\frac{(4n-1)R+x}{2\sqrt{\alpha^c t}}\right]^2\right)\right]$$
$$-\frac{h}{2}\sum_{n=1}^{\infty}h^{2(n-1)}\left[\left(T_{EC1,i}-T_{EC2,i}\right)\exp\left(-\left[\frac{(4n-2)R-x}{2\sqrt{\alpha^c t}}\right]^2\right)+\left(T_{EC1,i}-T_{EC2,i}\right)\exp\left(-\left[\frac{(4n-2)R+x}{2\sqrt{\alpha^c t}}\right]^2\right)\right]$$
$$-\frac{1}{1+K_\varepsilon}\sum_{n=1}^{\infty}h^{2(n-1)}\left[\left(T_{EC\ ,i}-T_{SO,i}\right)\exp\left(-\left[\frac{(4n-3)R-x}{2\sqrt{\alpha^c t}}\right]^2\right)-\left(T_{EC1,i}-T_{SI,i}\right)\exp\left(-\left[\frac{(4n-3)R+x}{2\sqrt{\alpha^c t}}\right]^2\right)\right]$$
$$\left.-\frac{\left(T_{EC1,i}-T_{EC2,i}\right)}{2}\sum_{n=1}^{\infty}h^{2(n-1)}\exp\left(-\left[\frac{(4n-4)R-x}{2\sqrt{\alpha^c t}}\right]^2\right)\right\} \quad (4.17)$$

## Temperature Gradient in EC2

$$\frac{\partial T_{EC2}(x,t)}{\partial x} = \frac{1}{\sqrt{\pi\alpha^c t}}$$
$$\times\Bigg\{-\frac{\left(T_{EC\ ,i} - T_{EC2,i}\right)h^2}{2}\sum_{n=1}^{\infty} h^{2(n-1)}\exp\left(-\left[\frac{(4n-0)R-x}{2\sqrt{\alpha^c t}}\right]^2\right)$$
$$+\frac{h}{1+K_\varepsilon}\sum_{n=1}^{\infty} h^{2(n-1)}\left[\left(T_{EC1,i} - T_{SI,i}\right)\exp\left(-\left[\frac{(4n-1)R-x}{2\sqrt{\alpha^c t}}\right]^2\right) - \left(T_{EC\ ,i} - T_{SI,i}\right)\exp\left(-\left[\frac{(4n-1)R+x}{2\sqrt{\alpha^c t}}\right]^2\right)\right]$$
$$-\frac{h}{2}\sum_{n=1}^{\infty} h^{2(n-1)}\left[\left(T_{EC\ ,i} - T_{EC\ ,i}\right)\exp\left(-\left[\frac{(4n-2)R-x}{2\sqrt{\alpha^c t}}\right]^2\right) + \left(T_{EC\ ,i} - T_{EC\ ,i}\right)\exp\left(-\left[\frac{(4n-2)R+x}{2\sqrt{\alpha^c t}}\right]^2\right)\right]$$
$$-\frac{1}{1+K_\varepsilon}\sum_{n=1}^{\infty} h^{2(n-1)}\left[\left(T_{EC2,i} - T_{SO,i}\right)\exp\left(-\left[\frac{(4n-3)R-x}{2\sqrt{\alpha^c t}}\right]^2\right) - \left(T_{EC\ ,i} - T_{SI,i}\right)\exp\left(-\left[\frac{(4n-3)R+x}{2\sqrt{\alpha^c t}}\right]^2\right)\right]$$
$$-\frac{\left(T_{EC\ ,i} - T_{EC\ ,i}\right)}{2}\sum_{n=1}^{\infty} h^{2(n-1)}\exp\left(-\left[\frac{(4n-4)R+x}{2\sqrt{\alpha^c t}}\right]^2\right)\Bigg\} \tag{4.18}$$

**Temperature Gradient in Source (SO)**

$$\frac{\partial T_{SO}(x,t)}{\partial x} = -\frac{K_\varepsilon}{1+K_\varepsilon}\frac{1}{\sqrt{\pi\alpha^o t}}$$
$$\times\Bigg\{\left(T_{EC2,i} - T_{SO,i}\right)h\sum_{n=1}^{\infty} h^{2(n-1)}\exp\left(-\left[\frac{x-R+(4n-0)RK_\alpha^{-1/2}}{2\sqrt{\alpha^o t}}\right]^2\right)$$
$$+\left(T_{EC\ ,i} - T_{EC\ ,i}\right)h\sum_{n=1}^{\infty} h^{2(n-1)}\exp\left(-\left[\frac{x-R+(4n-1)RK_\alpha^{-1/2}}{2\sqrt{\alpha^o t}}\right]^2\right)$$
$$-\frac{2\left(T_{EC1,i} - T_{SI,i}\right)}{(1+K_\varepsilon)}\sum_{n=1}^{\infty} h^{2(n-1)}\exp\left(-\left[\frac{x-R+(4n-2)RK_\alpha^{-1/2}}{2\sqrt{\alpha^o t}}\right]^2\right)$$
$$+\left(T_{EC1,i} - T_{EC2,i}\right)\sum_{n=1}^{\infty} h^{2(n-1)}\exp\left(-\left[\frac{x-R+(4n-3)RK_\alpha^{-1/2}}{2\sqrt{\alpha^o t}}\right]^2\right)$$
$$+\left(T_{EC2,i} - T_{SO,i}\right)\sum_{n=1}^{\infty} h^{2(n-1)}\exp\left(-\left[\frac{x-R+(4n-4)RK_\alpha^{-1/2}}{2\sqrt{\alpha^o t}}\right]^2\right)\Bigg\} \tag{4.19}$$

## 4.6 Heat Flux through the Interfaces

The conductive heat flow through the interfaces may be written as,

$$q_{SI|EC1}(t) = -k^o\left.\frac{\partial T_{SI}(x,t)}{\partial x}\right|_{x=-R} = -k^c\left.\frac{\partial T_{EC1}(x,t)}{\partial x}\right|_{x=-R} \tag{4.20}$$

$$q_{EC1|EC2}(t) = -k^c \left.\frac{\partial T_{EC1}(x,t)}{\partial x}\right|_{x=0} = -k^c \left.\frac{\partial T_{EC2}(x,t)}{\partial x}\right|_{x=0} \tag{4.21}$$

$$q_{EC2|SO}(t) = -k^c \left.\frac{\partial T_{EC2}(x,t)}{\partial x}\right|_{x=R} = -k^o \left.\frac{\partial T_{SO}(x,t)}{\partial x}\right|_{x=R} \tag{4.22}$$

The relations for heat flux through the interface SI|EC1, EC1|EC2 and EC2|SO may be determined by using temperature gradients (4.16) – (4.19) in the Eqs. (4.20), (4.21) and (4.22) respectively and the results have been in Eqs. (4.23) – (4.25).

**Heat Flux through the Interface SI|EC1**

$$\begin{aligned} q_{SI|EC1}(t) &= -k^o \left.\frac{\partial T_{SI}(x,t)}{\partial x}\right|_{x=-R} \\ &= -\frac{k^o}{\sqrt{\pi\alpha^o t}}\frac{K_\varepsilon}{1+K_\varepsilon} \\ &\quad \times \left\{ \left(T_{EC\ ,i} - T_{SI,i}\right) h \sum_{n=1}^{N} h^{2(n-1)} \exp\left(-\left[\frac{(4n-0)R}{2\sqrt{\alpha^c t}}\right]^2\right) \right. \\ &\quad - \left(T_{EC1,i} - T_{EC2,i}\right) h \sum_{n=1}^{N} h^{2(n-1)} \exp\left(-\left[\frac{(4n-1)R}{2\sqrt{\alpha^c t}}\right]^2\right) \\ &\quad - \frac{2\left(T_{EC\ ,i} - T_{SO,i}\right)}{(1+K_\varepsilon)} \sum_{n=1}^{N} h^{2(n-1)} \exp\left(-\left[\frac{(4n-2)R}{2\sqrt{\alpha^c t}}\right]^2\right) \\ &\quad - \left(T_{EC1,i} - T_{EC\ ,i}\right) \sum_{n=1}^{N} h^{2(n-1)} \exp\left(-\left[\frac{(4n-3)R}{2\sqrt{\alpha^c t}}\right]^2\right) \\ &\quad \left. + \left(T_{EC1,i} - T_{SI,i}\right) \sum_{n=1}^{N} h^{2(n-1)} \exp\left(-\left[\frac{(4n-4)R}{2\sqrt{\alpha^c t}}\right]^2\right) \right\} \end{aligned} \tag{4.23}$$

**Heat Flux through the Interface EC1|EC2**

$$q_{EC1|EC2}(t) = -k^c \left.\frac{\partial T_2(x,t)}{\partial x}\right|_{x=0}$$

$$= -\frac{k^c}{\sqrt{\pi\alpha^c t}}\Bigg\{-\frac{\left(T_{EC1,i} - T_{EC2,i}\right)}{2} h^2 \sum_{n=1}^{N} h^{2(n-1)} \exp\left(-\left[\frac{(4n-0)R}{2\sqrt{\alpha^c t}}\right]^2\right)$$

$$+ \frac{h}{1+K_\varepsilon}\left(T_{EC\ ,i} - T_{SI,i} - T_{EC2,i} + T_{SO,i}\right) \sum_{n=1}^{N} h^{2(n-1)} \exp\left(-\left[\frac{(4n-1)R}{2\sqrt{\alpha^c t}}\right]^2\right)$$

$$- \left(T_{EC\ ,i} - T_{EC\ ,i}\right) h \sum_{n=1}^{N} h^{2(n-1)} \exp\left(-\left[\frac{(4n-2)R}{2\sqrt{\alpha^c t}}\right]^2\right) \tag{4.24}$$

$$- \frac{1}{1+K_\varepsilon}\left(T_{EC2,i} - T_{SO,i} - T_{EC1,i} + T_{SI,i}\right) \sum_{n=1}^{N} h^{2(n-1)} \exp\left(-\left[\frac{(4n-3)R}{2\sqrt{\alpha^c t}}\right]^2\right)$$

$$- \frac{\left(T_{EC\ ,i} - T_{EC2,i}\right)}{2} \sum_{n=1}^{N} h^{2(n-1)} \exp\left(-\left[\frac{(4n-4)R}{2\sqrt{\alpha^c t}}\right]^2\right)\Bigg\}$$

**Heat Flux through the Interface EC2|SO**

$$q_{EC2|SO}(t) = -k^o \left.\frac{\partial T_{SO}(x,t)}{\partial x}\right|_{x=R}$$

$$= \frac{k^o}{\sqrt{\pi\alpha^o t}} \frac{K_\varepsilon}{1+K_\varepsilon} \times \Bigg\{\left(T_{EC\ ,i} - T_{SO,i}\right) h \sum_{n=1}^{N} h^{2(n-1)} \exp\left(-\left[\frac{(4n-0)R}{2\sqrt{\alpha^c t}}\right]^2\right)$$

$$+ \left(T_{EC1,i} - T_{EC2,i}\right) h \sum_{n=1}^{N} h^{2(n-1)} \exp\left(-\left[\frac{(4n-1)R}{2\sqrt{\alpha^c t}}\right]^2\right)$$

$$- \frac{2\left(T_{EC\ ,i} - T_{SI,i}\right)}{(1+K_\varepsilon)} \sum_{n=1}^{N} h^{2(n-1)} \exp\left(-\left[\frac{(4n-2)R}{2\sqrt{\alpha^c t}}\right]^2\right) \tag{4.25}$$

$$+ \left(T_{EC1,i} - T_{EC\ ,i}\right) \sum_{n=1}^{N} h^{2(n-1)} \exp\left(-\left[\frac{(4n-3)R}{2\sqrt{\alpha^c t}}\right]^2\right)$$

$$+ \left(T_{EC2,i} - T_{SO,i}\right) \sum_{n=1}^{N} h^{2(n-1)} \exp\left(-\left[\frac{(4n-4)R}{2\sqrt{\alpha^c t}}\right]^2\right)\Bigg\}$$

## 4.7 Heat Energy Transfer through the SI|EC1 and EC2|SO Interfaces

The energy per unit area through the interfaces SI|EC1 and EC2|SO may be determined by integrating heat flux over the time spans by using the relation (4.26) and is shown in Eqs.(4.27) & (4.28).

$$Q(t) = \int_0^t q(t)dt \tag{4.26}$$

The solution of the integral of the function $f(t) = \frac{1}{\sqrt{t}} \exp\left(-\frac{A}{t}\right)$ in limits from $0 \rightarrow t$, may be from any book of calculus or using Mathematica

$$\int_0^t \frac{1}{\sqrt{t}} \exp\left(-\frac{A}{t}\right) dt = 2\sqrt{t} \exp\left(-\frac{A}{t}\right) - 2\sqrt{A}\sqrt{\pi}\, \mathrm{erfc}\left(\frac{A}{\sqrt{t}}\right)$$

Where $1 - \mathrm{erf}(x) = \mathrm{erfc}(x)$,

Using the above relation, the total energy transfer through the interfaces SI|EC1 and EC2|SO in a specific time interval has been determined and given in Eqs. (4.27) and (4.28).

### 4.7.1 Heat Energy Transfer through the SI|EC1 Interface

$$Q_{SI|EC1} = \int_0^t q_{SI|EC1}(t)dt$$

$$\begin{aligned} Q_{SI|EC1} = -\frac{2k^o}{\sqrt{\pi\alpha^o}} \frac{K_\varepsilon}{1+K_\varepsilon} \\ \times \Bigg\{ \left(T_{EC\ ,i} - T_{SI,i}\right) h \sum_{n=1}^{N} h^{2(n-1)} \left[ \sqrt{t} \exp\left( -\left[ \frac{(4n-0)R}{2\sqrt{\alpha^c t}} \right]^2 \right) - \frac{(4n-0)R}{2\sqrt{\alpha^c}} \sqrt{\pi}\, \mathrm{erfc} \frac{(4n-0)R}{2\sqrt{\alpha^c t}} \right] \\ - \left(T_{EC\ ,i} - T_{EC\ ,i}\right) h \sum_{n=1}^{N} h^{2(n-1)} \left[ \sqrt{t} \exp\left( -\left[ \frac{(4n-1)R}{2\sqrt{\alpha^c t}} \right]^2 \right) - \frac{(4n-1)R}{2\sqrt{\alpha^c}} \sqrt{\pi}\, \mathrm{erfc} \frac{(4n-1)R}{2\sqrt{\alpha^c t}} \right] \\ - \frac{2\left(T_{EC2,i} - T_{SO,i}\right)}{(1+K_\varepsilon)} \sum_{n=1}^{N} h^{2(n-1)} \left[ \sqrt{t} \exp\left( -\left[ \frac{(4n-2)R}{2\sqrt{\alpha^c t}} \right]^2 \right) - \frac{(4n-2)R}{2\sqrt{\alpha^c}} \sqrt{\pi}\, \mathrm{erfc} \frac{(4n-2)R}{2\sqrt{\alpha^c t}} \right] \\ - \left(T_{EC1,i} - T_{EC2,i}\right) \sum_{n=1}^{N} h^{2(n-1)} \left[ \sqrt{t} \exp\left( -\left[ \frac{(4n-3)R}{2\sqrt{\alpha^c t}} \right]^2 \right) - \frac{(4n-3)R}{2\sqrt{\alpha^c}} \sqrt{\pi}\, \mathrm{erfc} \frac{(4n-3)R}{2\sqrt{\alpha^c t}} \right] \\ + \left(T_{EC1,i} - T_{SI,i}\right) \sum_{n=1}^{N} h^{2(n-1)} \left[ \sqrt{t} \exp\left( -\left[ \frac{(4n-4)R}{2\sqrt{\alpha^c t}} \right]^2 \right) - \frac{(4n-4)R}{2\sqrt{\alpha^c}} \sqrt{\pi}\, \mathrm{erfc} \frac{(4n-4)R}{2\sqrt{\alpha^c t}} \right] \Bigg\} \end{aligned} \tag{4.27}$$

### 4.7.2 Heat Energy Transfer through the EC2|SO Interface

$$Q_{EC2|SO} = \int_0^t q_{EC2|SO}(t)dt \tag{4.28}$$

$$Q_{EC2|SO} = \frac{2k^o}{\sqrt{\pi\alpha^o}}\frac{K_\varepsilon}{1+K_\varepsilon}$$
$$\times\left\{\left(T_{EC2,i}-T_{SO,i}\right)h\sum_{n=1}^{N}h^{2(n-1)}\left[\sqrt{t}\exp\left(-\left[\frac{(4n-0)R}{2\sqrt{\alpha^c t}}\right]^2\right)-\frac{(4n-0)R}{2\sqrt{\alpha^c}}\sqrt{\pi}\,\mathrm{erfc}\frac{(4n-0)R}{2\sqrt{\alpha^c t}}\right]\right.$$
$$+\left(T_{EC\ ,i}-T_{EC\ ,i}\right)h\sum_{n=1}^{N}h^{2(n-1)}\left[\sqrt{t}\exp\left(-\left[\frac{(4n-1)R}{2\sqrt{\alpha^c t}}\right]^2\right)-\frac{(4n-1)R}{2\sqrt{\alpha^c}}\sqrt{\pi}\,\mathrm{erfc}\frac{(4n-1)R}{2\sqrt{\alpha^c t}}\right]$$
$$-\frac{2\left(T_{EC\ ,i}-T_{SI,i}\right)}{(1+K_\varepsilon)}\sum_{n=1}^{N}h^{2(n-1)}\left[\sqrt{t}\exp\left(-\left[\frac{(4n-2)R}{2\sqrt{\alpha^c t}}\right]^2\right)-\frac{(4n-2)R}{2\sqrt{\alpha^c}}\sqrt{\pi}\,\mathrm{erfc}\frac{(4n-2)R}{2\sqrt{\alpha^c t}}\right]$$
$$+\left(T_{EC\ ,i}-T_{EC\ ,i}\right)\sum_{n=1}^{N}h^{2(n-1)}\left[\sqrt{t}\exp\left(-\left[\frac{(4n-3)R}{2\sqrt{\alpha^c t}}\right]^2\right)-\frac{(4n-3)R}{2\sqrt{\alpha^c}}\sqrt{\pi}\,\mathrm{erfc}\frac{(4n-3)R}{2\sqrt{\alpha^c t}}\right]$$
$$\left.+\left(T_{EC2,i}-T_{SO,i}\right)\sum_{n=1}^{N}h^{2(n-1)}\left[\sqrt{t}\exp\left(-\left[\frac{(4n-4)R}{2\sqrt{\alpha^c t}}\right]^2\right)-\frac{(4n-4)R}{2\sqrt{\alpha^c}}\sqrt{\pi}\,\mathrm{erfc}\frac{(4n-4)R}{2\sqrt{\alpha^c t}}\right]\right\}$$

It is worth mentioning here that the upper limit $n=\infty$ in Eqs. (4.23) – (4.25), (4.27) and (4.28) has been replaced with $n=N$. Where N is given by the relation below that has already been calculated in section 3.3 and is given here again for quick reference.

$$N=\frac{-\ln\delta-\ln(1-h^2\exp(-\gamma))}{\gamma-\ln h^2} \tag{3.57}$$

Where $\gamma=3a^2$ (> 0) in which $a = 4R/2\sqrt{\alpha^c t}$ (> 0) $\delta$ ($0<\delta<<1$) is the tolerance, and $|h|<1$.
In Eq. (3.57), the tolerance $\delta$ is defined as the ratio of summation of all terms of series for $(n > N+1)$ to the value of first term only of the series. That is, the smaller the δ is, the closer are the results of Eqs. (4.23) – (4.25) to the real results. If Eq. (3.57) results in a number smaller than 4, $N = 4$ should be used.

## 4.8 Net Heat Energy Transfer through the Interfaces in One Cycle

As it has already been discussed that operation of the heat pump comprises of three steps, so the net energy through the interface EC2|SO (or SI|EC1) may be determined using the initial conditions in Eq. (4.28) (or similarly in Eq. (4.27). The amount of heat energy flow in one cycle from step-I to step-III is shown in Eqs.(4.30) – (4.32). Longer time spans are required for the bodies in step-II and step-III to come at thermal equilibrium. At the thermal equilibrium, the energy through EC2|SO (and SI|EC1) cancels each other in the step-II and step-III so the energy that is transformed in the step-I is the net heat transfer during one complete cycle. After equilibrium, all bodies are at same temperature and then second cycle may be applied by external electric field and so on for a sustainable heat pumping operation. After a cycle of these three steps, one can get that the net heat flow through SO|EC2 interface is

$$Q_{SO}^{net} = -Q_{SO}^{I} - Q_{SO}^{II} + Q_{SO}^{III} \tag{4.29}$$

### 4.8.1 Heat Energy Transfer in Step-I

Putting ICs (4.5) in Eq. (4.28), we get

$$\begin{aligned} Q_{SO}^{I} = Q_{EC2|SO}^{I} = {} & \frac{2k^{o}}{\sqrt{\pi\alpha^{o}}}\frac{K_{\varepsilon}}{1+K_{\varepsilon}} \\ & \times\left\{(-\Delta T)\,h\sum_{n=1}^{N}h^{2(n-1)}\left[\sqrt{t}\exp\left(-\left[\frac{(4n-0)R}{2\sqrt{\alpha^{c}t}}\right]^{2}\right)-\frac{(4n-0)R}{2\sqrt{\alpha^{c}}}\sqrt{\pi}\,\mathrm{erfc}\frac{(4n-0)R}{2\sqrt{\alpha^{c}t}}\right]\right. \\ & +2(\Delta T)\,h\sum_{n=1}^{N}h^{2(n-1)}\left[\sqrt{t}\exp\left(-\left[\frac{(4n-1)R}{2\sqrt{\alpha^{c}t}}\right]^{2}\right)-\frac{(4n-1)R}{2\sqrt{\alpha^{c}}}\sqrt{\pi}\,\mathrm{erfc}\frac{(4n-1)R}{2\sqrt{\alpha^{c}t}}\right] \\ & -\frac{2(\Delta T)}{(1+K_{\varepsilon})}\sum_{n=1}^{N}h^{2(n-1)}\left[\sqrt{t}\exp\left(-\left[\frac{(4n-2)R}{2\sqrt{\alpha^{c}t}}\right]^{2}\right)-\frac{(4n-2)R}{2\sqrt{\alpha^{c}}}\sqrt{\pi}\,\mathrm{erfc}\frac{(4n-2)R}{2\sqrt{\alpha^{c}t}}\right] \\ & +2(\Delta T)\sum_{n=1}^{N}h^{2(n-1)}\left[\sqrt{t}\exp\left(-\left[\frac{(4n-3)R}{2\sqrt{\alpha^{c}t}}\right]^{2}\right)-\frac{(4n-3)R}{2\sqrt{\alpha^{c}}}\sqrt{\pi}\,\mathrm{erfc}\frac{(4n-3)R}{2\sqrt{\alpha^{c}t}}\right] \\ & \left.+(-\Delta T)\sum_{n=1}^{N}h^{2(n-1)}\left[\sqrt{t}\exp\left(-\left[\frac{(4n-4)R}{2\sqrt{\alpha^{c}t}}\right]^{2}\right)-\frac{(4n-4)R}{2\sqrt{\alpha^{c}}}\sqrt{\pi}\,\mathrm{erfc}\frac{(4n-4)R}{2\sqrt{\alpha^{c}t}}\right]\right\} \end{aligned} \tag{4.30}$$

### 4.8.2 Heat Energy Transfer in Step-II

Putting ICs (4.6) in Eq. (4.28),we get

$$\begin{aligned} Q_{SO}^{II} = Q_{EC2|SO}^{II} = {} & \frac{2k^{o}}{\sqrt{\pi\alpha^{o}}}\frac{K_{\varepsilon}}{1+K_{\varepsilon}} \\ & \times\left\{(-\Delta T)\,h\sum_{n=1}^{N}h^{2(n-1)}\left[\sqrt{t}\exp\left(-\left[\frac{(4n-1)R}{2\sqrt{\alpha^{c}t}}\right]^{2}\right)-\frac{(4n-1)R}{2\sqrt{\alpha^{c}}}\sqrt{\pi}\,\mathrm{erfc}\frac{(4n-1)R}{2\sqrt{\alpha^{c}t}}\right]\right. \\ & -\frac{2(-\Delta T)}{(1+K_{\varepsilon})}\sum_{n=1}^{N}h^{2(n-1)}\left[\sqrt{t}\exp\left(-\left[\frac{(4n-2)R}{2\sqrt{\alpha^{c}t}}\right]^{2}\right)-\frac{(4n-2)R}{2\sqrt{\alpha^{c}}}\sqrt{\pi}\,\mathrm{erfc}\frac{(4n-2)R}{2\sqrt{\alpha^{c}t}}\right] \\ & \left.+(-\Delta T)\sum_{n=1}^{N}h^{2(n-1)}\left[\sqrt{t}\exp\left(-\left[\frac{(4n-3)R}{2\sqrt{\alpha^{c}t}}\right]^{2}\right)-\frac{(4n-3)R}{2\sqrt{\alpha^{c}}}\sqrt{\pi}\,\mathrm{erfc}\frac{(4n-3)R}{2\sqrt{\alpha^{c}t}}\right]\right\} \end{aligned} \tag{4.31}$$

### 4.8.3 Heat Energy Transfer in Step-III

Putting ICs (4.7) in Eq. (4.28), we get

$$Q_{SO}^{III} = Q_{EC2|SO}^{III} = \frac{2k^o}{\sqrt{\pi\alpha^o}}\frac{K_\varepsilon}{1+K_\varepsilon}$$
$$\times\left\{(\Delta T)\,h\sum_{n=1}^{N}h^{2(n-1)}\left[\sqrt{t}\exp\left(-\left[\frac{(4n-0)R}{2\sqrt{\alpha^c t}}\right]^2\right)-\frac{(4n-0)R}{2\sqrt{\alpha^c}}\sqrt{\pi}\,\mathrm{erfc}\frac{(4n-0)R}{2\sqrt{\alpha^c t}}\right]\right.$$
$$+(-\Delta T)\,h\sum_{n=1}^{N}h^{2(n-1)}\left[\sqrt{t}\exp\left(-\left[\frac{(4n-1)R}{2\sqrt{\alpha^c t}}\right]^2\right)-\frac{(4n-1)R}{2\sqrt{\alpha^c}}\sqrt{\pi}\,\mathrm{erfc}\frac{(4n-1)R}{2\sqrt{\alpha^c t}}\right] \quad (4.32)$$
$$+(-\Delta T)\sum_{n=1}^{N}h^{2(n-1)}\left[\sqrt{t}\exp\left(-\left[\frac{(4n-3)R}{2\sqrt{\alpha^c t}}\right]^2\right)-\frac{(4n-3)R}{2\sqrt{\alpha^c}}\sqrt{\pi}\,\mathrm{erfc}\frac{(4n-3)R}{2\sqrt{\alpha^c t}}\right]$$
$$\left.+(\Delta T)\sum_{n=1}^{N}h^{2(n-1)}\left[\sqrt{t}\exp\left(-\left[\frac{(4n-4)R}{2\sqrt{\alpha^c t}}\right]^2\right)-\frac{(4n-4)R}{2\sqrt{\alpha^c}}\sqrt{\pi}\,\mathrm{erfc}\frac{(4n-4)R}{2\sqrt{\alpha^c t}}\right]\right\}$$

## 4.9 Temperature Profile and Corresponding Heat Flow through EC2|SO Interface

The directional heat transfer through the interfaces SI|EC1 and EC2|SO depends strongly on the interfacial temperature[143,147] $T_s$ and temperature profiles across the interface. Eqs. (4.33) – (4.35) give the interfacial temperature $T_s$ at interfaces S!|EC1, EC1|EC2, and EC2SO respectively.

$$T_s|_{SI|EC1}(t) = \left.\frac{T_{EC1}(t)\cdot K_\varepsilon + T_{SI}(t)}{1+K_\varepsilon}\right|_{x=-R} \quad (4.33)$$

$$T_s|_{EC1|EC2}(t) = \left.\frac{T_{EC1}(t)\cdot K_\varepsilon + T_{EC2}(t)}{1+K_\varepsilon}\right|_{x=0} \quad (4.34)$$

$$T_s|_{EC2|SO}(t) = \left.\frac{T_{EC2}(t)\cdot K_\varepsilon + T_{SO}(t)}{1+K_\varepsilon}\right|_{x=R} \quad (4.35)$$

That is, $T_s$ is determined by the surface temperature of two bodies at the surface and the relative thermal activity of bodies across the interface.

From Eq. (4.35), one can find that if SO/SI material is the same as ECM (i.e., $K_\varepsilon = 1$, all bodies are thermally same), $T_s$ is simply the average of two surface temperatures and there will be a smooth temperature profile across the interface. If the $K_\varepsilon \to 0$, $T_s$ will be very close to the temperature of the source surface $x$=$R$, $T_{SO}(t)|_{x=R}$. Therefore, $T_s(0^+)$ is close to the equilibrium temperature of SO, $T$. Similarly, if the $K_\varepsilon \to \infty$, $T_s$ will be very close to the temperature of the EC2 surface at $x$=$R$, $T_{EC}\ (t)|_{x=R}$.

For detailed study, numerical calculations were carried out using MATLAB based on the mathematical formulation described in the section 4.3. Thermal properties of some commonly used materials are shown in Appendix - D. Following three special cases were studied using the numerical method: 1) SO/SI material is the same as ECM (i.e., PMN-4.5PT), which results in $K_\varepsilon = 1$ (named as System-1); 2) PMN-4.5PT is used as ECM and Cu is used as SO/SI material, which corresponds to an $K_\varepsilon = 0.0172 \ll 1$ (named as System-2); 3) BT as ECM and air as SO/SI, which results in $K_\varepsilon = 794 \gg 1$ (named as System-3. R = 1 mm was used for all three systems. For the simulations, it was assumed that application/removal of an electric field on ECM (EC1 and EC2) results in a thermal change of $\Delta T_{EC} = \pm 1$ ℃, the corresponding change in heat energy is $\Delta Q = \rho R c_p \Delta T_{EC}$ for unity cross-section of EC1/EC2 and the equilibrium temperature is 0 ºC. That is, in the calculation, 0 ºC is used as the equilibrium temperature, but the results can be simply used to any equilibrium temperature T. Therefore, T is used as the equilibrium temperature in the figures hereafter.

### 4.9.1 Step-II and Step-III

For System-1, as discussed in section 4.2, the overall heat flow through the EC2|SO interface during Step-II and Step-III are not zero, but cancel each other as illustrated in Figure 4.4 for the temperature profiles at different times. Clearly, the peak temperature location does not change with time. That is, when the temperature in all four bodies reaches their equilibrium temperature, the heat transferred through SI|EC1 interface is exactly the same as the heat transferred through EC2|SO interface. If ΔQ is the heat absorbed by EC1 during Step-II and also the heat released by EC2 during Step-III, the net heat flows through EC2|SO is -ΔQ/2 and +ΔQ/2 during Step-II and Step-III, respectively.

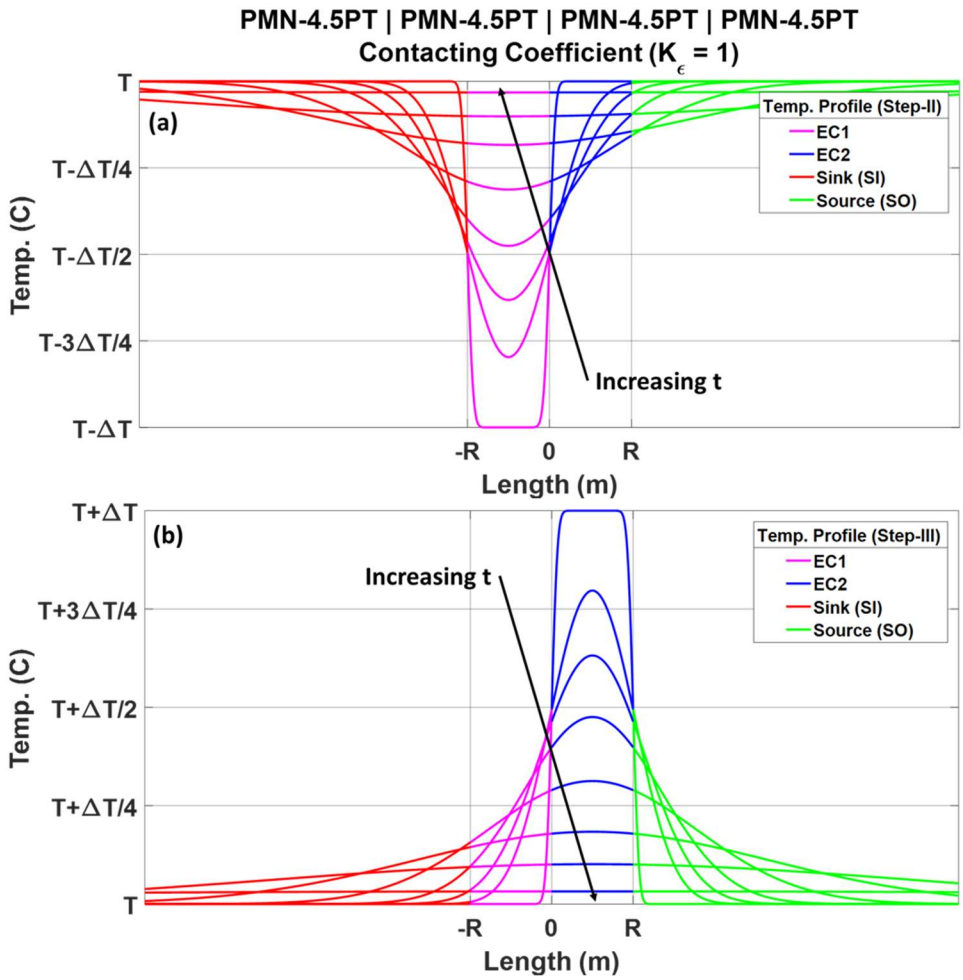


**Figure 4.4 Temperature profiles of system-1 during, (a). Step-II, (b). Step-III**

For system-2, the temperature profiles during Step-II and Step-III at different times are shown in Fig. 5. Clearly, at the beginning the heat is mainly exchanged between EC1 and EC2, which results in a very small amount heat flows through EC2|SO and SI|EC1 interface, as illustrated in Figure 4.5. In other words, the heat transferred between SI and EC1 and also between EC2 and SO mainly occurs after both EC1 and EC2 body reach the same temperature. Based on the results, it is concluded that the sum of the amount of net heat flows through EC2|SO interface during both Step-II and Step-III is zero as shown in Figure 4.6.

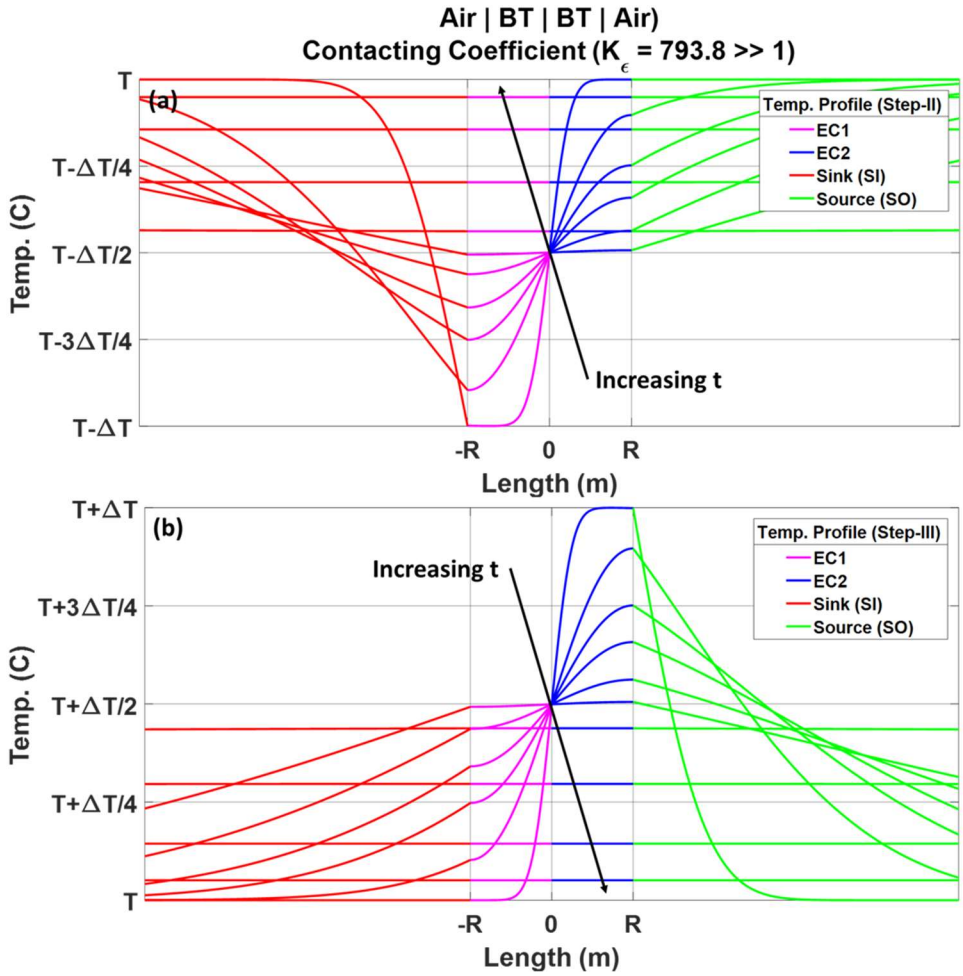


**Figure 4.5 Temperature profiles at different times for system-2, (a). Step-II, (b). Step-III**

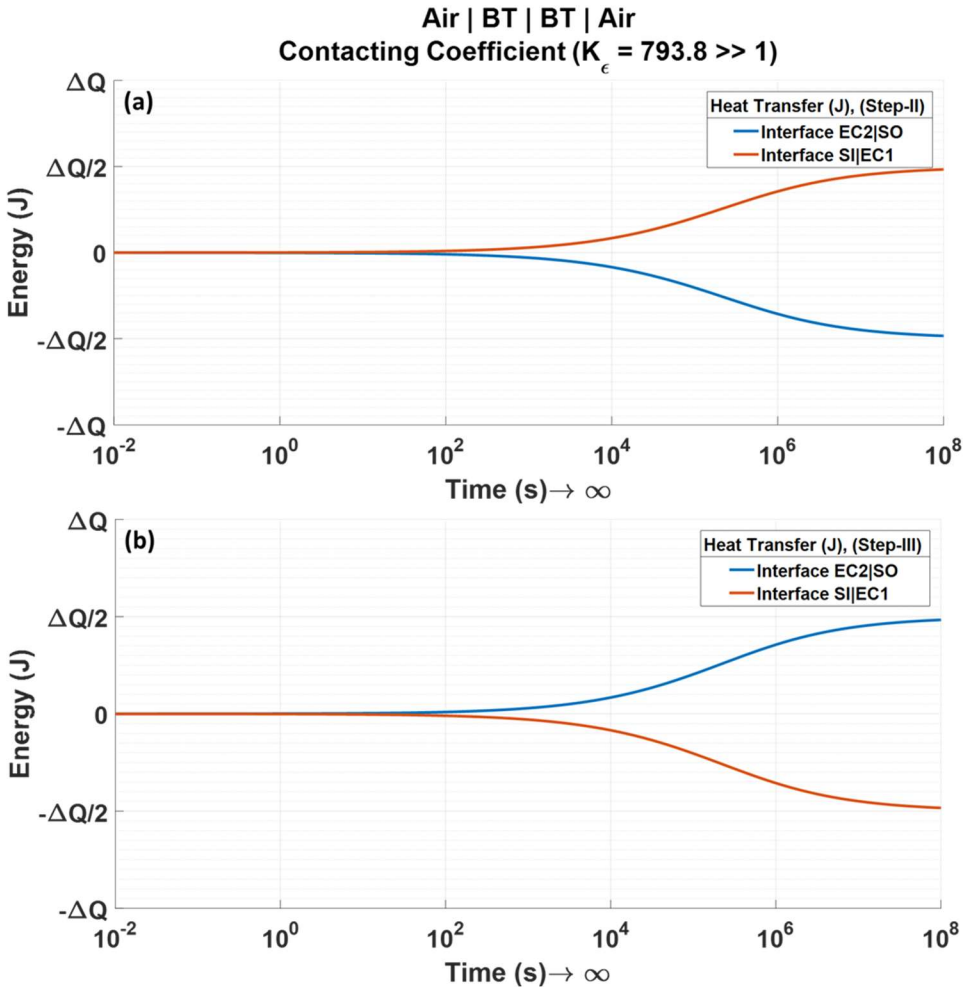


**Figure 4.6 Time dependence of heat energy transferred through SI|EC1 (blue) and EC2|SO (red) interface for system-2: (a). Step-II, (b). Step-III.**

For System-3, the temperature profiles at different times during Step-II and Step-III are plotted in Figure 4.7(a) and (b), respectively. For Step-II, EC1 has to absorb an amount of heat ($\Delta Q$) to reach the equilibrium temperature $T$ with all other bodies. There is a point at which the temperature is the minimum.

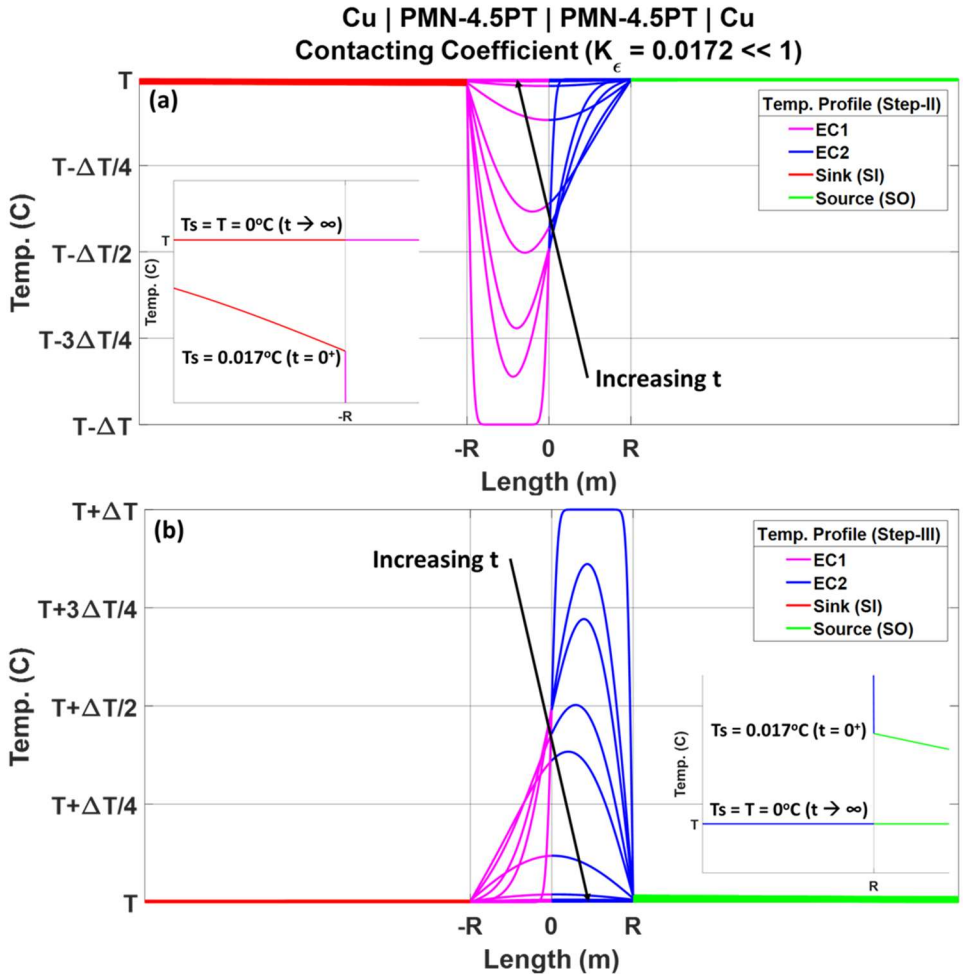


**Figure 4.7 Temperature profiles $K_\varepsilon$ << 1 at different times for system-3, (a). Step-II, (b). Step-III**

The location of the minimum temperature shifts to right with time. At a certain time, the minimum temperature point is at x=0. After this time, the heat flows from SO to EC2 with a higher rate than that from SI to EC1. Slowly, the minimum temperature point shifts to right further with time. At a certain time $t_{II}$, the minimum temperature point is at $x = R$. After $t_{II}$, the heat flows back from EC2 to SO at EC2|SO interface, while at SI|EC1 interface, the heat is continuously flowing from SI to EC1. All these characteristics can be clearly seen from the time dependence of heat energy transferred through both interfaces as shown in Figure 4.8.

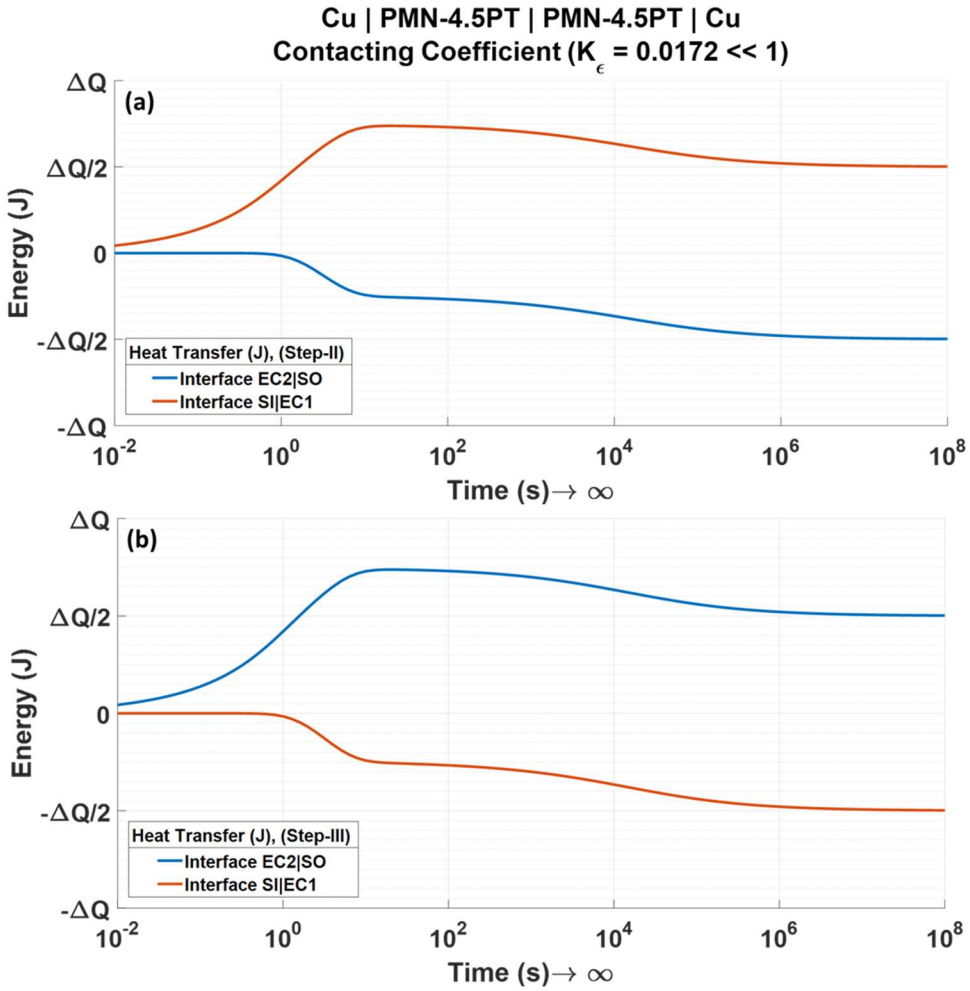


**Figure 4.8 Time dependence of heat energy transferred through SI|EC1 (blue) and EC2|SO (red) interface for system-3: (a). Step-II, (b). Step-III.**

As shown in Figure 4.8(a), during Step-II, the heat transferred from SO to EC2 is continuously increases, but the heat transferred from SI to EC1 increases initially and, then, decreases with time. Eventually, all four bodies reach their equilibrium temperature T and the heat transferred from SI to EC1 reaches the same value as the heat transferred from EC2 to SO. That is, for a complete Step-II, the net heat transferred from SO to EC2 is exactly ΔQ/2. Similarly, the heat transferred from SI to EC1 is also ΔQ/2.

The heat transformation during Step-III is exactly the same as during Step-II except the direction of heat flow. Again, eventually, all four bodies reach their equilibrium temperature T and the net heat transferred from EC2 to SO is exactly the same as the heat transferred from EC1 to SI (i.e., ΔQ/2) as shown in Figure 4.8(b). Based on the results obtained from Step-II and Step-III, it is

concluded that the summary of the amount of heat flows through EC2|SO interface during both Step-II and Step-III is zero.

### 4.9.2 Step-I

The temperature profile for system-1 at different times is shown in Figure 4.9 (a). Clearly, the temperature is symmetrical around $x = 0$. There are two characteristic points: one at which the temperature is the maximum, the other at which the temperature is minimum. The location of these two points, which shifts away from $x = 0$ with time, has the same distance from $x = 0$.

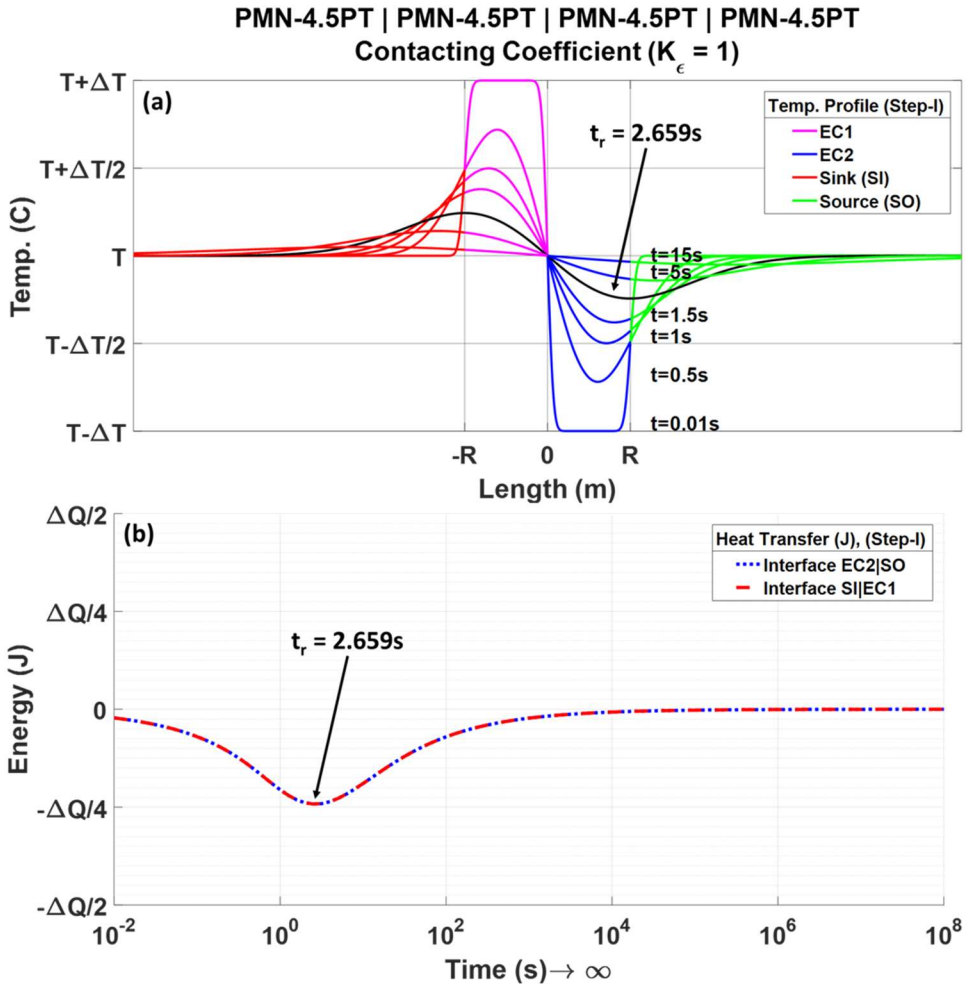


**Figure 4.9 Step-I of system-1, (a). Temperature profiles at different times, arrowhead shows the curve at the time $t_r$ ($\partial T_s(t_r)/\partial x|_R = 0$), (b). Time dependence of heat energy transferred through SI|EC1 and EC2|SO interfaces**

From the results shown in Figure 4.9 (a), one can find that at the beginning, temperature gradient at the interface is positive, meaning there is a heat flow from the source (SO) to EC2 (also from

EC1 to SI). As time goes on, the temperature gradient at the interface decreases, meaning heat flow rate decreases. At a certain time ($t_r$), the temperature gradient at the interface reaches zero. After time $t_r$, the heat flows back from EC2 to SO, which is illustrated in Figure 4.9 (b). In other words, after the time $t_r$, the process reduces the heat to be removed from the source.

All these indicate that $t_r$ is a critical time for the system. The value of $t_r$ for different systems that use different ECMs and SO/SI materials is presented in Table 4.1. The value of $t_r$ is dependent on the thermal conductivity of the materials. For example, as shown in Table 4.1, the $t_r$ is 2.659s and 0.218s for a system made of PMN-4.5PT and BT, respectively.

For System-2, the temperature profile is shown in Figure 4.10 (a) and corresponding heat exchange between SO and EC2 is illustrated in Figure 4.10 (b). Again, it is concluded that for a complete Step-1, there is no heat transferred between SO and SI.

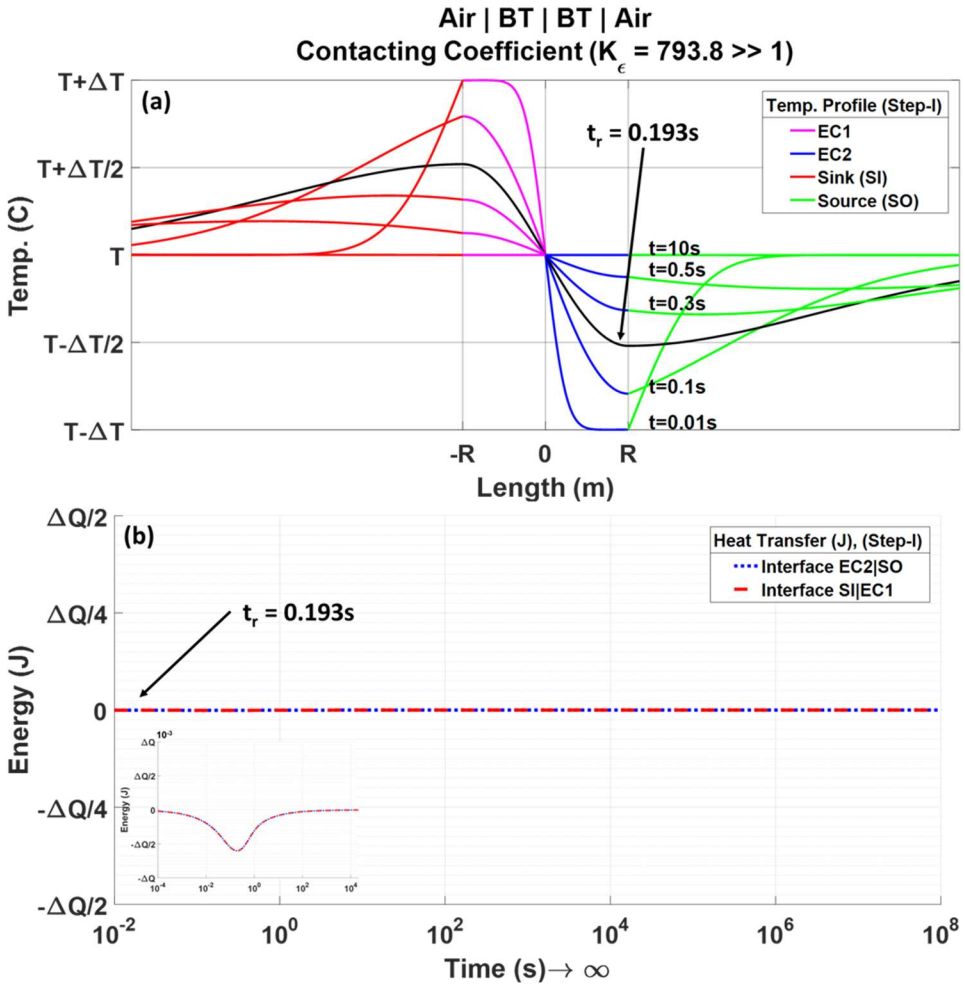


**Figure 4.10 Step-I of system-2, (a). Temperature profiles at different times, arrowhead shows the curve at the time $t_r$ ($\partial T_s(t_r)/\partial x|_R = 0$), (b). Time dependence of heat energy transferred through SI|EC1 and EC2|SO interfaces**

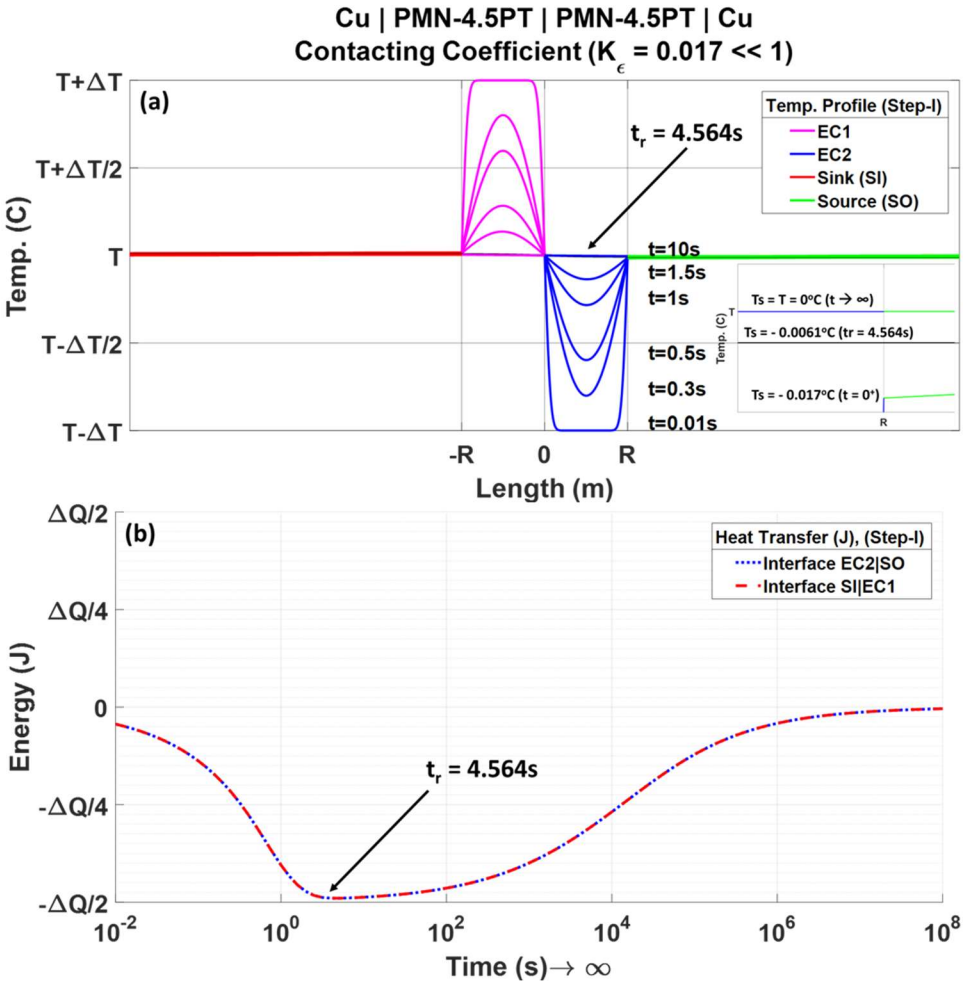


**Figure 4.11 Step-I of system-3 $K_\varepsilon = 0.0172 << 1$ with R = 1 mm, ΔT = 1°C, (a). Temperature profiles at different times, arrowhead shows the curve at the time $t_r$, $(\partial T_s(t_r)/\partial x|_R = 0)$, (b). Time dependence of heat energy transferred through SI|EC1 and EC2|SO interfaces**

The temperature profile for system-3 is shown in Figure 4.11(a). Like system-1, the temperature profile is symmetrical around $x = 0$ with a maximum and a minimum. The distance from the location of temperature maximum to x=0 is the same as that of temperature minimum to $x = 0$. The location of temperature maximum and minimum shifts away from $x = 0$ with time. At time $t_r$, the location of the temperature maximum is at $x = R$, while the location of the temperature minimum is at $x = -R$. After time $t_r$, the location of the temperature maximum is at $x > R$, while the location of the temperature minimum is at $x < -R$. In other words, the heat is initially transferred from SO to EC2 and EC1 to SI. However, after time $t_r$, the heat flows back from EC2 to SO and SI to EC1, as illustrated in Figure 4.11(b). If time is long enough, it is found that the

overall heat exchange between SO and EC2 is zero, as well as between SI and EC1. Therefore, for a completed Step-I, there is no heat transferred from SO to SI.

In a summary, for all three systems, it is found that when the time is long enough, all four bodies reach their equilibrium temperature $T$, which corresponds to an overall heat amount transferred through the interface is zero for Step-I.

### 4.9.3 Summary of an Ideal Three-step Process

Based on the results obtained above, for the three-step process described in Figure 4.2, if each step reaches its final equilibrium state (i.e., each step is operated with a long enough time), there is no net heat flow through the EC2|SO and SI|EC1 interfaces. In other words, after a complete cycle, no heat is transferred from SO to SI.

**Table 4.1 Contacting coefficient ($K_\varepsilon$), interface temperature ($T_s$) at EC2|SO interface at $t = 0$, time $t_r$ and $Q(t_r)$ for systems using BT and PMN-4.5PT as ECM and different materials as SO and SI ($\delta = 10^{-5}$)**

| EC1/EC2 | SI/SO | $\rho^o c_p^o$ ($10^6$) | $K_\varepsilon$ | $T_s = \Delta T\left(\frac{K_\varepsilon}{1+K_\varepsilon}\right)$ at $t = 0^+$ | $t_r$ (s) | $T_s(t_r)$ (°C) | $Q(t_r)$ (J) | System | $Q_r(\%) = \frac{Q(t_r)}{\Delta Q} \times 100$ |
|---|---|---|---|---|---|---|---|---|---|
| BT<br>ΔT = 1.0 °C<br>ΔQ = 3194 J<br>$\rho^c c_p^c = 3.19 \times 10^6$ | **Air** | 0.00117 | **793.8** | **-0.999** | **0.1932** | **-0.530** | **1.86** | **System-2** | **0.06** |
| | PMN-4.5PT | 1.620 | 6.878 | -0.908 | 0.1979 | -0.400 | 188.3 | | 6.0 |
| | BT | 3.190 | 1 | - ½ | 0.2184 | -0.076 | 749.8 | | 23.8 |
| | Gr | 0.056 | 0.708 | -0.412 | 0.2257 | -0.150 | 881.0 | | 27.6 |
| | Al | 2.557 | 0.178 | -0.15 | 0.2683 | -0.065 | 1294 | | 40.5 |
| | Ag | 2.468 | 0.135 | -0.12 | 0.2791 | -0.051 | 1346.5 | | 42.2 |
| | Cu | 3.439 | 0.118 | -0.11 | 0.2846 | -0.044 | 1368.1 | | 42.8 |
| PMN-4.5PT<br>ΔT = 1.0 °C<br>ΔQ = 1620 J<br>$\rho^c c_p^c = 1.62 \times 10^6$ | Air | 0.00117 | 115.4 | -0.990 | 2.3545 | -0.520 | 6.596 | | 0.41 |
| | **PMN-4.5PT** | 1.620 | **1** | **- ½** | **2.6585** | **-0.244** | **389.1** | **System-1** | **24.0** |
| | BT | 3.190 | 0.145 | -0.126 | 3.3601 | -0.0110 | 691.4 | | 42.6 |
| | Gr | 0.056 | 0.103 | -0.092 | 3.527 | -0.0389 | 719.9 | | 44.4 |
| | Al | 2.557 | 0.026 | -0.020 | 4.3121 | -0.0094 | 779.3 | | 48.1 |
| | Ag | 2.468 | 0.020 | -0.025 | 4.4812 | -0.0070 | 784.7 | | 48.4 |
| | **Cu** | 3.439 | **0.017** | **-0.017** | **4.5637** | **-0.0061** | **786.9** | **System-3** | **48.6** |

## 4.10 Operation to Achieve Net Heat Transfer from SO to SI for One Cycle for $K_\varepsilon << 1$

As discussed above, the heat transferred between EC2 and SO during Step-II and Step-III cancels each other. Therefore, the net heat transformation between SO and SI for the system and process described in SECTION 4.2 is dependent on Step-I. However, as demonstrated above, for Step-I, initially heat flows from SO to EC2, but after time $t_r$, the heat flows back from EC2 to SO. Therefore, if Step-II can start at the time $t_r$ of Step-I a non-zero net heat can be transferred from SO to SI. However, when $K_\varepsilon$ is big, the temperature in the ECM at $t_r$ is significantly different to the equilibrium temperature. Fortunately, when $K_\varepsilon$ is very small, the $T_s$ at $t_r$ is very close to the equilibrium temperature $T$ and at the same time a higher $Q(t_r)$ is obtained as shown in Table 4.1. From the data shown in Table 4.1, one can find that the smaller the $K_\varepsilon$, the higher the $Q(t_r)$ is and the smaller the $Ts$ is. Therefore, to build a cooling pump using the design reported here, a smaller $K_\varepsilon$ is better.

For System-3 ($K_\varepsilon = 0.0172$), at time $t_r$, the temperature at the surface of EC2 ($x = R$) is the highest temperature in EC2, which is only 0.0061 $^oC$ different from the equilibrium temperature $T$ or 0.61% of the temperature change ($\Delta T$ = 1 $^oC$) induced in ECM by the ECE. Considering the temperature in EC2 is not uniform, one side is always the same as the equilibrium temperature and the other side only 0.0061 $^oC$ different with the equilibrium temperature, the average temperature in EC2 is only less than 0.003 $^oC$ or less than 0.3% of $\Delta T$. Therefore, when Step-II starts at the time $t_r$ of Step-I, the results obtained in Section 4.9.1 for Step-II and Step-III are still valid. Therefore, after a three-step process cycle with Step-1 completed at $t_r$, a non-zero amount of heat is transferred from SO to EC2, which is also the heat transferred from EC1 to SI. It has to be mentioned that the initial temperature (i.e., equilibrium temperature) of both SO and SI are the same. In other words, for SO and SI with the same temperature, amount of heat, $Q(t_r)$, is transferred from SO to SI by one cycle. From Table 4.1, it is found that the overall heat transferred from SO to EC2, which is also the heat transferred from EC1 to SI, is about 49% of $\Delta Q$ – the thermal energy induced in the EC2 by the ECE.

**Table 4.2 Step-I of System-3 when it is operated with different ΔT. ($\delta = 10^{-5}$)**

| ΔT (℃) | ΔQ (J) $R = 1mm$ | $T_s(t = 0^+)$ (℃) | $t_r$(s) | $T_s(t_r)$ (℃) | $\frac{T_s(t_r)}{\Delta T}$ | $Q(t_r)$ | $Q_r = \frac{Q(t_r)}{\Delta Q}$ |
|---|---|---|---|---|---|---|---|
| 1 | 1620 | -0.017 | 4.564 | -0.0061 | -0.0061 | 786.9 | 48.6% |
| 2 | 3240 | -0.034 | 4.564 | -0.0121 | -0.0061 | 1573.8 | 48.6% |
| 5 | 8100 | -0.085 | 4.564 | -0.0304 | -0.0061 | 3935 | 48.6% |
| 10 | 16200 | -0.170 | 4.564 | -0.0607 | -0.0061 | 7869 | 48.6% |

For system-3, when different ΔT is used to operate it (i.e., different electric field is used), the results are shown in Table 4.2. One can find that all the values of $t_r$, $T_s(t_r)/\Delta T$ and Q(tr)/ΔQ do not change. In other words, the calculated results can be easily modified to the system operated under different electric field (i.e., different ΔT).

When system-3 is modified by using EC1/EC2 with different thicknesses, the results are shown in Table 4. From the results in Table 4, one can find that although the $t_r$ increases with the $R$, the $Ts(t_r)$ and $Q(t_r)/\Delta Q$ does not change with $R$. That is, the thickness does not affect the $Ts(t_r)$ which is only about 0.3% of ΔT.

Based on the results shown in Table 3 and 4, it is concluded that $Ts(t_r)/\Delta T$ is independent on the R and ΔT. In other words, Ts at $t_r$ during Step-1 is only 0.3% of ΔT. Therefore, the operation introduced here by starting Step-II at time $t_r$ of Step-I works for all the systems as long as $K_\varepsilon$ is very small. To achieve a larger amount of heat energy transferred from SO to SI during one cycle (i.e., a higher $Q(t_r)$), a smaller contacting coefficient ($K_\varepsilon$) is certainly required. Based on the definition in Section 4.3,

$$K_\varepsilon = \sqrt{\frac{k^c \rho^c C_p^c}{k^o \rho^o C_p^o}} \tag{4.36}$$

Where $\rho^c C_p^c$ and $\rho^o C_p^o$ are the volumetric specific heat capacity of ECM and SO/SI material, respectively. Therefore, to achieve a smaller contacting coefficient, SO/SI with a higher thermal conductivity and a higher volumetric heat capacity would be favorable.

To increase the power transformation rate, a smaller $t_r$ is desired. Additionally, from Eq. (4.30), one can find that the time dependence of the heat transfer through EC2|SO interface is actually dependent on $\alpha^c$ and $h = (1 - K_\varepsilon)/(1 + K_\varepsilon)$.

**Table 4.3 System-3 is modified to use different R, PMN-4.5PT as ECM and Cu as SO/SI**

| R (mm) | $t_r$ (s) | $Ts$ ($t_r$) | Q($t_r$) (J) | ΔQ (J) | Q($t_r$)/ΔQ (%) | Q($t_r$)/$t_r$ |
|---|---|---|---|---|---|---|
| 0.1 | 0.0457 | -0.0061 | 72.5 | 162 | 44.7 | 1586.4 |
| 0.3 | 0.4108 | -0.0061 | 231.2 | 486 | 47.6 | 562.8 |
| 0.5 | 1.1410 | -0.0061 | 390 | 810 | 48.1 | 341.8 |
| 0.7 | 2.2363 | -0.0061 | 548.7 | 1134 | 48.4 | 245.4 |
| **1.0** | **4.5637** | **-0.0061** | **786.9** | **1620** | **48.6** | **172.4** |
| 1.5 | 10.2683 | -0.0061 | 1183.7 | 2430 | 48.7 | 115.3 |
| 2.0 | 18.2548 | -0.0061 | 1580.6 | 3240 | 48.8 | 86.6 |
| 3.0 | 41.0740 | -0.0061 | 2374.4 | 4860 | 48.9 | 57.8 |
| 4.0 | 73.0189 | -0.0061 | 3168.2 | 6480 | 48.9 | 43.4 |
| 5.0 | 114.10 | -0.0061 | 3862.0 | 8100 | 48.9 | 33.84 |

## 4.11 Concluding Remarks

A new design of cooling pump using ECE is introduced by using two layers of ECM. The electric field in both ECM layers is independently controlled with a sequence (i.e., process) that includes three steps and can be repeated continuously. Among three steps, Step-1 is used to transfer heat from SO to SI, while Step-II and Step-III are used to restore the initial condition for Step-I. The time dependence of both the temperature profile in all four bodies and heat transformation through the interface was calculated using the newly introduced analytical solutions. It is concluded that the heat transformation during Step-II and Step-III cancel each other. Therefore, among of heat transferred from SO to SI during Step-I is the net heat transferred for one cycle. During Step-I, one layer of ECM increases, and the other layer of ECM decreases its temperature simultaneously using ECE. There is a critical time, $t_r$, at which the maximum and minimum point of the temperature profile are at ECM|SI and ECM|SO interface. Step-II has to start at *tr* of Step-I. To achieve a larger amount of heat transferred from SO to SI, it is concluded that: 1) the SO and SI should have a much higher thermal conductivity than the ECM; 2) the SO/SI material with a higher volumetric heat capacity is also favorable.

By using PMN-0.1PT as ECM and Cu as SI/SO material, it is demonstrated that during Step-I the amount of heat transferred from SO to SI is about 49% of the heat generated in one ECM layer due to the ECE, which is independent of both the thickness of ECM and the ΔT – temperature change in ECM due to the ECE. However, the time $t_r$ increases with increasing thickness of ECM layer, but does not change with the ΔT. That is, the EC heat pump introduced in this work can

transfer heat from SO to SI for both SO and SI with the same equilibrium temperature. It has to be mentioned that in this design, neither moving part nor heat switch was used.

**Application Remark**: Given that unidirectional heat flow was achieved without any moving parts with the EC heat pump unit concept presented in this article, future work might focus on staggering and cascading multiple EC heat pump units. Series and parallel configurations could produce larger temperature lifts and higher heat transfer rates more typical of heat pump systems for applications from electronic cooling to building and transportation HVAC systems.

# Chapter 5 Analytical Solution of a Multilayer Problem with Different Source and Sink

## 5.1 Model and Analytical Solution

In most of the prototype reported and in typical ECE-based devices, the ECM is alternatively coupled and decoupled thermally between source and sink in the absorption and rejection cycles. In that situation, during absorption, if ECM is in thermal contact with the source from the one end, then on the other end it is air and during rejection of heat, ECM is coupled with sink from the one end and it is air on the other end. It is considered inevitable that an analytical solution should be there so that the optimized devices may be designed and the relaxation time, heat fluxes and temperature profiles may be determined prior to actual prototype manufacturing. This solution will not only safe the cost and time but will also help to understand the physics of heat transfer in EE-based devices.

### 5.1.1 Physical Model

The thermal properties of the *center* bodies (EC1 and EC2) are same, whereas source and sink have different thermal properties. The problem has been solved for generalized initial conditions. The initial temperature profile is established in two ECMs using ECE. It is assumed that an electric field is applied on ECMs at time zero ($t = 0$) and prior to this all bodies have the same temperature (say T). SO|EC1, EC1|EC2, and EC2|SI are the interfaces through which the heat will transfer by heat conduction. The model has been shown in Figure 5.1. In the following, this model where the End bodies are different from each other (different thermal properties) and they are also different from the ECMs.

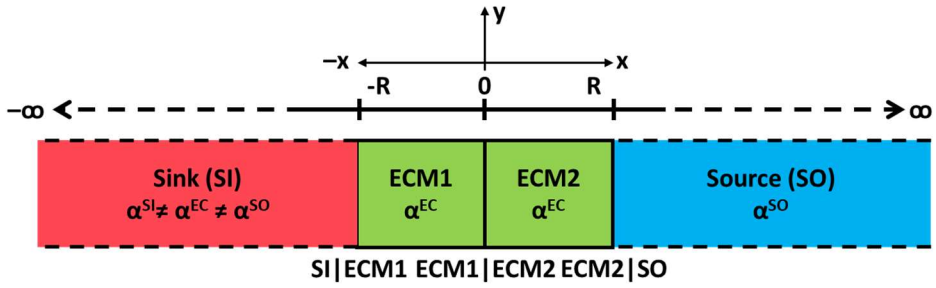


**Figure 5.1 Theoretical model of heat conduction problem for different source and sink bodies**

### 5.1.2 Mathematical Model and Governing Equations

#### 5.1.2.1 Assumptions and Considerations

To analytically solve the heat conduction in the system shown in Figure 5.1, the following assumptions are used: 1) there is no heat loss to the environment through convection and/or radiation, 2) the interfaces are considered the perfect thermal contacts (i.e. zero thermal resistance), 3) the gradients in the y and z direction are neglected, only the gradients along the x-direction are considered, 4) the materials properties are temperature invariant, 5) bodies B1 & B4 are considered infinite heat sink/source bodies. In this unsteady heat diffusion problem, the 1-D heat equations for each of the bodies are given in Eqs.(5.1) – (5.2).

$$\frac{\partial T_{SI}(x,t)}{\partial t} = \alpha^{SI}\frac{\partial^2 T_{SI}(x,t)}{\partial x^2} \qquad -\infty < \boldsymbol{x} < -\boldsymbol{R} \qquad (5.1)$$

$$\frac{\partial T_{EC1}(x,t)}{\partial t} = \alpha^{EC}\frac{\partial^2 T_{EC1}(x,t)}{\partial x^2} \qquad -\boldsymbol{R} < \boldsymbol{x} < \boldsymbol{0} \qquad (5.2)$$

$$\frac{\partial T_{EC2}(x,t)}{\partial t} = \alpha^{EC}\frac{\partial^2 T_{EC2}(x,t)}{\partial x^2} \qquad \boldsymbol{0} < \boldsymbol{x} < \boldsymbol{R} \qquad (5.3)$$

$$\frac{\partial T_{SO}(x,t)}{\partial t} = \alpha^{SO}\frac{\partial^2 T_{SO}(x,t)}{\partial x^2} \qquad \boldsymbol{R} < \boldsymbol{x} < \infty \qquad (5.4)$$

where $T_{SI}\ (x,t)$, $T_{EC1}\ (x,t)$, $T_{EC2}\ (x,t)$, and $T_{SO}\ (x,t)$, are the temperatures at time *t* and location *x* for sink, EC1, EC2 and source, respectively, $\alpha = k/\rho c_p$ ($m^2/s$) are the thermal diffusivity of each of the above mentioned four bodies, in which $k$ ($Wm^{-1}K^{-1}$), $\rho(kg/m^3)$, and $c_p(J/Kkg\ )$ are the thermal conductivity, mass density and specific heat capacity, respectively, of the respective body. The thermal properties of the ECMs are same, but the thermal properties of sink and source are different.

#### 5.1.2.2 Initial Conditions (ICs)

Based on the physical model shown in Figure 3.1, the ECE is used to change the temperature of bodies B2 and B3 by application/ removal of external electric field at any time. The followings are the generalized initial conditions,

$$T_{SI}(x,0) = T_{SI,i}$$

$$T_{EC}\ (x,0) = T_{EC1,i}$$

$$T_{EC2}(x,0) = T_{EC2,i} \tag{5.5}$$

$$T_{SO}(x,0) = T_{SO,i}$$

#### 5.1.2.3 Boundary Conditions (BCs)

**Interface SI|EC1 at $x = -R$**

$$T_{SI}(-R,t) = T_{EC1}(-R,t)$$
$$-k^{SI}\left.\frac{\partial T_{SI}(x,t)}{\partial x}\right|_{x=-R} = -k^{EC}\left.\frac{\partial T_{EC1}(x,t)}{\partial x}\right|_{x=-R} \tag{5.6}$$

**Interface EC1|EC2 at $x = 0$**

$$T_{EC1}(0,t) = T_{EC2}(0,t)$$
$$-k^{EC}\left.\frac{\partial T_{EC}\ (x,t)}{\partial x}\right|_{x=0} = -k^{EC}\left.\frac{\partial T_{EC2}(x,t)}{\partial x}\right|_{x=0} \tag{5.7}$$

**Interface EC2|SO at $x = R$**

$$T_{EC2}(R,t) = T_{SI}\ (R,t)$$
$$-k^{EC}\left.\frac{\partial T_{EC2}(x,t)}{\partial x}\right|_{x=R} = -k^{SI}\left.\frac{\partial T_{SO}(x,t)}{\partial x}\right|_{x=R} \tag{5.8}$$

#### 5.1.2.4 Physical Conditions (PCs)

The two semi-infinite end bodies (B1 & B4) being very large are considered a continuous source and sink of energy (i.e. infinite source/sink of heat energy). The perimeters are perfectly insulated and there is no heat transfer to the surroundings at $x = \pm\infty$.

$$\left.\frac{\partial T_{SI}(x,t)}{\partial x}\right|_{x=-\infty} = \left.\frac{\partial T_{SO}(x,t)}{\partial x}\right|_{x=\infty} = 0 \tag{5.9}$$

### 5.1.3 Solution of the Heat Equations

#### 5.1.3.1 Laplace Transformation

Laplace transform method[151] is used here to solve the system of Eqs. (5.1) – (5.4), so the Laplace transform of these equations may be given as,

$$W_{SI}(x,s) - \frac{T_{SI,i}}{s} = A_1\, e^{\sqrt{\frac{s}{\alpha^{SI}}}x} + B_1\, e^{-\sqrt{\frac{s}{\alpha^{SI}}}x} \tag{5.10}$$

$$W_{EC1}(x,s) - \frac{T_{EC\ ,i}}{s} = A_2\, e^{\sqrt{\frac{s}{\alpha^{EC}}}x} + B_2\, e^{-\sqrt{\frac{s}{\alpha^{EC}}}x} \tag{5.11}$$

$$W_{EC2}(x,s) - \frac{T_{EC2,i}}{s} = A_3\, e^{\sqrt{\frac{s}{\alpha^{EC}}}x} + B_3\, e^{-\sqrt{\frac{s}{\alpha^{EC}}}x} \tag{5.12}$$

$$W_{SO}(x,s) - \frac{T_{SO,i}}{s} = A_4\, e^{\sqrt{\frac{s}{\alpha^{SO}}}x} + B_4\, e^{-\sqrt{\frac{s}{\alpha^{SO}}}x} \tag{5.13}$$

There are 8 constants of integration that need to be determined. Boundary conditions may be used to calculate them. For the temperature of the bodies to be finite at $x = \pm\infty$, the constants $B_1$ & $A_4$ vanish instantly. (i.e. $B_1 = 0$ & $A_4 = 0$), and the Eqs. (5.10) – (5.13) become as follow,

$$W_{SI}(x,s) - \frac{T_{SI,i}}{s} = A_1\, e^{\sqrt{\frac{s}{\alpha^{SI}}}x} \tag{5.14}$$

$$W_{EC1}(x,s) - \frac{T_{EC1,i}}{s} = A_2\, e^{\sqrt{\frac{s}{\alpha^{EC}}}x} + B_2\, e^{-\sqrt{\frac{s}{\alpha^{EC}}}x} \tag{5.15}$$

$$W_{EC2}(x,s) - \frac{T_{EC2,i}}{s} = A_3\, e^{\sqrt{\frac{s}{\alpha^{EC}}}x} + B_3\, e^{-\sqrt{\frac{s}{\alpha^{EC}}}x} \tag{5.16}$$

$$W_{SO}(x,s) - \frac{T_{SO,i}}{s} = B_4\, e^{-\sqrt{\frac{s}{\alpha^{SO}}}x} \tag{5.17}$$

Now we are left with 06 constants of integration and boundary conditions on each interface will be used to get 06 equations to determine constants of integration.

### 5.1.3.2 Determining the Constants of Integration

Boundary conditions (5.6)– (5.8) and are used to determine the integration constants.

Two equations from the boundary conditions at $x = -R$

$$W_{SI}(-R,s) = W_{EC1}(-R,s)$$

$$\frac{T_{SI,i}}{s} + A_1\, e^{-\sqrt{\frac{s}{\alpha^{SI}}}R} = \frac{T_{EC1,i}}{s} + A_2\, e^{-\sqrt{\frac{s}{\alpha^{EC}}}R} + B_2\, e^{\sqrt{\frac{s}{\alpha^{EC}}}R} \tag{5.18}$$

$$-k^{SI}\frac{\partial W_1(x,s)}{\partial x}\Big|_{x=-R} = -k^{EC}\frac{\partial W_2(x,s)}{\partial x}\Big|_{x=-R}$$

$$\sqrt{\frac{s}{\alpha^{SI}}}\left(A_1\, e^{-\sqrt{\frac{s}{\alpha^{SI}}}R}\right) = \frac{k^{EC}}{k^{SI}}\sqrt{\frac{s}{\alpha^{EC}}}\left(A_2\, e^{-\sqrt{\frac{s}{\alpha^{EC}}}R} - B_2\, e^{\sqrt{\frac{s}{\alpha^{EC}}}R}\right)$$

$$\left(A_1\, e^{-\sqrt{\frac{s}{\alpha^{SI}}}R}\right) = \frac{k^{EC}}{k^{SI}}\sqrt{\frac{\alpha^{SI}}{\alpha^{EC}}}\left(A_2\, e^{-\sqrt{\frac{s}{\alpha^{EC}}}R} - B_2\, e^{\sqrt{\frac{s}{\alpha^{EC}}}R}\right)$$

$$A_1\, e^{-\sqrt{\frac{s}{\alpha^{SI}}}R} = K_{SI}\left(A_2\, e^{-\sqrt{\frac{s}{\alpha^{EC}}}R} - B_2\, e^{\sqrt{\frac{s}{\alpha^{EC}}}R}\right) \tag{5.19}$$

Two equations from the boundary conditions at interface $x = 0$

$$W_{EC1}(0,s) = W_{EC}\ (0,s)$$

$$\frac{T_{EC\ ,i}}{s} + A_2\, e^{\sqrt{\frac{s}{\alpha^{EC}}}(0)} + B_2\, e^{-\sqrt{\frac{s}{\alpha^{EC}}}(0)} = \frac{T_{EC\ ,i}}{s} + A_3\, e^{\sqrt{\frac{s}{\alpha^{EC}}}(0)} + B_3\, e^{-\sqrt{\frac{s}{\alpha^{EC}}}(0)}$$

$$\frac{T_{2i}}{s} + A_2 + B_2 = \frac{T_{3i}}{s} + A_3 + B_3 \tag{5.20}$$

$$-k^{EC}\frac{\partial W_{EC1}(x,s)}{\partial x}\Big|_{x=0} = -k^{EC}\frac{\partial W_{EC2}(x,s)}{\partial x}\Big|_{x=0}$$

$$\sqrt{\frac{s}{\alpha^{EC}}}\left(A_2\, e^{\sqrt{\frac{s}{\alpha^{EC}}}(0)} - B_2\, e^{-\sqrt{\frac{s}{\alpha^{EC}}}(0)}\right) = \sqrt{\frac{s}{\alpha^{EC}}}\left(A_3\, e^{\sqrt{\frac{s}{\alpha^{EC}}}(0)} - B_3\, e^{-\sqrt{\frac{s}{\alpha^{EC}}}(0)}\right)$$

$$A_2 - B_2 = A_3 - B_3 \tag{5.21}$$

Two equations from the boundary conditions at $x = R$

$$W_{EC2}(R,s) = W_{SO}(R,s)$$

$$\frac{T_{EC2,i}}{s} + A_3\, e^{\sqrt{\frac{s}{\alpha^{EC}}}R} + B_3\, e^{-\sqrt{\frac{s}{\alpha^{EC}}}R} = \frac{T_{SO,i}}{s} + B_4\, e^{-\sqrt{\frac{s}{\alpha^{SO}}}R} \tag{5.22}$$

$$-k^{EC}\frac{\partial W_3(x,s)}{\partial x}\Big|_{x=R} = -k^{SO}\frac{\partial W_4(x,s)}{\partial x}\Big|_{x=R}$$

$$\frac{k^{EC}}{k^{SO}}\sqrt{\frac{s}{\alpha^{c}}}\left(A_3\, e^{\sqrt{\frac{s}{\alpha^{EC}}}R} - B_3\, e^{-\sqrt{\frac{s}{\alpha^{EC}}}R}\right) = -\sqrt{\frac{s}{\alpha^{SO}}}\left(B_4\, e^{-\sqrt{\frac{s}{\alpha^{SO}}}R}\right)$$

$$\frac{k^{EC}}{k^{SO}}\sqrt{\frac{\alpha^{SO}}{\alpha^{EC}}}\left(A_3\, e^{\sqrt{\frac{s}{\alpha^{EC}}}R} - B_3\, e^{-\sqrt{\frac{s}{\alpha^{EC}}}R}\right) = -\left(B_4\, e^{-\sqrt{\frac{s}{\alpha^{SO}}}R}\right)$$

$$K_{SO}\left(A_3\, e^{\sqrt{\frac{s}{\alpha^{EC}}}R} - B_3\, e^{-\sqrt{\frac{s}{\alpha^{EC}}}R}\right) = -\left(B_4\, e^{-\sqrt{\frac{s}{\alpha^{SO}}}R}\right) \tag{5.23}$$

$K_{SI} = \frac{k^{EC}}{k^{SI}}\sqrt{\frac{\alpha^{SI}}{\alpha^{EC}}}$ and $K_{SO} = \frac{k^{EC}}{k^{SO}}\sqrt{\frac{\alpha^{SO}}{\alpha^{EC}}}$ are referred to as contacting coefficients. Both $K_{SI}$ and $K_{SO}$ characterize the thermal activity of one layer relative to next layer.

#### 5.1.3.3 Solving Simultaneous Equations

Eqs. (5.18) – (5.23) are solved simultaneously using Mathematica to find the constants of integration $(A_1, A_2, B_2, A_3, B_3, B_4)$ as given in Appendix - J.

#### 5.1.3.4 Manipulation of Constants of Integration

The denominator here are different than the denominator of constants that were solved in the Chapter 3, so they will be manipulated differently (see Appendix - K) and we get the relation.

$$\frac{1}{e^{4R\sqrt{\frac{s}{\alpha^{EC}}}}(1+K_{SI})(1+K_{SO})s-(1-K_{SI})(1-K_{SO})s}$$
$$=\frac{1}{s}\frac{e^{-4R\sqrt{\frac{s}{\alpha^{EC}}}}}{(1+K_{SI})(1+K_{SO})}\sum_{n=1}^{\infty}(h_{SI}h_{SO})^{n-1}\exp\left(-4nR\sqrt{\frac{s}{\alpha^{EC}}}\right) \quad (5.24)$$

where

$$h_{SI}=\frac{1-K_{SI}}{1+K_{SO}}\ |h_{SI}|<1$$
$$h_{SO}=\frac{1-K_{SO}}{1+K_{SO}}\ |h_{SO}|<1$$
$$K_{SI}=\frac{k^{EC}}{k^{SI}}\sqrt{\frac{\alpha^{SI}}{\alpha^{EC}}}$$
$$K_{SO}=\frac{k^{EC}}{k^{SO}}\sqrt{\frac{\alpha^{SO}}{\alpha^{EC}}}$$

Inserting the above relation (5.24) in constant of integrations given in Appendix - J and after further mathematical manipulation, and using the constants $A_1, A_2, B_2, A_3, B_3, B_4$ in Laplace solutions (5.14) – (5.17), we get

#### 5.1.3.5 Equations in Laplace Domain

$$W_{SI}(x,s)-\frac{T_{SI,i}}{s}=A_1\,e^{\sqrt{\frac{s}{\alpha^{SI}}}x}$$

$$\begin{aligned}W_{SI}(x,s)-\frac{T_{SI,i}}{s}&\\=\frac{K_{SI}}{1+K_{SI}}\Bigg\{&\frac{(T_{EC1,i}-T_{SI,i})\cdot h_{SO}}{s}\sum_{n=1}^{\infty}(h_{SI}h_{SO})^{n-1}\exp\left[-\left(-x-R+(4n-0)RK_{\alpha^{SI}}^{-1/2}\right)\sqrt{\frac{s}{\alpha^{SI}}}\right]\\&-\frac{(T_{EC1,i}-T_{EC2,i})\cdot h_{SO}}{s}\sum_{n=1}^{\infty}(h_{SI}h_{SO})^{n-1}\exp\left[-\left(-x-R+(4n-1)RK_{\alpha^{SI}}^{-1/2}\right)\sqrt{\frac{s}{\alpha^{SI}}}\right]\\&-\frac{2\,(T_{EC2,i}-T_{SO,i})}{(1+K_{SO})\,s}\sum_{n=1}^{\infty}(h_{SI}h_{SO})^{n-1}\exp\left[-\left(-x-R+(4n-2)RK_{SI}^{-1/2}\right)\sqrt{\frac{s}{\alpha^{SI}}}\right]\\&-\frac{T_{EC1,i}-T_{EC2,i}}{s}\sum_{n=1}^{\infty}(h_{SI}h_{SO})^{n-1}\exp\left[-\left(-x-R+(4n-3)RK_{\alpha^{SI}}^{-1/2}\right)\sqrt{\frac{s}{\alpha^{SI}}}\right]\\&+\frac{(T_{EC1,i}-T_{SI,i})}{s}\sum_{n=1}^{\infty}(h_{SI}h_{SO})^{n-1}\exp\left[-\left(-x-R+(4n-4)RK_{\alpha^{SI}}^{-1/2}\right)\sqrt{\frac{s}{\alpha^{SI}}}\right]\Bigg\}\end{aligned} \quad (5.25)$$

$K_{\alpha^{SI}}=\alpha^{EC}/\alpha^{SI}$ is relative thermal inertia of SI and EC1[144,145].

$$W_{EC1}(x,s) - \frac{T_{EC\ ,i}}{s} = A_2\, e^{\sqrt{\frac{s}{\alpha^{EC}}}x} + B_2\, e^{-\sqrt{\frac{s}{\alpha^{EC}}}x}$$

$$\begin{aligned}
W_{EC1}(x,s) - \frac{T_{EC1,i}}{s}
&= \frac{\left(T_{EC1,i} - T_{EC2,i}\right)\cdot\ h_{SI}h_{SO}}{2}\frac{1}{s}\sum_{n=1}^{\infty}(h_{SI}h_{SO})^{n-1}\exp\left(-\sqrt{\frac{s}{\alpha^{EC}}}\left((4n-0)R+x\right)\right)\\
&+\frac{1}{s}\sum_{n=1}^{\infty}(h_{SI}h_{SO})^{n-1}\left[\frac{h_{SO}}{1+K_{SI}}\left(T_{EC1,i}-T_{SI,i}\right)\exp\left(-\sqrt{\frac{s}{\alpha^{EC}}}\left((4n-1)R-x\right)\right)\right.\\
&\qquad\left.+\frac{h_{SI}}{1+K_{SO}}\left(T_{EC2,i}-T_{SO,i}\right)\exp\left(-\sqrt{\frac{s}{\alpha^{EC}}}\left((4n-1)R+x\right)\right)\right]\\
&-\frac{1}{2}\frac{1}{s}\sum_{n=1}^{\infty}(h_{SI}h_{SO})^{n-1}\left[h_{SO}\left(T_{EC1,i}-T_{EC2,i}\right)\exp\left(-\sqrt{\frac{s}{\alpha^{EC}}}\left((4n-2)R-x\right)\right)\right.\\
&\qquad\left.-h_{SI}\left(T_{EC\ ,i}-T_{EC\ ,i}\right)\exp\left(-\sqrt{\frac{s}{\alpha^{EC}}}\left((4n-2)R+x\right)\right)\right]\\
&-\frac{1}{s}\sum_{n=1}^{\infty}(h_{SI}h_{SO})^{n-1}\left[\frac{1}{1+K_{SO}}\left(T_{EC2,i}-T_{SO,i}\right)\exp\left(-\sqrt{\frac{s}{\alpha^{EC}}}\left((4n-3)R-x\right)\right)\right.\\
&\qquad\left.+\frac{1}{1+K_{SI}}\left(T_{EC\ ,i}-T_{SI,i}\right)\exp\left(-\sqrt{\frac{s}{\alpha^{EC}}}\left((4n-3)R+x\right)\right)\right]\\
&-\frac{\left(T_{EC1,i}-T_{EC\ ,i}\right)}{2}\frac{1}{s}\sum_{n=1}^{\infty}(h_{SI}h_{SO})^{n-1}\exp\left(-\sqrt{\frac{s}{\alpha^{EC}}}\left((4n-4)R-x\right)\right)
\end{aligned} \tag{5.26}$$

$$W_{EC2}(x,s) - \frac{T_{EC\ ,i}}{s} = A_3\, e^{\sqrt{\frac{s}{\alpha^{EC}}}x} + B_3\, e^{-\sqrt{\frac{s}{\alpha^{EC}}}x}$$

$$
\begin{aligned}
W_{EC2}(x,s)-\frac{T_{EC2,i}}{s} &= -\frac{\left(T_{EC1,i}-T_{EC2,i}\right)\cdot\ h_{SI}h_{SO}}{2}\frac{1}{s}\sum_{n=1}^{\infty}(h_{SI}h_{SO})^{n-1}\exp\left(-\sqrt{\frac{s}{\alpha^{EC}}}\left((4n-0)R-x\right)\right)\\
&+\frac{1}{s}\sum_{n=1}^{\infty}(h_{SI}h_{SO})^{n-1}\left[\frac{h_{SO}}{1+K_{SI}}\left(T_{EC1,i}-T_{SI,i}\right)\exp\left(-\sqrt{\frac{s}{\alpha^{EC}}}\left((4n-1)R-x\right)\right)\right.\\
&\left.+\frac{h_{SI}}{1+K_{SO}}\left(T_{EC2,i}-T_{SO,i}\right)\exp\left(-\sqrt{\frac{s}{\alpha^{EC}}}\left((4n-1)R+x\right)\right)\right]\\
&-\frac{1}{2s}\sum_{n=1}^{\infty}(h_{SI}h_{SO})^{n-1}\left[h_{SO}\left(T_{EC1,i}-T_{EC\ ,i}\right)\exp\left(-\sqrt{\frac{s}{\alpha^{EC}}}\left((4n-2)R-x\right)\right)\right.\\
&\left.-h_{SI}\left(T_{EC1,i}-T_{EC2,i}\right)\exp\left(-\sqrt{\frac{s}{\alpha^{EC}}}\left((4n-2)R+x\right)\right)\right]\\
&-\frac{1}{s}\sum_{n=1}^{\infty}(h_{SI}h_{SO})^{n-1}\left[\frac{1}{1+K_{SO}}\left(T_{EC2,i}-T_{SO,i}\right)\exp\left(-\sqrt{\frac{s}{\alpha^{EC}}}\left((4n-3)R-x\right)\right)\right.\\
&\left.+\frac{1}{1+K_{SI}}\left(T_{EC1,i}-T_{SI,i}\right)\exp\left(-\sqrt{\frac{s}{\alpha^{EC}}}\left((4n-3)R+x\right)\right)\right]\\
&+\frac{\left(T_{EC1,i}-T_{EC2,i}\right)}{2}\frac{1}{s}\sum_{n=1}^{\infty}(h_{SI}h_{SO})^{n-1}\exp\left(-\sqrt{\frac{s}{\alpha^{EC}}}\left((4n-4)R+x\right)\right)
\end{aligned}
\tag{5.27}
$$

$$
W_{SO}(x,s)-\frac{T_{SO,i}}{s}=B_4\,e^{-\sqrt{\frac{s}{\alpha^{SO}}}x}
$$

$$
\begin{aligned}
W_{SO}(x,s)-\frac{T_{SO,i}}{s}&\\
&=\frac{K_{SO}}{1+K_{SO}}\left\{\frac{\left(T_{EC2,i}-T_{SO,i}\right)\cdot h_{SI}}{s}\sum_{n=1}^{\infty}(h_{SI}h_{SO})^{n-1}\exp\left[-\left(x-R+(4n-0)RK_{\alpha^{SO}}^{-1/2}\right)\sqrt{\frac{s}{\alpha^{SO}}}\right]\right.\\
&+\frac{\left(T_{EC1,i}-T_{EC\ ,i}\right)\cdot h_{SI}}{s}\sum_{n=1}^{\infty}(h_{SI}h_{SO})^{n-1}\exp\left[-\left(x-R+(4n-1)RK_{\alpha^{SO}}^{-1/2}\right)\sqrt{\frac{s}{\alpha^{SO}}}\right]\\
&-\frac{2\left(T_{EC1,i}-T_{SI,i}\right)}{(1+K_{SI})\,s}\sum_{n=1}^{\infty}(h_{SI}h_{SO})^{n-1}\exp\left[-\left(x-R+(4n-2)RK_{\alpha^{SO}}^{-1/2}\right)\sqrt{\frac{s}{\alpha^{SO}}}\right]\\
&+\frac{T_{EC\ ,i}-T_{EC2,i}}{s}\sum_{n=1}^{\infty}(h_{SI}h_{SO})^{n-1}\exp\left[-\left(x-R+(4n-3)RK_{\alpha^{SO}}^{-1/2}\right)\sqrt{\frac{s}{\alpha^{SO}}}\right]\\
&\left.+\frac{\left(T_{EC2,i}-T_{SO,i}\right)}{s}\sum_{n=1}^{\infty}(h_{SI}h_{SO})^{n-1}\exp\left[-\left(x-R+(4n-4)RK_{\alpha^{SO}}^{-1/2}\right)\sqrt{\frac{s}{\alpha^{SO}}}\right]\right\}
\end{aligned}
\tag{5.28}
$$

$K_{\alpha^{SO}}=\alpha^{EC}/\alpha^{SO}$ is relative thermal inertia[144,145].

### 5.1.3.6 Inverse Laplace Transform of the System of Equations

The solution of the system of Eqs. (5.1) and (5.4) may be found by taking the inverse Laplace transform of Eq. (5.25) – (5.28) and the solution for temperature profiles in each body is given in Eqs. (5.29) – (5.32) as follows,

### 5.1.4 Temperature Profiles of the Bodies

## Temperature Profile of Sink (SI)

$$
\begin{aligned}
&T_{SI}(x,t) - T_{SI,i} \\
&= \frac{K_{SI}}{1+K_{SI}}\Bigg\{\left(T_{EC1,i} - T_{SI,i}\right) h_{SO} \sum_{n=1}^{\infty} (h_{SI}h_{SO})^{n-1} \operatorname{erfc}\frac{-x-R+(4n-0)K_{\alpha^{SI}}^{-1/2}R}{2\sqrt{\alpha^{SI}t}} \\
&\qquad - \left(T_{EC1,i} - T_{EC2,i}\right) h_{SO} \sum_{n=1}^{\infty} (h_{SI}h_{SO})^{n-1} \operatorname{erfc}\frac{-x-R+(4n-1)K_{\alpha^{SI}}^{-1/2}R}{2\sqrt{\alpha^{SI}t}} \\
&\qquad - \frac{2\left(T_{EC\ ,i} - T_{SO,i}\right)}{1+K_{SO}} \sum_{n=1}^{\infty} (h_{SI}h_{SO})^{n-1} \operatorname{erfc}\frac{-x-R+(4n-2)K_{\alpha^{SI}}^{-1/2}R}{2\sqrt{\alpha^{SI}t}} \\
&\qquad - \left(T_{EC\ ,i} - T_{EC2,i}\right) \sum_{n=1}^{\infty} (h_{SI}h_{SO})^{n-1} \operatorname{erfc}\frac{-x-R+(4n-3)K_{\alpha^{SI}}^{-1/2}R}{2\sqrt{\alpha^{SI}t}} \\
&\qquad + \left(T_{EC1,i} - T_{SI,i}\right) \sum_{n=1}^{\infty} (h_{SI}h_{SO})^{n-1} \operatorname{erfc}\frac{-x-R+(4n-4)K_{\alpha^{SI}}^{-1/2}R}{2\sqrt{\alpha^{SI}t}}\Bigg\}
\end{aligned}
\tag{5.29}
$$

## Temperature Profile of EC1

$$
\begin{aligned}
&T_{EC1}(x,t) - T_{EC1,i} \\
&= \frac{\left(T_{EC1,i} - T_{EC2,i}\right)h_{SI}h_{SO}}{2} \sum_{n=1}^{\infty} (h_{SI}h_{SO})^{n-1} \operatorname{erfc}\frac{(4n-0)R+x}{2\sqrt{\alpha^{EC}t}} \\
&\qquad + \sum_{n=1}^{\infty} (h_{SI}h_{SO})^{n-1}\left[\frac{h_{SO}}{1+K_{SI}}\left(T_{EC\ ,i} - T_{SI,i}\right)\operatorname{erfc}\frac{(4n-1)R-x}{2\sqrt{\alpha^{EC}t}} + \frac{h_{SI}}{1+K_{SO}}\left(T_{EC2,i} - T_{SO,i}\right)\operatorname{erfc}\frac{(4n-1)R+x}{2\sqrt{\alpha^{EC}t}}\right] \\
&\qquad - \frac{1}{2}\sum_{n=1}^{\infty} (h_{SI}h_{SO})^{n-1}\left[h_{SO}\left(T_{EC1,i} - T_{EC2,i}\right)\operatorname{erfc}\frac{(4n-2)R-x}{2\sqrt{\alpha^{EC}t}} - h_{SI}\left(T_{EC1,i} - T_{EC2,i}\right)\operatorname{erfc}\frac{(4n-2)R+x}{2\sqrt{\alpha^{EC}t}}\right] \\
&\qquad - \sum_{n=1}^{\infty} (h_{SI}h_{SO})^{n-1}\left[\frac{1}{1+K_{SO}}\left(T_{EC2,i} - T_{SO,i}\right)\operatorname{erfc}\frac{(4n-3)R-x}{2\sqrt{\alpha^{EC}t}} + \frac{1}{1+K_{SI}}\left(T_{EC1,i} - T_{SI,i}\right)\operatorname{erfc}\frac{(4n-3)R+x}{2\sqrt{\alpha^{EC}t}}\right] \\
&\qquad - \frac{\left(T_{EC1,i} - T_{EC2,i}\right)}{2} \sum_{n=1}^{\infty} (h_{SI}h_{SO})^{n-1} \operatorname{erfc}\frac{(4n-4)R-x}{2\sqrt{\alpha^{EC}t}}
\end{aligned}
\tag{5.30}
$$

## Temperature Profile of EC2

$$
\begin{aligned}
&T_{EC2}(x,t) - T_{EC2,i} \\
&= -\frac{\left(T_{EC1,i} - T_{EC2,i}\right)h_{SI}h_{SO}}{2} \sum_{n=1}^{\infty} (h_{SI}h_{SO})^{n-1} \operatorname{erfc}\frac{(4n-0)R-x}{2\sqrt{\alpha^{EC}t}} \\
&\qquad + \sum_{n=1}^{\infty} (h_{SI}h_{SO})^{n-1}\left[\frac{h_{SO}}{1+K_{SI}}\left(T_{EC1,i} - T_{SI,i}\right)\operatorname{erfc}\frac{(4n-1)R-x}{2\sqrt{\alpha^{EC}t}} + \frac{h_{SI}}{1+K_{SO}}\left(T_{EC2,i} - T_{SO,i}\right)\operatorname{erfc}\frac{(4n-1)R+x}{2\sqrt{\alpha^{EC}t}}\right] \\
&\qquad - \frac{1}{2}\sum_{n=1}^{\infty} (h_{SI}h_{SO})^{n-1}\left[h_{SO}\left(T_{EC1,i} - T_{EC2,i}\right)\operatorname{erfc}\frac{(4n-2)R-x}{2\sqrt{\alpha^{EC}t}} - h_{SI}\left(T_{EC1,i} - T_{EC\ ,i}\right)\operatorname{erfc}\frac{(4n-2)R+x}{2\sqrt{\alpha^{EC}t}}\right] \\
&\qquad - \sum_{n=1}^{\infty} (h_{SI}h_{SO})^{n-1}\left[\frac{1}{1+K_{SO}}\left(T_{EC\ ,i} - T_{SO,i}\right)\operatorname{erfc}\frac{(4n-3)R-x}{2\sqrt{\alpha^{EC}t}} + \frac{1}{1+K_{SI}}\left(T_{EC\ ,i} - T_{SI,i}\right)\operatorname{erfc}\frac{(4n-3)R+x}{2\sqrt{\alpha^{EC}t}}\right] \\
&\qquad + \frac{\left(T_{EC\ ,i} - T_{EC\ ,i}\right)}{2} \sum_{n=1}^{\infty} (h_{SI}h_{SO})^{n-1} \operatorname{erfc}\frac{(4n-4)R+x}{2\sqrt{\alpha^{EC}t}}
\end{aligned}
\tag{5.31}
$$

**Temperature Profile of Source (SO)**

$$
\begin{aligned}
&T_{SO}(x,t) - T_{SO,i} \\
&= \frac{K_{SO}}{1+K_{SO}}\Bigg\{\left(T_{EC\ ,i} - T_{SO,i}\right) h_{SI} \sum_{n=1}^{\infty} (h_{SI}h_{SO})^{n-1} \operatorname{erfc} \frac{x - R + (4n-0)K_{\alpha^{SO}}^{-1/2} R}{2\sqrt{\alpha^{SO} t}} \\
&\qquad + \left(T_{EC1,i} - T_{EC2,i}\right) h_{SI} \sum_{n=1}^{\infty} (h_{SI}h_{SO})^{n-1} \operatorname{erfc} \frac{x - R + (4n-1)K_{\alpha^{SO}}^{-1/2} R}{2\sqrt{\alpha^{SO} t}} \\
&\qquad - \frac{2\left(T_{EC1,i} - T_{SI,i}\right)}{1+K_{SI}} \sum_{n=1}^{\infty} (h_{SI}h_{SO})^{n-1} \operatorname{erfc} \frac{x - R + (4n-2)K_{\alpha^{SO}}^{-1/2} R}{2\sqrt{\alpha^{SO} t}} \\
&\qquad + \left(T_{EC\ ,i} - T_{EC2,i}\right) \sum_{n=1}^{\infty} (h_{SI}h_{SO})^{n-1} \operatorname{erfc} \frac{x - R + (4n-3)K_{\alpha^{SO}}^{-1/2} R}{2\sqrt{\alpha^{SO} t}} \\
&\qquad + \left(T_{EC2,i} - T_{SO,i}\right) \sum_{n=1}^{\infty} (h_{SI}h_{SO})^{n-1} \operatorname{erfc} \frac{x - R + (4n-4)K_{\alpha^{SO}}^{-1/2} R}{2\sqrt{\alpha^{SO} t}}\Bigg\}
\end{aligned}
\tag{5.32}
$$

### 5.1.5 Heat Flux through the Interfaces

The conductive heat flux can be written by Fourier law in 1-D as follows,

$$q = -k \frac{\partial T}{\partial x}$$

The temperature gradients are determined used the relation

$$
\begin{aligned}
\frac{\partial}{\partial x}\left[\operatorname{erfc}\left(\frac{x}{2\sqrt{\alpha t}}\right)\right] &= -\frac{1}{\sqrt{\pi \alpha t}} \exp\left(-\frac{x^2}{4\alpha t}\right) \\
\frac{\partial}{\partial x}\left[\operatorname{erfc}\left(\frac{-x}{2\sqrt{\alpha t}}\right)\right] &= \frac{1}{\sqrt{\pi \alpha t}} \exp\left(-\frac{x^2}{4\alpha t}\right)
\end{aligned}
\tag{5.33}
$$

**Heat Flux through the Interface SI|EC1 at $x = -R$**

$$q_{SI|EC} = -k^{SI} \left.\frac{\partial T_{SI}(x,t)}{\partial x}\right|_{x=-R} = -k^{EC} \left.\frac{\partial T_{EC1}(x,t)}{\partial x}\right|_{x=-R}$$

Differentiating Eq. **(5.29)**, substituting in above equation and putting $x = -R$, we get

$$q_{SI|EC1}(t) = -k^{SI}\frac{\partial T_{SI}(x,t)}{\partial x}\bigg|_{x=-R}$$

$$= -\frac{k^{SI}}{\sqrt{\pi\alpha^{SI}t}}\frac{K_{SI}}{1+K_{SI}}$$

$$\times\Bigg\{\left(T_{EC1,i}-T_{SI,i}\right)h_{SO}\sum_{n=1}^{\infty}(h_{SI}h_{SO})^{n-1}\exp\left(-\left[\frac{(4n-0)R}{2\sqrt{\alpha^{EC}t}}\right]^2\right)$$

$$-\left(T_{EC1,i}-T_{EC\ ,i}\right)h_{SO}\sum_{n=1}^{\infty}(h_{SI}h_{SO})^{n-1}\exp\left(-\left[\frac{(4n-1)R}{2\sqrt{\alpha^{EC}t}}\right]^2\right) \tag{5.34}$$

$$-\frac{2\left(T_{EC2,i}-T_{SO,i}\right)}{1+K_{SO}}\sum_{n=1}^{\infty}(h_{SI}h_{SO})^{n-1}\exp\left(-\left[\frac{(4n-2)R}{2\sqrt{\alpha^{EC}t}}\right]^2\right)$$

$$-\left(T_{EC\ ,i}-T_{EC\ ,i}\right)\sum_{n=1}^{\infty}(h_{SI}h_{SO})^{n-1}\exp\left(-\left[\frac{(4n-3)R}{2\sqrt{\alpha^{EC}t}}\right]^2\right)$$

$$+\left(T_{EC1,i}-T_{SI,i}\right)\sum_{n=1}^{\infty}(h_{SI}h_{SO})^{n-1}\exp\left(-\left[\frac{(4n-4)R}{2\sqrt{\alpha^{EC}t}}\right]^2\right)\Bigg\}$$

**Heat Flux through the Interface EC1|EC2 at *x = 0***

$$q_{EC1|EC2} = -k^{EC}\frac{\partial T_{EC}\ (x,t)}{\partial x}\bigg|_{x=0} = -k^{EC}\frac{\partial T_{EC}\ (x,t)}{\partial x}\bigg|_{x=0}$$

Differentiating Eq. **(5.30)** and substituting in above equation., and using $x = 0$

$$q_{EC1|EC2}(t) = -k^{EC}\frac{\partial T_{EC2}(x,t)}{\partial x}\bigg|_{x=0}$$

$$= -\frac{k^{EC}}{\sqrt{\pi\alpha^{EC}t}}\Bigg\{-\frac{\left(T_{EC1,i}-T_{EC2,i}\right)}{2}h_{SI}h_{SO}\sum_{n=1}^{\infty}(h_{SI}h_{SO})^{n-1}\exp\left(-\left[\frac{(4n-0)R}{2\sqrt{\alpha^{EC}t}}\right]^2\right)$$

$$+\sum_{n=1}^{\infty}(h_{SI}h_{SO})^{n-1}\left[\frac{h_{SO}}{1+K_{SI}}\left(T_{EC\ ,i}-T_{SI,i}\right)\exp\left(-\left[\frac{(4n-1)R}{2\sqrt{\alpha^{EC}t}}\right]^2\right)\right.$$

$$\left.-\frac{h_{SI}}{1+K_{SO}}\left(T_{EC2,i}-T_{SO,i}\right)\exp\left(-\left[\frac{(4n-1)R}{2\sqrt{\alpha^{EC}t}}\right]^2\right)\right]$$

$$-\frac{1}{2}\sum_{n=1}^{\infty}(h_{SI}h_{SO})^{n-1}\left[h_{SO}\left(T_{EC1,i}-T_{EC2,i}\right)\exp\left(-\left[\frac{(4n-2)R}{2\sqrt{\alpha^{EC}t}}\right]^2\right)\right. \tag{5.35}$$

$$\left.+h_{SI}\left(T_{EC\ ,i}-T_{EC\ ,i}\right)\exp\left(-\left[\frac{(4n-2)R}{2\sqrt{\alpha^{EC}t}}\right]^2\right)\right]$$

$$-\sum_{n=1}^{\infty}(h_{SI}h_{SO})^{n-1}\left[\frac{1}{1+K_{SO}}\left(T_{EC\ ,i}-T_{SO,i}\right)\exp\left(-\left[\frac{(4n-3)R}{2\sqrt{\alpha^{EC}t}}\right]^2\right)\right.$$

$$\left.-\frac{1}{1+K_{SI}}\left(T_{EC1,i}-T_{SI,i}\right)\exp\left(-\left[\frac{(4n-3)R}{2\sqrt{\alpha^{EC}t}}\right]^2\right)\right]$$

$$-\frac{\left(T_{EC\ ,i}-T_{EC2,i}\right)}{2}\sum_{n=1}^{\infty}(h_{SI}h_{SO})^{n-1}\exp\left(-\left[\frac{(4n-4)R}{2\sqrt{\alpha^{EC}t}}\right]^2\right)\Bigg\}$$

**Heat Flux through the Interface EC2|SO at *x = R***

$$q_{EC\ |SO} = -k^{EC}\left.\frac{\partial T_{EC2}(x,t)}{\partial x}\right|_{x=R} = -k^{SO}\left.\frac{\partial T_{SO}(x,t)}{\partial x}\right|_{x=R}$$

Differentiating Eq. **(5.32)** and substituting in above equation, and using $x = R$

$$q_{EC2|SO}(t) = -k^{SO}\left.\frac{\partial T_{SO}(x,t)}{\partial x}\right|_{x=R}$$

$$= \frac{k^{SO}}{\sqrt{\pi\alpha^{SO}t}}\frac{K_{SO}}{1+K_{SO}}$$

$$\times\left\{\left(T_{EC2,i} - T_{SO,i}\right)h_{SI}\sum_{n=1}^{\infty}(h_{SI}h_{SO})^{n-1}\exp\left(-\left[\frac{(4n-0)R}{2\sqrt{\alpha^{EC}t}}\right]^2\right)\right.$$

$$+\left(T_{EC1,i} - T_{EC2,i}\right)h_{SI}\sum_{n=1}^{\infty}(h_{SI}h_{SO})^{n-1}\exp\left(-\left[\frac{(4n-1)R}{2\sqrt{\alpha^{EC}t}}\right]^2\right) \quad (5.36)$$

$$-\frac{2\left(T_{EC\ ,i} - T_{SI,i}\right)}{1+K_{SI}}\sum_{n=1}^{\infty}(h_{SI}h_{SO})^{n-1}\exp\left(-\left[\frac{(4n-2)R}{2\sqrt{\alpha^{EC}t}}\right]^2\right)$$

$$+\left(T_{EC\ ,i} - T_{EC\ ,i}\right)\sum_{n=1}^{\infty}(h_{SI}h_{SO})^{n-1}\exp\left(-\left[\frac{(4n-3)R}{2\sqrt{\alpha^{EC}t}}\right]^2\right)$$

$$\left.+\left(T_{EC2,i} - T_{SO,i}\right)\sum_{n=1}^{\infty}(h_{SI}h_{SO})^{n-1}\exp\left(-\left[\frac{(4n-4)R}{2\sqrt{\alpha^{EC}t}}\right]^2\right)\right\}$$

### 5.1.6 Heat Energy Transfer through the Interfaces

The total amount of heat transfer per unit area through the interface may be determined by integrating heat flux over time as follows,

$$Q = \int_0^t q\,dt \quad (5.37)$$

## 5.2 Estimating the Infinite Series

For numerical calculations, the upper limit $n = \infty$ in Eqs.(5.34) – (5.36) may be replaced with $n = N$, where N needs to be determined here again (see SECTION 3.3) as now two different values of $h$ (i.e. $h_{SI}$ and $h_{SO}$) are involved. The procedure and assumptions are, however, same as adopted before in SECTION 3.3.

The heat flux solutions obtained in Eqs. (5.34) – (5.36) have series with infinite number of terms, which cannot be directly used for any numerical calculation. Therefore, it is important to find the summation of each series to a reasonable approximation for any numerical calculation. All the

series in the solution for heat fluxes can be represented by the series $S_n(x,t)$ (n=1,2,3…) or $S_{n'}(x,t)$ ($n'=1,2,3\ldots$) (i.e., n'= n – 1 or n = n' + 1) as:

$$S_n(x,t) = (h_{SI}h_{SO})^{n-1} \exp\left(-\left[\frac{(4n-m)R}{2\sqrt{\alpha^{EC}t}}\right]^2\right) \tag{5.38}$$

$$S_{n'}(x,t) = (h_{SI}h_{SO})^{n'} \exp\left(-\left[\frac{(4n'+4-m)R}{2\sqrt{\alpha^{EC}t}}\right]^2\right) \tag{5.39}$$

where m = 0, 1, 2, 3, 4, respectively. Based on the nature of the problem and the physics, the sum of the series shown in Eqs. (5.38) and (5.39) should be a finite number. It is also found that

$$\begin{aligned}
\frac{S_{n+2}}{S_{n+1}} &= \frac{(h_{SI}h_{SO})^{n+1} \exp\left(-\left[\frac{(4(n+2)-m)R}{2\sqrt{\alpha^{EC}t}}\right]^2\right)}{(h_{SI}h_{SO})^{n} \exp\left(-\left[\frac{(4(n+1)-m)R}{2\sqrt{\alpha^{EC}t}}\right]^2\right)} \\
&= (h_{SI}h_{SO}) \exp\left(-\left[\frac{(4n-m)R+8R}{2\sqrt{\alpha^{EC}t}}\right]^2 + \left[\frac{(4n-m)R+4R}{2\sqrt{\alpha^{EC}t}}\right]^2\right) \\
&= (h_{SI}h_{SO}) \exp\left(-\frac{48R^2+8(4n-m)R^2}{4\alpha^{EC}t}\right) \\
&= (h_{SI}h_{SO}) \exp\left(-\frac{12R^2-2mR^2}{\alpha^{EC}t} - \frac{8R^2}{\alpha^{EC}t}n\right)
\end{aligned}$$

Therefore, it can be simplified as:

$$\frac{S_{n+2}}{S_{n+1}} = h_{SI}h_{SO}B \exp(-A \cdot n) \tag{5.40}$$

where $A = \frac{8R^2}{\alpha^{EC}t} > 0$ and $B = \exp\left(-\frac{(12-2m)R^2}{\alpha^{EC}t}\right) < 1$ are constants that depend on the device (i.e., $R$ and $\alpha^{EC}$) and time ($t$). As mentioned in SECTION 5.1.3.4, $|h_{SI}| < 1$ and $|h_{SO}| < 1$, one can get from Eq. (5.40) that $|S_{n+2}/S_{n+1}| < 1$ and, more importantly, $|S_{n+2}/S_{n+1}|$ decreases with increasing $n$, which means that these series are convergent. That is, there should be a sufficiently

large integer *N* such that the subsequent terms have no significant effect on the overall summation value. That is,

$$\begin{aligned}\sum_{n=1}^{\infty} S_n(x,t) &= \sum_{n=1}^{N} S_n(x,t) + \sum_{n=N+1}^{\infty} S_n(x,t) \\ &= \sum_{n=1}^{N} S_n(x,t) + \Delta \\ &\cong \sum_{n=1}^{N} S_n(x,t)\end{aligned} \tag{5.41}$$

where Δ is a small number that should be much smaller than the summation of the series or that is very close to zero (either positive or negative). To determine the value of Δ, we can set $|\Delta| = |S_1(x,t)|\,\delta$, where $S_1(x,t)$ (>0) is the value of the series' first term and $\delta$ ($0 < \delta \ll 1$) is the control of the approximate calculation using Eq. (5.41). The smaller is the δ, the better is the approximation using Eq. (23). That is, as long as δ is smaller enough, |Δ| can be ignored for the calculation of series' summation. Using Eq. (5.39), the Δ can be manipulated as follows,

$$\begin{aligned}\Delta &= \sum_{n'=N}^{\infty} S_{n'}(x,t) \\ &= \sum_{n'=N}^{\infty} (h_{SI}h_{SO})^{n'} \exp\left(-\left[\frac{4R}{2\sqrt{\alpha^{EC}t}}n' + \frac{(4-m)R}{2\sqrt{\alpha^{EC}t}}\right]^2\right) \\ &= \sum_{n'=N}^{\infty} (h_{SI}h_{SO})^{n'} \exp(-[an'+b]^2) \\ &= \sum_{n'=N}^{\infty} (h_{SI}h_{SO})^{n'} \exp\left(-a^2 n'^2\right) \exp(-2abn') \exp(-b^2)\end{aligned}$$

where $a = 4R/2\sqrt{\alpha^{EC}t} > 0$ & $b = (4-m)R/2\sqrt{\alpha^{EC}t} \geq 0$. Considering that the value of $h_{SI}h_{SO}$ can be positive or negative as defined in SECTION 5.1.3.4, the calculation of Δ is replaced by the calculation of |Δ|. That is, as long as |Δ| is small enough, Eq. (5.41) can be used to calculate the summation of a series. Considering that $n'^2 \geq 3n'$ when $n' \geq 3$, we can get:

$$
\begin{aligned}
|\Delta| &= \left| \sum_{n'=N}^{\infty} (h_{SI} h_{SO})^{n'} \exp\left(-a^2 n'^2\right) \exp(-2abn') \exp(-b^2) \right| \\
&\leq \left| \sum_{n'=N}^{\infty} (h_{SI} h_{SO})^{n'} \exp(-3a^2 n') \exp(-2abn') \exp(-b^2) \right| \\
&= \left| C \sum_{n'=N}^{\infty} (h_{SI} h_{SO} \exp(-\gamma))^{n'} \right|
\end{aligned} \tag{5.42}
$$

where $C = \exp(-b^2) > 0$, $\gamma = 3a^2 + 2ab > 0$, and $N \geq 4$. For the series, $(h_{SI} h_{SO} \exp(-\gamma))^{n'}$, it is a geometric progression with $|h_{SI} h_{SO} \exp(-\gamma)| < 1$ since $|h_{SO}| < 1$, $|h_{SI}| < 1$, and $\exp(-\gamma) < 1$. Therefore,

$$
\sum_{n'=N}^{\infty} (h_{SI} h_{SO} \exp(-\gamma))^{n'} = \frac{(h_{SI} h_{SO})^N \exp(-\gamma N)}{1 - h_{SI} h_{SO} \exp(-\gamma)}
$$

Now, Eq. (5.42) can be written as

$$
\begin{aligned}
|\Delta| &\leq \left| C \frac{(h_{SI} h_{SO})^N \exp(-\gamma N)}{1 - h_{SI} h_{SO} \exp(-\gamma)} \right| \\
&= C \frac{(|h_{SI} h_{SO}|)^N \exp(-\gamma N)}{1 - h_{SI} h_{SO} \exp(-\gamma)}
\end{aligned}
$$

Now, we can set

$$
C \frac{(|h_{SI} h_{SO}|)^N \exp(-\gamma N)}{1 - h_{SI} h_{SO} \exp(-\gamma)} = S_1(x,t) \cdot \delta
$$

That is,

$$
\Delta \leq C \frac{(|h_{SI} h_{SO}|)^N \exp(-\gamma N)}{1 - h_{SI} h_{SO} \exp(-\gamma)} = S_1(x,t) \cdot \delta
$$

Or,

$$
\Delta < \exp(-b^2) \frac{(|h_{SI} h_{SO}|)^N \exp(-\gamma N)}{1 - h_{SI} h_{SO} \exp(-\gamma)} = \delta \cdot \exp(-[a_1]^2)
$$

where $a_1 = (4 - m)R/2\sqrt{\alpha^{EC} t} = b$ so that

$$(|h_{SI}h_{SO}|)^N \exp(-\gamma N) == \delta \cdot [1 - h_{SI}h_{SO} \exp(-\gamma)] \tag{5.43}$$

Therefore, the N (≥ 4) can be written as:

$$N = \frac{-\ln \delta - \ln(1 - h_{SI}h_{SO} \exp(-\gamma))}{\gamma - \ln(|h_{SI}h_{SO}|)} \tag{5.44}$$

Where $\gamma = 3a^2 = 12R^2/(\alpha^{EC}t)$. Eq. (5.45) can be used to determine the *N*.

From Eq.(5.44), one can find that if $|h_{SI}h_{SO}| \to 1$ and $\gamma \to \infty$ (i.e., either R is very big or t is very small), $N \to 0$. In this case, the sum of first four terms of the series (i.e., *N=4*) shown in Eq. (5.41) can be used as the sum of the series. On the other side, if $|h_{SI}h_{SO}| \to 0$, the $N \to 0$ for all values of $\gamma$. In this case, again the sum of only first four terms of the series (i.e., *N=4*) shown in Eq. (5.41) can be used as the sum of the series. For a constant $|h_{SI}h_{SO}|$, the *N* decreases as the $\gamma$ increases. Typical value of $|h_{SI}|$ and $|h_{SI}|$ for ceramics as ECM and metals for end materials is 0.5 – 0.9. As long as the $\gamma$ is more than 3 (i.e., $4R^2 > \alpha^c t$), the *N* is less than 4 for the δ being $10^{-5}$ or bigger. Again, in this case, the *N* = 4 can be used for the calculation of the series.

## 5.3 Application of Analytical Solution on Real Scenarios

In most of the ECE-based devices reported in literature, heat is absorbed from the source during depolarization by thermal coupling of the ECM with the source. In that case, the one side of the ECM is coupled with source while on the other side, there is air or some other material like heat switch, etc. Similarly, during polarization, the ECM rejects heat to the sink by thermal coupling with sink and now on the other side of ECM is air/some other material. This scenario may be observed in Figure 1.44. This EC device has been prototyped and its experimental observations have been reported[13]. This scenario has been simulated as a case study using our analytical solution to determine the temperature profiles and heat fluxes through interface in both absorption and rejection of heat steps based on the information provided in the article. It is discussed that how this analytical solution may be used for the determination of relaxation time, temperature profiles and heat fluxes in this already reported device. The analytical solution discussed above has been implemented in the MATLAB to find the simulation results of heat fluxes and temperature profiles.

### 5.3.1 Case Study of a Device

An electrostatic actuation based EC cooler (already discussed in section 1.5.2.2) has used PVDF elements as ECM and two aluminum blocks that act as source and sink in between ECM actuates and makes alternative thermal coupling to absorb and reject heat respectively. It may be noticed that in this step shown in Figure 5.2 it is absorbing heat from the source during its depolarization phase. Heat is transferring from AL block and on the other side, there is air that separates ECM from the sink. This situation has been simulated in MATLAB code using the analytical solution discussed above. In the heat absorption step, we may use the following inputs in our solution to find the temperature profiles and heat fluxes through the PVDF|AL interface in both absorption and rejection steps.

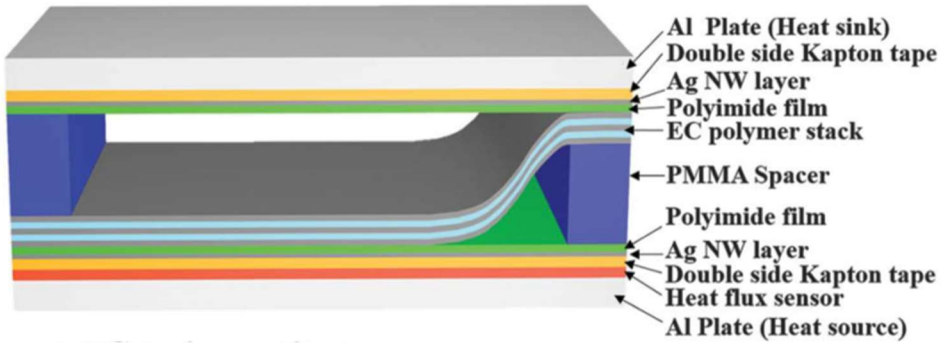


**Figure 5.2 An electrostatic actuation based EC cooler: ECM is PVDF and sink/source are AL blocks**

#### 5.3.1.1 Parameters to be Used in the Simulation

The ECM is PVDF (6mm) and Aluminum plates have been used as sink and source. The following initial conditions have been used in the heat absorption step.

$$T_{Air}(x,0) = T_{Air,i}$$

$$T_{EC}\ (x,0) = T_{EC}\ (x,0) = T_{EC\ ,i} = T_{EC\ ,i} \tag{5.45}$$

$$T_{SO}(x,0) = T_{SO,i}$$

Using the above ICs, our system convers into three body system. As it has already been mentioned that the analytical solution is much flexible to be molded depending on the situation and may be used to simulate most of the EC-based devices reported in literature.

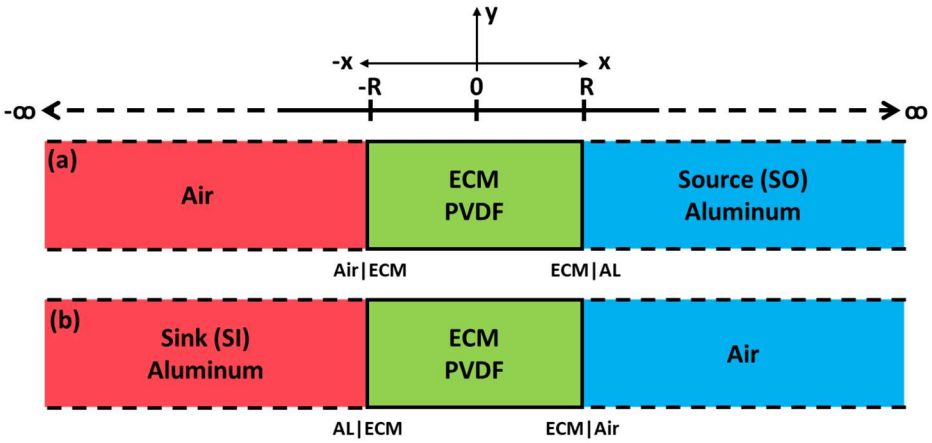


**Figure 5.3 Schematic diagram for working principle of EC cooler shown in Figure 5.2, (a). Heat absorption, (b). Heat rejection**

### 5.3.1.2 Temperature Profiles and Heat Flux

Given the data available in the article[13], the temperature profiles for the absorption of the heat step, determined using the analytical solution, are shown in Figure 5.5. The frequency of the heating and cooling cycles is 0.06 Hz (time period = 16.67 s). The thickness of the ECM (PVDF) along with electrodes (60 μm negligible) is 6mm.

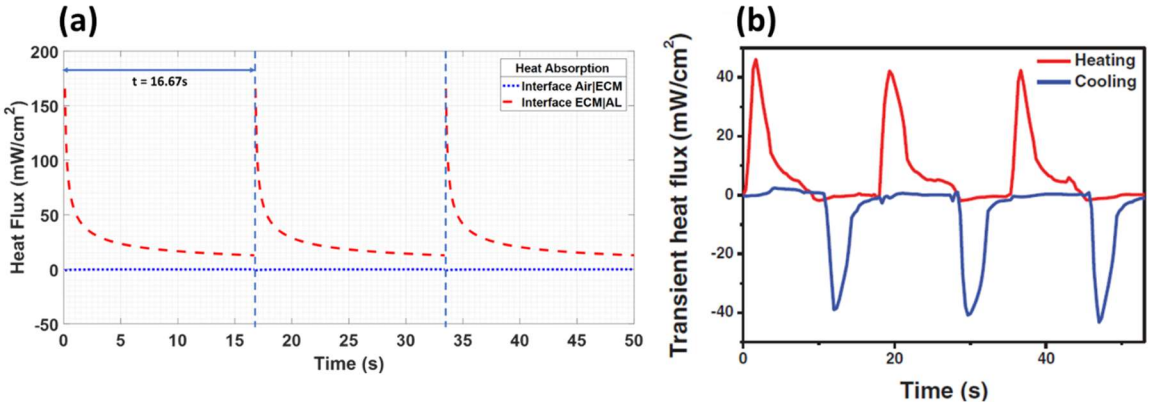


**Figure 5.4 Heat flux through ECM|SO interface for ΔT = 1.3 °C at 50MV/m[13] taking PVDF (thickness 6mm) as ECM and AL as source at frequency (0.06 Hz); (a). Simulation using analytical solution, (b). Experimental results[13]**

It may be inferred from the above temperature profile that for the time period reported in the article, the ECM has not come to the equilibrium to the Source and a small amount of energy has transferred, that might be the reason for a small efficiency $COP/COP_S = 0.06$[13]. Figure 5.4 shows

the comparison between the heat flux ($W/m^2$) deduced from the analytical solution and the experimentally measured heat flux ($mW/cm^2$) reported. A complete agreement of heat flux values of analytical solution and experimental results (notice the units; 1 $mW/cm^2$ =10$W/m^2$) may be noticed, for instant at about 1 sec the heat flux is about 500 $W/m^2$ and it decreases gradually. The negative heat flux shows that heat is moving in the negative direction (i.e. from source to ECM) as shown in Figure 5.3 (a). The low initial heat flux values in the experimentally reported heat flux may be due to the slow response of the heat flux meter, and in addition there are other parts involved in the device that have not been taken into account in the analytical solution. Also the convective/radiation losses and finite thermal resistance of the interface have not been considered in the analytical solution. Analytical solution has been solved on ideal conditions of perfect thermal interface with no heat losses due to radiation and convection from the lateral surfaces.

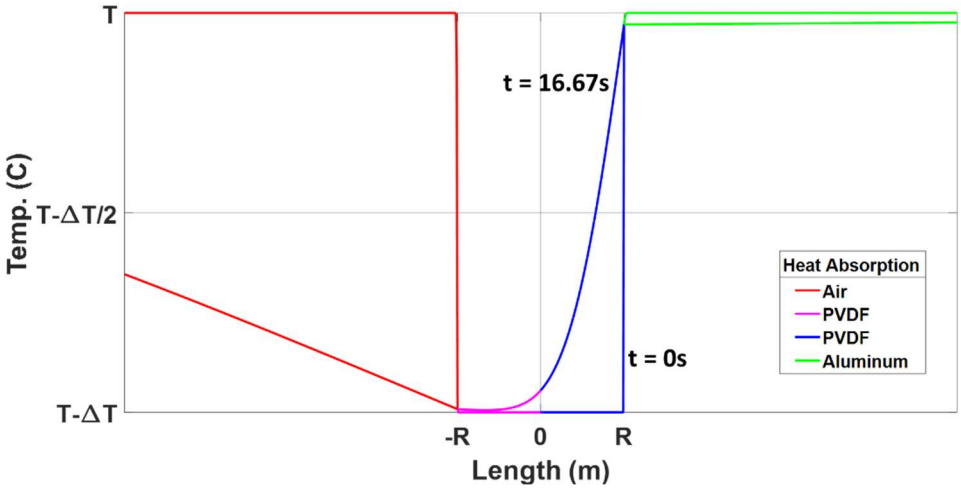


**Figure 5.5 Heat absorption for PVDF as ECM, AL as source for f = 0.06 Hz (using analytical solution)**

From the information given in the article, the absorption time is about 17 sec (f = 0.06 Hz) and after that the ECM is decoupled from the source and is coupled thermally with the sink to reject the heat under the polarization of the ECM. At that time, the expected temperature profile of the ECM is shown in Figure 5.5 determined from the analytical solution using the thermal properties of PVDF and Aluminum given in Appendix - D. It may be inferred that a small amount of energy has been extracted from source (Al block) as ECM is not in complete thermal equilibrium with source. Moreover, there is a temperature gradient in ECM, so after few thermal cycles, a thermal gradient will establish inside the ECM and further transfer of heat from the source to sink will stop.

To achieve high performance, the maximum amount of energy needs to be transferred from source. For this purpose, a simulation has been run on MATLAB code based on analytical solution for the extended time periods. The temperature profile evolution with the time has been shown in Figure 5.6 and the heat flux has been determined as shown in Figure 5.7. It may be noticed from the temperature profile that longer times are required to bring the ECM in equilibrium with source for high energy absorption in one cycle. It will increase the efficiency of the device. On the other hand, it will decrease the cooling power as longer time periods (low cyclic frequency) are required to complete one thermal cycle.

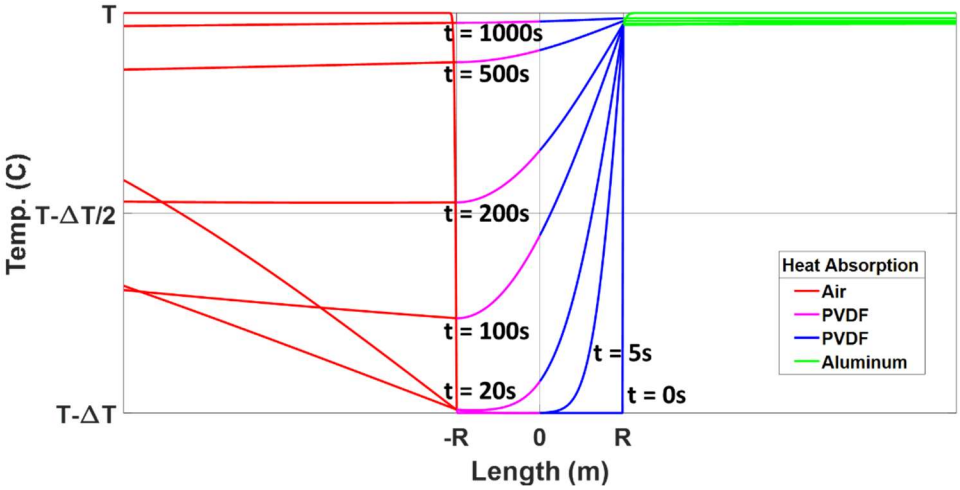


**Figure 5.6 Temperature profile of EC cooler for extended times to absorb more heat energy from source**

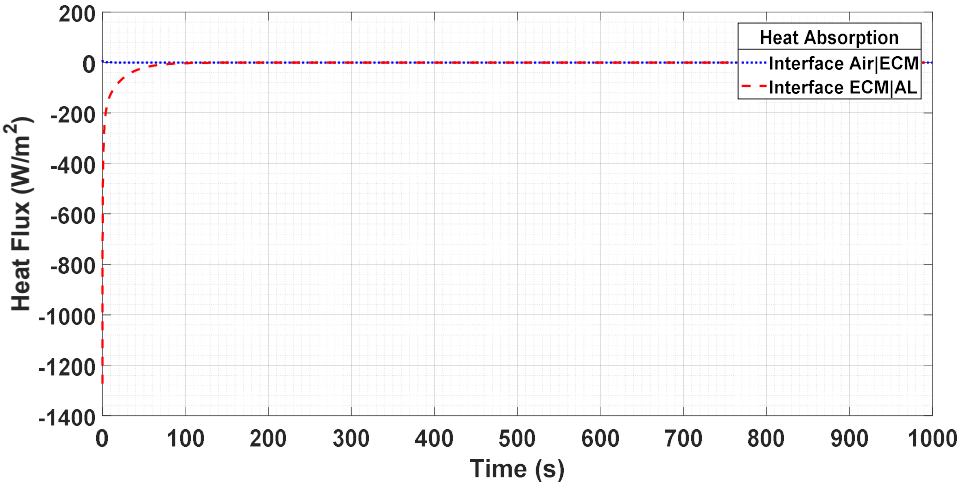


**Figure 5.7 Heat flux through the interfaces during heat absorption from the source**

It may also be noticed that heat through the interface Air|ECM is negligibly small as it is quite logical from experimental point of view and has been discussed in Chapter 4 in detail.

Now let us implement this device based on the two-layered idea given in this research. In that case, the sink will be brough in thermal contact with the ECM to achieve the directional heat flow with complete silent operation (No moving parts) as discussed in Chapter 4. Now the model shown in Figure 5.3(a) – (b) will transform to the model shown in Figure 5.8.

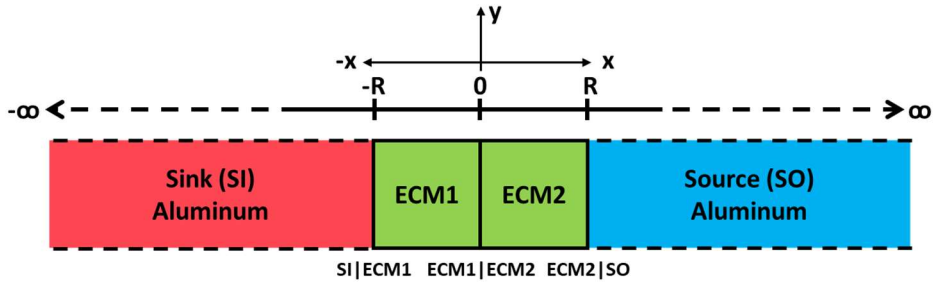


**Figure 5.8 Modification of device shown in Figure 5.3 to two-layered model**

The temperature profile of the ECM is shown in Figure 5.9 and as there is a big mismatch between thermal properties of PVDF and Aluminum, that is very low contacting coefficient (i.e. $K_\varepsilon = 0.03$), so there is large temperature gradient for heat to transfer from Source to ECM2 and from ECM1 to sink in the same step (i.e. Step-I). Comparing Figure 5.7 and Figure 5.9, it can be clearly noticed that in the two layered design, it took almost 10 times less time for ECM bodies to come to the thermal equilibrium, which will increase its cooling power. Two layered model will have however, less efficiency as it will absorb a maximum of 50% energy from the source, the rest heat will be mutually exchanged between ECM1 and ECM2. System given in Figure 5.3 will have one more step to reject heat to sink, whereas this model shown in Figure 5.8 needs two more steps (Step-II and Step-III) to recover it for the next cycle.

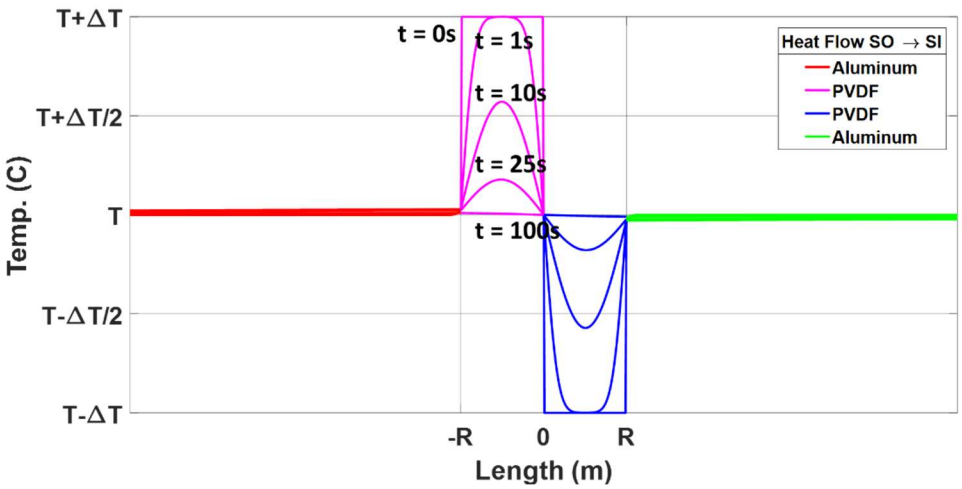


**Figure 5.9 Temperature profile showing the quick relaxation of ECMs in two-layered heat pump as compared to profile shown in Figure 5.6**

### 5.3.2 Implementing the Analytical Solution in Thin Film Characterization

As it is discussed that the direct measurement of the temperature change in thin films is a big challenge as due to less thermal mass, the substrate acts as a thermal anchor and the thin film comes to thermal equilibrium with substrate very quickly and the ECE is difficult to measure with accuracy during this short interval of time. Thermal devices like thermocouples and thermistors are difficult to attach, so infrared cameras are currently used to measure the temperature change, but they have their own limitations of response time to measure the temperature change quickly before the thin film comes to thermal equilibrium. This analytical solution determined in this chapter may be used to determine the heat flux through the substrate|thin-film interface, and the internal temperature profile of the thin film as a function of space (1D) and time. This information can help in the accurate measurements of ΔT upon the application/ removal of electric field on the EC thin films. As it has already been mentioned that the solution is flexible enough to be molded on the real time situations, so the model may be changed to three body system as it is typical of thin film measurements as shown in Figure 5.10.

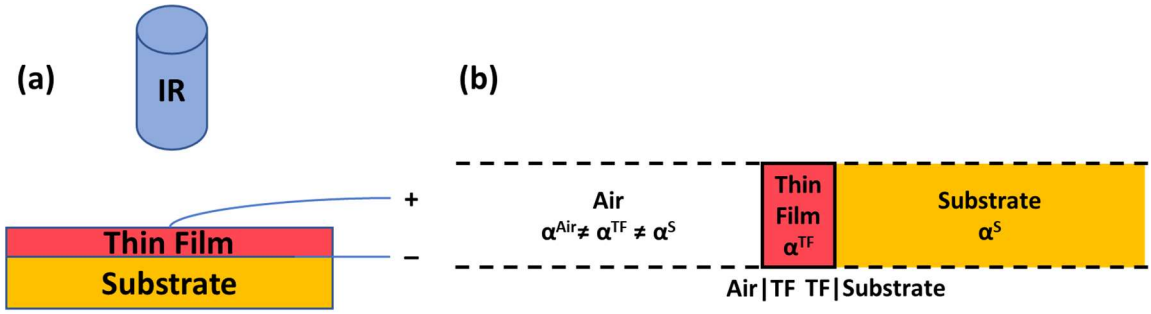


**Figure 5.10 (a) Typical arrangements of direct ECE measurement in thin film by infrared (IR) camera, (b). Physical model of thin film measurements**

The analytical solution is based on the perfect interface (no thermal resistance), when it is used for real applications, the imperfectness of interface will affect the results. Additionally, the piezoelectric effect of ECM was not considered. But all ECMs should have piezoelectric effect. Therefore, the strain/stress induced during the EC operation may results in the change in materials properties since some of these properties are dependent on the mechanical condition.

## 5.4 Concluding Remarks

We may conclude that the analytical solution presented in this chapter offers a great flexibility in choosing ECMs, sink/source materials, initial conditions and working principle to absorb and reject heat either by solid-solid contact or by circulating fluids. This analytical solution will be a key to the thermal analysis of the future novel ideas of the practical devices and can be used to find the relaxation time, temperature profiles and heat fluxes in the system. This solution is a quick tool to optimize the design parameters before manufacturing the prototype. The analytical approach adopted in this research is new in the field of ECE-based cooling technology and it will not only ease the designing methodology but will also open the new aspects of the research in this field.

As the ECE-based solid-state cooling technology is going through its evolutional stages with ultimate goal of high efficient, small-scale and completely silent devices for microscale applications for the thermal management of high power processors and other future technologies, so the analytical solutions were inevitable to understand the physics and engineering aspects of the ECE-based devices. Moreover, the concept of complete solid-state and noise free heat pump presented in this research will contribute significantly towards achieving the goals set by the

research community, and its experimental realization and prototyping in future may lead towards the manufacturing of high efficient and miniaturized solid-state coolers without involvement of any additional mechanism and will help reduction in the complexities of currently reported devices.

## Bibliography


1. Cline, W. R. *The Economics of Global Warming*. (Institute for International Economics, 1992).
2. UN. *Montreal Protocol on Substances that Deplete the Ozone Layer*. **C**, (1987).
3. UN. *Kyoto Protocol ot the United Nations Framework Convension on Climate Change*. (1997).
4. Sand, J. R., Fischer, S. K. & Baxter, V. D. *Energy and Global Warming Impacts of HFC Refrigerants and Emerging Technologies*. (1997).
5. Jaeger, C. R. Introduction to Microelectronic Fabrication. *Modular Series on Solid State Devices* 332 (2002). doi:10.1016/0026-2714(88)90019-4
6. Zhang, Q. Electrocaloric Materials; New Generation of Coolers. (2014).
7. Aprea, C., Greco, A., Maiorino, A. & Masselli, C. A comparison between electrocaloric and magnetocaloric materials for solid state refrigeration. *Int. J. Heat Technol.* **35**, 225–234 (2017).
8. Qian, S. *et al.* Not-in-kind cooling technologies: A quantitative comparison of refrigerants and system performance. *Int. J. Refrig.* **62**, 177–192 (2016).
9. Zhang, Q. & Correia, T. Electrocaloric Effect: An Introduction. in *Electrocaloric Matrials: New Generation of Coolers* 1–14 (Heidelberg, Springer, 2014).
10. Kutnjak, Z. & Rožič, B. Electrocaloric Effect : Theory, Measurements , and Applications. in *Wiley Encyclopedia of Electrical and Electronics Engineering* (John Wiley & Sons).
11. Kitanovski, A., Plaznik, U., Tomc, U. & Poredoš, A. Present and future caloric refrigeration and heat-pump technologies. *Int. J. Refrig.* **57**, 288–298 (2015).
12. Ožbolt, M., Kitanovski, A., Tušek, J. & Poredoš, A. Electrocaloric refrigeration: Thermodynamics, state of the art and future perspectives. *Int. J. Refrig.* **40**, 174–188 (2014).
13. Ma, R. *et al.* Highly efficient electrocaloric cooling with electrostatic actuation. *Science (80-. ).* **357**, 1130–1134 (2017).
14. Hehlen, M. P., Mueller, A. H., Weisse-Bernstein, N. R. & Epstein, R. I. Electrocaloric refrigerator using electrohydrodynamic flows in dielectric fluids. 86380D (2013). doi:10.1117/12.2004009
15. Ožbolt, M., Kitanovski, A., Tušek, J. & Poredoš, A. Electrocaloric vs. magnetocaloric energy conversion. *Int. J. Refrig.* **37**, 16–27 (2014).
16. Thomson, W. On the thermoelastic, thermomagnetic, and pyroelectric properties of matter. *Philos. Mag.* **5**, 4–27 (1878).
17. Kobeko, P. & Kurtschatov, J. Dielektrische Eigenschaften der Seignettesalykristalle. **66**, 192–205 (1930).
18. Hautzenlaub, J. . Electric and dielectric behavior of potassium dihydrogen Phosphate. (Massachussets Institute of Technology, 1943).
19. Radebaugh, R., Lawless, W. N., Siegwarth, J. D. & Morrow, A. J. Feasibility of electrocaloric refrigeration for the 4-15 K temperature range. *Cryogenics (Guildf).* **19**, 187–208 (1979).
20. Mischenko, A. S. Giant Electrocaloric Effect in Thin-Film PbZr0.95Ti0.05O3. *Science (80-. ).* **311**, 1270–1271 (2006).
21. Neese, B. *et al.* Large Electrocaloric Effect in Ferroelectric Polymers Near Room Temperature. *Science (80-.*

*)*. **321**, 821–823 (2008).

22. Li, X. *et al.* Giant electrocaloric effect in ferroelectric poly(vinylidenefluoride- trifluoroethylene) copolymers near a first-order ferroelectric transition. *Appl. Phys. Lett.* **101**, (2012).
23. Valant, M. Electrocaloric materials for future solid-state refrigeration technologies. *Prog. Mater. Sci.* **57**, 980–1009 (2012).
24. Qian, X. S. *et al.* Giant electrocaloric response over a broad temperature range in modified BaTiO3 Ceramics. *Adv. Funct. Mater.* **24**, 1300–1305 (2014).
25. Liu, Y. & Zheng, G. Anelastic analyses on the relaxation of anti-ferroelectric states in 0.94Bi0.5Na0.5TiO3-0.06BaTiO3 solid solutions under electric fields. *J. Electroceramics* **34**, 38–42 (2015).
26. Jian, X.-D. *et al.* Direct Measurement of Large Electrocaloric Effect in Ba(Zr x Ti 1– x )O 3 Ceramics. *ACS Appl. Mater. Interfaces* **10**, 4801–4807 (2018).
27. Guo, D. The giant electrocaloric effect and high effective cooling power near room temperature for BaTiO 3 thick film. *J. Appl. Phys.* **110**, 094103 (2011).
28. Pakhomov, O. V, Karmanenko, S. F., Semenov, A. A. & Starkov, A. S. Thermodynamic Estimation of Cooling Efficiency Using an Electrocaloric Solid State Line. **55**, 1155–1160 (2010).
29. Kitanovski, A. *et al.* Alternative Caloric Energy Conversions. in *Magnetocaloric Energy Conversion: From Theory to Applications* 395–420 (Springer, 2014).
30. Kitanovski, A. *et al.* The Thermodynamics of Magnetocaloric Energy Conversion. in *Magnetocaloric Energy Conversion From Theory to Applications* 1–21 (Springer, [2015], 2015). doi:10.1007/978-3-319-08741-2
31. Nye, J. *Physicsal Properties of Crystals*. (Oxford Science Publications, 1985).
32. Lines, M. . & Glass, A. M. *Principles and Applications of the Ferrolectircs and Realted Materials*. (Clarendon Press, 1977).
33. Jona, F. & Shirane, G. *Internaitonal Series of Monograph on Solid State Physics*. (The Macmillan Company, 1962).
34. Mitsui, T., Tatsuzaki, I. & Nakamura, E. General Phenomenological Theories. in *An Introduction to the Physics of Ferroelectrics* 21–77 (Gordon and Breach Science Publishers, 1976).
35. Mason, W. *Piezoelectric Crystals and their Applications to Ultrasonics*. (D. Van Nostrand Company, Inc., 1950).
36. Cady, W. *Piezoelectricity*. (McGraw-Hill Book Company, Inc., 1946).
37. Mitsui, T., Tatsuzaki, I. & Nakamura, E. *An Introdution to the Physics of Ferroelectrics*. (Gordon and Breach Science Publishers, 1976).
38. Ikeda, T. Thermodynamic aspects of electromechanical interaction and piezoelectric relations. in *Fundamentals of Piezoelectricty* 5–30 (Oxford University Press, 1990).
39. Mason, W. P. *Crystal Physics of Interaction Processes*. (Academic Press, 1966).
40. Lee, M. H., Guo, R. & Bhalla, A. S. Pyroelectric sensors. *J. Electroceramics* **2**, 229–242 (1998).
41. Li, X. *et al.* Pyroelectric and electrocaloric materials. *J. Mater. Chem. C* 23–37 (2013).
42. Newnham, R. E. *Properties of Materials: Anisotropy, Symmetry, Structure*. (Oxford University Press, 2004).

43. Kitanovski, A. *et al.* Alternative Caloric Energy Conversion. in *Magnetocaloric Energy Conversion: From Therory to Applications* 395–450 (Springer, 2015).
44. Lines, M. . & Glass, A. M. Macroscopics and Phenomenology. in *Principles and Application of Ferroelectrics and Related Materials* 59–81 (Oxford University Press, 1977).
45. Lu, S. & Zhang, Q. Electrocaloric Materials for Solid-State Refrigeration TL - 21. *Adv. Mater.* **21 VN-r**, 1983–1987 (2009).
46. Cao, W. Constructing Landau-Ginzburg-Devonshire type models for ferroelectric systems based on symmetry. *Ferroelectrics* **375**, 28–39 (2008).
47. Landau, L. D. On the theory of phase transition. *Nuovo Cim. Ser. 10* **37**, (1937).
48. Ginzburg, V. L. & Landau, L. D. On the theory of Superconductivity. *Zh. Eksp. Teor. Fiz.* 1064 (1950).
49. Ginzburg, V. L. & Landau, L. D. On Superconductivity and superfluidity. in *On the theory of Supercondicity* (Springer, Berlin, Heidelberg, 2009). doi:https://doi.org/10.1007/978-3-540-68008-6_4
50. Devonshire, A. . Theory of Barium Titanate Part-I. *Philos. Mag.* **40**, 1040–1062 (1949).
51. Devonshire, A. . Theory of Barium Titanate Part-II. *Philos. Mag.* **42**, 1065–1079 (1951).
52. Kutnjak, Z. & Rožič, B. Indirect and Direct Measurements of the Electrocaloric Effect. in *Electrocaloric Matrials: New Generation of Coolers* 147–182 (Springer, 2014).
53. Mitsui, T., Tatsuzaki, I. & Nakamura, E. *An Introduction to the Physics of the Ferroelectrics*. (Gordon and Breach Science Publishers, 1976).
54. Li, D. & Lu, S.-G. Electrocaloric Effect and Phase Transitions in Ferroelectrics. *Int. J. Metall. Mater. Eng.* **4**, 4–8 (2018).
55. Liu, Y., Scott, J. F. & Dkhil, B. Direct and indirect measurements on electrocaloric effect: Recent developments and perspectives. *Appl. Phys. Rev.* **3**, (2016).
56. Lu, S. G. *et al.* Comparison of directly and indirectly measured electrocaloric effect in relaxor ferroelectric polymers. *Appl. Phys. Lett.* **97**, 1–4 (2010).
57. Guyomar, D., Sebald, G., Guiffard, B. & Seveyrat, L. Ferroelectric electrocaloric conversion in 0.75(PbMg1/3Nb 2/3O3)-0.25(PbTiO3) ceramics. *J. Phys. D. Appl. Phys.* **39**, 4491–4496 (2006).
58. Lu, S. G. *et al.* Organic and inorganic relaxor ferroelectrics with giant electrocaloric effect. *Appl. Phys. Lett.* **97**, 1–4 (2010).
59. Kar-Narayan, S. *et al.* Direct electrocaloric measurements of a multilayer capacitor using scanning thermal microscopy and infra-red imaging. *Appl. Phys. Lett.* **102**, 1–5 (2013).
60. Rožič, B. *et al.* Giant electrocaloric response over a broad temperature range in modified BaTiO3 Ceramics. *Appl. Phys. Lett.* **110**, 1–4 (2017).
61. Crossley, S. *et al.* Direct electrocaloric measurement of 0.9Pb(Mg 1/3 Nb 2/3 )O 3 -0.1PbTiO 3 films using scanning thermal microscopy. *Appl. Phys. Lett.* **108**, 032902 (2016).
62. Molin, C. *et al.* Comparison of direct electrocaloric characterization methods exemplified by 0.92 Pb(Mg1/3Nb2/3)O3-0.08 PbTiO3 multilayer ceramics. *J. Am. Ceram. Soc.* **100**, 2885–2892 (2017).
63. Le Goupil, F., Berenov, A., Axelsson, A.-K., Valant, M. & Alford, N. M. Direct and Indirect Electrocaloric

Measurements on 001 PMN-PT Single Crsytals. *J. Appl. Phys.* **111**, 1–8 (2012).

64. Kim, D. S. *et al.* Direct and indirect measurements of the electro-caloric effect in (Bi,Na)TiO3-SrTiO3 ceramics. *J. Appl. Phys.* **126**, (2019).
65. Li, J. *et al.* Direct and indirect characterization of electrocaloric effect in (Na,K)NbO3 based lead-free ceramics. *Appl. Phys. Lett.* **109**, 2–6 (2016).
66. Lu, B. *et al.* Large Electrocaloric Effect in Relaxor Ferroelectric and Antiferroelectric Lanthanum Doped Lead Zirconate Titanate Ceramics. *Sci. Rep.* **7**, 1–8 (2017).
67. Dai, G. *et al.* Direct and indirect measurement of large electrocaloric effect in barium strontium titanate ceramics. *Int. J. Appl. Ceram. Technol.* **17**, 1354–1361 (2020).
68. Lu, S. G. *et al.* Comparison of directly and indirectly measured electrocaloric effect in relaxor ferroelectric polymers. *Appl. Phys. Lett.* **97**, 1–4 (2010).
69. Blinc, R. *Advanced Ferroelectricity*. (Oxford University Press, 2011).
70. Scott, J. F. Electrocaloric Materials. *Annu. Rev. Mater. Res.* **41**, 229–240 (2011).
71. Kar-Narayan, S. & Mathur, N. D. Direct and indirect electrocaloric measurements using multilayer capacitors. *J. Phys. D. Appl. Phys.* **43**, 3–7 (2010).
72. Kar-Narayan, S. & Mathur, N. D. Predicted cooling powers for multilayer capacitors based on various electrocaloric and electrode materials. *Appl. Phys. Lett.* **95**, 1–4 (2009).
73. Bai, Y., Zheng, G. & Shi, S. Direct measurement of giant electrocaloric effect in BaTiO[sub 3] multilayer thick film structure beyond theoretical prediction. *Appl. Phys. Lett.* **96**, 192902 (2010).
74. Smullin, S. J., Wang, Y. & Schwartz, D. E. System optimization of a heat-switch-based electrocaloric heat pump. *Appl. Phys. Lett.* **107**, (2015).
75. Shebanoves, L., Borman, K., Lawless, K. & Kalvane, A. Electrocaloric Effect in Some Perovskite Ferroelectric Ceramics and Multilayer Capacitors. *Ferroelectrics* **273**, 137–142 (2002).
76. Kumar, A., Thakre, A., Jeong, D. Y. & Ryu, J. Prospects and challenges of the electrocaloric phenomenon in ferroelectric ceramics. *J. Mater. Chem. C* **7**, 6836–6859 (2019).
77. Chu, B., Zhou, Y. & Zhnag, S. Dielectric Polymer Materials for High-Density Energy Storage. in *https://www.sciencedirect.com/science/book/9780128132159* 500 (Elsevier Inc., 2018). doi:https://doi.org/10.1016/B978-0-12-813215-9.00010-5
78. Hongbo, C., Zhenxing, Y., Ouyang, J., Wei, Z. & Fangren, H. Recent progress in ferroelectric thin film capacitors for high density energy storage. in *Nanostructures in Ferroelectric Films for Energy Applications* 386 (Elsevier Inc., 2019). doi:https://doi.org/10.1016/C2017-0-00379-8
79. Geng, W. *et al.* Giant negative electrocaloric effect in antiferroelectric La-doped Pb(ZrTi)O3 thin films near room temperature. *Adv. Mater.* **27**, 3165–3169 (2015).
80. Zhao, Y., Hao, X. & Zhang, Q. Energy-storage properties and electrocaloric effect of Pb (1-3 x /2)LaxZr0.85Ti0.15O 3 antiferroelectric thick films. *ACS Appl. Mater. Interfaces* **6**, 11633–11639 (2014).
81. Peng, B., Fan, H. & Zhang, Q. A giant electrocaloric effect in nanoscale antiferroelectric and ferroelectric phases coexisting in a relaxor Pb0.8Ba 0.2ZrO3 thin film at room temperature. *Adv. Funct. Mater.* **23**, 2987–

2992 (2013).

82. Pirc, R. *et al.* Anomalous dielectric and thermal properties of Ba-doped PbZrO3 ceramics. *J. Phys. Condens. Matter* **27**, (2015).
83. Peräntie, J., Correia, T., Hagberg, J. & Uusimaki, A. Electrocaloric Effect in Relaxor Ferroelectric-Based Materials. in *Electrocaloric Matrials: New Generation of Coolers* 253 (Springer-Verlag Berlin Heidelberg, 2014).
84. BOKOV, A. A. & YE, Z.-G. Dielectric Relaxation in Relaxor Ferroelectrics. *J. Adv. Dielectr.* **02**, 1241010 (2012).
85. Cheng, Z.-Y., Katiyar, R. S., Yao, X. & Bhalla, A. . Temperature dependence of the dielectric constant of relaxor ferroelectrics. *Phys. Rev. B* **57**, 8166–8177 (1998).
86. Cheng, Z., Katiyar, R. & Yao, X. Dielectric behavior of lead magnesium niobate relaxors. *Phys. Rev. B - Condens. Matter Mater. Phys.* **55**, 8165–8174 (1997).
87. Hagberg, J., Uusimäki, A. & Jantunen, H. Electrocaloric characteristics in reactive sintered 0.87 Pb (Mg13 Nb23) O3 -0.13 PbTi O3. *Appl. Phys. Lett.* **92**, 2006–2009 (2008).
88. Moya, X. *et al.* Giant electrocaloric strength in single-crystal BaTiO3. *Adv. Mater.* **25**, 1360–1365 (2013).
89. Zhang, T. F. *et al.* Enhanced electrocaloric analysis and energy-storage performance of lanthanum modified lead titanate ceramics for potential solid-state refrigeration applications. *Sci. Rep.* **8**, 1–12 (2018).
90. Pirc, R., Kutnjak, Z., Blinc, R. & Zhang, Q. M. Electrocaloric effect in relaxor ferroelectrics. *J. Appl. Phys.* **110**, (2011).
91. Li, M. D. *et al.* Giant electrocaloric effect in BaTiO3–Bi(Mg1/2Ti1/2)O3lead-free ferroelectric ceramics. *J. Alloys Compd.* **747**, 1053–1061 (2018).
92. Moya, X. & Mathur, N. D. Caloric materials near ferroic phase transitions. *Nat. Publ. Gr.* **13**, 439–450 (2014).
93. Novak, N., Pirc, R. & Kutnjak, Z. Effect of Electric Field on Ferroelectric Phase Transition in BaTiO3 Ferroelectric. *Ferroelectrics* **469**, 61–66 (2013).
94. Lin, G. C., Xiong, X. M., Zhang, J. X. & Wei, Q. Latent heat study of phase transition in Ba0.73Sr0.27TiO3 induced by electric field. *J. Therm. Anal. Calorim.* **81**, 41–44 (2005).
95. Zhnag, W. *et al.* Preparation and Characterization of (1 - x) Pb Mg13Nb23† O3 x PbTiO3 Electrocaloric Ceramics. **33**, 827–832 (1998).
96. Zhao, Y., Hao, X. & Zhang, Q. Enhanced energy-storage performance and electrocaloric effect in compositionally graded Pb(1-3x/2)LaxZr0.85Ti0.15O3antiferroelectric thick films. *Ceram. Int.* **42**, 1679–1687 (2016).
97. Guo, M., Wu, M., Gao, W., Sun, B. & Lou, X. Giant negative electrocaloric effect in antiferroelectric PbZrO 3 thin films in an ultra-low temperature range. *J. Mater. Chem. C* **7**, 617–621 (2019).
98. Zhao, Y., Hao, X. & Zhang, Q. A giant electrocaloric effect of a Pb0.97La0.02(Zr0.75Sn0.18Ti0.07)O3 antiferroelectric thick film at room temperature. *J. Mater. Chem. C* **3**, 1694–1699 (2015).
99. Uršič, H. *et al.* Specific heat capacity and thermal conductivity of the electrocaloric (1-x)Pb(Mg1/3Nb2/3)O3-xPbTiO3 ceramics between room temperature and 300°C. *Inf. MIDEM* **45**, 260–265 (2015).

100. Mischenko, A. S., Zhang, Q., Whatmore, R. W., Scott, J. F. & Mathur, N. D. Giant electrocaloric effect in the thin film relaxor ferroelectric 0.9 Pb Mg1/3Nb2/3O3-0.1 PbTiO3 near room temperature. *Appl. Phys. Lett.* **89**, 1–4 (2006).
101. Rožič, B. *et al.* Influence of the critical point on the electrocaloric response of relaxor ferroelectrics. *J. Appl. Phys.* **110**, 0–5 (2011).
102. Zhang, G. *et al.* Ferroelectric polymer nanocomposites for room-temperature electrocaloric refrigeration. *Adv. Mater.* **27**, 1450–1454 (2015).
103. Li, J. *et al.* Electrocaloric effect in lead-free relaxor (1-x)(Sr0.7Bi0.2)TiO3+x(Na0.5Bi0.5)TiO3material system. *Mater. Lett.* **187**, 68–71 (2017).
104. Feng, D., Yao, S., Zhang, T. & Zhang, Q. Modeling of Smart Heat Pump Using Thermoelectric and Electrocaloric Materials. *Vol. 1 Multifunct. Mater. Mech. Behav. Act. Mater. Integr. Syst. Des. Implementation; Struct. Heal. Monit.* **138**, V001T04A003 (2016).
105. Weyland, F., Perez-Moyet, R., Rossetti, G. & Novak, N. Material Measure of Electrocaloric Cooling Power in Perovskite Ferroelctrics. (2018). doi:10.1002/ente.201800136
106. Chukka, R., Shannigrahi, S. & Chen, L. Investigations of cooling efficiencies in solid-state electrocaloric device. *Integr. Ferroelectr.* **133**, 3–8 (2012).
107. Applications, C. Electrocaloric refrigeration : an innovative , emerging , eco-friendly refrigeration technique Electrocaloric refrigeration : an innovative , emerging , eco- friendly refrigeration technique. (2017). doi:10.1088/1742-6596/755/1/011001
108. Defay, E. *et al.* Enhanced electrocaloric efficiency via energy recovery. *Nat. Commun.* **9**, 1827 (2018).
109. Epstein, R. I. & Malloy, K. J. Electrocaloric devices based on thin-film heat switches. *J. Appl. Phys.* **106**, (2009).
110. Gschneidner, A., Pecharsky, V. K. & Tsokol, A. O. Recent developments in magnetocaloric materials. *Reports Prog. Phys.* **68**, 1479–1539 (2005).
111. Correia, T. M. *et al.* PST thin films for electrocaloric coolers. *J. Phys. D. Appl. Phys.* **44**, (2011).
112. Agency, D. E. Energy technology. 2007–2008 (2008). doi:10.1002/ente.201800139
113. Blumenthal, P. & Raatz, A. Classification of electrocaloric cooling device types. *Epl* **115**, (2016).
114. Kitanovski, A. *et al.* Active Magneic Regeneration. in *Magnetocaloric Energy Conversion: From Theory to Applications* 97–166 (2015). doi:10.1007/978-3-319-08741-2
115. Barclay, J. & Steyert, W. Active Magnetic Regenerator. 11 (1982).
116. Tušek, J., Kitanovski, A., Zupan, S., Prebil, I. & Poredoš, A. A comprehensive experimental analysis of gadolinium active magnetic regenerators. *Appl. Therm. Eng.* **53**, 57–66 (2013).
117. Sinyavsky, Y. V. & Brodyansky, V. M. Experimental testing of electrocaloric cooling with transparent ferroelectric ceramic as a working body. *Ferroelectrics* **131**, 321–325 (1992).
118. Guo, D. *et al.* Design and modeling of a fluid-based micro-scale electrocaloric refrigeration system. *Int. J. Heat Mass Transf.* **72**, 559–564 (2014).
119. Jia, Y. & Sungtaek Ju, Y. A solid-state refrigerator based on the electrocaloric effect. *Appl. Phys. Lett.* **100**,

(2012).

120. Plaznik, U. *et al.* Bulk relaxor ferroelectric ceramics as a working body for an electrocaloric cooling device. *Appl. Phys. Lett.* **106**, (2015).
121. Blumenthal, P., Molin, C., Gebhardt, S. & Raatz, A. Active electrocaloric demonstrator for direct comparison of PMN-PT bulk and multilayer samples. *Ferroelectrics* **497**, 1–8 (2016).
122. Gu, H. *et al.* A chip scale electrocaloric effect based cooling device. *Appl. Phys. Lett.* **102**, (2013).
123. Gu, H., Qian, X. S., Ye, H. J. & Zhang, Q. M. An electrocaloric refrigerator without external regenerator. *Appl. Phys. Lett.* **105**, (2014).
124. Hakuraku, Y. Thermodynamic simulation of a rotating Ericsson-cycle magnetic refrigerator without a regenerator. *J. Appl. Phys.* **62**, 1560–1563 (1987).
125. Zhang, T., Qian, X. S., Gu, H., Hou, Y. & Zhang, Q. M. An electrocaloric refrigerator with direct solid to solid regeneration. *Appl. Phys. Lett.* **110**, 1–5 (2017).
126. Wang, Y. D. *et al.* A heat-switch-based electrocaloric cooler. *Appl. Phys. Lett.* **107**, (2015).
127. Ju, Y. S. Solid-State Refrigeration Based on the Electrocaloric Effect for Electronics Cooling. *J. Electron. Packag.* **132**, 041004 (2010).
128. Bradesko, A. *et al.* Coupling of the electrocaloric and electromechanical effects for solid-state refrigeration. *Appl. Phys. Lett.* **109**, (2016).
129. Chukka, R., Vandrangi, S., Shannigrahi, S. & Chen, L. An electrocaloric device demonstrator for solid-state cooling. *Epl* **103**, (2013).
130. Feng, D., Yao, S., Zhang, T. & Zhang, Q. Modeling of Smart Heat Pump Using Thermoelectric and Electrocaloric Materials. in *ASME 2016 Conference on Smart Materials, Adaptive Structures and Intelligence System* **1**, V001T04A003-1-V001T04A003-12 (2016).
131. Basiulis, A. & Berry, L. Solid State Electrocaloric Cooling System and Method. (1988).
132. Karmanenko, S. F., Pakhomov, O. V., Prudan, A. M., Starkov, A. S. & Eskov, A. Layered ceramic structure based on the electrocaloric elements working as a solid state cooling line. *J. Eur. Ceram. Soc.* **27**, 3109–3112 (2007).
133. Es'kov, A. V., Karmanenko, S. F., Pakhomov, O. V. & Starkov, A. S. Simulation of a solid-state cooler with electrocaloric elements. *Phys. Solid State* **51**, 1574–1577 (2009).
134. Khodayari, A. & Mohammadi, S. Solid-state cooling line based on the electrocaloric effect. in *IEEE Transactions on Ultrasonics, Ferroelectrics, and Frequency Control* **58**, 503–508 (2011).
135. Bai, Y., Zheng, G. P. & Shi, S. Q. Kinetic electrocaloric effect and giant net cooling of lead-free ferroelectric refrigerants. *J. Appl. Phys.* **108**, 0–4 (2010).
136. Frohlich, H. *Theory of Dielectrics*. (Clarendon Press, 1958).
137. Frohlich, H. Macroscopic Theory. in *Theory of Dielectrics* (eds. Jackson, W., Mott, N. & Bullard, E.) 9–13 (Orford, 1958).
138. Zheludev, I. *Physics of Crystalline Dielectrics*. (Plenum Press, 1971).
139. Cheng, Z. Y., Wang, X. L. & Yao, X. Dielectric properties and glassy behaviour in the solid-solution ceramics

Pb(Zn‖Nb‖)O3-PbTiO3-BaTiO3. *Philos. Mag. B Phys. Condens. Matter; Stat. Mech. Electron. Opt. Magn. Prop.* **78**, 279–293 (1998).

140. Plaznik, U. *et al.* Bulk relaxor ferroelectric ceramics as a working body for an electrocaloric cooling device. *Appl. Phys. Lett.* **106**, (2015).
141. Crossley, S., McGinnigle, J. R., Kar-Narayan, S. & Mathur, N. D. Finite-element optimisation of electrocaloric multilayer capacitors. *Appl. Phys. Lett.* **104**, (2014).
142. Crank, J. *The Mathematics of Diffusion*. (Claredon Press, Oxford, 1975).
143. Luikov, A. . Infinite Plate. in *Analytical Heat Diffusion Theory* (ed. Hartnett, J. P.) 422–428 (Academic Express, 1968).
144. Luikov, A. . System of Two Bodies (Two Semi-Infinite Rods). in *Analytical Heat Diffusion Theory* (ed. Hartnett, J. P.) 401–406 (1968).
145. Luikov, A. . Temperature Field With Pulse-type Heat Sources. in *Analytical Heat Diffusion Theory* 377–398 (Academic Press, 1968).
146. Kakac, S. & Yener, Y. Plane Wall. in *Heat Conduction* 269–272 (Taylor & Francis, 1993).
147. Xin, R. C. & Tao, W. Q. Analytical Solution for Transient Heat Conduction in Two Semi-infinite Bodies in Contact. *ASME* **116**, 224–228 (1994).
148. Carslaw, H. S. & Jaeger, J. C. *Conduction of Heat in Solids*. (Clarendon Press, 2011).
149. Kakac, S. & Yaner, Y. Fourier's Law of Heat Conduction. in *Heat Conduction* 363 (1993).
150. Luikov, A. . End Conditions. in *Analytical Heat Diffusion Theory* (ed. Hartnett, J. P.) 24–31 (Academic Press, 1968).
151. Kreyszic, E. Partial Differential Equations. in *Advanced Engineering Matthemtics* (ed. Pirtle, R.) 645–716 (Don Ford, 1988).
152. Stewart, J. *Calculus*. (Cengage Learning, 2014).

**APPENDIX - A GENERIC SOLUTION OF THE HEAT EQUATION**

Let us consider a 1D heat equation

$$\frac{\partial T(x,t)}{\partial t} = \alpha \frac{\partial^2 T(x,t)}{\partial x^2}$$

$$\frac{\partial^2 T(x,t)}{\partial x^2} - \frac{1}{\alpha}\frac{\partial T(x,t)}{\partial t} = 0$$

Taking Laplace Transform

$$L\left\{\frac{\partial^2 T(x,t)}{\partial x^2}\right\} - \frac{1}{\alpha} L\left\{\frac{\partial T(x,t)}{\partial t}\right\} = L\{0\}$$

Let $L\{T(x,t)\} = W(x,s)$

$$\frac{\partial^2 W(x,s)}{\partial x^2} - \frac{1}{\alpha}\{sW(x,s) - T(x,0)\} = 0$$

Initial condition $T(x,0) = T_i$

$$\frac{\partial^2 W(x,s)}{\partial x^2} - \frac{s}{\alpha} W(x,s) + \frac{1}{\alpha} T_i = 0$$

It is an ordinary second order differential equation and the solution of this eq. may be given as

$$\boldsymbol{W(x,s) - \frac{T_i}{s} = C_1\, e^{\sqrt{\frac{s}{\alpha}}x} + C_2\, e^{-\sqrt{\frac{s}{\alpha}}x}}$$

The constant of integration $C_1$ and $C_2$ may be determined using the boundary conditions. Then after taking the inverse transform, the solution for temperature as a function of time and space (1D) *T(x,t),* is determined.

**APPENDIX - B CONSTANTS OF INTEGRATION (ANALYTICAL SOLUTION FOR SAME SINK/SOURCE)**

$$A_1 = \frac{e^{R\sqrt{\frac{s}{\alpha^o}}}K_\varepsilon\left\{(1-K_\varepsilon)(T_{2i}-T_{1i}) - e^{R\sqrt{\frac{s}{\alpha^c}}}(1-K_\varepsilon)(T_{2i}-T_{3i}) - 2e^{2R\sqrt{\frac{s}{\alpha^c}}}(T_{3i}-T_{4i}) - e^{3R\sqrt{\frac{s}{\alpha^c}}}(1+K_\varepsilon)(T_{2i}-T_{3i}) + e^{4R\sqrt{\frac{s}{\alpha^c}}}(1+K_\varepsilon)(T_{2i}-T_{i1})\right\}}{e^{4R\sqrt{\frac{s}{\alpha^c}}}(1+K_\varepsilon)^2 s - (1-K_\varepsilon)^2 s}$$

$$A_2 = \frac{2e^{R\sqrt{\frac{s}{\alpha^c}}}(1-K_\varepsilon)(T_{2i}-T_{1i}) - e^{2R\sqrt{\frac{s}{\alpha^c}}}(1-K_\varepsilon{}^2)(T_{2i}-T_{3i}) - 2e^{3R\sqrt{\frac{s}{\alpha^c}}}(1+K_\varepsilon)(T_{3i}-T_{4i}) - e^{4R\sqrt{\frac{s}{\alpha^c}}}(1+K_\varepsilon)^2(T_{2i}-T_{3i})}{2e^{4R\sqrt{\frac{s}{\alpha^c}}}(1+K_\varepsilon)^2 s - 2(1-K_\varepsilon)^2 s}$$

$$B_2 = \frac{(1-K_\varepsilon)^2(T_{2i}-T_{3i}) + 2e^{R\sqrt{\frac{s}{\alpha^c}}}(1-K_\varepsilon)(T_{3i}-T_{4i}) + e^{2R\sqrt{\frac{s}{\alpha^c}}}(1-K_\varepsilon{}^2)(T_{2i}-T_{3i}) - 2e^{3R\sqrt{\frac{s}{\alpha^c}}}(1+K_\varepsilon)(T_{2i}-T_{1i})}{2e^{4R\sqrt{\frac{s}{\alpha^c}}}(1+K_\varepsilon)^2 s - 2(1-K_\varepsilon)^2 s}$$

$$A_3 = \frac{-(1-K_\varepsilon)^2(T_{2i}-T_{3i}) + 2e^{R\sqrt{\frac{s}{\alpha^c}}}(1-K_\varepsilon)(T_{2i}-T_{1i}) - e^{2R\sqrt{\frac{s}{\alpha^c}}}\left(1-K_\varepsilon{}^2\right)(T_{2i}-T_{3i}) - 2e^{3R\sqrt{\frac{s}{\alpha^c}}}(1+K_\varepsilon)(T_{3i}-T_{4i})}{2e^{4R\sqrt{\frac{s}{\alpha^c}}}(1+K_\varepsilon)^2 s - 2(1-K_\varepsilon)^2 s}$$

$$B_3 = \frac{2e^{R\sqrt{\frac{s}{\alpha^c}}}(1-K_\varepsilon)(T_{3i}-T_{4i}) + e^{2R\sqrt{\frac{s}{\alpha^c}}}(1-K_\varepsilon{}^2)(T_{2i}-T_{3i}) - 2e^{3R\sqrt{\frac{s}{\alpha^c}}}(1+K_\varepsilon)(T_{2i}-T_{1i}) + e^{4R\sqrt{\frac{s}{\alpha^c}}}(1+K_\varepsilon)^2(T_{2i}-T_{3i})}{2e^{4R\sqrt{\frac{s}{\alpha^c}}}(1+K_\varepsilon)^2)s - 2(1-K_\varepsilon)^2 s}$$

$$B_4 = \frac{e^{R\sqrt{\frac{s}{\alpha^o}}}K_\varepsilon\left\{(1-K_\varepsilon)(T_{3i}-T_{4i}) + e^{R\sqrt{\frac{s}{\alpha^c}}}(1-K_\varepsilon)(T_{2i}-T_{3i}) - 2e^{2R\sqrt{\frac{s}{\alpha^c}}}(T_{2i}-T_{1i}) + e^{3R\sqrt{\frac{s}{\alpha^c}}}(1+K_\varepsilon)(T_{2i}-T_{3i}) + e^{4R\sqrt{\frac{s}{\alpha^c}}}(1+K_\varepsilon)(T_{3i}-T_{4i})\right\}}{e^{4R\sqrt{\frac{s}{\alpha^c}}}(1+K_\varepsilon)^2)s - (1-K_\varepsilon)^2 s}$$

where

$$h = \frac{1-K_\varepsilon}{1+K_\varepsilon} \quad |h| < 1$$

**APPENDIX - C MANIPULATING THE DENOMINATOR FOR ANALYTICAL SOLUTION IN CHAPTER 3**

$$Deno = \frac{1}{2e^{4R\sqrt{\frac{s}{\alpha}}}(1+K_\varepsilon)^2 s - 2(1-K_\varepsilon)^2 s}$$

$$= \frac{1}{2e^{4R\sqrt{\frac{s}{\alpha}}}(1+K_\varepsilon)^2\left[1-\frac{(1-K_\varepsilon)^2}{(1+K_\varepsilon)^2}e^{-4R\sqrt{\frac{s}{\alpha}}}\right]}\frac{1}{s}$$

$$= \frac{e^{-4R\sqrt{\frac{s}{\alpha}}}}{2(1+K_\varepsilon)^2\left[1-\frac{(1-K_\varepsilon)^2}{(1+K_\varepsilon)^2}e^{-4R\sqrt{\frac{s}{\alpha}}}\right]}\frac{1}{s}$$

$$= \frac{e^{-4R\sqrt{\frac{s}{\alpha}}}}{2(1+K_\varepsilon)^2\left[1-h^2 e^{-4R\sqrt{\frac{s}{\alpha}}}\right]}\frac{1}{s}$$

$$Deno = \frac{1}{s}\frac{e^{-4R\sqrt{\frac{s}{\alpha}}}}{2(1+K_\varepsilon)^2}\frac{1}{\left[1-h^2 e^{-4R\sqrt{\frac{s}{\alpha}}}\right]}$$

Using the following relation (Geometric Series)

$$\frac{1}{1-x} = \sum_{n=0}^{\infty} x^n = 1 + x + x^2 + x^3 + \cdots$$

The above equation may be written as

$$Deno = \frac{1}{s}\frac{e^{-4R\sqrt{\frac{s}{\alpha}}}}{2(1+K_\varepsilon)^2}\sum_{n=0}^{\infty}\left(h^2\, e^{-4R\sqrt{\frac{s}{\alpha}}}\right)^n$$

$$= \frac{1}{s}\frac{e^{-4R\sqrt{\frac{s}{\alpha}}}}{2(1+K_\varepsilon)^2}\left[1 + h^2\exp\left(-4R\sqrt{\frac{s}{\alpha}}\right) + h^4\exp\left(-8R\sqrt{\frac{s}{\alpha}}\right) + h^6\exp\left(-12R\sqrt{\frac{s}{\alpha}}\right) + \cdots\right]$$

$$Deno = \frac{1}{s}\frac{1}{2(1+K_\varepsilon)^2}\sum_{n=1}^{\infty} h^{2(n-1)}\exp\left(-4nR\sqrt{\frac{s}{\alpha}}\right)$$

Hence

$$\frac{1}{2e^{4R\sqrt{\frac{s}{\alpha}}}(1+K_\varepsilon)^2 s - 2(1-K_\varepsilon)^2 s} = \frac{1}{s}\frac{1}{2(1+K_\varepsilon)^2}\sum_{n=1}^{\infty} h^{2(n-1)}\exp\left(-4nR\sqrt{\frac{s}{\alpha}}\right)$$

**APPENDIX - D VALIDATION OF THE ANALYTICAL SOLUTION**

If we put the following initial conditions in our solution, our solution will become equivalent to the problem discussed in section 3.1.5.

$$T_{2i} = T_{3i}$$

$$T_{1i} = T_{4i}$$

$$T_{2i} = T_{3i} > T_{1i} = T_{4i}$$

**Temperature Profile for Center Body $-R < x < R$: Combining Body2 and Body3**

Putting the above initial condition in the Eq. **(3.35)**, we get

$$T_2(x,t) - T_{2i} = \frac{h}{1+K_\varepsilon}\sum_{n=1}^{\infty} h^{2(n-1)}\left[(T_{2i}-T_{1i})\,\mathrm{erfc}\frac{(4n-1)R-x}{2\sqrt{\alpha^c t}} + (T_{3i}-T_{4i})\,\mathrm{erfc}\frac{(4n-1)R+x}{2\sqrt{\alpha^c t}}\right] - \frac{1}{1+K_\varepsilon}\sum_{n=1}^{\infty} h^{2(n-1)}\left[(T_{3i}-T_{4i})\,\mathrm{erfc}\frac{(4n-3)R-x}{2\sqrt{\alpha^c t}} + (T_{2i}-T_{1i})\,\mathrm{erfc}\frac{(4n-3)R+x}{2\sqrt{\alpha^c t}}\right]$$

$$T_2(x,t) - T_{2i} = \frac{h(T_{2i}-T_{1i})}{1+K_\varepsilon}\sum_{n=1}^{\infty} h^{2(n-1)}\left[\mathrm{erfc}\frac{(4n-1)R-x}{2\sqrt{\alpha^c t}} + \mathrm{erfc}\frac{(4n-1)R+x}{2\sqrt{\alpha^c t}}\right] - \frac{(T_{2i}-T_{1i})}{1+K_\varepsilon}\sum_{n=1}^{\infty} h^{2(n-1)}\left[\mathrm{erfc}\frac{(4n-3)R-x}{2\sqrt{\alpha^c t}} + \mathrm{erfc}\frac{(4n-3)R+x}{2\sqrt{\alpha^c t}}\right]$$

$$T_2(x,t) - T_{2i} = \frac{(T_{2i}-T_{1i})}{1+K_\varepsilon}\left\{h\sum_{n=1}^{\infty} h^{2(n-1)}\left[\mathrm{erfc}\frac{(4n-1)R-x}{2\sqrt{\alpha^c t}} + \mathrm{erfc}\frac{(4n-1)R+x}{2\sqrt{\alpha^c t}}\right] - \sum_{n=1}^{\infty} h^{2(n-1)}\left[\mathrm{erfc}\frac{(4n-3)R-x}{2\sqrt{\alpha^c t}} + \mathrm{erfc}\frac{(4n-3)R+x}{2\sqrt{\alpha^c t}}\right]\right\}$$

For n=1 the first terms give $3R \mp x$ and second two terms give us $R \mp x$

For n=2 the first terms give $7R \mp x$ and second two terms give us $5R \mp x$

Let us write some terms for above equation

$$T_2(x,t) - T_{2i} = \frac{(T_{2i}-T_{1i})}{1+K_\varepsilon}\left\{h\sum_{n=1}^{\infty} h^{2(n-1)}\left[\mathrm{erfc}\frac{(4n-1)R-x}{2\sqrt{\alpha^c t}} + \mathrm{erfc}\frac{(4n-1)R+x}{2\sqrt{\alpha^c t}}\right] - \sum_{n=1}^{\infty} h^{2(n-1)}\left[\mathrm{erfc}\frac{(4n-3)R-x}{2\sqrt{\alpha^c t}} + \mathrm{erfc}\frac{(4n-3)R+x}{2\sqrt{\alpha^c t}}\right]\right\}$$

$$T_2(x,t)-T_{2i}=\frac{(T_{2i}-T_{1i})}{1+K_\varepsilon}\Big\{h\left(\operatorname{erfc}\frac{3R-x}{2\sqrt{\alpha t}}+\operatorname{erfc}\frac{3R+x}{2\sqrt{\alpha t}}\right)+h^3\left(\operatorname{erfc}\frac{7R-x}{2\sqrt{\alpha t}}+\operatorname{erfc}\frac{7R+x}{2\sqrt{\alpha t}}\right)$$
$$-\left(\operatorname{erfc}\frac{R-x}{2\sqrt{\alpha t}}+\operatorname{erfc}\frac{R+x}{2\sqrt{\alpha t}}\right)-h^2\left(\operatorname{erfc}\frac{5R-x}{2\sqrt{\alpha t}}+\operatorname{erfc}\frac{5R+x}{2\sqrt{\alpha t}}\right)+\cdots\Big\}$$

Rearranging…

$$T_2(x,t)-T_{2i}=\frac{(T_{2i}-T_{1i})}{1+K_\varepsilon}\Big\{-\left(\operatorname{erfc}\frac{R-x}{2\sqrt{\alpha t}}+\operatorname{erfc}\frac{R+x}{2\sqrt{\alpha t}}\right)+h\left(\operatorname{erfc}\frac{3R-x}{2\sqrt{\alpha t}}+\operatorname{erfc}\frac{3R+x}{2\sqrt{\alpha t}}\right)$$
$$-h^2\left(\operatorname{erfc}\frac{5R-x}{2\sqrt{\alpha t}}+\operatorname{erfc}\frac{5R+x}{2\sqrt{\alpha t}}\right)+h^3\left(\operatorname{erfc}\frac{7R-x}{2\sqrt{\alpha t}}+\operatorname{erfc}\frac{7R+x}{2\sqrt{\alpha t}}\right)+\cdots.\Big\}$$

So, we may express this series with only two terms if we replace 4n with 2n and some manipulation with $h$ power.

$$T_2(x,t)-T_{2i}=-\frac{(T_{2i}-T_{1i})}{1+K_\varepsilon}\left\{\sum_{n=1}^{\infty}(-h)^{n-1}\left[\operatorname{erfc}\frac{(2n-1)R-x}{2\sqrt{\alpha t}}+\operatorname{erfc}\frac{(2n-1)R+x}{2\sqrt{\alpha t}}\right]\right\}$$

Above is the solution given in the reference book. Expanding above equation…

$$T_2(x,t)-T_{2i}=-\frac{(T_{2i}-T_o)}{1+K_\varepsilon}\Big\{\operatorname{erfc}\frac{R-x}{2\sqrt{\alpha t}}+\operatorname{erf}\frac{R+x}{2\sqrt{\alpha t}}-h\left(\operatorname{erf}\frac{3R-x}{2\sqrt{\alpha t}}+\operatorname{erf}\frac{3R+x}{2\sqrt{\alpha t}}\right)$$
$$+h^2\left(\operatorname{erf}\frac{5R-x}{2\sqrt{\alpha t}}+\operatorname{erf}\frac{5R+x}{2\sqrt{\alpha t}}\right)+\cdots.\Big\}$$

So, the above two relation are same, so it validates our solution as given in the reference book.

**Temperature Profile of End Bodies ( $-\infty < x < -R$ and $R < x < \infty$) (Body 1 or Body4)**

Putting the above initial condition in the Eq. **(3.37)**, we get

$$T_4(x,t)-T_{4i}$$
$$=\frac{K_\varepsilon}{1+K_\varepsilon}\Big\{(T_{3i}-T_{4i})\,h\sum_{n=1}^{\infty}h^{2(n-1)}\operatorname{erfc}\frac{x-R+(4n-0)K_\alpha^{-1/2}R}{2\sqrt{\alpha^o t}}$$
$$-\frac{2(T_{3i}-T_{4i})}{1+K_\varepsilon}\sum_{n=1}^{\infty}h^{2(n-1)}\operatorname{erfc}\frac{x-R+(4n-2)K_\alpha^{-1/2}R}{2\sqrt{\alpha^o t}}$$
$$+(T_{3i}-T_{4i})\sum_{n=1}^{\infty}h^{2(n-1)}\operatorname{erfc}\frac{x-R+(4n-4)K_\alpha^{-1/2}R}{2\sqrt{\alpha^o t}}\Big\}$$

$$T_4(x,t)-T_{4i}$$
$$=\frac{K_\varepsilon(T_{3i}-T_{4i})}{1+K_\varepsilon}\Big\{h\sum_{n=1}^{\infty}h^{2(n-1)}\operatorname{erfc}\frac{x-R+(4n-0)K_\alpha^{-1/2}R}{2\sqrt{\alpha^o t}}$$
$$-\frac{2}{1+K_\varepsilon}\sum_{n=1}^{\infty}h^{2(n-1)}\operatorname{erfc}\frac{x-R+(4n-2)K_\alpha^{-1/2}R}{2\sqrt{\alpha^o t}}+\sum_{n=1}^{\infty}h^{2(n-1)}\operatorname{erfc}\frac{x-R+(4n-4)K_\alpha^{-1/2}R}{2\sqrt{\alpha^o t}}\Big\}$$

$$\frac{T_4(x,t)-T_{4i}}{(T_{3i}-T_{4i})}$$

$$= \frac{K_\varepsilon}{1+K_\varepsilon}\left\{ h\sum_{n=1}^{\infty} h^{2(n-1)}\,\mathrm{erfc}\frac{x-R+(4n-0)K_\alpha^{-1/2}R}{2\sqrt{\alpha^o t}} - \frac{2}{1+K_\varepsilon}\sum_{n=1}^{\infty} h^{2(n-1)}\,\mathrm{erfc}\frac{x-R+(4n-2)K_\alpha^{-1/2}R}{2\sqrt{\alpha^o t}} + \sum_{n=1}^{\infty} h^{2(n-1)}\,\mathrm{erfc}\frac{x-R+(4n-4)K_\alpha^{-1/2}R}{2\sqrt{\alpha^o t}}\right\}$$

Expanding the above relation

$$\frac{T_4(x,t)-T_{4i}}{(T_{3i}-T_{4i})}$$

$$= \frac{K_\varepsilon}{1+K_\varepsilon}\left\{ h\left(\mathrm{erfc}\frac{x-R+4K_\alpha^{-1/2}R}{2\sqrt{\alpha^o t}} + h^2\,\mathrm{erfc}\frac{x-R+8K_\alpha^{-1/2}R}{2\sqrt{\alpha^o t}} + h^4\,\mathrm{erfc}\frac{x-R+12K_\alpha^{-1/2}R}{2\sqrt{\alpha^o t}} + \cdots\right) - \frac{2}{1+K_\varepsilon}\left(\mathrm{erfc}\frac{x-R+2K_\alpha^{-1/2}R}{2\sqrt{\alpha^o t}} + h^2\,\mathrm{erfc}\frac{x-R+6K_\alpha^{-1/2}R}{2\sqrt{\alpha^o t}} + h^4\,\mathrm{erfc}\frac{x-R+10K_\alpha^{-1/2}R}{2\sqrt{\alpha^o t}} + \cdots\right) + \left(\mathrm{erfc}\frac{x-R}{2\sqrt{\alpha^o t}} + h^2\,\mathrm{erfc}\frac{x-R+4K_\alpha^{-1/2}R}{2\sqrt{\alpha^o t}} + h^4\,\mathrm{erfc}\frac{x-R+8K_\alpha^{-1/2}R}{2\sqrt{\alpha^o t}} + \cdots\right)\right\}$$

Further manipulation…

$$\frac{T_4(x,t)-T_{4i}}{(T_{3i}-T_{4i})} = \frac{K_\varepsilon}{1+K_\varepsilon}\mathrm{erfc}\frac{x-R}{2\sqrt{\alpha^o t}} + \frac{K_\varepsilon}{1+K_\varepsilon}\left\{ h\left(\mathrm{erfc}\frac{x-R+4K_\alpha^{-1/2}R}{2\sqrt{\alpha^o t}} + h^2\,\mathrm{erfc}\frac{x-R+8K_\alpha^{-1/2}R}{2\sqrt{\alpha^o t}} + h^4\,\mathrm{erfc}\frac{x-R+12K_\alpha^{-1/2}R}{2\sqrt{\alpha^o t}} + \cdots\right) - (1+h)\left(\mathrm{erfc}\frac{x-R+2K_\alpha^{-1/2}R}{2\sqrt{\alpha^o t}} + h^2\,\mathrm{erfc}\frac{x-R+6K_\alpha^{-1/2}R}{2\sqrt{\alpha^o t}} + h^4\,\mathrm{erfc}\frac{x-R+10K_\alpha^{-1/2}R}{2\sqrt{\alpha^o t}} + \cdots\right) + \left(h^2\,\mathrm{erfc}\frac{x-R+4K_\alpha^{-1/2}R}{2\sqrt{\alpha^o t}} + h^4\,\mathrm{erfc}\frac{x-R+8K_\alpha^{-1/2}R}{2\sqrt{\alpha^o t}} + \cdots\right)\right\}$$

The above series may be written as

$$\frac{T_4(x,t)-T_{4i}}{(T_{3i}-T_{4i})} = \frac{K_\varepsilon}{1+K_\varepsilon}\mathrm{erfc}\frac{x-R}{2\sqrt{\alpha^o t}} - \frac{K_\varepsilon(1+h)}{1+K_\varepsilon}\left\{\sum_{n=1}^{\infty}(-h)^{n-1}\,\mathrm{erfc}\frac{x-R+2nRK_\alpha^{-1/2}}{2\sqrt{\alpha^o t}}\right\}$$

Where

$$\frac{1+K_\varepsilon}{2}=\frac{1}{1+h}=\sum_{n=1}^{\infty}(-h)^{n-1}$$

Note: there are two terms for each 4R, 6R, 8R. Expanding the second part of the above equation

$$=-\frac{K_\varepsilon(1+h)}{1+K_\varepsilon}\left\{\sum_{n=1}^{\infty}(-h)^{n-1}\,\mathrm{erfc}\frac{x-R+2nRK_\alpha^{-1/2}}{2\sqrt{\alpha^o t}}\right\}$$

$$=-\frac{K_\varepsilon(1+h)}{1+K_\varepsilon}\left(\mathrm{erfc}\frac{x-R+2RK_\alpha^{-1/2}}{2\sqrt{\alpha^o t}}\right)-\frac{K_\varepsilon(1+h)}{1+K_\varepsilon}\left(-h\,\mathrm{erfc}\frac{x-R+4RK_\alpha^{-1/2}}{2\sqrt{\alpha^o t}}\right)$$

$$-\frac{K_\varepsilon(1+h)}{1+K_\varepsilon}\left(h^2\,\mathrm{erfc}\frac{x-R+6RK_\alpha^{-1/2}}{2\sqrt{\alpha^o t}}\right)-\frac{K_\varepsilon(1+h)}{1+K_\varepsilon}\left(-h^3\,\mathrm{erfc}\frac{x-R+8RK_\alpha^{-1/2}}{2\sqrt{\alpha^o t}}\right)+\cdots$$

Hence, we proved that our results are the same as mentioned in the reference book and our solution is the more generalized form for the solution mentioned in the book (i.e. Book problem is a special case of our problem)

**APPENDIX - E THERMAL PROPERTIES OF SEVERAL EC AND NON-EC MATERIALS**

| **Materials** | **Density** $\rho\left(\frac{kg}{m^3}\right)$ | **Heat Capacity** $c_p\left(\frac{J}{K\ kg}\right)$ | **Thermal Conductivity** $k\left(\frac{W}{mK}\right)$ | **Thermal Diffusivity (x10$^{-6}$)** $\alpha\left(\frac{m^2}{s}\right)$ | **Ref.** |
|---|---|---|---|---|---|
| P(VDF-TrFE-CFE) Terpolymer | 1800 | 1500 | 0.2 | 0.074 | [123] |
| Barium Strontium Titanate (BST) | 6000 | 900 | 10 | 1.85 | [133] |
| PMN-25PT | 8000 | 321.5 | 0.25 | 0.097 | [134] |
| PZN-4.5PT | 8100 | 200 | 0.25 | 0.154 | [134] |
| BT | 6060 | 527 | 6 | 1.88 | - |
| Air | 1.1614 | 1007 | 0.026 | 22.2 | - |
| Graphite | 2250 | 25 | 709 | 12604 | - |
| Aluminum | 2689 | 951 | 237.5 | 92.9 | - |
| Silver | 10500 | 235 | 429 | 174 | - |
| Copper | 8933 | 385 | 400 | 116 | - |

**APPENDIX - F DEFINITIONS OF MATERIAL PROPERTIES OF A DIELECTRIC MATERIAL**

| Gibbs Free Energy | Material Property | Effect Description |
|---|---|---|
| $G(E=0, T=T_0, X=0)$ | $G_0$ | Initial Value of Gibbs Free Energy |
| $\left(\frac{\partial G}{\partial E_m}\right)_{T,X}$ | $D_m$ | Electric Displacement |
| $\left(\frac{\partial G}{\partial T}\right)_{E,X}$ | $S$ | Entropy |
| $\left(\frac{\partial G}{\partial X_\mu}\right)_{E,T}$ | $x_\mu$ | Strain |
| $\left(\frac{\partial^2 G}{\partial E_m \partial E_n}\right)_{T,X}$ | $\varepsilon_{mn}^{T,X} = \left(\frac{\partial D_m}{\partial E_n}\right)_{T,X}$ | Permittivity (Dielectric Constant) |
| $\left(\frac{\partial^2 G}{\partial T \partial T}\right)_{E,X}$ | $\frac{C^{E,X}}{T} = \left(\frac{\partial S}{\partial T}\right)_{E,X}$ | Heat Capacity |
| $\left(\frac{\partial^2 G}{\partial X_\mu \partial X_\upsilon}\right)_{E,T}$ | $s_{\mu\upsilon}^{E,T} = \left(\frac{\partial x_\mu}{\partial X_\upsilon}\right)_{E,T}$ | Elastic Compliance |
| $\left(\frac{\partial^2 G}{\partial E_m \partial T}\right)_{X}$ | $p_m^X = \left(\frac{\partial D_m}{\partial T}\right)_X = \left(\frac{\partial S}{\partial E_m}\right)_X$ | Pyroelectric Effect<br>Electrocaloric Effect |
| $\left(\frac{\partial^2 G}{\partial T \partial X_\mu}\right)_{E}$ | $\alpha_\mu^E = \left(\frac{\partial x_\mu}{\partial T}\right)_E = \left(\frac{\partial S}{\partial X_\mu}\right)_E$ | Thermal Expansion<br>Piezocaloric Coefficient |
| $\left(\frac{\partial^2 G}{\partial E_m \partial X_\mu}\right)_{T}$ | $d_{m\mu}^T = \left(\frac{\partial x_\mu}{\partial E_m}\right)_T = \left(\frac{\partial D_m}{\partial X_\mu}\right)_T$ | Converse Piezoelectric Effect<br>Piezoelectric Effect |
| $\left(\frac{\partial^3 G}{\partial E_m \partial T \partial X_\mu}\right)$ | $Z_{m\mu} = \left(\frac{\partial p_m^X}{\partial X_\mu}\right)_{E,T} = \left(\frac{\partial \alpha_\mu^E}{\partial E_m}\right)_{T,X} = \left(\frac{\partial d_{m\mu}^T}{\partial T}\right)_{E,X}$ | Stress dependence of Pyroelectric Effect<br>Field dependence of Thermal Expansion<br>Temperature dependence of Piezoelectric Effect |

| | | |
|---|---|---|
| $\left(\frac{\partial^3 G}{\partial E_m \partial E_n \partial E_p}\right)_{T,X}$ | $\eta_{mnp}^{T,X} = \left(\frac{\partial \varepsilon_{mn}^{T,X}}{\partial E_p}\right)_{T,X}$ | Electric Field dependence of Permittivity |
| $\left(\frac{\partial^3 G}{\partial T \partial T \partial T}\right)_{E,X}$ | $\delta^{E,X}$ | Temperature dependence of Heat Capacity |
| $\left(\frac{\partial^3 G}{\partial X_\mu \partial X_\upsilon \partial X_\xi}\right)_{E,T}$ | $\varphi_{\mu\upsilon\xi}^{E,T} = \left(\frac{\partial x_\mu}{\partial X_\upsilon \partial X_\xi}\right)_{E,T} = \left(\frac{\partial s_{\mu\upsilon}^{E,T}}{\partial X_\xi}\right)_{E,T}$ | Stress dependence of Elastic Coefficient |
| $\left(\frac{\partial^3 G}{\partial E_m \partial E_n \partial T}\right)_X$ | $L_{mn}^X = \left(\frac{\partial \varepsilon_{mn}^{T,X}}{\partial T}\right)_X$ | Field dependence of Pyroelectric Effect<br>Temperature dependence of Permittivity |
| $\left(\frac{\partial^3 G}{\partial E_m \partial T \partial T}\right)_X$ | $M_m^X \equiv \left(\frac{\partial p_m^X}{\partial T}\right)_X = \left(\frac{\partial (C^{E,X}/T)}{\partial E_m}\right)_X$ | Temperature dependence of Pyroelectric Effect<br>Field dependence of Heat Capacity |
| $\left(\frac{\partial^3 G}{\partial T \partial T \partial X_\mu}\right)_E$ | $N_\mu^E \equiv \left(\frac{\partial \alpha_\mu^E}{\partial T}\right)_E = \left(\frac{\partial (C^{E,X}/T)}{\partial X_\mu}\right)_E = \left(\frac{\partial^2 x_\mu^E}{\partial T^2}\right)_E$ | Temperature dependence of Thermal Expansion<br>Stress dependence of Heat Capacity |
| $\left(\frac{\partial^3 G}{\partial T \partial X_\mu \partial X_\upsilon}\right)_E$ | $O_{\mu\upsilon}^E = \left(\frac{\alpha_\mu^E}{\partial X_\upsilon}\right)_E = \left(\frac{\partial s_{\mu\upsilon}^{E,T}}{\partial T}\right)_E$ | Stress dependence of Thermal Expansion<br>Temperature dependence of Elastic Compliance |
| $\left(\frac{\partial^3 G}{\partial E_m \partial E_n \partial X_\mu}\right)_T$ | $R_{mn\mu}^T = \left(\frac{\partial d_{m\mu}^T}{\partial E_n}\right)_T = \left(\frac{\partial \varepsilon_{mn}^{T,X}}{\partial X_\mu}\right)_T = \left(\frac{\partial^2 x_\mu}{\partial E_n \partial E_m}\right)_T$ | Field dependence of Piezoelectric Coefficient,<br>*("Electrostriction")*<br>Stress dependence of Permittivity (Dielectric Constant) |
| $\left(\frac{\partial^3 G}{\partial E_m \partial X_\mu \partial X_\upsilon}\right)_T$ | $V_{m\mu\upsilon}^T = \left(\frac{s_{\mu\upsilon}^{E,T}}{\partial E_m}\right)_T = \left(\frac{\partial d_{m\mu}^T}{\partial X_\upsilon}\right)_T$ | Field dependence of Elastic Compliance<br>Stress dependence of Piezoelectric Coefficient (Nonlinear Piezoelectric Coefficient) |
| $\left(\frac{\partial^4 G}{\partial E_m \partial E_n \partial E_p \partial E_q}\right)_{T,X}$ | $\lambda_{mnpq}^{T,X}$ | Nonlinear Effect of Fourth Order |
| $\left(\frac{\partial^4 G}{\partial T^4}\right)_{E,X}$ | $\chi^{E,X}$ | Nonlinear Effect of Fourth Order |
| $\left(\frac{\partial^3 G}{\partial X_\mu \partial X_\upsilon \partial X_\xi \partial X_\lambda}\right)_{E,T}$ | $\psi_{\mu\upsilon\xi\lambda}^{E,T}$ | Nonlinear Effect of Fourth Order |

## APPENDIX - G TENSORIAL RANKS OF MATERIAL PROPERTIES

| Parameter | Rank of Tensor | Parameter | Rank of Tensor | Parameter | Rank of Tensor |
|---|---|---|---|---|---|
| Electric Field | 1st (Vector) | Electric Displacement | 1st | Permittivity | 2nd |
| Temperature | 0th (scalar) | Entropy | 0th | Heat Capacity | 0th |
| Stress | 2nd | Strain | 2nd | Elastic Compliance | 4th |
| Electric Field | 1st | Entropy | 0th | Pyroelectricity | 1st |
| Temperature | 0th | Strain | 2nd | Thermal Expansion | 2nd |
| Stress | 2nd | Elect. Disp. | 1st | Piezoelectricity | 3rd |

**APPENDIX - H MATRIX AND TENSOR NOTATIONS**

| Parameter | Symbol | No. of Terms | Matrix Notation | Tensor Notation |
|---|---|---|---|---|
| Electric Field | $E_m$ | $m = 1,2,3$ | $[E_1\ E_2\ E_3]$ | Vector |
| Electric Displacement | $D_m$ | $m = 1,2,3$ | $[D_1\ D_2\ D_3]$ | Vector |
| Permittivity | $D_m = \varepsilon_{mn}E_n$ | $m = 1,2,3$<br>$n = 1,2,3$ | $\begin{bmatrix}\varepsilon_{11} & \varepsilon_{12} & \varepsilon_{13}\\ \varepsilon_{21} & \varepsilon_{22} & \varepsilon_{23}\\ \varepsilon_{31} & \varepsilon_{32} & \varepsilon_{33}\end{bmatrix}$ | $\varepsilon_{mn}$ |
| Stress | $X_\mu$ | $\mu = 1,2,3,4,5,6$ | $X_{11} = X_1$<br>$X_{22} = X_2$<br>$X_{33} = X_3$<br>$X_{23} = X_{32} = X_4$<br>$X_{31} = X_{13} = X_5$<br>$X_{12} = X_{21} = X_6$<br>$[X_1\ X_2\ X_3\ X_4\ X_5\ X_6]$ | $X_{ij}$<br>$i = 1,2,3$<br>$j = 1,2,3$<br>$\begin{bmatrix}X_{11} & X_{12} & X_{13}\\ X_{21} & X_{22} & X_{23}\\ X_{31} & X_{32} & X_{33}\end{bmatrix}$ |
| Strain | $x_\mu$ | $\mu = 1,2,3,4,5,6$ | $x_{11} = x_1$<br>$x_{22} = x_2$<br>$x_{33} = x_3$<br>$x_{12} = x_{21} = x_6$<br>$x_{23} = x_{32} = x_4$<br>$x_{31} = x_{13} = x_5$<br>$[x_1\ x_2\ x_3\ x_4\ x_5\ x_6]$ | $x_{ij}$<br>$i = 1,2,3$<br>$j = 1,2,3$<br>$\begin{bmatrix}x_{11} & x_{12} & x_{13}\\ x_{21} & x_{22} & x_{23}\\ x_{31} & x_{32} & x_{33}\end{bmatrix}$ |
| Elastic Compliance | $x_\mu = s_{\mu\upsilon}X_\upsilon$ | $\mu = 1,2,3,4,5,6$<br>$\upsilon = 1,2,3,4,5,6$ | $\begin{bmatrix}s_{11} & s_{12} & \cdots & s_{16}\\ s_{21} & s_{22} & \cdots & s_{26}\\ \vdots & \vdots & \ddots & \vdots\\ s_{61} & s_{62} & \cdots & s_{66}\end{bmatrix}$ | $x_{ij} = s_{ijkl}X_{kl}$ |
| Piezoelectricity | $x_\mu = d_{m\mu}E_m$<br>$D_m = d_{m\mu}X_m$ | $m = 1,2,3$<br>$\mu = 1,2,3,4,5,6$ | $\begin{bmatrix}d_{11} & d_{12} & \cdots & d_{16}\\ d_{21} & d_{22} & \cdots & d_{26}\\ d_{31} & d_{32} & \cdots & d_{36}\end{bmatrix}$ | $x_{ij} = d_{mij}E_m$<br>$D_m = d_{mij}X_{ij}$ |
| Pyroelectricity | $\Delta S = p_m E_m$<br>$D_m = p_m \Delta T$ | $m = 1,2,3$ | $[p_1\ p_2\ p_3]$ | Vector |
| Thermal Expansion | $\Delta S = \alpha_\mu X_\mu$<br>$x_\mu = \alpha_\mu \Delta T$ | $\mu = 1,2,3,4,5,6$ | $\alpha_{11} = \alpha_1$<br>$\alpha_{22} = \alpha_2$<br>$\alpha_{33} = \alpha_3$<br>$\alpha_{12} = \alpha_{21} = \alpha_6$<br>$\alpha_{23} = \alpha_{32} = \alpha_4$<br>$\alpha_{31} = \alpha_{13} = \alpha_5$<br>$[\alpha_1\ \alpha_2\ \alpha_3\ \alpha_4\ \alpha_5\ \alpha_6]$ | $\Delta S = \alpha_{ij}X_{ij}$<br>$x_{ij} = \alpha_{ij}\Delta T$ |

**APPENDIX - I PROOF OF GEOMETRIC SERIES**

$$S_n = h^{2(n-1)} \exp\left(-\left[\frac{(4n-m)R}{2\sqrt{\alpha^c t}}\right]^2\right)$$

$$\frac{S_{n+2}}{S_{n+1}} = \frac{h^{2(n+2-1)} \exp\left(-\left[\frac{(4(n+2)-m)R}{2\sqrt{\alpha^c t}}\right]^2\right)}{h^{2(n+1-1)} \exp\left(-\left[\frac{(4(n+1)-m)R}{2\sqrt{\alpha^c t}}\right]^2\right)}$$

$$= \frac{h^{2(n+1)} \exp\left(-\left[\frac{(4n-m+8)R}{2\sqrt{\alpha^c t}}\right]^2\right)}{h^{2n} \exp\left(-\left[\frac{(4n-m+4)R}{2\sqrt{\alpha^c t}}\right]^2\right)}$$

$$= \frac{h^2 \exp\left(-\left[\frac{(4n-m)^2R^2 + 16(4n-m)R^2 + 64R^2}{4\alpha^c t}\right]\right)}{\exp\left(-\left[\frac{(4n-m)^2R^2 + 8(4n-m)R^2 + 16R^2}{4\alpha^c t}\right]\right)}$$

$$= h^2 \exp\left(-\left[\frac{(4n-m)^2R^2 + 16(4n-m)R^2 + 64R^2}{4\alpha^c t}\right] + \left[\frac{(4n-m)^2R^2 + 8(4n-m)R^2 + 16R^2}{4\alpha^c t}\right]\right)$$

$$= h^2 \exp\left(\frac{-(4n-m)^2R^2 - 16(4n-m)R^2 - 64R^2 + (4n-m)^2R^2 + 8(4n-m)R^2 + 16R^2}{4\alpha^c t}\right)$$

$$= h^2 \exp\left(\frac{-8(4n-m)R^2 - 48R^2}{4\alpha^c t}\right)$$

$$= h^2 \exp\left(\frac{-32nR^2 + 8mR^2 - 48R^2}{4\alpha^c t}\right)$$

$$= h^2 \exp\left(-\frac{4(12-2m)R^2}{4\alpha^c t} - \frac{32R^2}{4\alpha^c t}n\right)$$

$$= h^2 \exp\left(-\frac{(12-2m)R^2}{\alpha^c t}\right) \exp\left(-\frac{8R^2}{\alpha^c t}n\right)$$

$$\frac{S_{n+2}}{S_{n+1}} = h^2 B \exp(-A \cdot n) \quad (< 1)$$

Where

$$A = \exp\left(-\frac{8R^2}{\alpha^c t}\right) > 0$$

$$\mathrm{B} = \exp\left(-\frac{(12-2m)R^2}{\alpha^c t}\right) < 1$$

**APPENDIX - J CONSTANTS OF INTEGRATION (ANALYTICAL SOLUTION FOR DIFFERENT SINK/SOURCE)**

$$A_1 = \frac{e^{R\sqrt{\frac{s}{\alpha^{SI}}}}K_{SI}\left\{(1-K_{SO})\left(T_{EC1,i}-T_{SI,i}\right) - e^{R\sqrt{\frac{s}{\alpha^{EC}}}}(1-K_{SO})\left(T_{EC1,i}-T_{EC2,i}\right) - 2e^{2R\sqrt{\frac{s}{\alpha^{EC}}}}\left(T_{EC2,i}-T_{SO,i}\right) - e^{3R\sqrt{\frac{s}{\alpha^{EC}}}}(1+K_{SO})\left(T_{EC1,i}-T_{EC2,i}\right) + e^{4R\sqrt{\frac{s}{\alpha^{EC}}}}(1+K_{SO})(T_{EC1,i}-T_{SI,i})\right\}}{e^{4R\sqrt{\frac{s}{\alpha^{EC}}}}(1+K_{SI})(1+K_{SO})s - (1-K_{SI})(1-K_{SO})s}$$

$$A_2 = \frac{2e^{R\sqrt{\frac{s}{\alpha^{EC}}}}(1-K_{SO})\left(T_{EC1,i}-T_{SI,i}\right) - e^{2R\sqrt{\frac{s}{\alpha^{EC}}}}(1+K_{SI})(1-K_{SO})(T_{EC1,i}-T_{EC2,i}) - 2e^{3R\sqrt{\frac{s}{\alpha^{EC}}}}(1+K_{SI})(T_{EC2,i}-T_{SO,i}) - e^{4R\sqrt{\frac{s}{\alpha^{EC}}}}(1+K_{SI})(1+K_{SO})(T_{EC1,i}-T_{EC2,i})}{2e^{4R\sqrt{\frac{s}{\alpha^{EC}}}}(1+K_{SI})(1+K_{SO})s - 2s((1-K_{SI})(1-K_{SO})}$$

$$B_2 = \frac{(1-K_{SI})(1-K_{SO})\left(T_{EC1,i}-T_{EC2,i}\right) + 2e^{R\sqrt{\frac{s}{\alpha^{EC}}}}(1-K_{SI})\left(T_{EC2,i}-T_{SO,i}\right) + e^{2R\sqrt{\frac{s}{\alpha^{EC}}}}(1-K_{SI})(1+K_{SO})\left(T_{EC\ ,i}-T_{EC2,i}\right) - 2e^{3R\sqrt{\frac{s}{\alpha^{EC}}}}(1+K_{SO})(T_{EC1,i}-T_{SI,i})}{2e^{4R\sqrt{\frac{s}{\alpha^{EC}}}}(1+K_{SI})(1+K_{SO})s - 2s((1-K_{SI})(1-K_{SO})}$$

$$A_3 = \frac{-(1-K_{SI})(1-K_{SO})\left(T_{EC1,i}-T_{EC2,i}\right) + 2e^{R\sqrt{\frac{s}{\alpha^{EC}}}}(1-K_{SO})\left(T_{EC\ ,i}-T_{SI,i}\right) - e^{2R\sqrt{\frac{s}{\alpha^{EC}}}}(1-K_{SI})(1+K_{SO})\left(T_{EC1,i}-T_{EC2,i}\right) - 2e^{3R\sqrt{\frac{s}{\alpha^{EC}}}}(1+K_{SO})(T_{EC\ ,i}-T_{SO,i})}{2e^{4R\sqrt{\frac{s}{\alpha^{EC}}}}(1+K_{SI})(1+K_{SO})s - 2s((1-K_{SI})(1-K_{SO})}$$

$$B_3 = \frac{2e^{R\sqrt{\frac{s}{\alpha^{EC}}}}(1-K_{SI})\left(T_{EC2,i}-T_{SO,i}\right) + e^{2R\sqrt{\frac{s}{\alpha^{EC}}}}(1-K_{SI})(1+K_{SO})\left(T_{EC1,i}-T_{EC2,i}\right) - 2e^{3R\sqrt{\frac{s}{\alpha^{EC}}}}(1+K_{SO})\left(T_{EC1,i}-T_{SI,i}\right) + e^{4R\sqrt{\frac{s}{\alpha^{EC}}}}(1+K_{SI})(1+K_{SO})(T_{EC1,i}-T_{EC2,i})}{2e^{4R\sqrt{\frac{s}{\alpha^{EC}}}}(1+K_{SI})(1+K_{SO})s - 2s((1-K_{SI})(1-K_{SO})}$$

$$\boldsymbol{B_4} = \frac{\boldsymbol{e^{R\sqrt{\frac{s}{\alpha^{SO}}}}K_{SO}\left\{(1-K_{SI})\left(T_{EC2,i}-T_{SO,i}\right) + e^{R\sqrt{\frac{s}{\alpha^{EC}}}}(1-K_{SI})\left(T_{EC1,i}-T_{EC2,i}\right) - 2e^{2R\sqrt{\frac{s}{\alpha^{EC}}}}\left(T_{EC1,i}-T_{SI,i}\right) + e^{3R\sqrt{\frac{s}{\alpha^{EC}}}}(1+K_{SI})\left(T_{EC1,i}-T_{EC2,i}\right) + e^{4R\sqrt{\frac{s}{\alpha^{EC}}}}(1+K_{SI})(T_{EC2,i}-T_{SO,i})\right\}}}{\boldsymbol{e^{4R\sqrt{\frac{s}{\alpha^{EC}}}}(1+K_{SI})(1+K_{SO})s - (1-K_{SI})(1-K_{SO})s}}$$

where

$$h_{SI} = \frac{1-K_{SI}}{1+K_{SI}} \ |h| < 1$$

$$h_{SO} = \frac{1-K_{SO}}{1+K_{SO}} \ |h| < 1$$

**APPENDIX - K MANIPULATING THE DENOMINATOR FOR ANALYTICAL SOLUTION IN CHAPTER 5**

$$
\begin{aligned}
Deno &= \frac{1}{e^{4R\sqrt{\frac{s}{\alpha^{EC}}}}(1+K_{SI})(1+K_{SO})s-(1-K_{SI})(1-K_{SO})s} \\
&= \frac{1}{e^{4R\sqrt{\frac{s}{\alpha^{EC}}}}(1+K_{SI})(1+K_{SO})\left[1-\frac{(1-K_{SI})(1-K_{SO})}{(1+K_{SI})(1+K_{SO})}e^{-4R\sqrt{\frac{s}{\alpha^{EC}}}}\right]}\frac{1}{s} \\
&= \frac{e^{-4R\sqrt{\frac{s}{\alpha^{EC}}}}}{(1+K_{SI})(1+K_{SO})\left[1-\frac{(1-K_{SI})(1-K_{SO})}{(1+K_{SI})(1+K_{SO})}e^{-4R\sqrt{\frac{s}{\alpha^{EC}}}}\right]}\frac{1}{s} \\
&= \frac{e^{-4R\sqrt{\frac{s}{\alpha^{EC}}}}}{(1+K_{SI})(1+K_{SO})\left[1-h_{SI}h_{SO}e^{-4R\sqrt{\frac{s}{\alpha^{EC}}}}\right]}\frac{1}{s} \\
&= \frac{1}{s}\frac{e^{-4R\sqrt{\frac{s}{\alpha^{EC}}}}}{(1+K_{SI})(1+K_{SO})}\frac{1}{\left[1-h_{SI}h_{SO}e^{-4R\sqrt{\frac{s}{\alpha^{EC}}}}\right]}
\end{aligned}
$$

Using the following relation (Geometric Series)

$$\frac{1}{1-x}=\sum_{n=0}^{\infty}x^n=1+x+x^2+x^3+\cdots$$

The above equation may be written as

$$
\begin{aligned}
Deno &= \frac{1}{s}\frac{e^{-4R\sqrt{\frac{s}{\alpha^{EC}}}}}{(1+K_{SI})(1+K_{SO})}\sum_{n=0}^{\infty}\left(h_{SI}h_{SO}e^{-4R\sqrt{\frac{s}{\alpha^{EC}}}}\right)^n \\
&= \frac{1}{s}\frac{e^{-4R\sqrt{\frac{s}{\alpha^{EC}}}}}{(1+K_{SI})(1+K_{SO})}\left[1+h_{SI}h_{SO}\exp\left(-4R\sqrt{\frac{s}{\alpha^{EC}}}\right)+h_{SI}^2h_{SO}^2\exp\left(-8R\sqrt{\frac{s}{\alpha^{EC}}}\right)\right. \\
&\qquad \left.+h_{SI}^2h_{SO}^2\exp\left(-12R\sqrt{\frac{s}{\alpha^{EC}}}\right)+\cdots\right] \\
&= \frac{1}{s}\frac{e^{-4R\sqrt{\frac{s}{\alpha^{EC}}}}}{(1+K_{SI})(1+K_{SO})}\sum_{n=1}^{\infty}h_{SI}^{n-1}h_{SO}^{n-1}\exp\left(-4nR\sqrt{\frac{s}{\alpha^{EC}}}\right)
\end{aligned}
$$

Hence

$$\frac{1}{e^{4R\sqrt{\frac{s}{\alpha^{EC}}}}(1+K_{SI})(1+K_{SO})s-(1-K_{SI})(1-K_{SO})s}=\frac{1}{s}\frac{e^{-4R\sqrt{\frac{s}{\alpha^{EC}}}}}{(1+K_{SI})(1+K_{SO})}\sum_{n=1}^{\infty}(h_{SI}h_{SO})^{n-1}\exp\left(-4nR\sqrt{\frac{s}{\alpha^{EC}}}\right)$$